PROCEEDINGS

Cosmic Ray Summer School

Nor Amberd International Conference Center
June 1-7, 2012

Edited by A. Chilingarian


Cosmic Ray Division

A. Alikhanyan National Laboratory

Yerevan Physics Institute

Published by CRD
Cosmic Ray division, A.Alikhanyan National Laboratory
Yerevan Physics Institute
Alikhanyan Brothers 2, Yerevan, Armenia

http://aragats.am

Printed by **TIGRAN METS**
2, Arshakouniats Avenue, Yerevan, Armenia
Tel:+37410-521 775

ISBN 978-99941-0-478-9 July 2012

Copies 150

Preface

A summer school “A century of cosmic rays” was held on June 1-7, 2012 in the International Conference Center of Yerevan Physics Institute in Nor Amberd, Armenia, 40 km from Armenia’s capital Yerevan. A cycle of invited lectures was delivered to the students of Yerevan State University work in Cosmic Ray Division (CRD) of A.Alikhanyan National laboratory, for graduate and PhD students and young scientists of CRD. During the summer school also sessions devoted to International Science and Technology (ISTC) project A1554, completed recently by CRD staff, were held. Last 10 years ISTC was the main funding body supporting research on high altitude stations Aragats and Nor Amberd and facilitating creation of new scientific directions of CRD, namely, Space Weather and Solar terrestrial connections; High energy Phenomena in thunderstorm atmospheres. Young scientists and students have presented 13 reports covering recent research in the framework of the A1554 ISTC project “Space Weather Research and Forecasting by Networks of Hybrid Particle Detectors Measuring Neutral and Charged Fluxes”.

On 6 June, early in the morning, the summer school participants and professors observed the Venus transit on solar disc; the same day afternoon School students welcomed at Republic square in the center of Yerevan the group of bicyclist from the USA and Armenia cycling from Artsakh province to memorize 100 years of cosmic ray invention and successes of CRD physicists. Also school participants installed a new optical telescope and weather station in Nor Amberd, to detect Thunderstorm Ground Enhancements (TGEs) registered by facilities of Aragats and Nor Amberd labs; the students were introduced to the data analysis methodologies developed in CRD; climbed to the Aragats research station on 3200 m all in snow.

Program of Lectures

Prof. Johannes Knapp

1) Introduction to Astroparticle Physics; Cosmic Rays and Photons.
2) Cosmic Ray Physics in the energy range 10^14 … 10^18 eV.
3) Air shower simulations with the Corsika Program.
4) Ultra High Energy Cosmic Rays & Recent Results from the Pierre Auger Observatory.
5) Gamma Ray Astronomy and the Cherenkov Telescope Array.

Prof. Razmik Mirzoyan

1) Discovery of Cherenkov emission and instrumentation based on this discovery.
2) Ground-based Very High Energy Astroparticle Physics by Means of Gamma Rays: Status of the Field.
3) Ultra-fast Light sensors for Astroparticle Physics.
4) Pulsed gamma rays from the Crab pulsar.
5) The Galactic source W51.

Prof. Hartmut Gemmeke

1) Signals from the particle detectors and their treatment; modern trends.
2) Particle radio emission in the atmosphere; history of detection, instrumentation and opened possibilities.
3) European and American radio detecting arrays; goals, results, problems.
4) Status and Results from the Auger Engineering Array (AERA).
5) AERA Hardware and Self-Trigger.
6) First Results from the KIT 3D Computer Tomography.

Prof. Ashot Chilingarian

1) Thunderclouds - another source of MeV electrons, gamma rays and neutrons.

Videography of lectures and slides are available from http://crd.yerphi.am

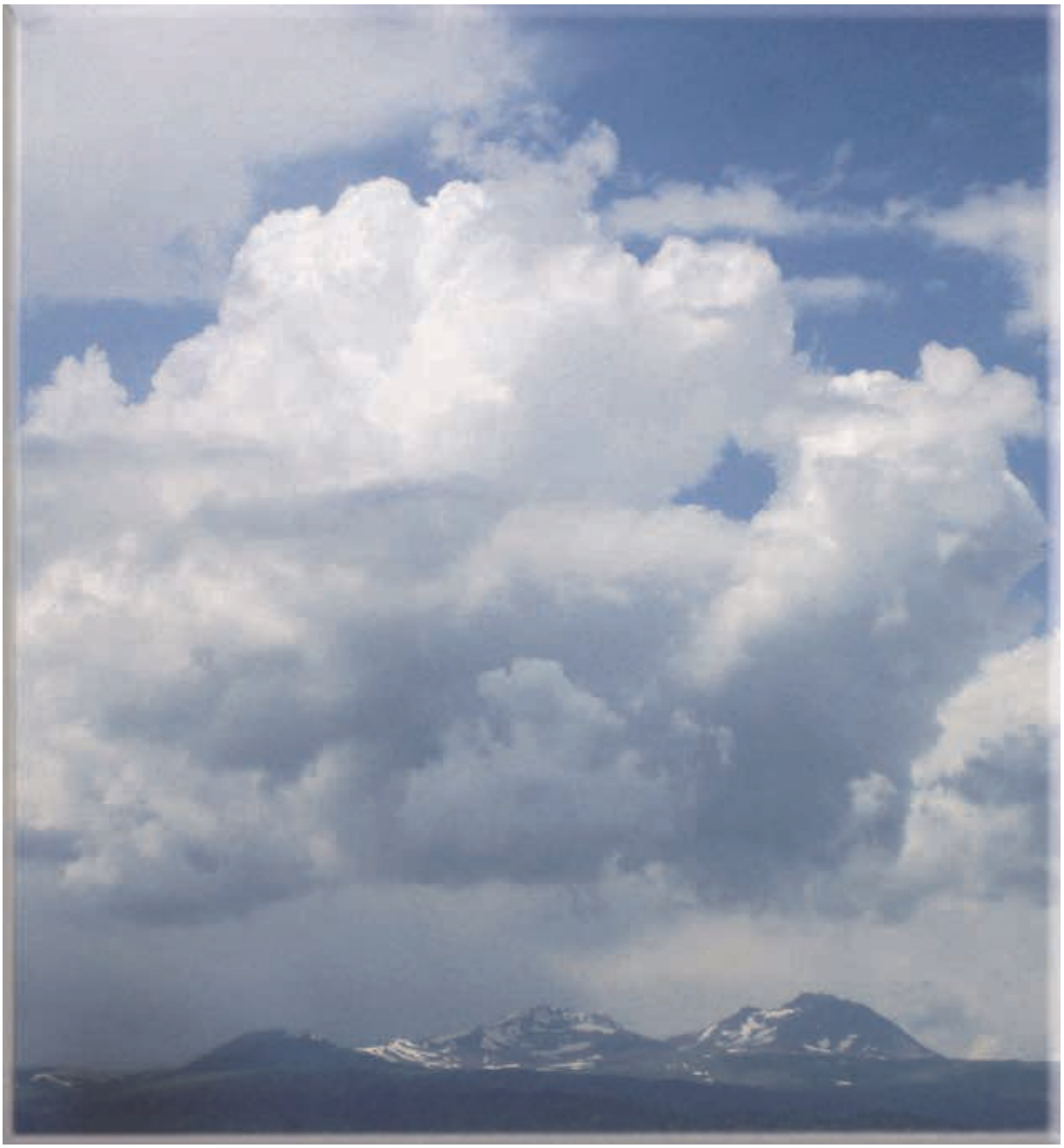

Thunderclouds above Aragats

Table of Contents

Thunderstorm Ground Enhancements (TGEs) - New High-Energy Phenomenon Originated in the Terrestrial Atmosphere…….9
A. Chilingarian

Recovering of the TGE Electron and Gamma ray Energy Spectra..…….12
A. Chilingarian, B. Mailyan

Simulations of the Secondary Cosmic Ray Propagation in the Thunderstorm Atmospheres Resulting in the Thunderstorm Ground Enhancements (TGEs).…….15
A. Chilingarian, L. Vanyan

Geophysical Research Network Operating in the Aragats Space Environmental Center ...……...……18
A. Reymers, S. Chilingarian

Magnetometric Measurements at Mt. Aragats...……21
T. Karapetyan,

NaI Detector Network at Aragats ……23
K. Avakyan, K. Arakelyan, A. Chilingarian, A. Daryan, L. Kozliner, B. Mailyan, G. Hovsepyan, D. Pokhsraryan, D. Sargsyan

New Low Threshold Detectors for Measuring Electron and Gamma Ray Fluxes from Thunderclouds ...…….25
K. Arakelyan, K. Avakyan, A. Chilingarian, A. Daryan, L. Kozliner, G. Hovsepyan, L. Melkumyan, D. Pokhsraryan, D. Sargsyan

Space Environmental Viewing and Analysis Network (SEVAN) – Characteristics and First Operation Results……..…….27
A. Chilingarian, K. Avakyan, K. Arakelyan, N. Bostanjyan, S. Chilingarian, L. Kozliner, D. Pokhsraryan, D. Sargsyan, A. Reymers

Simulation of MuSTAnG Telescope Response to Cosmic Rays..…….30
R. Hippler, M. Zazyan

CME-CME Interaction and Forbush Decrease: a case study of 13th ; 14th; 15th February 2011 CMEs……...……32
D. Maričić, N. Bostasyan, M. Dumbović, A. Chilingarian, K. Arakelyan, H. Rostomyan, B. Vršnak, D. Roša, D. Hržina, I. Romštajn and A. Veronig

Depletion of High Energy Muon Flux during TGEs – a Possibility to Measure Potential Drop in Thunderclouds ……32
A. Chilingarian, G. Karapetyan, K. Bostanjyan, L. Vanyan

Extensive Cloud Showers (ECS) – High-Energy Phenomena Resulting from the Thunderstorm Atmospheres...…….33
A. Chilingarian, G. Hovsepyan

Comments on Recent Results on Neutron Production in Thunderclouds…….34
A. Chilingarian, N. Bostanjyan, T. Karapetyan, L. Vanyan

Role of the Lower Positive Charge Region (LPCR) in Initiation of the Thunderstorm Ground Enhancements (TGEs)……...…….39
A. Chilingarian, H. Mkrtchyan

Ground-Based Observations of Thunderstorm-Correlated
Fluxes of High-Energy Electrons, Gamma Rays, and Neutrons……..….48
A. Chilingarian, A. Daryan, K. Arakelyan, A. Hovhannisyan, B. Mailyan,
L. Melkumyan, G. Hovsepyan, S. Chilingaryan, A. Reymers, and L. Vanyan;
PHYSICAL REVIEW D 82, 043009 (2010)

Particle Bursts from Thunderclouds:
Natural Particle Accelerators above our Heads…….59
A. Chilingarian, G. Hovsepyan, A. Hovhannisyan;
PHYSICAL REVIEW D 83, 062001 (2011)

Recovering of the Energy Spectra of Electrons and
Gamma Rays Coming from the Thunderclouds...…….…….70
A. Chilingarian, B. Mailyan, L. Vanyan;
ATMOSPHERIC RESEARCH 114–115 (2012) 1–16

Neutron Bursts Associated with Thunderstorms..…….…….86
A. Chilingarian, N. Bostanjyan, L. Vanyan;
PHYSICAL REVIEW D 85, 085017 (2012)

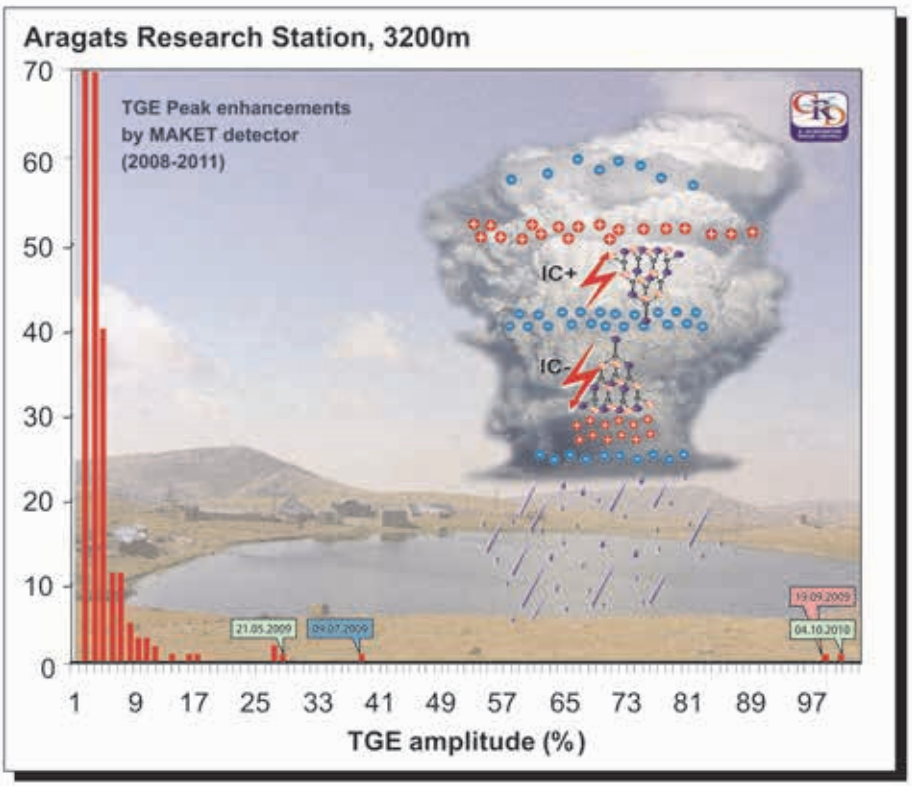

The histogram of the amplitudes of TGE events detected by ASEC detectors in 2008-2010. The peak values of the cosmic ray flux increase above rather stable secondary cosmic ray background were measured by the outdoor plastic scintillators.

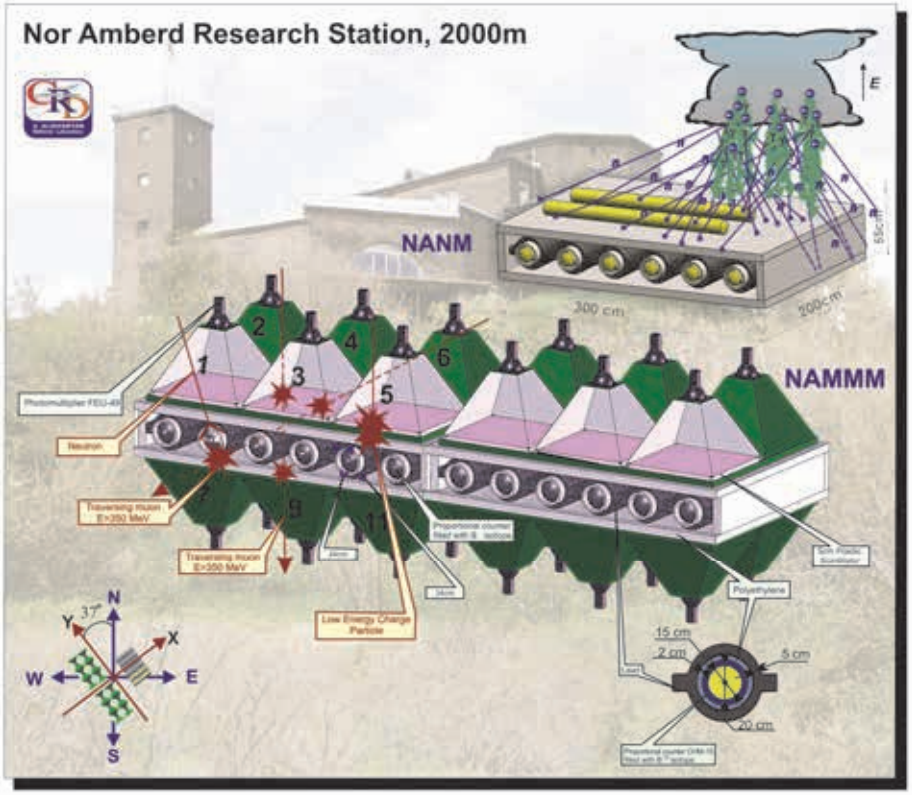

Nor Amberd multidirectional muon monitor (NAMMM) arranged above and below 2 sections of the Nor Amberd Neutron Monitor (NANM); on the third section of NANM 2 "bare" proportional counters are located

Examples 3 classes of TGE events

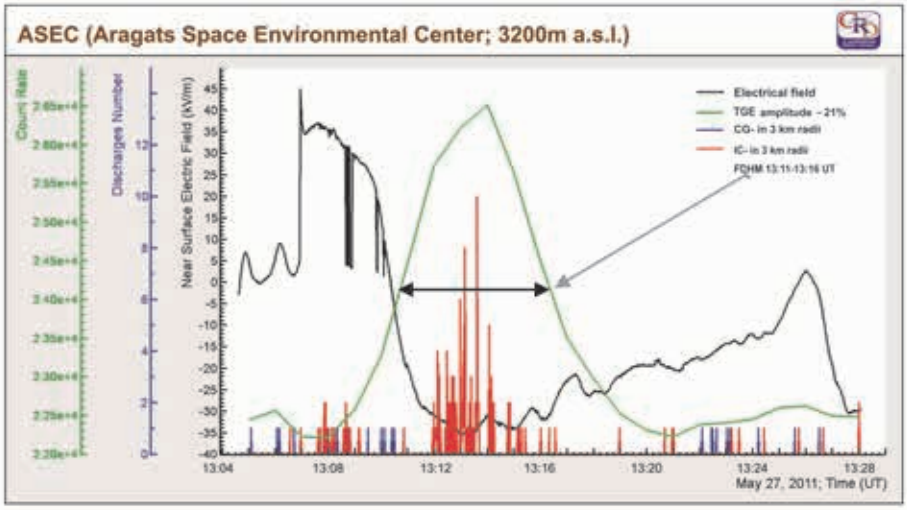

TGE of the first type according to pattern of the electric field disturbances; the black curve shows changing electric field; red lines - IC- lightning and blue CG- lightning occurrences within 3 km radius; the green curve shows the time series of the particle flux minutely counts. Particle flux peaked at 21% above CR background.

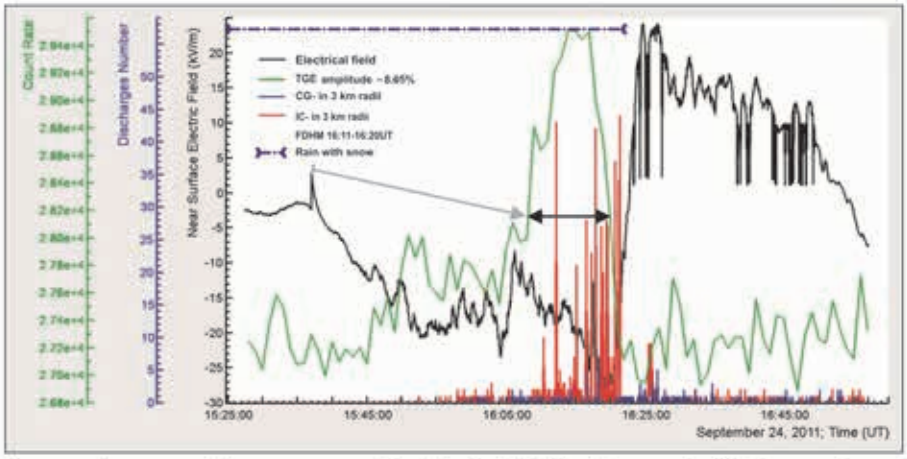

TGE of the second type according to pattern of the electric field disturbances; the black curve shows changing electric field; red lines - IC- lightning and blue CG- lightning occurrences within 3 km; the green curve - the time series of the particle flux minutely counts. Particle flux peaked at 8% above CR background.

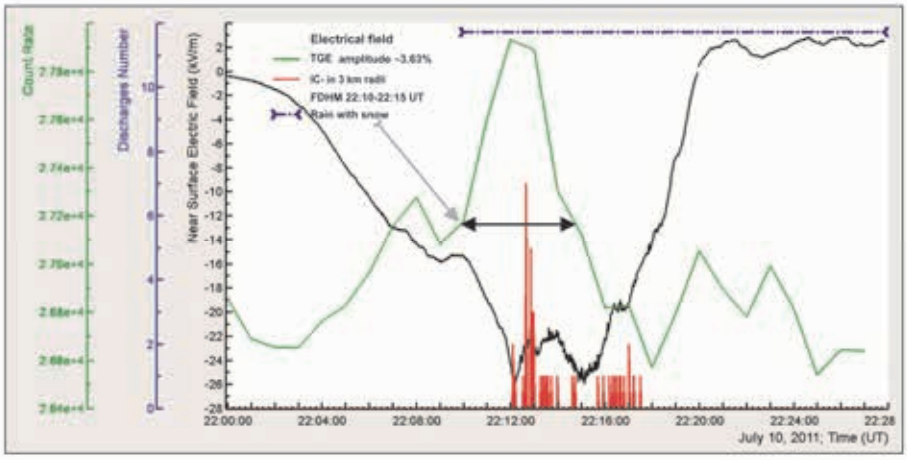

TGE of the third type according to pattern of the electric field disturbances; the black curve shows changing electric field; red lines - IC- occurrences within 3 km; the green curve - the time series of the particle flux minutely counts. Particle flux peaked at 3.6% above CR background. Rain was detected during 22:15-22:35 UT.

Thunderstorm Ground Enhancements (TGEs) - New High-Energy Phenomenon Originated in the Terrestrial Atmosphere

A. Chilingarian

Abstract: Space based gamma ray observatories; sensors on aircraft and surface particle detectors observe fluxes of gamma rays, which are correlated with thunderstorms. In some, yet fully unknown circumstances electrons are accelerated upward in direction to space and downward in direction to the Earth and dramatically enhance usually rather stable cosmic ray background. These very important phenomena are now intensively researched both in space and on Earth's surface. Numerous particle detectors and field maters located on the slopes of mountain Aragats and in Yerevan 24 hours 12 months are monitoring changing geophysical conditions. After analyzing near 300 detected at Aragats Thunderstorm ground enhancements (TGEs) we present the physical model of new phenomena.

1. THUNDERSTORM GROUND ENHANCEMENTS (TGES)

Rapidly expanding field of energetic particle and radiation physics in terrestrial atmosphere, namely, High-Energy Atmospheric Physics, impacts traditional atmospheric electricity and lightning physics, study of cosmic-ray extensive air showers, discharge physics, space physics, plasma physics, and aviation safety [1]. One of the most exciting manifestations of the new field is so called Thunderstorm Ground Enhancement (TGE, [2]): abrupt enhancements of surface particle detector count rates correlated with thunderstorm activity. Facilities of the Aragats Space Environment Center (ASEC, [3]) observe charged and neutral fluxes of secondary cosmic rays by the variety of particle detectors located in Yerevan and on slopes of Mount Aragats at altitudes 1000, 2000 and 3200 m. ASEC detectors measure particle fluxes with different energy thresholds as well as Extensive Air Shower (EAS) initiated by primary proton or stripped nuclei with energies greater than 50–100 TeV and Extensive Cloud Showers (ECS) initiated by the electron-gamma ray avalanches in the thunderstorm atmosphere. TGEs detected during 2008-2011 bring vast amounts (243 events) of small and very few large TGEs (only 6 TGE events with amplitude exceeding 20%) allowing the detailed analyses and taxonomy of the new high-energy phenomena in the atmosphere[1]. In Fig. 1, we present the histogram of the 243 TGE amplitudes measured by the MAKET detector in 2008-2011; the dates of 4 largest TGE events are displayed as boxed text; flux enhancement is presented in percentage relative to rather stable background of the ambient population of secondary cosmic rays. As we can see in the left corner of histogram of Fig. 1, majority of TGE events have amplitude less than 10 %. These small TGEs and analogical TGEs reported by other groups can be explained by the modification of the energy spectra of charged particles in the electric field of thunderclouds. Due to asymmetry of positive-to-negative flux of secondary cosmic rays in the terrestrial atmosphere, peaks and dips can arise in time series of count rates of surface particle detectors. These effects have been theoretically analyzed in [4] and detected on Mount Norikura [5] and in Baksan, Russia [6]. Measurements at ASEC and simulations with GEANT4 package [7] confirm additional flux of gamma rays up to 1000% in the energy range 2-20 MeV and up to 10% in the energy range up to 100 MeV. Simultaneously dips in the muon flux at energies above 200 MeV were obtained by GEANT4 simulations and detected by ASEC detectors.

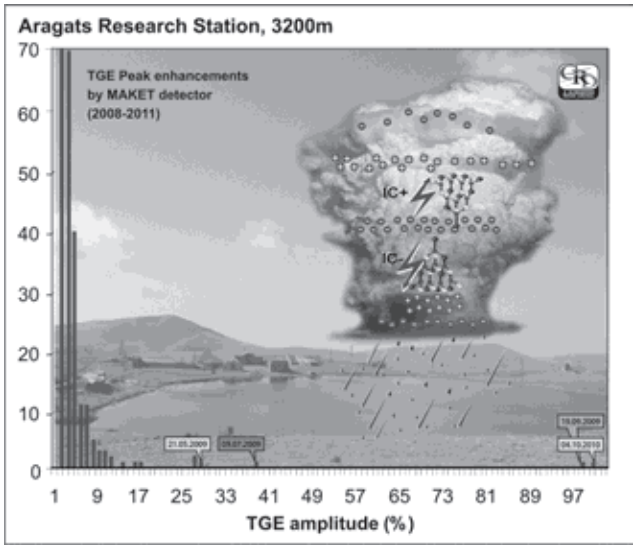

Figure 1. The histogram of the amplitudes of TGE events detected by ASEC detectors in 2008-2010. The peak values of the cosmic ray flux increase above rather stable secondary cosmic ray background were measured by the outdoor plastic scintillators.

Few very large enhancements seen in the right corner of Fig. 1 can be explained only by invoking the Runaway Breakdown (RB) process [8], also referred as Relativistic Runaway Electron avalanche (RREA, [9-11]. Ambient population of secondary cosmic ray electrons in the electric fields with strength greater than critical value[2] unleash the electron-gamma ray avalanches and total number of particles on the exit from cloud can be multiplied by several orders of magnitude. Proceeding from the measurements of the charged and neutral fluxes as well as from the energy deposit of particles in thick scintillators we recover the energy spectra of TGE electrons and gamma rays for the 2 largest TGE events of September 19, 2009 and October 4, 2010 [12]. Installed at Aragats field meters and lightning

[1] Time series of changing particle fluxes registered from ASEC monitors, as well as magnetometer and electrical mill measurements are available from http://adei.crd.yerphi.am/adei/.

[2] The critical electric field E_t = 1.534; 1.625, 1.742 kV/cm at 4500, 4000 and 3400m respectively. E_t dependence on altitude follows the air density dependence on altitude.

detectors allow correlating the measured particle fluxes with near-surface electric field disturbances and with occurrences of lightning of different types.

Lightning occurrences, as well as sketch of the RREA process in upper and lower dipoles also are depicted in Fig. 1. The indispensable condition of TGE initiation is the creation of the lower dipole accelerating electrons downward. The temporarily emerging Lower positive charge region (LPCR, [13]) is smaller than the mid-level negative and upper positive layers of the main upper thundercloud dipole [14]. Therefore TGE phenomena is local and its duration coincide with duration of the existence of LCPR, at Aragats usually ~10 minutes.

2. SUMMARY OF TGE RESEARCH

Thunderstorm ground enhancements (TGEs) manifest themselves by at least 6 physical effects:

- Large fluxes of the electrons and gamma rays;
- Neutron fluxes;
- Microsecond bursts of the electrons;
- Depletion of the high energy muon flux;
- Large negative near-surface electrical field;
- Depletion of the cloud-ground lightning occurrences and enhancement of the intracloud lightning occurrences.

Origin of TGE is a radiating region in the bottom of the cloud [15] coincided with LPCR, which forms a lower dipole with the main negative charge region in the middle of the cloud. Intensive electrical field between these layers accelerates electrons downward and give birth to 2 processes:

- Relativistic runaway electron avalanches (RB/RREA) process sustaining electron and gamma ray fluxes up to 10 times above cosmic ray;
- Modification of CR energy spectra (MOS) process, which is responsible for the gamma ray and electron flux enhancements and depletion of high-energy muon flux.

Electrical fields in thunderclouds effectively transfers field energy to electrons; electrons generate gamma rays and gamma rates by photonuclear reactions born neutrons detected on earth's surface [16-18]; RREA can generate particle bursts with duration less than 50 microseconds [19] ; overall duration of TGE is ~ 10 minutes, during 10 minutes large amount of short bursts occurs; Largest TGE events allows to estimate energy spectra: energy spectra of electrons and low energy gamma rays are exponential; energy spectra of gamma rays above 10 MeV are described by power law in overall agreement with GEANT4 simulation; TGEs usually occurred on negative near surface electrical field varied from -10 to -30 kV/m; During TGEs the fraction of IC- lightning occurrences is strictly increased, CG- lightnings are suppressed; observed behavior of lightning occurrences supports emergence of the LCPR and, consequently, lower dipole. The upper dipole accelerates electrons upward to the space where electrons, positrons and gamma rays are detected by space born gamma ray observatories [20]. This founding is very important for geophysics, atmospheric physics and climatology. Ongoing climate change can lead to significant increase of lightning occurrences mostly in globe dry regions. Monitoring lightnings by worldwide networks of antennas and by space born monitors, planned in coming decade at International Space Station [21,22]will help to establish the forewarning services on disastrous weather conditions greatly enlarged recently. The increasing rate of lightnings and simultaneous increase of their height can alert on the upcoming huge thunderstorm with possible flooding. The increasing rate of positive cloud to ground lightnings is manifestation of possible hailing. Numerous particle detectors and field maters located on the slopes of mountain Aragats and in Yerevan 24 hours 12 months are monitoring changing geophysical conditions. Planned geophysical station near Sevan lake with existing 3 stations on slopes of Mt. Aragats will monitor particle fluxes from sun, thunderclouds and Galaxy as well as magnetic and electrical fields and lightning occurrences; issue alerts and forewarnings on upcoming dangerous consequences of space and thunder-storms.

REFERENCES

[1] Dwyer J.R., Smith D.M., Cummer S.A., Space Sci Rev, DOI 10.1007/s11214-012-9894-0, 2012.

[2] Chilingarian, A., et al., Nucl. Inst. and Methods in Phys. Res. Sect A, 543, 483, 2005.

[3] Chilingarian, A., et al., Phys. Rev. D 82, 043009 (2010).

[4] Dorman, L.I., et al., Advances in Space Research 35, 476-483, 2005.

[5] [5] Muraki, Y., et al., Phys. Rev. D 69, 123010, 2004.

[6] Alexeenko, V. V., et al., Phys. Lett. A, 301, 299–306, 2002.

[7] Agostinelli, S., et al. Nucl. Instrum. Methods Phys. Res., Sect. A, 506(3), 250–303, 2003.

[8] [8] Gurevich, A. V., et al., Phys. Lett. A, 165, 463, 1992.

[9] Babich, L. P., et al, Phys. Lett. A, 245, 460–470,1998.

[10] Dwyer J.R., Geophys. Res. Lett., 30(20), 2055, 2003.

[11] Carlson, B. E., Lehtinen, N. G., Inan, U. S., J. Geophys. Res.Lett. 34, L08809, 2008.

[12] Chilingarian A., Mailyan B., Vanyan L., Atmospheric research, V. 114-115, pp. 1-16

[13] Qie, X., et al., *Geophys. Res. Lett.*, *32*, L05814, 2005.

[14] Williams, E.R., J.Geophys.Res., 94, 13151-13167, 1989.

[15] Torii, T., et al., J. Geophys. Res. 107, 4324, 2002.

[16] Chilingarian, et al., Phys.Rev.D 85, 085017, (2012).

[17] Gurevich, A.V. et al., PRL 108, 125001, (2012).

[18] Tsuchiya, H. et al., arX:1204.2578v1 [physics.geo-ph], Phys. Rev. D accepted, (2012).

[19] Chilingarian, A. et al., Phys. Rev. D 83, 062001 (2011).

[20] G.J. Fishman et al., Science 264, 1313 (1994).
[21] V. Kuznetsov, Y. Ružín, V.M. Sinelnikov, Kosm. Nauka Teh. 17, 12 (2011).
[22] T. Neubert, Coupling of thunderstorms and lightning discharges to near-Earth space, in AIP Conf. Proc. 1118, p. 8(2009)

Recovering of the TGE Electron and Gamma Ray Energy Spectra

A. Chilingarian, B. Mailyan

Abstract: The strong electric fields inside thunderclouds give rise to enhanced fluxes of high-energy electrons and, consequently, gamma rays and neutrons. During thunderstorms at Mount Aragats, hundreds of Thunderstorm Ground Enhancements (TGEs) comprising millions of energetic electrons and gamma rays, as well as neutrons, were detected at Aragats Space Environmental Center (ASEC) on 3200 m altitude. Observed large TGE events allow for the first time to measure the energy spectra of electrons and gamma rays well above the cosmic ray background. We describe the methodology of solving cosmic ray physics inverse problem to recover the energy spectra of electrons and gamma rays incident on particle detectors located at mountain altitudes. The energy spectra of the electrons have an exponential shape and extend up to 30-40 MeV. Recovered energy spectrum of the gamma rays is also exponential in the energy range 5-10 MeV, then turns to power law and is extending up to 100 MeV.

1. INTRODUCTION: THUNDERSTORM GROUND ENHANCEMENTS (TGES)

The attempts to discover high-energy phenomena in the atmosphere, so called, Thunderstorm Ground Enhancement (TGE), in spite of a long history since the prediction of C.R.T. Wilson in 1916 [1], were discrepant and rare [2-7]. Facilities of the Aragats Space Environmental Center (ASEC) [8] observe charged and neutral fluxes of secondary cosmic rays by a variety of particle detectors located in Yerevan and on slopes of Mount Aragats at altitudes 1000, 2000 and 3200 m. ASEC detectors measure particle fluxes with different energy thresholds, as well as, EAS initiated by primary proton or stripped nuclei with energies greater than 50– 100 TeV [9]. TGEs detected during 2008-2011 bring vast amounts of small and very few large TGEs (only 6 TGE events from 243 exceed 20% of cosmic ray background) allowing the detailed analyses and taxonomy of the new high-energy phenomena in the atmosphere. Few very large enhancements can be explained only by invoking the Runaway Breakdown (RB) process [10], also referred as Relativistic Runaway Electron avalanche (RREA), [11, 12]. Proceeding from the measurements of the charged and neutral fluxes, as well as, from the energy deposit of particles in thick scintillators, we recover the energy spectra of TGE electrons and gamma rays for the 2 largest TGE events of September 19, 2009 and October 4, 2010 and considerably smaller event on 27 May 2011.

1.1. THE ENERGY SPECTRA OF THE TGE ELECTRONS

Among hundreds of TGE events detected at ASEC only September 19, 2009 and October 4, 2010 TGEs allow the electron energy spectra recovering. In Figure 1, electron spectra of September 19, 2009 and October 4, 2010 TGEs are presented. The spectrum of September 19, 2009 TGE was obtained by additional counts of plastic scintillators with energy threshold of 9,12,15,18 and 25 MeV. The spectrum was approximated with exponential function; corresponding mean energy equals to ~3.3 MeV. Scintillators with thresholds of 2, 7 and 12 MeV were used to recover the October 4, 2010 TGE electron integral spectrum; for this event, the mean energy equal to ~2.3 MeV; both values are significantly smaller than estimates based on simulations of the RREA [13, 14]; however the 7.2 MeV value was obtained for the electrons just exiting electrical field and for rather large electrical field strengths; the particle source of considered measurements at Aragats were located according to our estimates 50-150 m above detectors.

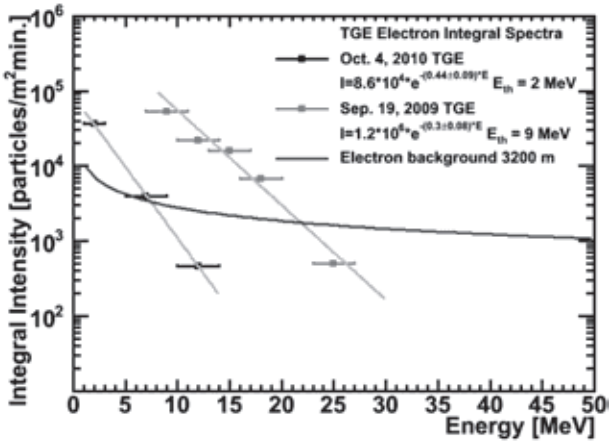

Figure 1. Electron integral energy spectra of the September 19, 2009 and October 4, 2010 TGEs measured at 3200 m compared with the background energy spectrum.

1.2. THE ENERGY SPETRA OF THE TGE GAMMA RAYS

The energy spectra of September 19, 2009 and October 4, 2010 TGE gamma rays are recovered based on the energy deposit spectra measured by Cube and ASNT detectors (see details of detector operation in [9]). Both Cube and ASNT detectors are measuring the energy deposit spectra and store them each minute. These histograms reproduce the energy spectrum of gamma rays, however they are folded by the detector response very different for Cube and ASNT detector assemblies. Recovering the energy spectrum by the energy deposit histograms, i.e. solving the inverse problem of cosmic ray physics is rather complicated task and we use multiple trial spectra for solving it. For October 4, 2010 TGE, we recover the gamma ray energy spectrum in the range of 5-10 MeV. The spectrum was approximated by both exponential and power law functions. Exponential function with mean energy of ~3.8 MeV provides slightly better approximation of the measured energy deposit with simulated one.

We use the energy deposit spectra measured by Cube detector for the calibration of ASNT detector. Above 10 MeV, the energy spectra are better approximated with power law. The spectral indices of gamma ray differential energy spectra were estimated to be 3.3±0.7 and 3.4±0.8.

The recovered gamma ray energy spectra posted in Figure 2 have no error bars due to the spectra recovering method; we chose a particular power index (the power was found to be the best model), which provides simulated energy deposit histogram (obtained by simulation of the detector response) closest to the experimentally measured one. The uncertainties of the procedure, including the possible errors in estimating detector response are included in the errors of the estimated power law indices.

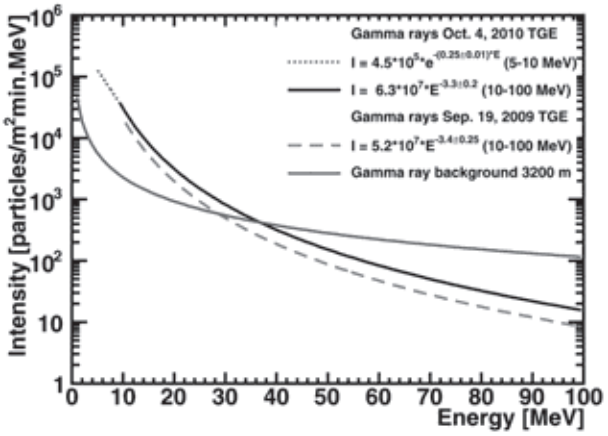

Figure 2. The Differential energy spectra of the gamma rays detected on September 19, 2009 and October 4, 2010.

2. MAY 27, 2011 TGE MEASURED BY NAI DETECTORS

In 2011, several TGEs were detected by newly installed NaI crystals network and also by Cube detector providing veto signal for charged particles and by STAND assembly allowing detection of charged flux with various energy thresholds. These detectors enabling us to disentangle charged and neutral fluxes and recover energy spectra of TGE gamma rays and electrons. Since NaI gamma ray registration efficiency is much higher than one for the plastic scintillators, the measured energy deposit is closer to the energy spectra above the detector. Therefore, for obtaining gamma ray energy spectra we use simpler method that was used for the energy recovering by the measured energy release histograms in plastic scintillators [15]. Proceeding from the simulation of the energy release in NaI crystals we calculated corrections to be applied to measured energy release spectrum in each histogram bin. These corrections are dependent on assumed in simulation energy spectrum of gamma rays (power law with different indices); however corrections corresponding to indices -1.5, -2 and -3 are very close to each other. Moreover, after corrections for the efficiency, the shape and index of energy deposit spectrum doesn't change much and the differences are within the errors bars. The energy deposit spectrum of the gamma rays registered on May 27, 2011 by the NaI crystal of thickness 13.5 x 13.5 x 21 cm in aluminum case of 0.7 mm is shown in Figure 3. In the same figure, one also can see the "corrected" spectrum. According to the calculations, there were ~130,000 particles/m^2/min at the energy range 3 - 20 MeV on May 27, 2011. The power spectrum index of these gamma rays is ~1.7±0.1. It is worth mentioning, that Stand detector's data show the absence of electrons > 7 MeV and presence of electrons of 4-7 MeV, which can contaminate gamma ray flux observed by NaI crystals, however, by our estimates the electron fraction can not exceed 5 % of the gamma ray flux.

3. CONCLUSIONS

We present electron and gamma ray energy spectra of 2 large events observed by facilities of Aragats Space Environmental Center (ASEC) in 2009 and 2010, and considerably smaller event (without electrons above 7 MeV) detected by NaI crystals in 2011. Integral energy spectra of the TGE electrons of super events on September 19, 2009 and October 4, 2010 have exponential shape with mean energy ~3.3 and ~2.3 MeV. The gamma ray differential energy spectrum also is better fitted by an exponential function at energies below 10 MeV with mean energy ~4 MeV; in the energy range 10 – 100 MeV spectra are fitted by power law function with indices -3.3 and -3.4. The spectral index of the May 27 2011 event (energy range 3-20 MeV) equal to approximately -1.7 is in a good agreement with indices reported by Gamma-Ray Observation of Winter Thunderclouds (GROWTH) collaboration in the energy range up to 10 MeV[6].

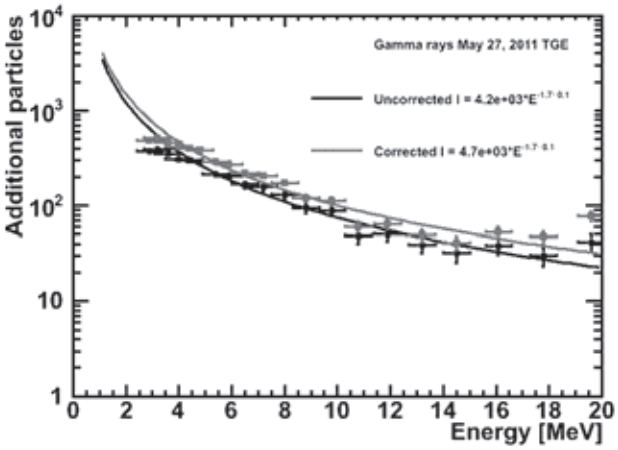

Figure 3. The gamma ray energy spectra of the NaI detector,

REFERENCES

[1] Wilson,C.T.R., Proc. R. Soc., London, A92, 555, 1916.

[2] Torii, T. et al., J. Geophys. Res., 107, 4324, 2002.

[3] Torii, T., et al., Geophys. Res. Lett., 36, L13804, 2009.

[4] Lidvansky, A. S. and Khaerdinov, N. S., Izvestiya Rossiiskoi Akademii Nauk. Seriya Fizicheskaya 73, 418, 2009.

[5] Gurevich, A. V. et al., Physics Letters A, 373, 3550, 2009.

[6] Tsuchiya, H., et al., J. Geophys. Res., 116, D09113, 2011.

[7] Torii, T., et al., Geophys. Res. Lett., 38, L24801, 2011

[8] Chilingarian, A., et al., Nucl. Inst. and Methods in Phys. Res. Sect A, 543, 483, 2005.

[9] Chilingarian, A., et al., Phys. Rev. D, 82, 043009, 2010.
[10] Gurevich, A. V., et al., Phys. Lett. A, 165, 463, 1992.
[11] Dwyer, J. R., Phys. Plasmas 14, 042901, 2007.
[12] Carlson, B. et al., J. Geophys. Res.Lett., 34, L08809, 2008.
[13] Lehtinen, N. G. et al., J. Geophys. Res., 104, 24699, 1999.
[14] Dwyer, J. R., Geophys. Res. Lett., 31, L12102, 2004.
[15] Chilingarian, A., Mailyan, B. and Vanyan, L., Atmospheric research, 114–115, 1–16, 2012.

Simulations of the Secondary Cosmic Ray Propagation in the Thunderstorm Atmospheres Resulting in the Thunderstorm Ground Enhancements (TGEs)

A. Chilingarian, L. Vanyan

Abstract. GEANT4 simulations of the propagation of electrons in the thunderstorm atmospheres were performed to explain the Thunderstorm Ground Enhancements (TGEs), detected by the particle detectors of the Aragats Space Environmental Center (ASEC) operating at altitude 3200 m on the slopes of Mt. Aragats in Armenia. The charged particle propagation and multiplication processes were simulated in the uniform electric fields of different strengths and elongation. The Gamma ray, electron and neutron energy spectra were obtained on the exit of the electric field and beneath. Simulation results prove existence of 2 mechanisms of particle enhancements, first connected with electron – gamma ray avalanche process; and the second – with modification of energy spectra of particles in the strong electric fields of the thunderclouds. The avalanche process can multiply the number of electrons and gamma rays by several orders of magnitude well above the cosmic ray background in the energy range up to 40 MeV; the energy spectra modifications lead to a few percent enhancements in the energy range up to 100 MeV, as well as to the depletion of the high-energy muon flux. Consequently the energy spectra at low energy are better fitted by an exponential law; at high energies – by the power law.

1. INTRODUCTION:

Creation of a detailed model to explain the TGE events is hampered by unknown strength and structure of the electric field in the thunderclouds. The location and time evolution of the charged layers in the thundercloud (sources of electric field) is very poor studied domain due to missing of suitable and reliable experimental techniques. In these circumstances the experimentation with the computer models of the propagation of radiation through thunderstorm atmosphere is only available method for developing of the quantitative models of TGE events. The theoretical knowledge on the acceleration of electrons in the atmospheric electric fields as well as interactions of electrons, gamma rays and neutrons with atmosphere nuclei and molecules are well established and simulated in the applied program packages [1]. The limits on possible values and elongations of electric fields are known from registered soundings of balloons launched during thunderstorms [2] and from theoretical limits [3]. The density and energy spectra of populations of cosmic rays (CR) electrons at different altitudes in the atmosphere are also very well measured in last century. Therefore, by computer experiments, assuming plausible values of strength and structure of electric field we get valuable information to be compared with experimental results. One of the first simulations [4] was performed to explain a rocket-triggered lightning experiment. From simulation experiments of Relativistic Runaway Electron Avalanche (RREA, [5], also referred as Runaway breakdown, RB – process [6]) were obtained RREA electron energy spectra approximated by the exponential function. To explain the measurements of hard gamma radiation from winter thunderstorms in Japan, (Torii et al. 2004), a tripol model of thundercloud electric field was used [7] and was obtain a significant flux of secondary bremsstrahlung gamma rays from the RREA process, some portion of which was capable to reach the ground. Another simulation code [8] estimates photon energy spectra, number of photons in the source, full bremsstrahlung energy, which in the best way fit the spectra of gamma ray flux published in [9]. The shift of the energy spectrum of the electrons/positrons and negative/positive muons entering large electric field region in thunderclouds can lead to dips and peaks in time series of the count rates of surface particle detectors (see theory of meteorological effects in [10]. These effects were investigated in experimentally in [11] and [12].

2. SIMULATIONS OF THE PARTICLE PROPAGATION IN THE ELECTRIC FIELDS

We used the following approximations in our simplified model of the electrical structure of the thundercloud:

Electric field within thundercloud is uniform (no "pockets" with enhanced field, and no different layers with opposite field directions). The electric field strength of 1.8kV/cm which is greater than threshold value $E_t \approx$ 1.7kV/cm was used. The length of electric fields equals to L = 1650m, from 5000m till 3350 above the detectors located at 3200m.

As seed particles secondary Cosmic Ray (CR) electrons in the energy range of 1-300 MeV and with fixed energy 1 MeV (simulating "pure" RREA process, ~1 MeV electrons commit minimal ionization losses in the atmosphere) were used. Incident electron spectrum was estimated by EXPACS WEB-calculator, which estimates secondary cosmic ray spectra at different altitudes and latitudes (Sato, 2009).

The following interactions were considered:

For electrons and positrons – ionization, bremsstrahlung, multiple scattering;

For positrons also –annihilation;

For gamma rays– Compton scattering, conversion, photoelectric effect, photonuclear reaction.

3. ELECTRON AND GAMMA RAY ENERGY SPECTRA DERIVED FROM SIMULATIONS

To explain numerous TGEs detected at Aragats Space environmental center (ASEC, [13, 14, 15]) we implement simulations using described above simple model of the electric fields in the thundercloud. Results of the simulation are posted in Fig. 1, where we can apparently see 2 modes of particle generation. The RREA mode with maximal energy of electrons is 30-40 MeV and gamma rays - 20-30

MeV and MOS (modification of spectra) mode accelerating electrons up to 60-70 MeV; gamma ray spectrum prolonged up to 80-90 MeV. The electron and gamma ray energy spectra in the energy range 1-10 MeV demonstrate large multiplication of electrons in the RREA process and huge amplitudes of the TGEs. MOS regime is fast fading after 50 MeV and needs large surfaces of particle detectors to be measured above the background of ambient population of secondary cosmic rays.

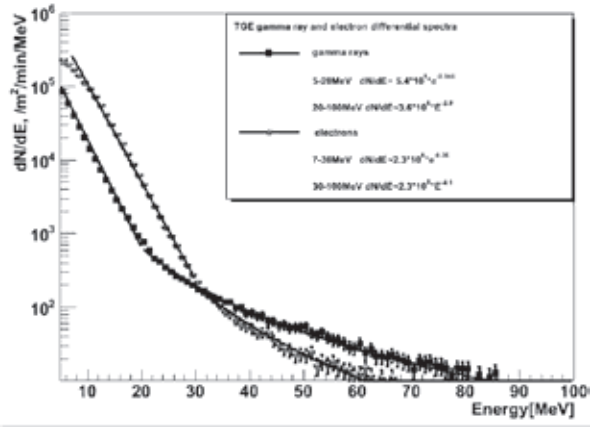

Figure 1. TGE electron and gamma ray spectra obtained from GEANT4 simulation of RREA process in electric field of 1.8 kV/cm with seed electrons 1-300 MeV.

The high-energy tail of the gamma ray spectrum is due to enhanced bremstrahlung radiation of the higher energy electrons traversing the electric field of the cloud. Because of highly enlarged radiation losses, high energy electrons cannot unleash the RREA, however, the additional flux of gamma rays radiated by these electrons can reach the mountain altitudes and be registered as small and modest enhancement over CR background.

To prove our hypothesis on 2-component origin of TGE, we perform the same simulation with a fixed flux of 1 MeV seed electrons. The shape of electron and gamma ray spectra coincides with spectra obtained with 1-300 MeV electron seeds (exponential function – reflecting the particle multiplication in the avalanche process), however there are no high energy tails, see Figure 2. Thus, pure RREA process with chosen electric field parameters cannot produce TGE electrons with energies above 30-40 MeV and gamma rays with energies above 20-30 MeV.

To prove that MOS process can provide high-energy gamma rays we perform simulations of the electron propagation in the moderate electric field below RREA initiation threshold (1.5 kV/cm). In Figure 3 we see that only modification of the energy spectra of electrons can significantly enlarge the yield of the gamma rays reaching the earth surface. Electrons attenuate in the atmosphere after exiting from the cloud; however, as we can see from Figure 3, the gamma rays survive.

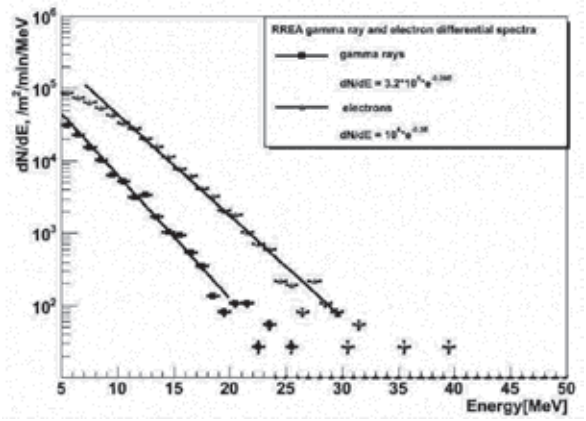

Figure 2. The electron and gamma energy spectra obtained in electric field of 1.8 kV/m prolonged from 5000 till 3400 m with 1 MeV electron as seeds.

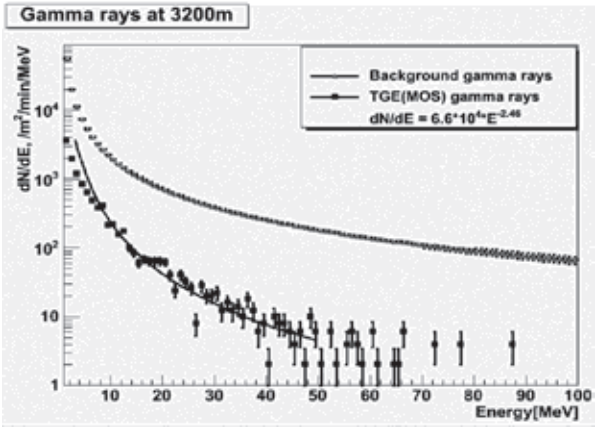

Figure 3. Comparison of background gamma ray spectrum with the surplus gamma ray spectrum generated by electrons accelerated in the field of strength 1.5 kV/m below the critical field for the RREA initiation; the background cosmic ray gamma ray flux and TGE gamma ray flux are calculated at 3200 m altitude after exiting from the uniform electric field at 3350 m altitude

4. CONCLUSION

Our simulations supports 2 component model of the TGE origin: the RRRE avalanches in energy domain up to 30-40 MeV and Modification Of energy Spectra (MOS) process operating on all energy scales and providing extension of TGE gamma ray energy spectra up to 100 MeV. The RREA process can multiply particle flux up to 10 times above ambient background of secondary cosmic rays; the MOS process can provide several percentage excess above cosmic rays, however for the much higher energies.

REFERENCES

[1] Agostinelli, S., et al. Nucl. Instrum. Methods Phys. Res., Sect. A, 506(3), 250–303, 2003.

[2] Marshall, T. C., et al., Geophys. Res. Lett., 32, L03813, 2005.

[3] Dwyer J.R., Geophys. Res. Lett., 30(20), 2055, 2003.

[4] Dwyer, J. R., Geophys. Res. Lett., 31, L12102, 2004.

[5] Babich, L. P., et al, Phys. Lett. A, 245, 460–470,1998.
[6] Gurevich, A. V., et al., Phys. Lett. A, 165**,** 463, 1992.
[7] Torii, T., et al., J. Geophys. Res. 107, 4324, 2002.
[8] Babich L.P. et al., J. Geophys. Res., 115, A09317, 2010.
[9] Tsuchiya H., et al., Phys. Rev. Lett., 99, 165002, 2007,
[10] Dorman, L.I., et al., Advances in Space Research 35, 476-483, 2005.
[11] Muraki, Y., et al., Phys. Rev. D 69, 123010, 2004.
[12] Alexeenko, V. V., et al., Phys. Lett. A, 301, 299–306, 2002.
[13] Chilingarian, A., et al., Phys. Rev. D 82, 043009 (2010).
[14] Chilingarian, A. et al., Phys. Rev. D 83, 062001 (2011).
[15] Chilingarian, A. et al., Phys.Rev.D 85, 085017, (2012).

Geophysical Research Network Operating in the Aragats Space Environmental Center

A. Reymers, S. Chilingarian

Abstract. In the Aragats Space Environmental center (ASEC) operate hundreds of measuring channels detecting the changing fluxes of secondary cosmic rays and geophysical parameters, including magnetic and electrical fields, low and high frequency radio emissions, lightning intensity. We also plan to measure the height and structure of thunderclouds and electrical field inside; provide optical monitoring of the transient luminous events. The network of the particle detectors and field meters is rather large including several locations out of Armenia. The created scientific infrastructure is intended for the research of the solar modulation effects, high-energy atmospheric events and for issuing warnings and alerts on the violent consequences of solar eruptions and catastrophic meteorological events. Information from all measuring channels should be assessable on-line in fast and user-friendly fashion. Also forecast and now cast of the events under development requires fast joint analysis of the multivariate information and decision making on the level of risks. We present the structure and operation characteristics of the ASEC as well as MySQL databases and mirror sites, as well as software support codes for solving this problem.

1. INTRODUCTION

Geophysical research network of the Aragats Space-Environmental Center (ASEC) (‘[1]’) provides monitoring of different species of secondary cosmic rays and geophysical parameters. ASEC network monitors located at two high altitude stations on Mt. Aragats in Armenia and Yerevan headquarters of Cosmic Ray Division (CRD) of A. Alikhanian National Laboratory.

First research station, Aragats, located at 3200m altitude, geographic coordinates 40°28'N, 44°10'E. Second station is Nor-Amberd, altitude 2000m and geographic coordinates 40°22'N, 44°15'E. The third observation altitude is1000m, Yerevan headquarters of CRD; geographic coordinates 40°11'N, 44°31'E. Geomagnetic cutoff rigidity ~7.1 GV for allocations. At these 3 destinations different types of particle detectors are continuously measure the intensity of the secondary cosmic ray fluxes; one second and one minute time series of all ASEC channels are available from the CRD web page (http://adei.crd.yerphi.am) in real time.

Also ASEC manage Space Environmental Viewing and Analyses Network (SEVAN) monitors (‘[2]’). At this moment SEVAN network consist of 7 monitors, 4 of them installed in the Armenia, 3 other in Bulgaria (Mt. Musala 42°10'45"N, 23°35'8"E, 2925m asl), Croatia (Zagreb, 45°49'7"N, 15°58'30"E, 160m asl), and India, New Delhi (Jawaharlal Nehru University, 28°32'26"N, 077°09'46"E, 258m asl).

Since Jun 2009 we start to measure geomagnetic field at Nor-Amberd research station; in 2010 September geomagnetic measurements also started at Aragats research station. Since August 2010 we measure near surface atmospheric electric field, 4 types lightning occurrences at Aragats station. Later we establish the same instruments (Boltek EFM100 and Boltek Storm Tracker) in Yerevan and Nor Amberd. In 2011 also started measure weather parameters by the Vantage Pro2 weather station.

2. MONITORS OF THE ASEC

ASEC operates since 2012 13 monitors at Aragats station. Number of physical channels (each monitor comprises from multiple sensors) at Aragats station is 197. Number of software channels (various logical combinations of monitor channels) which are available online in our home page is 579. In Nor-Amberd station we have 7 monitors. Also near to Nor-Amberd, in Burakan we have 2 monitors. Number of physical channels is 58. Number of software channels number is 383. In Yerevan located only 5 monitors. Number of physical channels is 14. Number of software channels is 79.

Several particle monitors measure not only second or minute counts of incident particle, but also energy release spectra in the thick plastic scintillator and NaI crystals. According to chosen trigger conditions data for various experiments are continuously collected. For instance one of, so called, selected events consists in registering horizontal muon flux, within 1 degree. Another “event” consists in selecting short bursts of electrons incident on 1000 m^2 area 50 microseconds. After multiyear operation this kind of information will be analyzed and published. This type of data we do not share in the web.

Each monitor at the station has its own Data acquisition (DAQ) electronics and on-line PC. Electrical pulses from the monitor channels are digitized and stored. At the stage of analyses we could obtain any combination of count rates. Along with count rate of the particles per second detected in each channel we can obtain count rate of the any coincidences between different channels. For instance, we can organize veto trigger to measure neutral fluxes from the thick scintillators fully covered by thin ones. After obtaining all type of interested count rates electronic device send information to local PC. Local PC could also generate additional software channels and store information and share it in local network. Different monitors have different DAQ electronics and PCs with different operating system. Some of them share information by http, some of them - by ssh.

DAQ electronic developed at CRD has also its own data acquisition system (Advanced Data Acquisition System - ADAS). By the ADAS software PCs communicate with electronics, download data from it and share data in the network. Also, by ADAS it is possible to control parameters of the electronics (for instance - thresholds of particle detectors). By the http protocols it is

possible to download data from the PC in different formats (XML, CSV, TXT).

At this moment, geophysical research network consist from 30 monitors, 338 physical channels and 1059 software channels. Daily size of the data, which we are collecting from the geophysical network monitors, approximately equal to 5GB.

3. NETWORK ORGANIZATION

ASEC geophysical research network physically could be divided in 4 sections. Aragats research station, Nor-Amberd research station, Yerevan headquarters of CRD and SEVAN monitors located outside of Armenia. Main servers of CRD located at Yerevan headquarters.

Doubled wireless connection between Yerevan and Aragats, Yerevan and Nor-Amberd provide stable and reliable connections with stations. Now we have 11Mb/s link between Yerevan and research stations. Around 60 hosts (PCs, servers, wireless bridges, routers etc.) are in the ASEC network. The Nagios Core software (http://nagios.org) controls operation of all these devices. .

On each station we have local file server, to which connected GPS antenna and this file server works also as NTP server to synchronize all on-line PCs. In Yerevan SyncServer S250 GPS Network Time Server provides ultra-precise time even if GPS antenna loses signals from the satellites. Station file server downloads data from the on-line PCs in real time, store and share this data in local network. Also station file server download data from other station file servers. It was done to have copy of all our data in all file servers. At this moment we have 3 File Servers, at Aragats, Nor-Amberd and Yerevan. File servers store data in raw format without any changes. File servers shares data by http protocol. They are available by the web browser. The final storage place of our data is MySQL database. Usage of MySQL facilitates software developments for data analysis. To increase access speed to MySQL database, we use MySQL database on separate server. Also we use separate server (we called it application server) to run scripts, which are working with MySQL and file servers. Application server takes data from the File Server and fills this data to MySQL server. Also application server takes data from MySQL server and sends it to mirrors. Filtration and correction of the data also are doing by Application server.

4. ADEI

Advanced Data Extraction Infrastructure (ADEI) has been developed to provide data exploration capabilities to a broad range of physical experiments dealing with time series. ADEI shares our data in the Internet. You can connect to ADEI server by the web browser and very quickly make a plot of our data for any time window. After that you can download selected data in different formats. The web address of this server is http://adei.crd.yerphi.am . To provide such broad coverage ADEI utilizes highly modular architecture. The system consists of backend and frontend parts communicating over HTTP protocol using Asynchronous JavaScript and XML (AJAX) approach (‘[3]’). The ADEI backend defines few abstract interfaces which are used to implement various capabilities using simple plugins. The data sources are interfaced with dedicated drivers implemented data access abstraction layer. The higher levels of system are relaying on this abstract interface to get data in a uniform way from arbitrary storage. ADEI web frontend is inspired by Google Maps interface. The navigation through the data is feasible using mouse only. Single or multiple time series are plotted using the data from currently selected time interval. Then, the plot could be dragged and zoomed over time and value axes. Detailed information is provided about the graphics around mouse pointer. The region of plot may be selected and exported in one of supported formats. ADEI is licensed under GNU General Public License and uses only free open source technologies. It is currently implemented at Aragats Space Environmental Center to providing data access (‘[4]’), (‘[5]’).

In Fig. 1 we post an example of the ADEI interface. To check the possibility to detect the neutrons from lightnings we turn the Aragats neutron monitor (ANM) to one-second data-recording regime. To see if there are coincidences with lightning occurrences we correlate ANM time series with one-second near surface electrical field data. In the Fig.1we see 2 abrupt increases of the near-surface electrical field, which could be attributed to the lightning occurrences. In the same second we detect abrupt increase of the “bare”[3] proportional counter and other 18 counters of ANM. Proportional counter is made from 2 m long and 15 cm diameter iron tube that is excellent antenna. In spite of grounding when lightning hits nearby all channels of neutron monitor register inference signals due to extremely powerful radio pulses from lightning bolt, as we see in the Fig. 1.

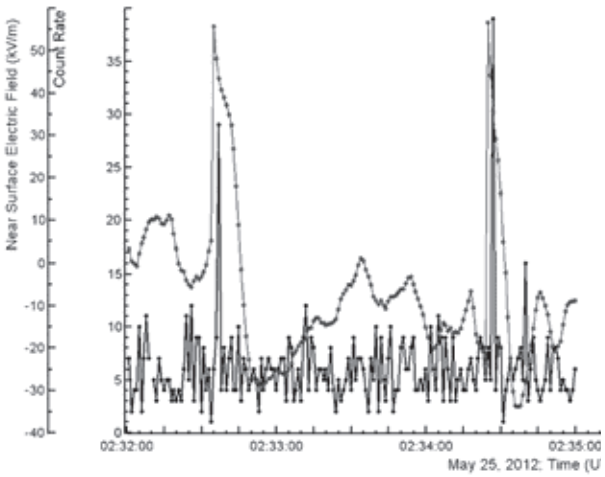

Figure 1. One second time series of near surface electric field (blue) and counts of the “bare” proportional counter located on the Aragats neutron monitor (black).

REFERENCES

[1] A. Chilingarian, K. Arakelyan, K. Avakyan et al. 2005 Nucl. Inst. Meth. D A543 483–496

[3] Bare proportional counter of the same type as used for the ANM (HC-15) is sensitive only to thermal (0.01 – 1 eV) neutrons. The same counter surrounded by lead producer and polyethylene moderator is sensitive to MeV-GeV neutrons.

[2] A. Chilingarian, G. Hovsepyan, K. Arakelyan, et al; Earth, Moon and Planets: Volume 104, Issue 1 (2009), page 195
[3] Brett McLaughlin 2005 Mastering ajax URL http://www.ibm.com/developerworks/web/library/wa-ajaxintro1.html.
[4] A. Chilingarian, K. Avakyan, V. Babayan et al. 2003 J. of Phys. G 29 939–951
[5] S. Chilingaryan, A. Beglarian, A. Kopmann and S. Vöcking:2010 J. Phys.: Conf. Ser. 219 042034

Magnetometric Measurements at Mt. Aragats

T. Karapetyan

Abstract. Magnetometric station LEMI-018, and LEMI-417 commissioned by the Lviv center of Space Research Institute of Ukrainian Academy of Science, have been installed on slopes mountain Aragats (Armenia) at heights 2000 and 3200m above sea level. Operation of magnetometric station started on July 2009 and 2011 accordingly. LEMI-417 is measuring also components of the electric field. One-second time series of the 3-dimensional measurements of the geomagnetic field enter the database of the Aragats Space Environmental Center (ASEC). This information can highly improve the research of correlations of the geomagnetic field, changes of the fluxes of secondary cosmic rays measured by ASEC monitors with parameters of the solar wind and interplanetary magnetic field (IMF) measured by facilities on board space station located 1.5 million km from Earth. Measurements of geomagnetic field at Nor Amberd (2000m) and Aragats (3200m) research stations of A.Alikhanyan national lab will support forewarning of the upcoming major geomagnetic storms. We present the detection of the first geomagnetic storms of the 24 solar activity cycle detected by new installed magnetometric stations.

1. INTRODUCTION

Interplanetary coronal mass ejections (ICMEs) are known as major drivers of severe space weather conditions when arriving at the Earth. On their way to Earth, ICMEs also ‘‘modulate’’ the flux of galactic cosmic rays (GCRs) introducing anisotropy and changing the energy (rigidity) spectra. These anisotropies of GCRs manifested themselves as peaks and deeps in time series of secondary cosmic rays, detected by surface particle detectors. Presence of a strong and long-duration southward magnetic field component in the sheath region of ICMEs is the primary requirement for their geoeffectiveness [1, and references therein]. The size and magnetic field strength of ICMEs are correlated with the ICME modulation effects on the energy spectra and the direction of GCRs [2]. Therefore, simultaneous measurements of the particle fluxes and disturbances of magnetic field will allow better understanding solar modulation processes and helping to build the model of solar-terrestrial connections. Facilities of the Aragats Space Environment Center (ASEC) [3] observe charged and neutral fluxes of secondary cosmic rays by the variety of particle detectors located in Yerevan and on slopes of Mount Aragats at altitudes 1000, 2000 and 3200 m. ASEC detectors measure particle fluxes with different energy thresholds starting from 2 MeV and register solar modulation effects in wide range of secondary particle energies and types. We present results of detected geomagnetic storms by new magnetometric stations operated on slopes of Mt. Aragats and also comparisons of Nor Amberd and Aragats magnetometers data with LVIV, Furstenfeldbruck, and Novosibirsk magnetometers as well as with geomagnetic Dst index.

2. THE MAIN TECHNICAL PARAMETERS OF MAGNETOMETER LEMI -018 AND LEMI-417

In Table 1 are shown the main technical parameters of magnetometer LEMI-018 and LEMI-417. LEMI-417 magnetotelluric station has the same main technical parameters of measuring magnetic field as LEMI-01.

Table 1. Main technical parameters of magnetometer LEMI-018

Measured range of total magnetic field	± 65000 nT
Resolution along each component both at the display and registered into the internal FLASH-memory	0.01 nT
Temperature drift	<0.2 nT/°C
Frequency band	DC-0.3 Hz
Magnetometer output noise in frequency band(0.03…0.3)Hz	< 10 pT rms
Magnetic sensor components orthogonality error	<30 min of arc
Automated offset compensation band along each magnetic component	65000 nT
Noise of electric meter in the frequency band 0.03 – 0.3Hz	<0.5 μV rms
Sample rate (LEMI018)	1.2. 4. 10. 60 sec
Volume of the internal FLASH-memory	Up to 2 GB
Digital output	RS-232
GPS timing and coordinates determination	
Operating temperature range	Minus 10 to +50°C
Temperature sensors (both in magnetic sensor and electronic units) resolution	0.1 °C
Power supply	9…12 V
Power consumption	<0.7 W

3. OBSERVATIONS

Active sunspot 1401 erupted in Jan. 19th, on 2012 between 15:15 and 16:30 UT. The long-duration blast produced an M3-class solar flare and a CME heading towards Earth (http://spaceweather.com). At Jan. 22thhas been registered geomagnetic storm, see Figures 1-3, where we present 1-second time series of geomagnetic field components measurements in Nor Amberd (Armenia), LVIV (Ukraine), Furstenfeldbruck (Germany), Novosibirsk (Russia). Data of Lviv, Furstenfeldbruck, Novosibirsk, stations were taken from web pageof International Real-time Magnetic Observatory Network(intermagnet.org). In Figure 4 we present comparisons of Nor Amberd magnetometer 1-hour measurements, Dst index calculated by Kyoto data center and Bz component of magnetic field of CME measured by ACE magnetometer. As we can see in figures our data are in good agreement with others.

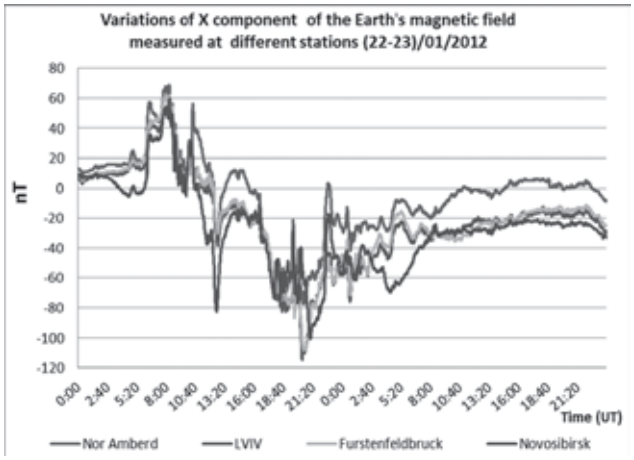

Figure 1. One second data comparison of X component of the Earth's magnetic field of Nor Amberd, Lviv, Furstenfeldbruck, and Novosibirsk magnetometers

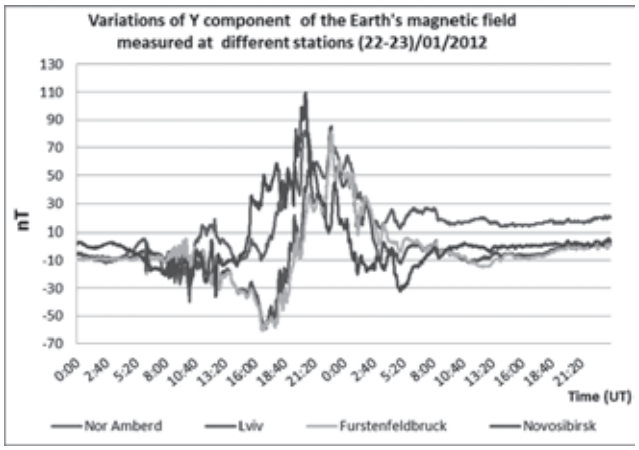

Figure 2. One second data comparison of Y component of the Earth's magnetic field of Nor Amberd, Lviv, Furstenfeldbruck, and Novosibirsk magnetometers

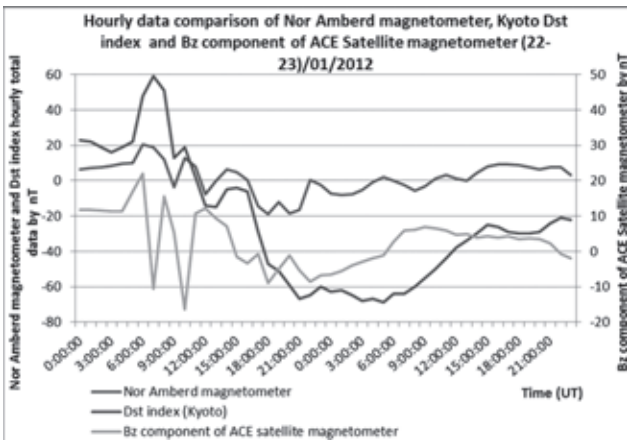

Figure 3. One second data comparison of Z component of the Earth's magnetic field of Nor Amberd, LVIV, Furstenfeldbruck, Novosibirsk magnetometers

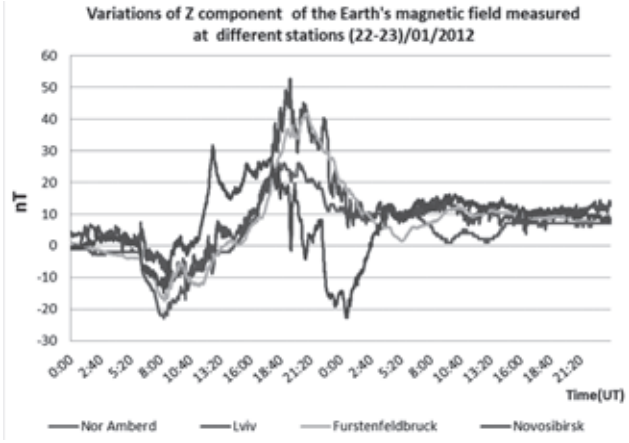

Figure 4. Hourly total magnetic field data comparison of Nor Amberd magnetometer, Dst index of Kyoto and Bz component of ACE satellite magnetometer.

4. CONCLUSION

For the first time we present geomagnetic field measurements on the slope of mountain Aragats. The comparison of data from new installed magnetometers in January and March 2012 during strong solar activity with data from Lviv, Furstenfeldbruck, Novosibirsk magnetometers as well as with geomagnetic Dst index proves relevance and applicability of new devices for global research of solar-terrestrial connections.

REFERENCES

[1] Valtonen, E. In "Solar Eruptions and Energetic Particle", Geophys. Monogr. Ser., vol. 165, ed. by N. Gopalswamy, R. Mewaldt, and J. Torsti, pp. 335– 344, AGU, Washington, DC, 2007.

[2] Chilingarian A. and Bostanjyan N. 2009, Journal of geophysical research, VOL. 114, A09107,

[3] Chilingarian, A., et al., Nucl. Inst. and Methods in Phys. Res. Sect A, 543, 483, 2005.

NaI Detector Network at Aragats

K. Avakyan, K. Arakelyan, A. Chilingarian, A. Daryan, L. Kozliner, B. Mailyan, G. Hovsepyan, D. Pokhsraryan, D. Sargsyan

Abstract The Aragats Space Environmental Center (ASEC) [1] provides monitoring of different species of secondary cosmic rays and consists of two high altitude research stations on Mt. Aragats in Armenia. Energy spectra and correlations between fluxes of different particles, measured on Earth's surface address the important issues of the solar modulation effects and the atmospheric high-energy phenomena. Along with solar modulation effects, ASEC detectors register several coherent enhancements associated with thunderstorm activity. The experimental techniques used allowed for the first time to simultaneously measure changing fluxes of the electrons, muons, gamma rays, and neutrons correlated with thunderstorm activity [2,3]. Ground-based observations with a complex of surface particle detectors, measuring in systematic and repeatable fashion, gamma quanta, electrons, muons and neutrons from atmospheric sources are necessary for proving the theory of particle acceleration and multiplication during thunderstorms. Established on May 26 2011, network of 5 NaI(Tl) (thallium-doped sodium iodide) scintillation detectors in the new ASEC laboratory on Aragats is of great importance for the investigation of thunderstorm phenomena because NaI(Tl) detectors have a higher efficiency of gamma ray detection comparing with plastic ones.

1. NETWORK DESIGN

The NaI network consists of 5 NaI crystal scintillators of size 12.5 x 12.5 x 30 cm and plastic one of the same shape; the plastic scintillator is installed for comparison purposes. The scheme of detector and detector distribution in the network are presented in Figs.1 and 2 respectively. The NaI crystal is placed into sealed aluminium (1 mm thick) housing (because the crystal is hygroscopic) with transparent window attached to the photo-cathode of the photomultiplier tube (PM).

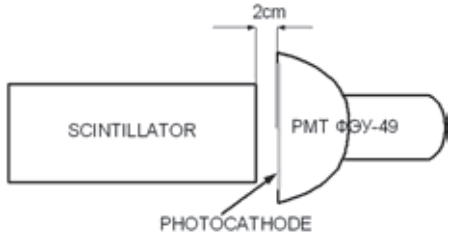

Figure 1. NaI(Tl) and PM assembly

The PM-49 type PM has large photocathode (15 cm diameter) and therefore provides good light collecting. Spectral sensitivity range of PM-49 is 300-850 nm, that covers the spectrum of NaI(Tl) emission light.

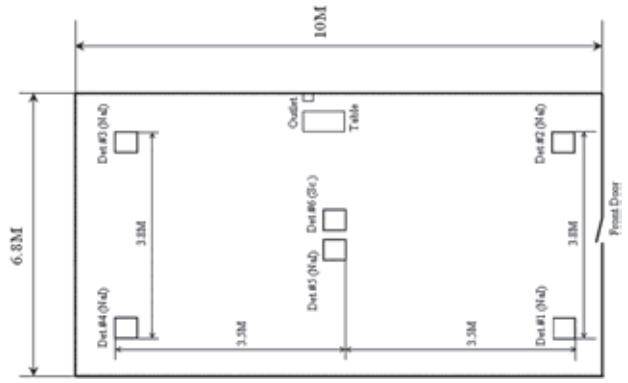

Figure 2. Disposition of NaI & plastic scintillation detectors at Aragats Cosmic Ray Station

2. DETECTOR RESPONSE SIMULATION

Calculation of the detector response to the secondary cosmic ray flux has been carried out with "EXPACS" cosmic ray flux WEB calculator [4] and "GEANT3" code. All particle fluxes providing considerable contribution to the detector counts was taken into account in simulation. Obtained registration efficiencies are plotted in the Fig. 3. Simulations demonstrate that efficiency of the NaI exceeds that of the plastic one 3 – 4 times in the energy range 3 -100 MeV.

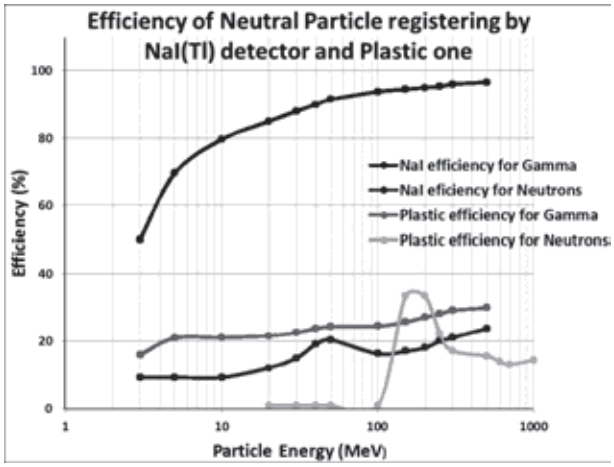

Figure 3. Registration efficiency of NaI crystal and plastic scintillator

3. 27 MAY OF 2011 THUNDER GROUND ENHANCEMENT (TGE) EVENT AT ARAGATS MOUNTAIN.

Just after installing NAI network, on 27 May 2011 a Thunderstorm Ground enhancement (TGE) was observed at Aragats. The maximum of enhancement was at 13:13 UT. In Fig. 4 we can see that the TGE amplitude is much larger for NaI crystals comparing with plastic scintillator.

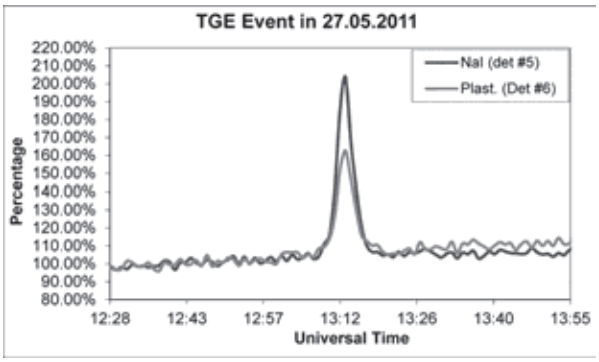

Figure 4. TGE event detected by NaI and plastic scintillator

On 26 May, 2012 very interesting TGE was detected by ASEC particle detectors on Aragats. In Figs. 5 and 6 we post the one-minute time series of several ASEC particle detectors sensitive to neutral flux (Fig. 5) and charged flux (Fig. 6). Also the one-second time series of near-surface electric field are posted in both Figures.[4]

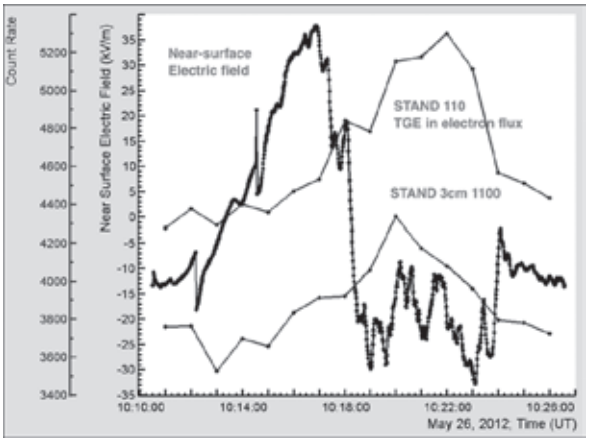

Figure 5. During positive near-surface electrical field ASEC detectors sensitive to gamma rays detected ~20% TGE with absolutely identical shape peaking at 10:17

The NaI crystals and inner 20 cm thick plastic scintillators of Cube detector, fully surrounded by the 1-cm thick veto scintillators, also r5egistered gamma ray flux with deeply suppressed charged flux. As we see in Figure 5 both detectors demonstrate identical time history of TGE detection, peaking at 10:17 UT. After field reversal the particle detectors sensitive to charged flux and insensitive to gamma rays; namely "110" combination of the STAND 1 cm detector and "1100"[5] combination of STAND 3 cm detector, register ~ 25% TGE mostly in electron flux, see Fig. 6. During positive near surface electric field and, expected negative electric field in thundercloud electrons cannot be accelerated in direction to earth and only gamma rays can reach detectors. During negative near-surface electrical field electrons are accelerated downwards and along with gamma rays can be detected by surface particle detectors.

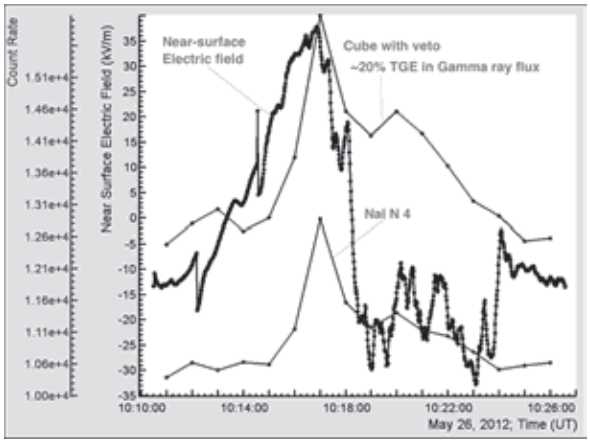

Figure 6. During negative near-surface electrical field ASEC detectors sensitive to charged particles detect ~25% TGE, peaking at 10:20-10:22

4. CONCLUSION

New detector network is taking data 24 hours a day, detecting high energy phenomena in atmosphere and solar modulation effects: efficiency of detecting gamma rays is ~4 times larger than that of plastic scintillators. Detection of TGE events in 2011 and 2012 proves high efficiency and reliability of the NaI crystal network.

REFERENCES

[1] Chilingarian, A. et al., Nucl. Instrum. & Methods, Phys. Res., Sect. A 543, 483 (2005).
[2] Chilingarian, A., et al., Phys. Rev. D 82, 043009 (2010).
[3] Chilingarian, A. et al., Phys. Rev. D 83, 062001 (2011).
[4] EXPACS ver2.17 http://phits.jaea.go.jp/expacs/)

[4] The Boltek firm EFM-100 electrical mill is continuously monitoring monitored the near-surface electrical field at Aragats.
[5] Stand detectors comprise from stacked horizontally 1 and 3 cm thick plastic scintillators. Count rates of all combinations of scintillator hits are registered and stored. Combinations 110 and 1100 denote the situation when signals come only from 2 upper scintillators. The probability that gamma ray initiate these combinations is veru low.

New Low Threshold Detectors for Measuring Electron and Gamma Ray Fluxes from Thunderclouds

K. Arakelyan, K. Avakyan, A. Chilingarian, A. Daryan, L. Kozliner, G. Hovsepyan, L. Melkumyan, D. Pokhsraryan, D. Sargsyan

Abstract. Space Environmental Viewing and Analysis Network is a worldwide network of identical particle detectors located at middle and low latitudes aimed to improve fundamental research of space weather conditions and to provide short- and long-term forecasts of the dangerous consequences of space storms. SEVAN detected changing fluxes of different species of secondary cosmic rays at different altitudes and latitudes, thus turning SEVAN into a powerful integrated device used to explore solar modulation effects. Till to now the SEVAN modules are installed at Aragats Space Environmental Centre in Armenia (3 units at altitudes 800, 2000 and 3200 m a.s.l.), Bulgaria (Moussala), Croatia and India (New-Delhi JNU.) and now under installation in Slovakia, LomnitskySchtit). Recently SEVAN detectors were used for research of new high-energy phenomena originated in terrestrial atmosphere – Thunderstorm Ground Enhancements (TGEs). In 2011 first joint measurements of solar modulation effects were performed by SEVAN network, now under analysis.

1. DESIGN OF THE STAND STACKED DETECTOR

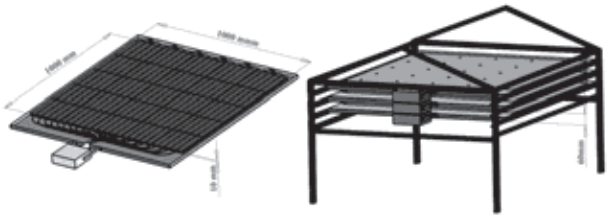

Figure 1. Stand assembly and design of 1 cm thick molded plastic scintillator with optical spectrum-shifter fibers; details of detector construction see in [2].

"STAND" detector comprise of three-layer assembly of 1 cm thick 1 m2 sensitive area molded plastic scintillators one above the other and one 3 cm thick scintillator located aside (Figure 1). Detector operates in particle counter regime[6]. Outdoors location, 1-cm thickness and three-layer design allow to measure flux of TGE electrons with 3 different energy thresholds starting from 1.5 MeV and to recover integral spectrum of TGE electrons. Light from scintillator by optical spectrum-shifter fibers is reradiated to the long-wavelength region and passed to the FEU-115M type photomultiplier (PM). Maximum of luminescence is on about 420nm wavelength and luminescence time is about 2.3 ns (http://www.ihep.su/). The tuning of STAND detector consists in selections of PM high voltage and discrimination threshold. The threshold should be chosen to guarantee both high efficiency of signal detection and maximal suppression of noise. Tuning of STAND was made by means of the 8-channel signal analyzer developed in CRD for online experimental data processing in real time [1]. Proper tuning of the detector provides 98-99% signal detection efficiency simultaneously suppressing electronic noise down to 1-2%. The SEVAN DAQ along with separate channel counts is measuring and storing all coincidences of the detector channels. Coincidence "111" means that all 3 layers register particle, minimal energy of charged particles giving signal in all 3 layers should be ~10 MeV; coincidence "100" means that only upper detector register particle – we estimate the minimal energy of this coincidence to be ~1.5 MeV. The energy threshold of 3cm thick scintillators is ~5MeV.

2. CUBE SCINTILLATOR ASSEMBLY DESIGN

The CUBE assembly (Figure 2) consists of two 20cm thick scintillation detectors of 0.25 m2 area each surrounded by 1cm thick 1 m2 area scintillators. This design ensures that no particle can hit the inside 20cm detectors without passing through at least one of 1cm scintillators.

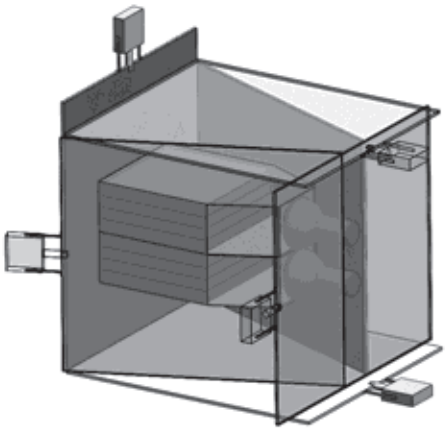

Figure 2. CUBE assembly design.

The 20cm thick plastic scintillator with 0.25 sq. meter area is overviewed by the photomultiplier (PM) ФЭУ-49 with large cathode, operating in low-noise operation mode. Surrounding detectors (6 units) are 1 cm thick molded plastic scintillators fabricated in High Energy Institute of Russian academy of sciences.

The efficiency of neutral component detection by 1cm scintillators calculated by Monte-Carlo simulation is ~2% and weakly depends on energy of gamma ray. The energy deposit of passing muons in 20 cm thick plastic scintillator is ~40 MeV. Taking into account construction material of detector (2 mm plastic and 1 cm thick scintillator above, detection threshold is estimated to be about 9 MeV. The

[6] 4-layered 3 cm thick version of STAND also measures 1-minute histograms of the energy deposit

efficiency of gamma ray detection by 20 cm thick scintillator was calculated by GEANT3 code, in the range 10 - 120 MeV. Obtained efficiency of gamma ray registration equals ~30% and weakly depends on energy. Efficiency of neutron detection in the range 4-100 MeV, in 20 cm thick scintillator is ~27%. CUBE assembly has been tested in Yerevan at 1000 m. a.s.l. and in 2010 installed at high altitude "Aragats" research station (3200 m a.s.l.). It has been included into Aragats Space Environmental Center (ASEC, [3]) since September 15, 2010; the on-line time series are available from the CRD portal: http://adei.crd.yerphi.am/adei/.

3. TGE EVENT AT OCTOBER 4, 2010.

ASEC particle detectors have recorded a huge TGE event in October 4, 2010 [4]. The count rate enhancement at maximum minute (18:23 UT) amounts to 232%, 229% and 190% for top, middle and bottom STAND layers respectively (Fig. 3). The total number of additional particles registered in that minute was 103873, 111941 and 73279 accordingly. The total number of TGE particles registered in the 3cm detector amounts to 91200 that is 267% enhancement. The enhancement varies in layers of STAND due to difference in energy thresholds.

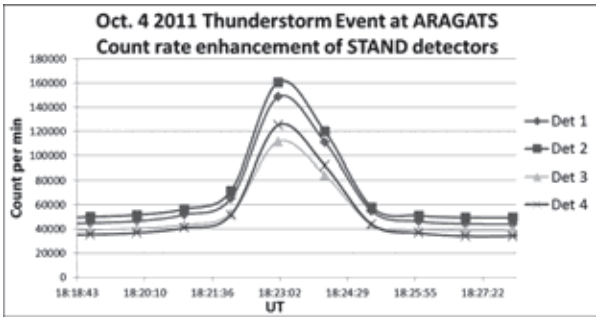

Figure 3. Count rate enhancements for STAND assembly's detectors.

CUBE count rate enhancement at maximum minute (18:23 UT) amounts to 390% and 304% for detectors #7 and #8 respectively (Figure 4). Lower count rate of bottom detector is connected with additional matter above it, which causes attenuation of the gamma ray flux. Number of TGE particles detected by upper thick scintillator (detector surface 0.25 m^2, see Figure 19) at 18:23, 4 October 2010 was N (20cm) = 43,439 with veto and N^v(20 cm) = 44,956 without veto, the difference is $N - N^v = 1517$. By these counts we recover the flux (number of particles per m^2 per minute) of gamma rays n_g above the detector (see details in [5]) by solving the inverse problem of cosmic rays:

$dE/dn = 5.4e+07 * \exp(-0.25*E)$ for the energy range of 5-10 MeV;

$dE/dn = 1.93e+08 * E^{-3.3}$ for the energy range of 10-50MeV.

The energy spectrum of gamma rays obtained by the Cube detector was used to calculate the detector response of the STAND detector. In Table 1 we compare the measured at 18:23 4 October 2010 coincidences statistics with simulated detector response on reconstructed by Cube gamma ray energy spectrum.

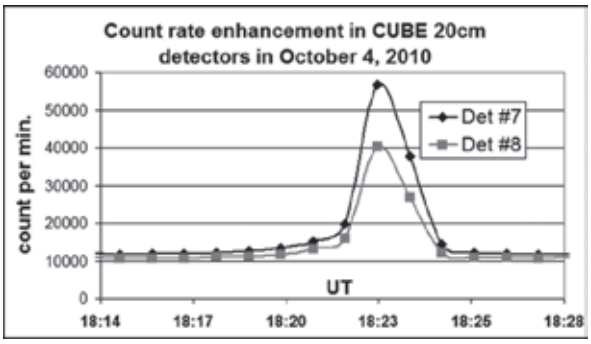

Figure 4. Count rate enhancement of Cube inner scintillators; October 4, 2010.

Table 1. Measured and simulated STAND statistics; 18:23, 4 October 2010.

	100	110	111
Experiment	95025	7366	1836
Simulated gamma rays	62832	3929	1377
Simulated electrons	32193	3437	459

Rather good coincidence of the sum of simulated electrons and gamma rays with measured particle confirms that used gamma ray energy spectrum is valid. Furthermore, by the electron fraction of the total counts we can recover integral spectrum of the TGE electrons.

4. CONCLUSION

Cube and STAND type detectors are precisely suited for the TGE research, measuring separately fluxes of electrons and gamma rays with rather low energy threshold. Same type detectors are operating now also in Yerevan (Cube with 3 cm thick) and a 3 cm thick STAND at Aragats, a vertically stacked assembly of the four 3 cm thick molded plastic scintillators with optical guided light-shifters. New ASEC detector has rich possibilities to detect charged and neutral cosmic ray flux. Measured and stored statistics of 4 layered coincidences of scintillator operation will be used to check and confirm the fraction of gamma rays and electrons in TGE; as well as to estimate with high precision the integral energy spectrum of the TGE electrons in energy range from 2 till 30 MeV.

REFERENCES

[1] Arakelyan, K., et al, Proc.FORGES 2008, pp 105-116, Tigran Mets, (2008).

[2] Britvich, G., et al. Instrum. Exp. Tech., 45:664-676, (2002).

[3] Chilingarian, A. et al., Nucl. Instrum. & Methods, Phys. Res., Sect. A 543, 483 (2005).

[4] Chilingarian, A. et al., Phys. Rev. D 83, 062001 (2011).

[5] Chilingarian, A., et al., Atmos. Res. (2012), doi:10.1016/j.atmosres.2012.05.008

Space Environmental Viewing and Analysis Network (SEVAN) – Characteristics and First Operation Results

A. Chilingarian, K. Avakyan, K. Arakelyan, N. Bostanjyan, S. Chilingarian, L. Kozliner, D. Pokhsraryan, D. Sargsyan, A. Reymers

Abstract. Space Environmental Viewing and Analysis Network is a worldwide network of identical particle detectors located at middle and low latitudes aimed to improve fundamental research of space weather conditions and to provide short- and long-term forecasts of the dangerous consequences of space storms. SEVAN detected changing fluxes of different species of secondary cosmic rays at different altitudes and latitudes, thus turning SEVAN into a powerful integrated device used to explore solar modulation effects. Till to now the SEVAN modules are installed at Aragats Space Environmental Centre in Armenia (3 units at altitudes 800, 2000 and 3200 m a.s.l.), Bulgaria (Moussala), Croatia and India (New-Delhi JNU.) and now under installation in Slovakia, LomnitskySchtit). Recently SEVAN detectors were used for research of new high-energy phenomena originated in terrestrial atmosphere – Thunderstorm Ground Enhancements (TGEs). In 2011 first joint measurements of solar modulation effects were performed by SEVAN network, now under analysis.

1. INTRODUCTION

For the basic research of solar physics, solar-terrestrial connections and Space weather, as well as for establishing services of alerting and forecasting of dangerous consequences of space storm the networks of particle detectors located at different geographical coordinates and measuring various species of secondary cosmic rays are of vital importance.A network of particle detectors located at middle to low latitudes known as SEVAN (Space Environment Viewing and Analysis Network, [1.2]) was developed in the framework of the International Heliophysical Year (IHY-2007) and now operates and continue to growth within International Space Weather Initiative (ISWI). SEVAN detectors measure time series of charged and neutral secondary particles born in cascades originating in the atmosphere by nuclear interactions of protons and nuclei accelerated in the Galaxy and nearby the sun. SEVAN modules are operating in Armenia (4 one m^2 standard modules and 2 super modules of 12 identical SEVAN units each arranged above and below 2 standard sections of Nor Amberd neutron monitor 6NM-64; both super modules are capable of muon direction estimation), in Croatia (Zagreb observatory), Bulgaria (Mt. Moussala, India (New-Delhi JNU Univ.) and are under construction in Slovakia (Mt. Lomnicky Stit).The analogical detector is in operation in Tibet [3].

The particle fluxes measured by the new network at medium to low latitudes, combined with information from satellites and particle detector networks at high latitudes, will provide experimental evidence on the most energetic processes in the solar system and will constitute an important element of the global space weather monitoring and forecasting service. SEVAN network measure charged and neutral fluxes; energy spectra of the solar protons by registering the ground level enhancements (GLEs); distinguish between neutron- and proton-initiated GLEs. SEVAN modules also register Thunderstorm ground enhancements (TGEs), new high-energy phenomena in the atmosphere. SEVAN modules, operated at slopes of Mt. Aragats in Armenia during recent years detect many TGE events in fluxes of gamma rays and high-energy muons, proving existence of the strong electrical fields in the thunderclouds initiating relativistic runaway electron avalanches in the thunderstorm atmospheres [4,-6]. SEVAN detectors was calibrated by the gamma ray flux of the most powerful TGEs and furthermore, the time series of the high energy muons detected by SEVAN open possibility to estimate the electrical structure of the thunderclouds, the key parameter for creating models of both TGE and lightning occurrences.

2. DESIGN OF SEVAN PARTICLE DETECTORS

The basic detecting unit of the SEVAN network (see Figure 1) is assembled from standard slabs of 50 x 50 x 5 cm^3 plastic scintillators. Between two identical assemblies of 100 x 100 x 5 cm^3 scintillators (four standard slabs) are located two 100 x 100 x 5 cm^3 lead absorbers and thick 50 x 50 x 25 cm^3 scintillator assembly (5 standard slabs). A scintillator light capture cone and photo multiplier tube (PMT) are located on the top, bottom and the intermediate layers of detector. The detailed detector charts with all sizes are available from http://aragats.am/SEVAN.

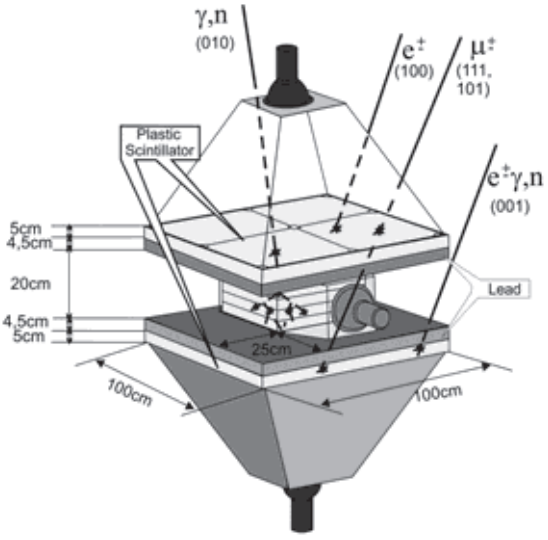

Figure 1. Basic detecting unit of the SEVAN network.

Incoming neutral particles undergo nuclear reactions in the thick 25 cm plastic scintillator and produce protons and

other charged particles. In the upper 5 cm thick scintillator charged particles are registered very effectively; however for the nuclear interactions of neutral particles there is not enough matter. When a neutral particle traverses the top thin (5 cm) scintillator, usually no signal is produced. The absence of the signal in the upper scintillators, coinciding with the signal in the middle scintillator, points to neutral particle detection. The coincidence of signals from the top and bottom scintillators indicates the traversal of high-energy muons. Lead absorbers improve the efficiency of the neutral flux detection and filtered low energy charged particles

If we denote by ‘‘1’’ the signal from a scintillator and by ‘‘0’’ the absence of a signal, then the following combinations of the 3-layered detector output are possible:

111 and 101—traversal of high energy muon; 010—traversal of a neutral particle;100—traversal of a low energy charged particle stopped in the scintillator or in the first lead absorber (energy less than *100 MeV).110—traversal of a higher energy charged particle stopped in the second lead absorber. 001—registration of inclined charged particles

3. FORBUSH DECREASE EVENTS DETECTED BY THE SEVAN NETWORK IN THE BEGINNING OF THE 24-TH SOLAR ACTIVITY CYCLE

In the middle of February 2011 the active region AR 11158 unleashed 3 solar flares of class M6.6 (13 February, solar coordinates S19, W03), M2.2 (14 February, solar coordinates S20, W14) and strongest X2.2 (15 February, solar coordinates S19, W03S21, W18). All 3 flares were accompanied with CMEs headed to the earth direction. The worldwide network of neutron monitors detects at 18 February sizeable Forbush decrease (FD). The SEVAN network as well detects FD by 3 monitors located in Armenia and by Balkanian monitors located in Zagreb observatory (Croatia) and Mt. Moussala (Bulgaria). The SEVAN module locates in India do not register FD due to large geomagnetic cutoff.

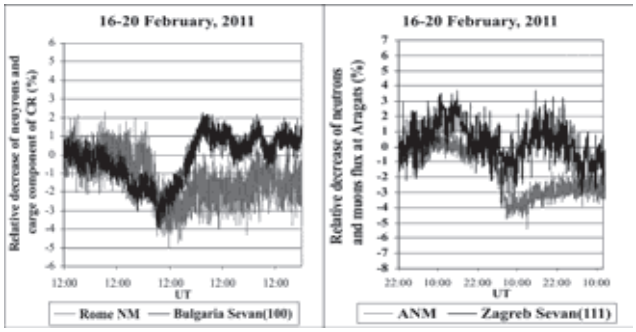

Figure 2. The time profiles of the FD on 18 February, 2011 measured by Zagreb and Moussala SEVAN monitors in comparison with Rome Neutron monitor and Aragats Neutron monitor. The low energy charged particles (combination 100) and high-energy muons (combination 111) are recovering much faster comparing with neutrons measured by Rome and Aragats Neutron monitors.

As we can see in Figure 2 the overall patterns of FD detected in charged particle fluxes are very similar to the ones measured by neutron monitors. However, there are several differences due to location of detectors at different latitudes, longitudes and altitudes. The FD phenomena is global phenomena influenced all globe (may be not the equatorial regions only where the cutoff rigidity is very large); nevertheless the detection of the local differences in time profiles of FD produced by primary particles of different energies is very important and allows to recover the event anisotropy and sometimes also the shape of the ICME. The SEVAN network located on different longitudes (from Zagreb to Delhi) gives possibility to explore FD’s shape and the magnitude longitudinal dependence and character of the disturbance and its source. The amplitude of FD is dependent on the speed, size, and value of magnetic field of ICMEs [7]. In this respect registration of FD also in low and high energy charged particle fluxes can bring additional information for the developing of the model of ICME – magnetosphere interactions.

4. CONCLUSION

Networks of particle detectors on Earth’s surface provide timely information and constitute an important element of planetary Space Weather warning services. The big advantage of ground based particle detectors is their consistency, 24 h coverage, and multi- year operation. In contrast the planned life of the satellites and spacecraft is only a few years, they are affected by the same solar blast that they should alert, and space-born facilities instead of sending warnings are usually set in the stand-by mode. The multi-particle detectors probe different populations of primary cosmic rays. The basic detector of the SEVAN network is designed to measure fluxes of neutrons and gamma rays, of low energy charged particles and high-energy muons. The rich information obtained from the SEVAN network allows estimation of the energy spectra of the highest energy Solar CR (SCR). The SEVAN network is sensitive to very weak fluxes of SCR above 10 GeV, a very poorly explored region of the highest energy. Summarizing, the hybrid particle detectors, measuring neutral and charged fluxes provide the following advantages over existing detector networks measuring single species of secondary cosmic rays:

- Enlarged statistical accuracy of measurements;
- Probe different populations of primary cosmic rays with rigidities from 3 GV up to 20– 30 GV;
- Reconstruct SCR spectra and determine position of the spectral ‘‘knees’’;
- Classify GLEs in ‘‘neutron’’ or ‘‘proton’’ initiated events;
- Gives possibilities to investigate energy dependences of the barometric coefficients and diurnal wave;
- Estimate and analyze correlation matrices among different fluxes;
- Significantly enlarge the reliability of Space Weather alerts due to detection of three particle fluxes instead of only one in existing neutron monitor and muon telescope world-wide networks.

REFERENCES

[1] Chilingarian, A. and Reymers A., Ann. Geophys, 26, 249-257, (2008).
[2] Chilingarian, A., et al., Earth, Moon and Planets: Vol.104, Issue 1, 195, (2009).
[3] Zhang J.L., et al., NIMA, 623, 1030-1034, (2010).
[4] Chilingarian, A., et al., Phys. Rev. D 82, 043009 (2010).
[5] Chilingarian, A. et al., Phys. Rev. D 83, 062001 (2011).
[6] Chilingarian, et al., Phys.Rev.D 85, 085017, (2012).
[7] Chilingarian A. and Bostanjyan N., Journal of geophysical research, V. 114, A09107, (2009).

Simulation of MuSTAnG telescope response to cosmic rays

R. Hippler, M. Zazyan

Abstract. The Muon Space Weather Telescope for Anisotropies (MuSTAnG) is operating at present at Greifswald University in Germany for studying the variations of cosmic rays muon flux. MuSTAnG telescope is able to register incident muons with different zenith and azimuth angles. The mean incoming directions, as well as muon threshold energies for the different upper/lower layer detector combinations were computed using Geant4-based Monte Carlo simulation. The median energies of primary protons, responsible for detected muons, have been calculated using CORSIKA code.

1. INTRODUCTION

MuSTAnG telescope was constructed between 2004 – 2006 at Greifswald University in Germany. It consists of 32 muon detectors arranged in two (top and bottom) layers separated vertically by 95 cm, with an intermediate 5 cm thick layer of lead [1,2]. Each detector consists of a scintillator plate of size 50 cm x 50 cm x 5 cm. Muon traversing the scintillator plates produce intense flashes of light that are converted into electrical signals by the photomultipliers.

A Monte Carlo simulation has been performed to study the response of MuSTAnG telescope to cosmic rays. Atmospheric muons produced in the interactions of primary cosmic rays particles with Earth's atmosphere were simulated using CORSIKA code [3]. As input to CORSIKA, the primary angles of incidence and energy thresholds of muons were needed. In this connection, an additional Monte Carlo *simulation* of particle transport through MuSTAnG telescope was performed using GEANT4 (version 9.4) toolkit [4].

2. GEANT4 SIMULATION

The objective of GEANT4 simulations was to estimate muons energy thresholds for different arrival directions. In our simulation muons were randomly distributed over the surface of telescope. The energies were selected in the range 10 Mev to 800 MeV at random from a *uniform* distribution. The incident directions were also randomized over the range $0 \leq \theta \leq 75^{\circ}$ and $0 \leq \varphi \leq 360^{\circ}$. 5×10^{7} incident muons hitting the telescope have been simulated. Particles *were followed through* the detailed geometry of MuSTAnG telescope. The simulation program outputs energy deposits in all scintillators. If it was more than 4 MeV in any upper and any lower layer scintillators, muon was considered as recorded.

The propagation of incident muons and the secondary particles through the telescope is illustrated on Figure 1.

Energy distribution of vertically penetrating muons is shown in figure 2. Estimation of the threshold energy is illustrated.

Muon energy and angular distributions were obtained from simulation for different upper layer/lower layer combinations of the detectors that recorded the muons passage. If (UX, UY) is the position of upper detector and (LX, LY) is the position of lower detector, the *distance between* upper and *lower detectors can be expressed as* UX-LX= l·Δn, UY-LY = l·Δm (l m is a quadratic detector's length, n and m are the detectors numbers in X and Y directions). A matrix (7×7) spanning from -3 to 3 in X and Y represents all possible directions.

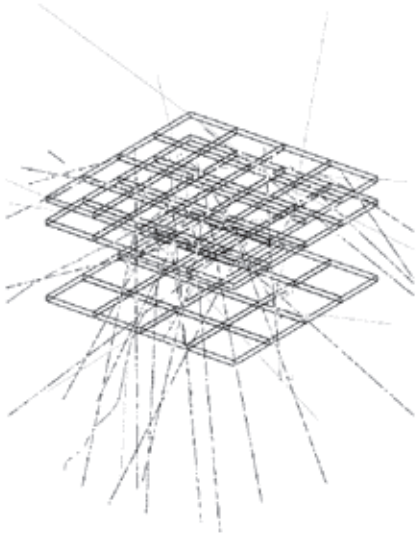

Figure 1. Cosmic ray muons passing through the layers of MuSTAnG telescope

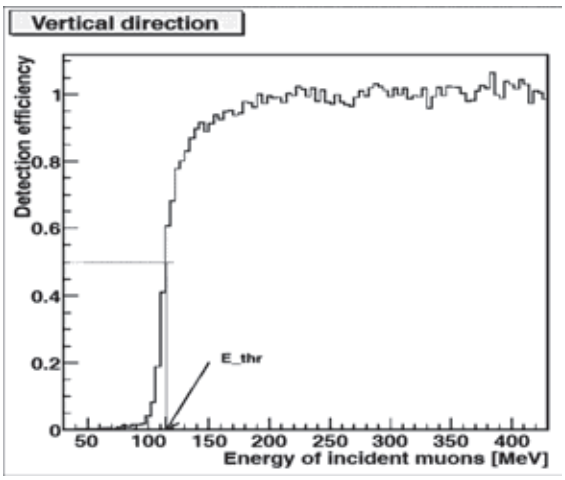

Figure 2. Estimation of the threshold energy for vertical muons.

Mean zenith and azimuthal angles θ and φ and muon energy threshold for each cell of matrix were derived from appropriating distributions (see example on Figure 3).

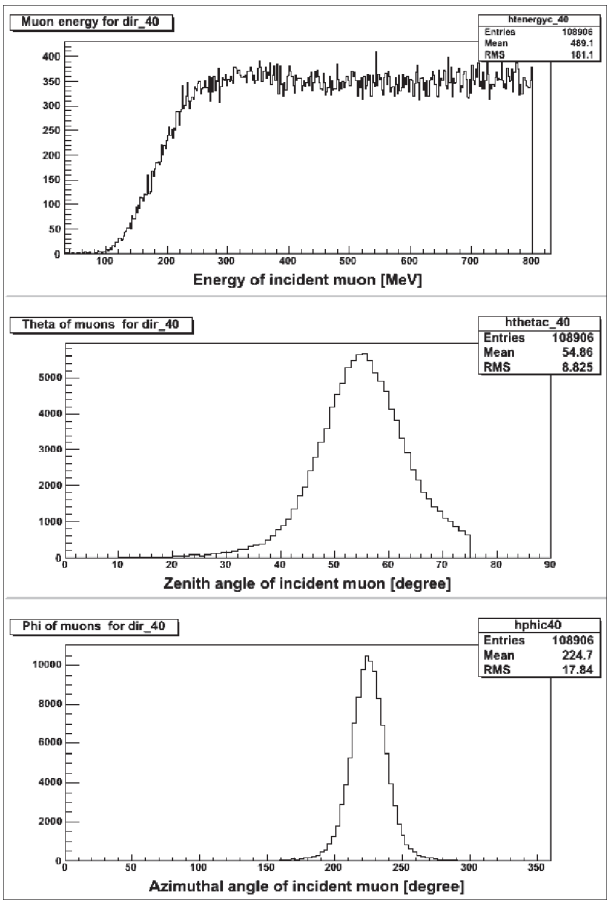

Figure 3. Muon energy, and zenith and azimuthal angle distributions for one of upper/lower layer detector combinations.

3. CORSIKA SIMULATION

To simulate particles propagation through the atmosphere CORSIKA code (version 6.900) has been used. In our simulation the primary energies vary between the geomagnetic cut-off of the MuSTAnG telescope location (2.4 GV) and 10000 GeV. The simulations have been done for Galactic cosmic rays (GCR) using for the primary particle's spectrum the expression: $JP(E) \sim E^{-2.7}$. For the simulation of hadronic interactions GHEISHA [5] and QGSJET [6] models have been used. The observation level was set to 15 m a.s.l. As input to CORSIKA, the angles of incidence and threshold energies of muons, obtained from GEANT4 simulation were used.

The median energies of primary particles responsible for muons detected by MuSTAnG telescope have been derived for different directions. 28 cm of concrete shield was included in GEANT4 simulation. *We have summarized the results of* GEANT4 and CORSIKA *simulations in* Table 1.

The dependence of primary proton median energy on the zenith angle for GCRs can be described by the formula $E_{med}(\theta) = 51.5 \cdot (\cos\theta) - 0.943$ GeV .

Table 1. Mean zenith angles θ, muon threshold energies and primary proton median energes for the different upper/lower layer detector combinations.

±Δm	±Δn	0	1	2	3
0	Θ (degree)	17.6	28.8	45.3	55.5
	Eμ_thr (MeV)	262	280	350	460
	Ep_med(GeV)	55.6	60.6	71.7	87.0
1	Θ (degree)	28.8	36.2	48.5	57.0
	Eμ_thr (MeV)	280	300	375	485
	Ep_med(GeV)	60.6	62.1	75.3	88.5
2	Θ (degree)	45.3	48.5	54.9	60.1
	Eμ_thr(MeV)	350	375	450	550
	Ep_med(GeV)	71.7	75.3	86.7	102.3
3	Θ (degree)	55.5	57.0	60.1	62.9
	Eμ_thr(MeV)	460	485	550	600
	Ep_med(GeV)	87.0	88.5	102.3	110.6

4. CONCLUSION

Mean angles of incidence, as well as threshold energies of muons for different upper/lower layer detector combinations were computed using GEANT4 code. It was found that MuSTAnG telescope detects muon flux in the zenith angle range $17.6° \leq \theta_{mean} \leq 63°$. The threshold energy of muons ranges from 0.262 to 0.6 GeV, depending on zenith angle. Using these parameters as input for CORSIKA simulation the median energies of primary protons, responsible for detected muons, have been calculated for different directions. It was shown, that MuSTAnG telescope selects primary cosmic rays in energy range from 55.6 to 110.6 GeV.

5. ACKNOWLEDGMENTS

This work was supported by the German DAAD research grant. Special thanks to Varlen Grabski (from Universidad Nacional Autonoma de Mexico) for the help in GEANT4 simulation.

REFERENCES

[1] Jansen F, Munakata K, Duldig M L and Hippler R 2001 Muon Detectors – the real-time, ground based forecast of geomagnetic storms in Europe, *ESA Space Weather Workshop: Looking towards a European Space Weather Programme*, ESA WPP-144

[2] Hippler R, Mengel A, Jansen F et al. 2007 First Space Observation at MuSTAnG – the Muon Spaceweather Telescope for Anisotropies at Greifswald, *30th Int. Cosmic Ray Conf.* (Mexico) v.1 p347

[3] Heck D et al. 1998 Forschungszentrum Karlsruhe, *FZKA Report 6019*

[4] Agostinelli S *et al.* 2003 GEANT4—a simulation toolkit *Nucl. Instrum. Methods Phys. Res.* A 506 pp 50–303

[5] Werner K 1993 *Phys. Rep*. 232 pp 87-299

[6] Kalmykov N et al. 1993 *Phys. At. Nucl*. 56 p 346

CME-CME Interaction and Forbush Decrease: a case study of 13th ; 14th; 15th February 2011 CMEs

D. Maričić, N. Bostasyan, M. Dumbović, A. Chilingarian, K. Arakelyan, H. Rostomyan, B. Vršnak, D. Roša, D. Hržina, I. Romštajn and A. Veronig

Abstract. *Aims.* We analyze the kinematics of three interplanetary coronal mass ejections (ICMEs) that occurred on 13th, 14th and 15th February 2011 in the active region AR11155 and showed that they have appeared at the Earth orbit on February, 18th and have causing Forbush decrease (FD). Furthermore, we investigate their connection to observed solar flares and the timing of the FD relative to the ICMEs arrival at the Earth.

Methods. The solar coordinates of flares are (S19W03), (S20W14) and (S21W18). The kinematic curves were obtained using STEREO (A&B) data. Additionally, we explore the possibility of the CME-CME interaction for these three events. We compare obtained estimates of ICME arrival with the in-situ measurements from WIND spacecraft at L1 point and with ground-based cosmic ray data obtained from SEVAN network.

Results. The acceleration of each CME is highly correlated with the associated SXR flares energy release. CMEs that erupted at 13 and 14 Feb 2011 are not associated with prominence eruption; maximum velocity was $v_{max} \approx 550 \pm 50$ km/s and $v_{max} \approx 400 \pm 50$ km/s, respectively. However, 15 Feb 2011 CME is connected with much more violent eruption associated with a prominence, with maximum velocity of $v_{max} \approx 1400 \pm 50$ km/s. The last overtakes 13th and 14th Feb CMEs at distances of 32 and 160 R , respectively. Therefore, the solar eruptions occurred at the 13-15 February represent an example of the colliding CMEs, which were the cause of Fd.

Conclusion. The estimated arrival times of the ICMEs, at the L1 point and at the Earth, obtained from *STEREO-A & B* data (t_A = 01:05 ± 120 UT,18 February 2011 and t_B = 02:20 ± 120 UT, 18 February 2011, respectively), are in good coincidence with the observed onset of the Space Weather disturbances (Storm Sudden Commencement – SSC, t_{ssc} = 00:42 ± 60 UT, 18 February 2011) and Forbush decrease (caused by the ICME, t_{FD} = 02:30 ± 60 UT by SEVAN Aragats on 18 February 2011).

Depletion of High Energy Muon Flux during TGEs – a Possibility to Measure Potential Drop in Thunderclouds

A. Chilingarian, G. Karapetyan, K. Bostanjyan, L. Vanyan

Abstract. Magnetometric station LEMI-018, and LEMI-417 commissioned by the Lviv center of Space Research Institute of Ukrainian Academy of Science, have been installed on slopes mountain Aragats (Armenia) at heights 2000 and 3200m above sea level. Operation of magnetometric station started on July 2009 and 2011 accordingly. LEMI-417 is measuring also components of the electric field. One-second time series of the 3-dimensional measurements of the geomagnetic field enter the database of the Aragats Space Environmental Center (ASEC). This information can highly improve the research of correlations of the geomagnetic field, changes of the fluxes of secondary cosmic rays measured by ASEC monitors with parameters of the solar wind and interplanetary magnetic field (IMF) measured by facilities on board space station located 1.5 million km from Earth. Measurements of geomagnetic field at Nor Amberd (2000m) and Aragats (3200m) research stations of A.Alikhanyan national lab will support forewarning of the upcoming major geomagnetic storms. We present the detection of the first geomagnetic storms of the 24 solar activity cycle detected by new installed magnetometric stations.

Extensive Cloud Showers (ECS) – High-Energy Phenomena Resulting from the Thunderstorm Atmospheres

A. Chilingarian, G. Hovsepyan

Abstract: In 2011 we report the phenomenon of the short TGEs (duration less than 50 us) detected by the surface particle detectors at mountain altitudes. Short particle bursts occur during a large near surface negative electrical field. Observed short TGEs, in contrast to prolonged ones (lasting ~10 minutes and more) are direct evidence of the RB/RREA process reaching the mountain altitudes from low located thunderclouds. In the report we present further analysis of these rare events including spatial distribution, density spectra and particle energy.

Comments on recent results on neutron production in thunderclouds

A. Chilingarian, N. Bostanjyan, T. Karapetyan, L. Vanyan

Abstract. We have analyzed the neutron fluxes correlated with thunderstorm activity recently measured at mountain altitudes by Tien-Shan, Tibet and Aragats groups. We perform simulations of the photonuclear reactions of gamma rays born in the electron-gamma ray avalanches in the thunderstorm atmosphere and calculate expected count rates of the neutron counters used by 3 groups. Also we present independent experiment performed at the slopes of Aragats Mountain in Armenia confirming the photonuclear nature of thunderstorm-correlated neutrons.

1. INTRODUCTION

Although the reported enhancements of the Neutron Monitor counts are rather consistent all 3 groups drastically differ in explanation of the origin of neutron flux. The Tien-Shan group reports large flux of thermal neutrons correlated with atmospheric discharges; Aragats and Tibet groups do not relate the neutron flux to lightning occurrences due to considerable difference of time scales of lightning (~ msec) and neutron flux (minutes); different at least 5 orders of magnitude. Both groups connect neutron flux with Relativistic Runaway Electron Avalanches (RREA, Babich et al., 1998, also referred as Runaway Breakdown, RB, Gurevich et al., 1992) process in the thunderstorm atmosphere; however Tibet group assumes that gamma rays born in the avalanche directly initiate NM counts by photonuclear reactions with lead producer of NM (Tsuchiya et. al., 2012); Aragats group accepts the hypothesis of the photonuclear reaction of the RREA gamma rays with the atmosphere as a source of neutrons (Chilingarian et al, 2012a).

Tien-Shan group founded their explanation on the large thermal neutron flux detected by outdoors and indoors thermal neutron detectors correlated in time with atmospheric discharges; no gamma ray flux was reported. Aragats group interpretation was based on the simultaneous detection of the electrons, gamma rays and neutron fluxes and was supported by the GEANT4 simulations of photonuclear reactions of gamma rays in the atmosphere.

To resolve apparent ambiguity and to clarify neutron production mechanisms we perform additional simulations and add new experimental evidence coming from another experimental setup located on slopes of Mt. Aragats in Nor Amberd research station on altitude 2000 m. Experimental facilities located in Nor Amberd operated as a part of the Aragats Space Environmental center (ASEC, Chilingarian et al., 2005) and measure fluxes of gamma rays, thermal and high energy neutrons, as well as high energy muons; we consider registration of multiple particle fluxes (Thunderstorm ground enhancements, TGEs, see Chilingarian et al., 2010, 2011, 2012b) as an absolutely necessary condition for making physical inference on the neutron origin.

2. THE RELATION BETWEEN ADDITIONAL GAMMA RAYS AND NEUTRONS DETECTED DURING TGEs; DO GAMMA RAYS DIRECTLY INITIATE COUNTS IN NEUTRON MONITOR?

The simulation performed by Tsuchiya et. al., 2012, showed that the arriving neutron flux at >1 keV is expected to be lower than that of arriving gamma rays at > 10 MeV by more than 2 orders of magnitude. Combining this estimate with an efficiency of NM to register gamma rays with energies above 10 MeV and neutrons above 1 KeV (Fig. 1 of Tsuchiya et. al., 2012) it was found that bremsstrahlung gamma rays interacting with lead producer of NM largely attribute the signal obtained by YBJ NM and neutrons born in photonuclear reactions in atmosphere give only a small contribution to the signal.

The authors of Tsuchiya et. al., 2012 conclude also "Consequently, not neutrons but gamma rays may possibly dominate enhancements detected by the Aragats neutron monitor".

Under plausible assumptions on the originated in the thunderclouds gamma ray spectrum and height of the gamma ray source several simulations (see for instance Babich et al., 2010, Carlson et al., 2010) estimate a yield rate of a photo- nuclear neutron per one gamma ray with energy >10 MeV to be ~0.3-0.4%. This estimate is consistent with the claim made in Tsuchiya et. al., 2012 on the relative rate of neutrons and gamma rays. However, as we discuss in Chilingarian et al., 2012a) the mentioned above estimate of ~0.3-0.4% is related to the axis-symmetric simulation of the neutron production and transport. The gamma ray flux reported in (Tsuchiya et. al., 2012) relate to a point source of gamma rays[7] rather than realistic extended one, as was proved in Tsuchiya et al., 2011 and Torii et al., 2011. The locality of gamma ray emitting region and drastically different angular distribution of the gamma rays and neutrons (see Figure 1) leads as we discuss in Chilingarian et al., 2012a to the large discrepancy of the neutron relative yield. Gamma rays are radiated in a rather narrow cone; therefore they are illuminated in a limited area below the thundercloud. The increasing offset of the projection of simulated point gamma ray source relative to the particle detector location as we can see in Fig. 8 of Chilingarian et al., 2012a, dramatically changes the neutron relative yield making it at offset distances of ~150 m ~12% instead of 0.3-0.4%. Therefore, the claim of

[7] The particular simulation scheme adopted by the authors of Tsuchiya et al, 2012 is apparent from discussion in the end of section 1.

prevailing contribution of gamma rays in NM counts is not valid.

Another argument against dominating "gamma ray" nature of NM counts is the absence of the expected under assumption of the gamma ray nature of NM counts linear correlation between number of additional gamma rays and NM counts as we can see in Fig. 3 of Chilingarian et al., 2012a.

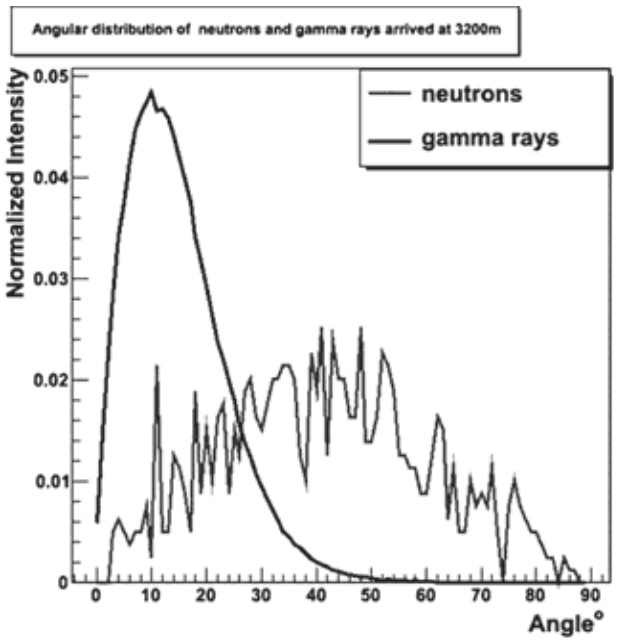

Figure 1. Angular distribution of gamma rays according to detected TGE on 4 October 2010 and neutron flux born by these gamma rays in the photonuclear reaction with atmospheric nuclei.
The source of gamma rays is located on 5000 m height, detection on 3200 m height.

In Figures 2 and 3 we post the histograms of the numbers of the additional gamma rays and neutrons of the TGEs detected in 2009-2010 at Aragats (from Table 2 of Chilingarian et al., 2012). The histogram ranges (difference between maximal value and minimal value) are quite different: by the gamma ray content events differ from 715 till 10,281, i.e. the range is 9,566 (Figure 2) and of the neutron content only 74 – from 50 till 124 neutrons (Figure 3). The relative range[8]of gamma ray histogram is ~3.6, and for the neutron histogram ~1. Thus, the neutron distribution of the TGE events is much more compact than gamma ray distribution. It demonstrates that there is no linear relation between gamma rays and neutrons fallen on the detector, expected if the origin of NM counts will be gamma rays as assumed in (Tsuchiya et al., 2008).

The large divergence of detected neutrons to gamma ray ratio can be explained by the different angular distribution of gamma rays and neutrons from thundercloud and by various locations of the thunderclouds relative to particle detector see Figure 1 (see also discussion in Chilingarian et al., 2012).

[8]Relative range equals to range divided to the sample mean and usually is used as an estimate of the standard deviation for small samples not belonging to an analytic probabilistic families (nonparametric estimate of standard deviation)

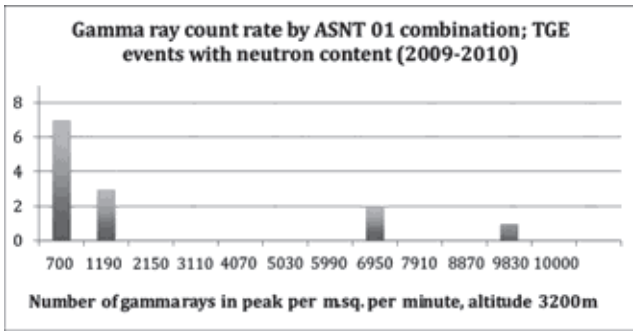

Figure 2. Histogram of the normalize to 1 m^2 gamma rays detected by ASNT during 13 TGE events in 2009-2010 (from Table 1); relative range (nonparametric estimate of standard deviation) ~ 3.6

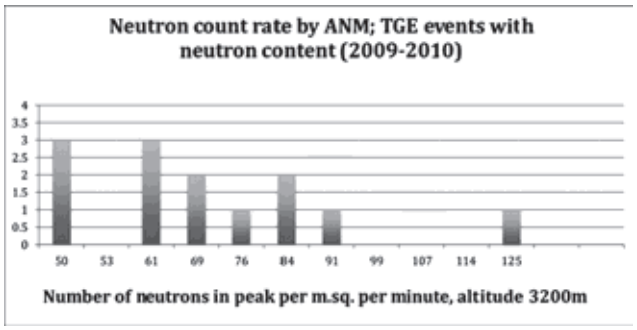

Figure 3. Histogram of the normalize to 1 m^2 neutrons detected by ANM during 13 TGE events in 2009-2010 (from Table 1); relative range (nonparametric estimate of standard deviation) ~ 1

3. THERMAL AND PHOTONUCLEAR NEUTRON FLUXES (ATTEMPT TO EXPLAIN TIEN-SHAN DATA)

Gurevich et al., 2012 reported for the first time about the registration of the extremely intensive fluxes of low-energy neutrons generated during thunderstorms. They also claim that these fluxes are connected with atmospheric discharges. Unfortunately the empiric data on neutron detector count rates were not supported by the detector response calculation and with a model of neutron generation. Only several episodes of the detected 1-minute count rate enhancements possibly correlated in time with lightning occurrences are presented.

Reported observations were done with Tien-Shan 18NM64 neutron monitor (TSNM) and thermal neutron counters (TSNC) located outdoors and indoors, see Figure 2 in (Chubenko et al., 2008). The counters are filled with 3He gas; because of the absence of producing and moderating material these counters can register only thermal neutrons having energies in the range (0.01 – 1 eV). From the published (Gurevich et al., 2012) outdoors (external) thermal neutron counts were taken into account reported in (Chubenko et al., 2008) efficiency and size of TSNC counters we readily obtain the flux of thermal neutrons for mentioning episodes to be:

3462, 1600, 1684, 4567, 3717 and 2722 neutrons per m^2 per minute.

These fluxes of the thermal neutrons are fallen on the building where TSNM and indoor TSNC are located. Having incident neutron fluxes and construction of the building roof reported in (Chubenko et al., 2008 and Gurevich et al., 2012) we simulate the transport of neutrons

through the roof material and using also reported in Gurevich et al., 2012 the neutron detection efficiencies we calculate the expected count rate of both indoor neutron detectors.

The indoor TSNC and TNNM are located in the building under 2 mm iron tilt, 20 cm carbon and 2.5 cm wood. Our GEANT4 simulations demonstrate that only 7% of thermal neutron flux can penetrate the roof matter. If we proceed from the recovered by outdoors TSNC neutron fluxes we come to following expected numbers of thermal neutrons to be detected by indoors TSNC:

109, 50, 53, 143, 117, 86 per m^2, per minute.

However, the reported numbers of detecting thermal neutrons are much larger:

641, 418, 323, 716, 927 and 922 per m^2, per minute.

The reported (recalculated to unit surface) numbers of counts detected by TSNM are:

44, 63, 51, 40, 156, 117 per m^2, per minute.

Assuming 0.5% efficiency (Gurevich et al., 2012) of TSNM to detect thermal neutrons we obtain the much lower expected number of the TSNM counts:

1, 1, 1, 2, 2, 1 per m^2, per minute.

Thus, measured by the outdoors TSNC thermal neutron flux[9] cannot explain the reported counts of indoors TSNC and TSNM.

As a possible explanation of the count rate enhancements reported by Tien Shan group we consider also flux of neutrons born in photonuclear reaction in the thunderstorm atmosphere, see Fig. 4.

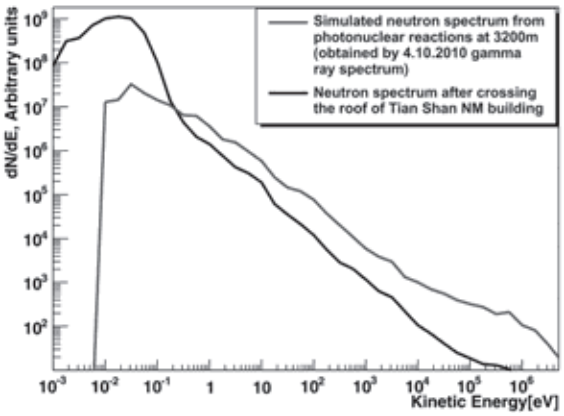

Figure 4. Energy spectra of photonuclear neutrons at 3350 m and in the building of Tien-Shan NM after crossing the roof matter

Maximal estimated neutron flux at Aragats up to date is ~5000 neutrons per m^2, per minute. By considering the higher location of Tien-Shan we can double this number and assume that photonuclear neutron flux at Tien-Shan can reach 10000 neutrons per m^2, per minute. GEANT4 simulations demonstrate that only ~20% of photonuclear neutrons can penetrate the roof material; additionally, as we can see in Fig. 4, the 20 cm thick carbon layer effectively termalized neutrons; 97% of the initial neutrons incident on the indoor detectors are termalized. 2000 neutrons entering indoor TSNC and TSNM will generate approximately the same number of counts as the thermal neutron flux calculated from counts of outdoor TSNC[10]; much less than reported. Thus the hypothesis of the photonuclear nature of neutron flux in Tien-Shan also cannot explain reported count rate enhancements.

Thermal neutron counters on Aragats and Nor Amberd only once detect enhancement of count rate at 4 October 2010, see Fig. 6 of (Chilingarian et al., 2012). Our simulations demonstrate that the MeV photonuclear neutron flux incident on the neutron monitor thermalized in the polyethylene moderator and a significant fraction of the thermal neutrons is emitted upwards from the polyethylene moderator covering the Aragats NM and registered by the bare proportional chamber located just on the moderator of neutron monitor.

4. NOR AMBERD HYBRID DETECTOR

Detector assembly measuring secondary cosmic ray fluxes originated from protons and ions accelerated on sun and in the Galaxy are located on the slopes of the mountain Aragats in Nor Amberd research station at 2000 m above sea level. Nor Amberd detecting system consists of 18NM64 neutron monitor (NANM, 3 sections of 6 neutron counters each) and - Multidirectional Muon Monitor (NAMMM) – 2 layers of 5 cm thick plastic scintillators overviewed by photomultiplier (PM) above and below 2 sections of NM; and include also 2 proportional counters without lead producer and polyethylene moderator for detecting thermal neutrons, see Fig. 5. The energy threshold of the upper scintillators is determined by the roof matter and by data acquisition electronics (DAQ) and equals ~ 7 MeV. The upper scintillator registered charged flux above the threshold with very high efficiency reaching 99%; however 5 cm plastic scintillator register also neutral flux (gamma rays and neutrons) although with much smaller efficiency - ~10%. The bottom layer of scintillators is located under a significant amount of matter including 10 cm of lead and its energy threshold is ~350 MeV; therefore the bottom layer measures mostly high energy muons.

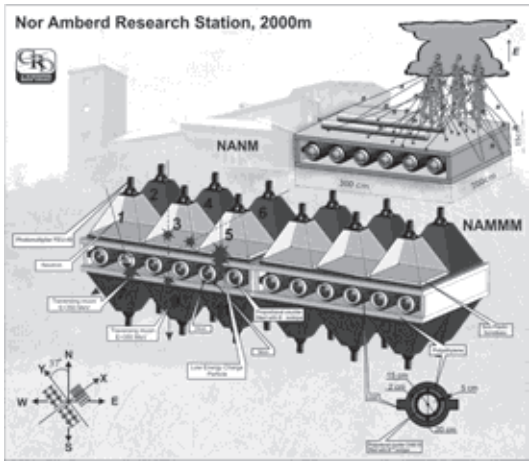

Figure 5. Nor Amberd multidirectional muon monitor (NAMMM) arranged above and below 2 sections of the Nor Amberd Neutron Monitor (NANM); on the third section of NANM 2 "bare" proportional counters are located

[9]Possibly generated in atmospheric discharge processes as assumed by the authors of Gurevichetal., 2012.

[10]Of course, under the assumption of the photonuclear nature of the neutron flux outdoors TSNC also should count much less neutrons than reported.

DAQ electronics calculates all possible coincidences of detector operation as well as count rates of each detector and total count rates of upper and bottom detectors of both sections of NAMMM. By counting one-to-one coincidences of upper and bottom scintillators it is possible to monitor muon fluxes for 12 directions. NANM operates with 3 dead times ranging from 0.4 to 1250 μs. The monitor counts with shortest dead time give possibility to count almost all thermal neutrons entering the sensitive volume of the proportional chamber; the long dead time provides a one-to-one relation between counts and high energy atmospheric hadrons incident on the detector. If neutron bursts are incident on detector the shortest dead time will provide registration of a majority of neutrons, the longer dead time will miss neutrons coming simultaneously within 1250 μs.

5. SIMULTANEOUS DETECTION OF CHARGED AND NEUTRAL FLUXES BY NOR AMBERD DETECTOR ASSEMBLY

In Fig.6 we post detected at 28 March 2009 time series of 1-minute count rates of NAMMM top and bottom layers as well as NANM 1 minute time series corresponding to shortest dead time.

The statistical accuracy of measurements and significances of detected peaks is posted in Table 1. In Figure 6 we see a large enhancement of the counts in the upper layer of NAMMM conditioned on absence of signal in the lower layer (we assume that most of them are gamma rays);

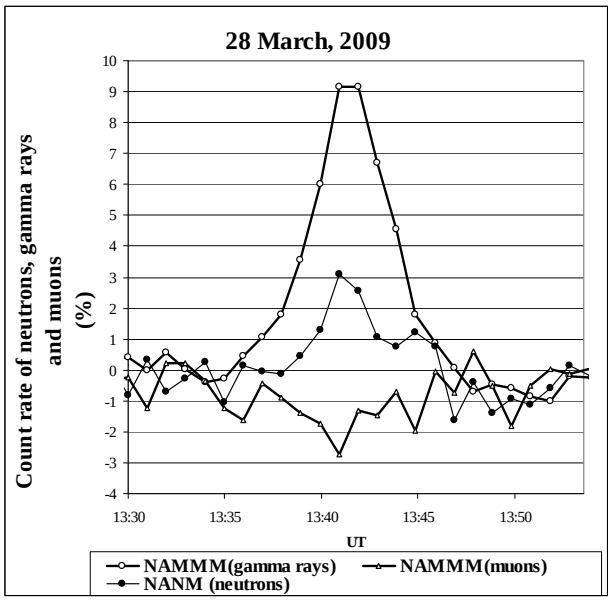

Figure 3 . The 1-minute time series of count rates of upper and top layers of NANM and NANM

significant enhancement of the count rate of neutron monitor and depletion of counts of high energy muons. The TGE in Nor-Amberd is alike of TGEs measured at Aragats; namely Fig. 1,4 and Table 1 of (Chilingarian et al., 2012) are very close to the ones presented here, obtained with different detector at different altitude.

Table 1 Statistical characteristics of detectors and detected peaks and dips at 28.03.2009, 13:43.

Detector	Mean count rate per minute	Standard deviation – SD (σ) and relative standard deviation (RSD)	Percent of enhancement	Number of SD (σ) in peak	Number of additional particles (or deficit for muons) at minute of maximal excess ($min^{-1} m^{-2}$)
NANM neutrons	30000	300 (1%)	3.2%	3.2σ	53
NAMMM upper (10)	121150	348 (0.29%)	9.2%	32σ	924
NAMMM (muons>350 MeV); Vertical direction excluded	24000	155(0.65%)	-2,2%	3.5σ	-45

6. CONCLUSION

We consider the data of recently reported neutron fluxes correlated with thunderstorms. The Tibet group explains the detected count rate enhancement in the neutron monitor by the previously neglected direct registration of gamma ray photons by NM. According to their estimates the gamma channel over performed the contribution of the neutrons born in the photonuclear reactions in the atmosphere by an order of magnitude. However, as we have shown they do not take into account the offset of neutron source related to detector location. Also, calculated linear correlation of gamma ray and neutron fluxes expected if the main mechanism of neutron production is a photonuclear reaction in the lead producer of NM is not supported by Aragats group neutron events.

Proceeding from the reported in (Gurevich et al., 2012) thermal neutron count rates measured by the outdoors Thermal neutron counter (TSNC) we calculate the expected counts of Tien-Shan neutron monitor (TSNM) and indoors TSNC taking into account the detector response. Calculated fluxes are much lower than reported ones. If we assume that additional neutrons were born in the photonuclear reactions of gamma rays in the atmosphere we come to approximately the same expected numbers due to effective thermalizing of neutrons in roof matter. Thus both thermal and photonuclear hypotheses of neutron origin contradict reported data.

The situation can be clarified by presenting measured gamma ray fluxes and by correlating the neutron bursts and atmospheric discharges on the second (better millisecond) scale. It will be also useful to estimate the negative muons contribution to TSNM counts, previously treated by members of group as the main cause of TSNM count rate enhancements during thunderstorms (Antonova et.al., 2011).

Also it is worth to mention that Aragats and Tibet measurements do not support the hypothesis of particle fluxes directly related to the atmospheric discharges, accepted by Tien-Shan group. Accordingly during the developed Lower positive charge region in the thundercloud (necessary condition of the creation of lower dipole accelerated electrons downward) the flash rate is quite low (Qui et al., 2005).

Based on previous discussions and also on TGE event detected on 28 March 2009 at Nor Amberd research station we confirm the existence of the atmospheric photonuclear neutron flux correlated with thunderstorms.

REFERENCES

V.P. Antonova, S.V. Kryukov, A.P. Chubenko, Yu.V. Shlyugaev, A.L. Shepetov, 2011, Izvestiya Rossiiskoi Akademii Nauk. Seriya Fizicheskaya, 2011, Vol. 75, No. 6, pp. 894–897; Bulletin of the Russian Academy of Sciences. Physics, 2011, Vol. 75, No. 6, pp. 843–846. © Allerton Press, Inc

Babich, L. P., I. M. Kutsyk, E. N. Donskoy, and A. Y. Kudryavtsev (1998), New data on space and time scales of a relativistic runaway electron ava- lanche for thunderstorms environment: Monte Carlo calculations, Phys. Lett. A, 245, 460–470, doi:10.1016/S0375-9601(98)00268-0.

L. P. Babich, E. I. Bochkov, I. M. Kutsyk, and R. A. Roussel-Dupre´, J. Geophys. Res. 115, A00E28 (2010).

B. E. Carlson, N. G. Lehtinen, and U. S. Inan, J. Geophys. Res. 115, a00e19 (2010).

A. Chilingarian et al., Nucl. Instrum. Methods Phys. Res., Sect. A 543, 483 (2005).

A. Chilingarian, A. Daryan, K. Arakelyan, A. Hovhannisyan, B. Mailyan, L. Melkumyan, G. Hovsepyan, S. Chilingaryan, A. Reymers, and L. Vanyan, Phys. Rev. D 82, 043009 (2010).

A. Chilingarian, G. Hovsepyan, and A. Hovhannisyan, Phys. Rev. D 83, 062001 (2011).

A.Chilingarian, N. Bostanjyan, and L. Vanyan, Neutron bursts associated with thunderstorms, Physical review d 85, 085017, 2012a.

Chilingarian A., Mailyan B., Vanyan L., *Recovering of the energy spectra of electrons and gamma rays coming from the thunderclouds*, Atmospheric Research 114–115, 1–16, (2012b).

A P Chubenko, A L Shepetov, V P Antonova, P A Chubenko and S V Kryukov, The influence of background radiation on the events registered in a neutron monitor at mountain heights, J. Phys. G: Nucl. Part. Phys. 35 (2008) 085202

V. Gurevich, V. P. Antonova, A. P. Chubenko, A. N. Karashtin, G. G. Mitko, M. O. Ptitsyn,V. A. Ryabov, A. L. Shepetov, Yu. V. Shlyugaev, L. I. Vildanova, and K. P. Zybin, Strong Flux of Low-Energy Neutrons Produced by Thunderstorms, PRL 108, 125001, 2012.

A. V. Gurevich, G. M. Milikh, and Roussel-Dupre, Phys. Lett. A 165, 463 (1992).

C.J. Hatton and H. Carmichel, Can. J. Phys. 42, 2443 (1964).

H. Tsuchiya, K. Hibino, K. Kawata, et al., Observation of thundercloud-related gamma rays and neutrons in Tibet, Phys. Rev. D 85, 092006, (2012).

H. Tsuchiya et al., J. Geophys. Res. 116, D09113 (2011).

T. Torii, T. Sugita, M. Kamogawa, Y. Watanabe, and K. Kusunoki, Geophys. Res. Lett. 38, L24801 (2011).

Role of the Lower Positive Charge Region (LPCR) in initiation of the Thunderstorm Ground Enhancements (TGEs)

A. Chilingarian, H. Mkrtchyan

Abstract. Despite the ubiquity of thunderstorms, lightning, and related electrical phenomena, many important electromagnetic processes in our atmosphere are poorly understood; the key questions about the thundercloud electrification and lightning initiation remain unanswered (Dwyer et al., 2012). The bulk information on particle fluxes correlated with thunderstorm can be used to better understand the electrical structure of thunderclouds. Only very specific electric configuration of the lower part of the cloud can support the sustainable acceleration of the electrons. Our analysis is based on the thunderstorm data from the Aragats mountain in Armenia, 3200 m a.s.l. The electrical mill and lightning detectors are monitoring the near surface electric field and type of lightning occurrences, particle detectors register fluxes of neutral and charged particles associated with thunderstorms. We relate particle fluxes to the electrical structure of thunderclouds and - to lightning occurrences. The origination of the Lower Positive Charged Region (LPCR) leads to the blocking of CG- lightning occurrences. High particle fluxes, associated with thunderstorms, so called Thunderstorm Ground Enhancements (TGEs) precede lightning activity, thus proving possibility that downward moving streamer uses the conductive channel opened by the electron-gamma ray avalanches.

1. INTRODUCTION

Thunderstorms, due to their potential to kill and cause extensive property damage are an important issue not only for researchers but also for the society. However, in spite of many experimental and theoretical studies the origin of electrification in clouds is still poorly understood; the layered structure of the thundercloud is variable and unexplained; relationship between electrification, lightning activity and particle fluxes have not been unambiguously established.

Although big varieties of measures in the thundercloud electric field profiles, the following basic structure of the electric field in thunderclouds is widely accepted: from the ground up to cloud base there is usually a low magnitude field (both positive or negative); relative small positively charged "pocket" is lowermost just at cloud base (comprising only ~20% of negative charge higher); larger positive field prolongs up to negative charge layer at 1-2 km above cloud base; and about 1-4 km above the negative layer the main positive charge is located (Stolzenburg et al., 1998). The Lower Positive Charge Region (LPCR) with a main negative layer in the middle of the cloud represents the, so called, lower dipole, responsible for the downward electron acceleration and also playing a major role in the initiation of cloud-to-ground (CG-) and intracloud (IC-) lightning occurrences.

The acceleration of electrons in the strong electric fields inside thunderclouds was postulated by C.R.T.Wilson in 1924, in 1992 Gurevich et al., developed theory of the Runaway breakdown (RB), now mostly referred to as Relativistic Runaway Electron Avalanches (RREA, Babich et al., 1998). In (Chilingarian et al., 2012b) we consider alternative mechanism of electron acceleration in thunderclouds, namely the Modification Of energy Spectra (MOS, Dorman et al., 2005) of charged cosmic ray particles. Both scenarios lead to enhancements of the secondary cosmic rays in the thunderclouds and if the height of clouds is not very large particle detectors located on the earth's surface can register enhancement of count rates of electrons, gamma rays and neutrons, lasting as much, as the electric field sustain electron acceleration, at Aragats usually ~ 10 minutes.

It has been suggested that RREAs seeded by cosmic-ray extensive air showers (EASs) could result in enough ionization to initiate lightning (Gurevich et al. 1999, 2003). However, Babich et al. (2009), Dwyer and Babich (2011) argue that lateral diffusion and the relativistic feedback threshold on the amount of avalanche multiplication are limited a joint action of EASs and RREAs to initiate lightning. Although, they do not rule out that RREA acting on the ambient cosmic-ray flux could discharge the large scale electrical field in such a way that local electric field enhancements occur, potentially providing a high enough field region to allow lightning to initiate (Dwyer 2005; Babich et al. 2011).

Additionally, Dwyer et al., 2012, pointed to the possibility that the gamma ray glows (the gamma ray component of the TGE) may be a manifestation of the steady state configuration of the electric field in which the charging currents are balanced by the discharge RREA currents. Lasting tens of minutes TGEs may affect lightning initiation and research of the correlations of lightning and TGE can provide long missing clues to understand the lightning physics.

In the paper the correlation between thundercloud electrification (near surface electrical field, type of lightning discharge and its distance from the detecting point) and measured particle fluxes was studied, thus invoking in the atmospheric electricity research a new type of key evidence – presence of the Thunderstorm Ground Enhancements (TGEs), the flux of gamma rays and electrons coming from thunderclouds and detected on the earth's surface by particle detectors (Chilingarian et al., 2010, 2011, 2012a). For the first time we present simultaneous measurements of the particle fluxes, disturbances in the near surface electrical field and lightning initiations of the different types.

2. THE LOWER POSITIVE CHARGE REGION (LPCR) AND ITS INFLUENCE ON THE NEGATIVE CLOUD-TO-GROUND (CG-) AND INTRACLOUD (IC-) LIGHTNING OCCURRENCES

During the last 3 years of TGE research on Aragats nearly 300 significant enhancements of particle detector count rates were detected. After locating the field meters and lightning detectors in 2010-2011 we found that all TGEs were accompanied by the disturbances of the near-surface electric field and most of them – with lightning occurrences. The research of TGE events started with classification of TGEs according to patterns of near-surface electrical field disturbances. Then we examine each class to get evidence how is the particle flux increasing and what happens with lightning occurrences as a flux enlarged. Our model of TGE initiation (Chilingarian et al., 2011, 2012b) suggests that electron acceleration could start only after the creation of the Lower positive charge region (LPCR) below the main negative charged region in the center of the cloud. If electric field between 2 differently charged regions is strong enough the RREA process is unleashed and runaway electrons generate gamma rays and gamma rays in turn if energetic enough can generate neutrons via phonuclear reactions. If the electric field is below the RREA threshold the MOS process can result in additional fluxes; however much weak comparing with RREA.

Simpson and Scrase, 1937, found that many thunderstorms contain a region of the positive charge located below the main negatively charged layer in the middle of a thundercloud; they speculated that the positive charge resided on precipitation particles. Measurements by (Holden et al., 1980) show that LPCR's are not always found because they are localized to a fairly small volume and are transient phenomena as well. LPCR's are short-lived because, being composed of precipitation, they fall out of the cloud and carry their charge to the ground. As the LPCR approaches the ground, it should alter (at least locally) the field at the ground; thus LPCRs are responsible for the field reversals (Moore et al., 1977). Many researchers outline the dominant role lower positive charge region plays in initiating/triggering an intracloud and the cloud-to-ground lightning discharge (Pawar and Kamra, 2004, Nag and Rakov 2009, Qui et.al., 2009). The influence of the LPCR on lightning leader propagation can be considered in the following steps:

a. While the negative charge accumulates at mid level, it may not be energetically favorable to transfer the negative charge to ground in -CG lightning. Starting to develop lower positive charge results in the enhancement of the electric field strength within the cloud, allows for negative charge transfer to ground in -CG lightning occurrence (Williams, 1989).
b. When the magnitude of LPCR is becoming considerably large negative intracloud discharges IC- (attempted leader) are expected to occur. The “normal” IC+ intracloud lightning occurs between main negative and positive layers of the dipole; the electric field is negative and electrons are accelerated upward. IC- lightning bridging the main negative and large lower positive charge regions have been reported by (Qie et al., 2005); due to screening positive charge descending negative leader may change its direction of propagation to horizontal.

Thus, the existence of the LPCR is a necessary condition for the TGE unleashing and, also, for the lightning initiation. As LPCR is just forming or decaying the clod-ground CG- lightning occurrences should be often, during the mature stage of LPCR mostly intracloud IC- lightning should occur. An example of the above-described scenario gives lightning studies on the central Tibetan Plateau at an altitude of 4508 m. The registered on Tibet IC- flashes were usually polarity-inverted and occurred in the lower dipole. The large LPCR did not cause positive CG+ flashes to occur during the whole storm lifetime, and only negative CG- flashes were observed in the late stage of the storm (Qui et al., 2005). Also there were observed that the flash rate was quite low. It is worth to note that recently the TGE detection on Tibet also was reported (Salvini, 2011).

3. PARTICLE FLUXES, ELECTRIC FIELDS AND LIGHTNING OCCURRENCES

Electric field meters[11] and lightning detectors[12] installed at Aragats as well as multipurpose weather station[13] allows to correlateTGEs with electric field disturbances, with occurrences of lightning of different types and with other meteorological conditions (rain, atmospheric pressure, temperature, humidity…). The TGE amplitude (the percentage of enhancement of particle flux relative to the rather stable background of secondary cosmic rays) was measured by the outdoor 5 and 3 cm thick, 1 m2 area plastic scintillators. Time series of particle intensity, electric field measurements, lightning occurrences and meteorological information are entering the MySql database and are visualized with ADEI multivariate visualization code[14]. Examining disturbances of near-surface electric field we outline following most typical patterns accompanied with TGE (see Figure 1):

1. Electric field reversal from positive to negative: field strength changes from large (up to 50 kV/m) positive electric field to low (down to -35 kV/m) negative value. We select 6 events of this type, see Figure a) and Table 1

[11] Boltek firm electrical mill EFM100, measurement accuracy 5%, http://www.boltek.com/efm100.html

[12] Boltek's StormTracker Lightning Detection System powered by the software from Astrogenic systems, defining 4 types of lightning occurrences (CG- , CG+ cloud-to ground negative and positive, IC-, IC_+ intracloud positive and negative, - in radius of 1, 3 and 5 km around location of its antenna, http://www.boltek.com/stormtracker

[13] Professional Davis Instruments Vantage Pro2, http://www.davisnet.com/

[14] ADEI (Advances Data Extraction Infrastructure) is AJAX based dynamic web interface facilitating browsing and extraction time-series from various data sources. http://adei.crd.yerphi.am/adei/

2. Electric field reversal from negative to positive: changes from low (down to -35 kV/m) negative electric field to large positive electric field (~50 kV/m). We select 3 events of this type, see Figure b) and Table 2.
3. Electric field's abrupt decreases: changes started from fair weather value (few hundred volts) down to large negative values (-30 kV/m); we select 5 events of this type, see Figure c) and Table 3.

Usually 3 types of TGE events were accompanied with lightning occurrence and rain; however sometimes lightnings and rain are missing.

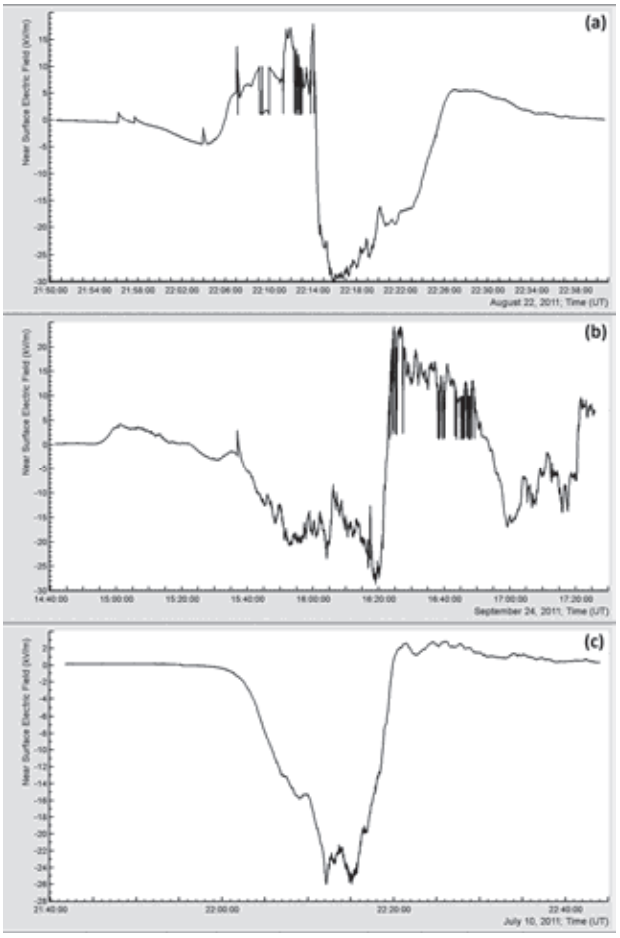

Figure 1. Three patterns of the electric field disturbances during TGE events on Aragats.

4. TGE EVENTS OF THE FIRST TYPE

During the first type of events, see Figure 2, the near-surface positive electric field reaching a strength of 40 kV/m after a series of lightning occurrences (those types are usually equally distributed among intraclaud positive and negative lightning IC+ and IC- and cloud-to-ground negative lightning CG- when the near surface electric field is positive, see Figure 3) started to reverse and simultaneously particle flux started to slowly rise at 13:10 discharging the electric field. The evolution of the surface electric field as in shown in Figure 2 suggests occurrence of the "special type thunderstorm", according to classification introduced in (Qui et al., 2009). A special-type thunderstorm suggests the long period of negative surface electric field. During this period larger in dimension and high in charge magnitude LPCR exists at the base of the storm. Electron acceleration downward is possible only if the electric field in the thundercloud is positive; i.e. if the lower dipole is formed or under formation. Lasting ~10 minutes the negative near-surface electric field coincides in time with large particle flux, proving that the positive charge region at the base of thundercloud is larger in dimension and charge magnitude. Developed LPCR creates a larger positive electric field in the cloud that increases the particle flux downward, peaking at ~13:13 when the negative field approaching minimal strength of -35 kV/m. During several minutes of particle flux maximum IC+ and CG- lightning occurrences are highly suppressed and only IC- lightnings were observed, see Figure 4. Emerging large LPCR blocks the step leader propagation to the ground and turn it to intracloud IC- flash because the abundant lower positive charge made IC-discharges energetically preferable. At 13:20 the LPCR contracted and particle flux decayed. Consequently diminished LPCR cannot block any more the lightning leader propagation to the ground and several CG- lightning occurred at 13:23 at fully stopped particle flux.

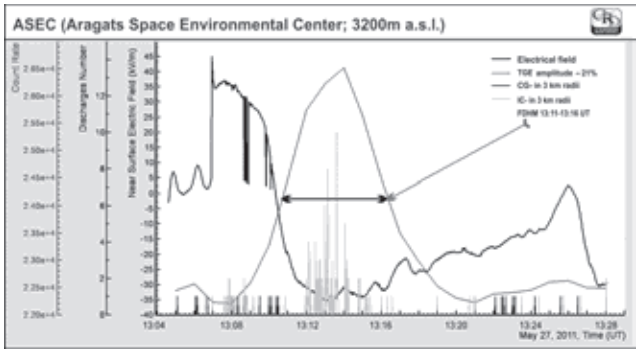

Figure 2. TGE of the first type according to pattern of the electric field disturbances; the black curve shows changing electric field; red lines - IC- lightning and blue CG- lightning occurrences within 3 km radius; the green curve shows the time series of the particle flux minutely counts. Particle flux peaked at 21% above CR background .

The information on the first type TGEs is posted in the Table 1. TGE duration comprises ~10 minutes; however sometimes we detect long lasting tails of particle fluxes. To avoid possible ambiguity we "normalize" the TGE duration by calculating the full duration of the TGE peak on the half-maximum (FDHM).

In the first column we post the date of the TGE event. The durations of the positive and negative fields with maximal and minimal field values, the full duration of the TGE peak at the half-maximum (FDHM) and TGE amplitudes present in the fourth column. In the columns 5-7 we post fractions of lightnings of different types during positive and negative fields and during FDHM in different radiuses around particle detector location (1, 3 and 5 km). Last column depicts the rain duration and rain rate, if any. As we see in Table 2 the range of the maximal values of the positive electric field varies 14 – 45 kV/m, duration 5-20 minutes. The maximal value of negative field is changing from -28 till -35 kV/m; duration 5-20 minutes.

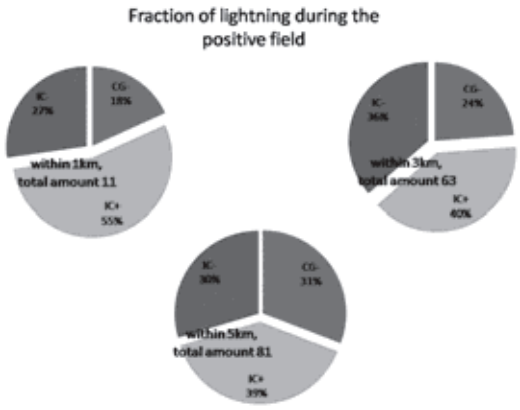

Figure 3. Fractions of lightning occurrences of different type

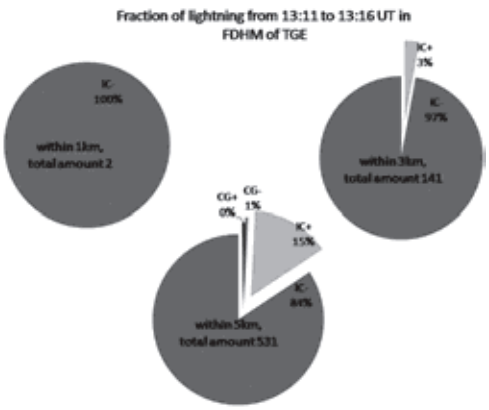

Figure 4. May 27 2011. Fractions of lightning occurrences of

Table 1 . Selected first type of TGE event according to changing pattern of the near-surface electric field

Event's date	Duration of positive field / Max value of electric field	Duration of negative field / Min value of electric field	FDHM of TGE / Flux increase (percents)	Fraction of lightnings of different type within 1km				Fraction of lightnings of different type within 3km				Fraction of lightnings of different ty within 5km			
				Time	**Positive field**	**Negative field**	**FDHM of TGE**	**Time**	**Positive field**	**Negative field**	**FDHM of TGE**	**Time**	**Positive field**	**Negative field**	**FDHM TGE**
04.10.10	18:14-18:20	18:20-18:25	18:22-18:23	**Total**	**0**	**5**	**1**	**Total**	**1**	**17**	**2**	**Total**	**3**	**32**	**9**
				IC-	0%	100%	100%	**IC-**	0%	76.5%	100%	**IC-**	66.7%	81.3%	100%
	28.8 kV/m	-28.8 kV/m	76%	**IC+**	0%	0%	0%	**IC+**	100%	11.8%	0%	**IC+**	33.3%	12.5%	0%
				GC-	0%	0%	0%	**GC-**	0%	5.8%	0%	**GC-**	0%	3.13%	0%
				GC+	0%	0%	0%	**Gc+**	0%	5.8%	0%	**Gc+**	0%	3.13%	0%
24.05.11	13:17-13:26	13:26-13:40	13:29-13:38	**Time**	**Positive field**	**Negative field**	**FDHM of TGE**	**Time**	**Positive field**	**Negative field**	**FDHM of TGE**	**Time**	**Positive field**	**Negative field**	**FDHM TGE**
				Total	**1**	**3**	**2**	**Total**	**2**	**10**	**5**	**Total**	**4**	**41**	**33**
				IC-	0%	100%	100%	**IC-**	0%	90%	80%	**IC-**	25%	61.0%	58%
	22.15 kV/m	-35.2 kV/m	3%	**IC+**	0%	0%	0%	**IC+**	0%	10%	20%	**IC+**	25%	34%	39%
				GC-	100%	0%	0%	**GC-**	100%	0%	0%	**GC-**	50%	4.87%	3%
				GC+	0%	0%	0%	**GC+**	0%	0%	0%	**GC+**	0%	0%	0%
27.05.11	13:05-13:10	13:10-13:25	13:11-13:16	**Time**	**Positive field**	**Negative field**	**FDHM of TGE**	**Time**	**Positive field**	**Negative field**	**FDHM of TGE**	**Time**	**Positive field**	**Negative field**	**FDHM TGE**
				Total	**10**	**9**	**2**	**Total**	**60**	**173**	**141**	**Total**	**74**	**735**	**531**
				IC-	30%	33%	100%	**IC-**	38%	86%	97%	**IC-**	32%	77.1%	84%
	45 kV/m	-35.5 kV/m	21%	**IC+**	60%	22%	0%	**IC+**	38%	6.9%	3%	**IC+**	39%	20%	14.9%
				GC-	10%	44%	0%	**GC-**	23%	5.8%	0%	**GC-**	28%	2.30%	0.6%
				GC+	0%	0%	0%	**GC+**	0%	1.70%	0%	**GC+**	0%	0.50%	0.2%
15.07.11	21:05-21:23:45	21:23:46-21:41:06	21:26-21:35	**Time**	**Positive field**	**Negative field**	**FDHM of TGE**	**Time**	**Positive field**	**Negative field**	**FDHM of TGE**	**Time**	**Positive field**	**Negative field**	**FDHM TGE**
				Total	**0**	**10**	**8**	**Total**	**0**	**146**	**104**	**Total**	**0**	**383**	**328**
				IC-	0%	100%	100%	**IC-**	0%	80.0%	97%	**IC-**	0%	88%	97%
	14.05kV/m	-29.3kV/m	2.44%	**IC+**	0%	0%	0%	**IC+**	0%	8.9%	2%	**IC+**	0%	7%	2%
				GC-	0%	0%	0%	**GC-**	0%	8.9%	0%	**GC-**	0%	4%	0%
				GC+	0%	0%	0%	**GC+**	0%	2.0%	1%	**GC+**	0%	1%	1%
22.08.11	22:06-22:14	22:14-22:25	22:14-22:20	**Time**	**Positive field**	**Negative field**	**FDHM of TGE**	**Time**	**Positive field**	**Negative field**	**FDHM of TGE**	**Time**	**Positive field**	**Negative field**	**FDHM TGE**
				Total	**0**	**17**	**15**	**Total**	**0**	**26**	**20**	**Total**	**0**	**32**	**22**
				IC-	0%	94.1%	100%	**IC-**	0%	88.5%	100%	**IC-**	0%	87.5%	100%
	17.9 kV/m	-29.95 kV/m	8%	**IC+**	0%	0%	0%	**IC+**	0%	3.85%	0%	**IC+**	0%	6.25%	0%
				GC-	0%	5.89%	0%	**GC-**	0%	7.70%	0%	**GC-**	0%	6.25%	0%
				GC+	0%	0%	0%	**GC+**	0%	0%	0%	**GC+**	0%	0%	0%
20.09.11	10:08:34-10:19:45	10:19:47-10:40:30	10:22-10:28	**Time**	**Positive field**	**Negative field**	**FDHM of TGE**	**Time**	**Positive field**	**Negative field**	**FDHM of TGE**	**Time**	**Positive field**	**Negative field**	**FDHM TGE**
				Total	**0**	**30**	**0**	**Total**	**0**	**65**	**6**	**Total**	**0**	**221**	**31**
				IC-	0%	20%	0%	**IC-**	0%	28%	98%	**IC-**	0%	44%	65%
	21.05 kV/m	-29.45 kV/m	2.55%	**IC+**	0%	37%	0%	**IC+**	0%	31%	2%	**IC+**	0%	32%	23%
				GC-	0%	40%	0%	**GC-**	0%	34%	0%	**GC-**	0%	19%	10%
				GC+	0%	3%	0%	**GC+**	0%	8%	0%	**GC+**	0%	5%	3%

TGE amplitude changes from 2.5 till 76%, FDHM is usually 4-9 minute, only once it falls to 1 minute for the super TGE at October 4, 2010.

The circular diagrams (Figure 3 and 4) demonstrate the frequencies of lightning occurrences at positive and negative near-surface electric field. The pattern of frequencies is drastically different. If at positive field the share of 3 types of lightning occurrences (intracloud positive and negative and cloud-to-ground negative) is approximately equal, at negative field we detect strong suppression of CG- and IC+ lightning occurrences (positive cloud-to-ground lightning IC+ is rather a rare occasion). In the just vicinity of particle detectors we detect only IC- lightnings, with enlarging the radius around the detection site other types of lightnings occur; however their fraction was negligible, only once reaching 20% (IC+ type at 24 May, 2011 in 3 km radius). The total number of lightning occurrences was very moderate within 1 km radius ranging from 3 to 30; confirming the results of the Tibet plateau lightning occurrences study (Qui et al., 2005) in 3 km radius the range is significantly larger: from 10 till 146 during negative near-surface electric field. This founding supports resent results of the Japanese groups measuring the size of the radiation region within the thundercloud to be ~1 km (Tsuchiya, 2011, Torii, 2011).

5. TGE EVENTS OF THE SECOND TYPE

During the second type of the TGE events, see Figure 5, the near-surface electric field gradually decreases from the near-zero value at 15:40 UT and remain in the negative domain near 40 minutes. At 16:10 – 16:22 UT particle flux reaches maximum of 8%, electric field peaks -28 kV/m at 16:19 UT and simultaneously we observe highly enlarged lightning occurrences, see Figure 6, mostly of the IC- type, CG- lightning occurrences again were suppressed. At 16:24 UT abrupt reversal of the field occurred and positive field peaked on 24.2 kV/m at 16:26 UT. The pattern of the lightning occurrences changed accordingly; see Figures and 6 and 7.

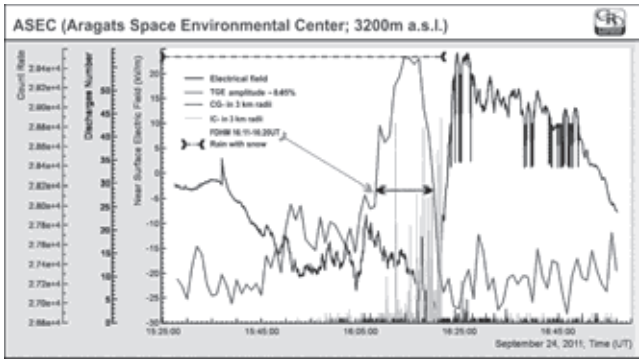

Figure 5. TGE of the second type according to pattern of the electric field disturbances; the black curve shows changing electric field; red lines - IC- lightning and blue CG- lightning occurrences within 3 km; the green curve - the time series of the particle flux minutely counts. Particle flux peaked at 8% above CR background .

In Figures 6 and 7 were depicted the frequencies of lightning occurrences around the maximum of TGE and during positive near-surface electric field. As we see the second type of events is different from the first one. Around the time of maximal particle flux we detect the lightnings of all types, although the fraction of the IC- lightnings is again overwhelming. During positive near-surface electric field we detect all types of lightnings including positive cloud-to-ground lightning (CG+) almost missing in type 1 events.

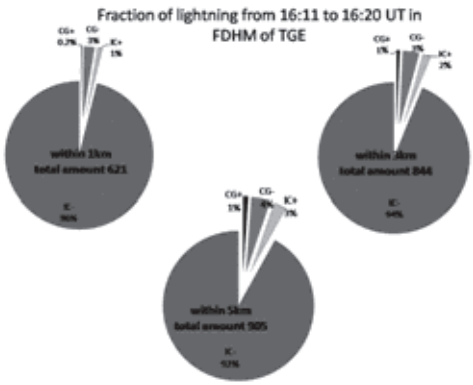

Figure 6. Fractions of lightning occurrences of different type in FDHM of TGE (16:11-16:20 UT); negative field peaked - 28.65kV/m at 16:19:06 UT.

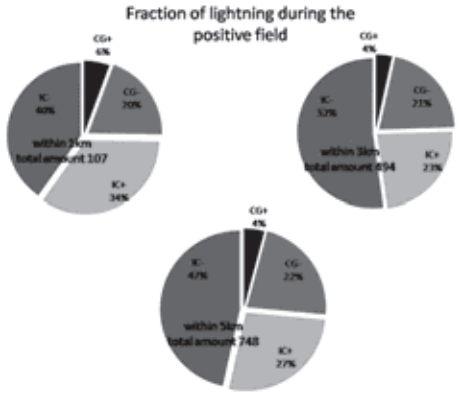

Figure 7. Positive field duration is 16:22:47-16:53:36 UT; max value is 24.2kV/m at 16:26:48 UT. TGE ended at 16:22 UT.

We registered 3 events of the second type, see Table 2; the Table filling is the same as Table 1. Depend on distance fractions of lightnings changed insignificantly. In the vicinity of particle detectors we detect plenty IC- lightnings, with enlarging the radius other types of lightnings occur. All 3 TGE started during negative field; field strength is changing from -32 to -18 kV/m; duration range is 20-45 minutes. The range of the positive electric field is 12 – 25 kV/m, duration - 7-30 minutes. TGE amplitude changes from 2.8 till 8%, FDHM is changing from 7 till 9 minutes. Very large numbers of lightnings were registered on September 24 2011; considerable fraction was registered in the minute of peak of the particle flux; most of them were IC-. The rain started during negative field and ended with TGE fading. On September 25 2011 during negative field we registered a large number of IC- lightnings, however during positive field we did not register any lightning. This day the rain started during the positive field. On October 17 we have very few lightning occurrences. Naturally, numbers of lightnings of all types increased depending on the growth of the distance.

Table 2. Selected second type of TGE event according to changing pattern of the near-surface electric field

Event's date	Duration of negative field	Duration of positive field	FDHM of TGE	Fraction of lightnings of different type within 1km				Fraction of lightnings of different type within 3km				Fraction of lightnings of different type within 5km				Rain duration
	Min value of electric field	Max value of electric field	Flux increase (percents)													Rain rate
24.09.11	15:37:24-16:22:46	16:22:47-16:53:36	16:11-16:20	**Time**	**Negative field**	**Positive field**	**FDHM of TGE**	**Time**	**Negative field**	**Positive field**	**FDHM of TGE**	**Time**	**Negative field**	**Positive field**	**FDHM of TGE**	15:17-16:26
				Total	**1207**	**107**	**621**	**Total**	**1606**	**494**	**844**	**Total**	**1818**	**748**	**905**	
				IC-	94.5%	40.1%	96%	**IC-**	90.5%	52.2%	94%	**IC-**	86.9%	46.5%	92%	
	-28.6kV/m	24kV/m	8.05%	**IC-+**	1.8%	34.6%	1%	**IC-+**	3.1%	23.3%	2%	**IC-+**	5.0%	27.0%	3%	
				GC-	2.1%	19.6%	3%	**GC-**	4.3%	21.1%	3%	**GC-**	5.7%	22.3%	4%	
				GC+	1.5%	5.6%	0.2%	**GC+**	2.1%	3.4%	1%	**GC+**	2.4%	4.1%	1%	
25.09.11	11:30:40-11:53:07	11:53:09-12:08:45	11:38-11:47	**Time**	**Negative field**	**Positive field**	**FDHM of TGE**	**Time**	**Negative field**	**Positive field**	**FDHM of TGE**	**Time**	**Negative field**	**Positive field**	**FDHM of TGE**	11:58-12:37
				Total	**356**	**0**	**176**	**Total**	**564**	**5**	**271**	**Total**	**678**	**22**	**360**	
				IC-	96%	0%	98%	**IC-**	95%	60%	94.5%	**IC-**	90%	27%	86.1%	
	-32kV/m	12kV/m	3.74%	**IC-+**	1%	0%	2%	**IC-+**	3%	40%	5.2%	**IC-+**	8%	50%	13.6%	
				GC-	1%	0%	0%	**GC-**	1%	0%	0.4%	**GC-**	1%	14%	0.3%	
				GC+	1%	0%	0%	**GC+**	1%	0%	0%	**GC+**	1%	9%	0%	
17.10.11	13:41:40-14:01:17	14:01:18-14:07:34	13:50-13:56	**Time**	**Negative field**	**Positive field**	**FDHM of TGE**	**Time**	**Negative field**	**Positive field**	**FDHM of TGE**	**Time**	**Negative field**	**Positive field**	**FDHM of TGE**	
				Total	**1**	**0**	**1**	**Total**	**2**	**0**	**2**	**Total**	**10**	**1**	**4**	no
				IC-	100%	0%	100%	**IC-**	50%	0%	50%	**IC-**	30%	0%	50%	
	-18kV/m	25kV/m	2.82%	**IC+**	0%	0%	0%	**IC+**	50%	0%	50%	**IC+**	50%	0%	50%	
				GC-	0%	0%	0%	**GC-**	0%	0%	0%	**GC-**	10%	100%	0%	
				GC+	0%	0%	0%	**GC+**	0%	0%	0%	**GC+**	10%	0%	0%	

6. TGE EVENTS OF THE THIRD TYPE

During the third type of events, see Figure 8, the near-surface electric field gradually decreases from the near-zero value at 22:00 UT and remain in the negative domain near 20 minutes, peaking -26 kV/m at 22:12 and 22:15 UT; the particle flux starts to rise and peak at 3.6% at 22:13 UT. After the start of the rain the negative field very fast returns to near-zero value and consequently particle flux stopped.

IC- lightning occurrences started at maximum of particle flux and continued till flux faded. CG- lightning occurrences were not detected; IC+ lightnings occurred within 3 km radius around the particle detector location, see Figure 9.

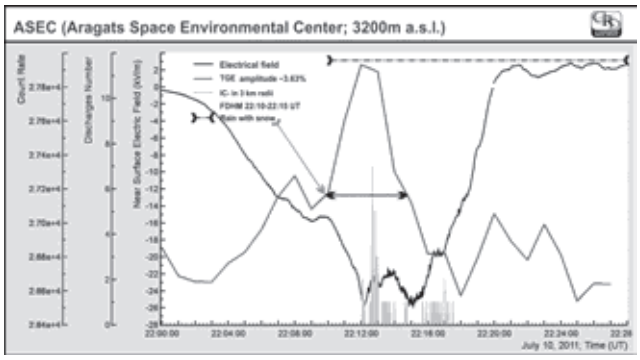

Figure 8. TGE of the third type according to pattern of the electric field disturbances; the black curve shows changing electric field; red lines - IC- occurrences within 3 km; the green curve - the time series of the particle flux minutely counts. Particle flux peaked at 3.6% above CR background . Rain was detected during 22:15-22:35 UT.

The third type of TGEs differs from the others as lightnings were registered only during the particle flux. We detect 5 events of the third type, during some of them large number of lightnings were registered see Table 3.

As we see in **Error! Reference source not found.** the value of the negative electric field varies from -34.5 to -18 kV/m, duration was - 25-55 minutes. TGE amplitude changes from 2.27 till 12%, FDHM of TGE varies from 4 till 9 minutes. In two events we detected 100% IC- lightnings in 1 and 3 km radius. During the other events fraction of IC- lightnings predominate and lightning occurrences of CG- and IC+ were suppressed see Table 3.

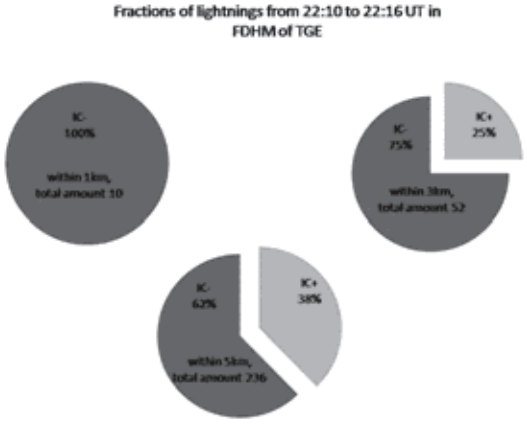

Figure 9. Fractions of lightning occurrences of different type in FDHM of TGE (16:11-16:20 UT); negative field peaked -28.65kV/m at 16:19:06 UT.

7. CONCLUSION

Incorporation of the information on the changing particle fluxes measured during thunderstorms proves the model of LPCR as it was formulated in the points a) and b) of section 2. LPCR and lower dipole are transient and local phenomena; LPCR is created during minutes, with consequent acceleration of electrons in lower dipole resulting in enlarged particle flux (TGE). Particle flux is a measure of the LPCR maturity; it reaches maximum at the largest LPCR size and decays on LPCR contracting fully agreeing with foundlings made in Tibet (Qui et al., 2005, 2009). The negative polarity signals that the LPCR is creating and with developing of LPCR the particle flux has consequently been rising; simultaneously mature LPCR prevents negative CG- flashes due to abundant lower positive charge making intraclaud IC- flashes preferable (see also Nag and Rakov, 2009). The negative CG-discharges occurred in the late stage of the storm on the degradation of the LPCR when particle flux stopped. Therefore, scenarios a) and b) of the section 2 are enabled successively during one and the same thunderstorm. Aragats thunderstorm data also confirm founding from Tibetan thunderstorms that emerged LPCR did not cause positive CG+ flashes. The characteristic time scale of maturing the LPCR is ~10 minutes coinciding with estimates from thunderstorms at Tibet plateau.

The technique of measuring particle fluxes simultaneously with near-surface electric field and lightning occurrences of different types first developed and used on Aragats allows following up the creation of the LPCR and its contraction. The maximal flux of gamma rays detected at the surface (and corresponding maximal flux of the electrons within the lower dipole) pointed at the maximal positive electric field in the cloud and, correspondingly on the maximal dimension and charge of the LPCR. The distance between the main negatively charged layer in the middle of a cloud and LPCR should be significantly larger to provide large potential drop necessary for the electron acceleration. Fading of the gamma ray flux evidences the degradation of the LPCR. Measured particle flux along with registered lightning occurrences of the different type allows researching the fine structure of the thunderstorm, including the time evolution of the LPCR and ongoing processes of intracloud lightning initiation and electron avalanche propagation.

In several events the particle fluxes (TGEs) precede lightning occurrences, thus demonstrating that downward moving streamer can use the conductive channel opened by the downward electron-gamma ray avalanche (see Smith et al., 2010); however for some of TGEs the frequency of lightning occurrences at maximal particle flux is very low signaling that in some circumstances the particle acceleration and IC- lightning occurrences can compete.

8. ACKNOWLEDGEMENT

Authors highly appreciate the discussions of the topics related to the presented letter at seminars of the cosmic ray division of Alikhanyan national lab. Arakelyan Karen and Pokhsraryan David were instrumental in installing and preparing software for treating of the time series of electric field and lightning measurements. Reymers Artur provides

data transfer from the particle detectors to databases at CRD headquarters. Suren Chilingaryan tuned ADEI data visualization code for cosmic ray monitoring. Narine Khachatryan designed figures. To all of them authors express gratitude for fruitful collaboration.

Table 3. Selected third type of TGE event according to changing pattern of the near-surface electric field.

Event's date	Duration of negative field Min value of electric field	FDHM of TGE Flux increase (percents)	Fraction of lightnings of different type within 1km		Fraction of lightnings of different type within 3km		Fraction of lightnings of different type within 5km		Rain duration Rain rate
07.05.11	20:35-21:30	21:11-21:15	**Time**	**FDHM of TGE**	**Time**	**FDHM of TGE**	**Time**	**FDHM of TGE**	missing data
			Total	**235**	**Total**	**1002**	**Total**	**1089**	
			IC-	96.2%	**IC-**	98.2%	**IC-**	98.2%	
	-34.5 kV/m	4.36%	**IC+**	21.27%	**IC+**	1.3%	**IC+**	1.28%	
			GC-	1.07%	**GC-**	0.4%	**GC-**	0.37%	
			GC+	0%	**GC+**	0.1%	**GC+**	0.18%	
08.05.11	01:43-02:09	01:45-01:51	**Time**	**FDHM of TGE**	**Time**	**FDHM of TGE**	**Time**	**FDHM of TGE**	missing data
			Total	**6**	**Total**	**157**	**Total**	**266**	
			IC-	50%	**IC-**	92.4%	**IC-**	93%	
	-32 kV/m	7.50%	**IC+**	0%	**IC+**	0.6%	**IC+**	1%	
			GC-	50%	**GC-**	5.7%	**GC-**	5%	
			GC+	0%	**GC+**	1.3%	**GC+**	1%	
10.07.11	21:56-22:20	22:10-22:15	**Time**	**FDHM of TGE**	**Time**	**FDHM of TGE**	**Time**	**FDHM of TGE**	22:15-22:35
			Total	**8**	**Total**	**50**	**Total**	**234**	
			IC-	100%	**IC-**	74%	**IC-**	62%	
	-26.05 kV/m	4.36%	**IC+**	0%	**IC+**	26%	**IC+**	38%	
			GC-	0%	**GC-**	0%	**GC-**	0%	
			GC+	0%	**GC+**	0%	**GC+**	0%	
13.10.11	11:24-11:50	11:32-11:39	**Time**	**FDHM of TGE**	**Time**	**FDHM of TGE**	**Time**	**FDHM of TGE**	short time
			Total	**103**	**Total**	**112**	**Total**	**115**	
			IC-	100%	**IC-**	100%	**IC-**	99%	
	-29.5 kV/m	12.00%	**IC+**	0%	**IC+**	0%	**IC+**	1%	
			GC-	0%	**GC-**	0%	**GC-**	0%	
			GC+	0%	**GC+**	0%	**GC+**	0%	
25.10.11	23:08-23:37	23:24-23:33	**Time**	**FDHM of TGE**	**Time**	**FDHM of TGE**	**Time**	**FDHM of TGE**	no rain
			Total	**346**	**Total**	**503**	**Total**	**719**	
			IC-	100%	**IC-**	100%	**IC-**	100%	
	-18.55kV/m	2.27%	**IC+**	0%	**IC+**	0%	**IC+**	0%	
			GC-	0%	**GC-**	0%	**GC-**	0%	
			GC+	0%	**GC+**	0%	**GC+**	0%	

REFERENCES

Babich, L. P., Kutsyk I.M., Donskoy E. N., and Kudryavtsev A. Y., New data on space and time scales of a relativistic runaway electron ava- lanche for thunderstorms environment: Monte Carlo calculations, Phys. Lett. A, 245, 460–470 (1998).

Babich, L.P., Bochkov E.I., Kutsyk I.M., Numerical simulation of a conducting channel initiated by an extensive air shower in a thunderstorm electric field, Geomagn. Aeron. 49(2), 232–238 (2009)

Babich, L.P., Bochkov E.I., Kutsyk I.M., Lightning initiation mechanism based on the development of relativistic runaway electron avalanches triggered by background cosmic radiation: Numerical simulation, J. Exp. Theor. Phys. 112, 902–909 (2011)

Chilingarian, A., Arakelya, K., Avakyan, K., et al.: Correlated mea- surements of secondary cosmic ray fluxes by the Aragats Space – Environmental Center monitors, Nucl. Instrum. Methods Phys. Res., Sect. A, 483–496 (2005).

Chilingarian, A., Avakyan, K., Babayan, V., et al.: Aragats Space- Environmental Center: status and SEP forecasting possibilities, J. Phys. G: Nucl. Part. Phys., 29, 939–952 (2003).

Chilingarian, A., et al., Ground-based observations of thunderstorm-correlated fluxes of high-energy electrons, gamma-rays, and neutrons, Phys. Rev. D, 82: 043009 (2010).

Chilingarian, A., G. Hovsepyan and A.Hovhannisyan, Particle bursts from thunderclouds: Natural particle accelerators above our heads, Phys. rev. D, 83, 062001 (2011).

Chilingarian A., Mailyan B., Vanyan L., *Recovering of the energy spectra of electrons and gamma rays coming from the thunderclouds*, Atmospheric Research 114–115, 1–16, (2012).

Holden, D. N., C. R. Holmes, C. B. Moore, W. P. Winn, J. W. Cobb, J. E. Griswold, and Lytle D. M., Local charge concentration in thunderclouds, in Sixth International Conference on Atmospheric Electricity, University of Manchester, Manchester, England, (1980).

Dwyer J.R., Smith D.M., Cummer S.A., High-Energy Atmospheric Physics: Terrestrial Gamma-Ray Flashes and Related Phenomena, Space Sci Rev, DOI 10.1007/s11214-012-9894-0, 2012.

Dwyer J.R., Babich, L., Low-energy electron production by relativistic runway electron avalanches in air, J. Geophys. Res. 116, A09301 (2011).

Gurevich, A.V., G.M. Milikh, and R.A. Roussel-Dupré (1992), Runaway electron mechanism of air breakdown and preconditioning during a thun- derstorm, Phys. Lett. A, 165, 463, doi:10.1016/0375-9601(92)90348-P.

Gurevich A.V., Milikh G.M., R.A. Roussel-Dupré, Nonuniform Runaway Air-Breakdown, Phys. Lett. A 187, 197–203 (1994).

Gurevich A.V., Milikh G.M., Generation of x-rays due to multiple runaway breakdown inside thunderclouds,, Phys. Lett. A 262, 457–463 (1999).

Gurevich, A.V., Duncan L.M., Karashtin A.N., Zybin K.P., Runaway Breakdown and the Mysteries of Lightning, Phys. Lett. A 312, 228–237 (2003).

Marshall and T.C. Winn P.W., Measurements of Charged Precipitation in a New Mexico Thunderstorm' Lower Positive Charge Centers, JGR, 87, 7141-7157 (1982).

Moore, C. B., and B. Vonnegut, The thundercloud, in Lightning, edited by R. H. Golde, Academic, New York, (1977).

Nag, A., and V. A. Rakov, Some inferences on the role of lower positive charge region in facilitating different types of lightning, Geophys. Res. Lett., 36, L05815 (2009).

Qie, X., T. Zhang, G. Zhang, T. Zhang, and W. Wei, The lower positive charge center and its effect on lightning discharges on the Tibetan Plateau, *Geophys. Res. Lett.*, *32*, L05814, (2005).

Qie, X., T. Zhang, C. Chen, G. Zhang, T. Zhang, and Kong X., Electrical characteristics of thunderstorms in different plateau regions of China, Atmospheric Research 91 244–249 (2009).

Pawar S. D. and Kamra A. K., Evolution of lightning and the possible initiation/triggering of lightning discharges by the lower positive charge center in an isolated thundercloud in the tropics, *J. Geophys. Res.*, 109, D02205, (2004).

Salvini P., Study of the correlation between atmospheric electric field variations measured on the ground and cosmic rays by the ARGO-YBJ experiment, Proceedings of the workshop, Aragats-2011, Nor Amberd, Armenia, (2011).

Simpson,G., and F. J. Scrase,The distributionof electricityin thunderclouds, Proc.R. Soc.London, Ser.A, 161,309-352 (1937).

Smith, D. M., et al.,J. Geophys. Res., 115, A00E49, (2010).

Steiger S M, Orville R E and Carey L., Total lightning signatures of thunderstorm intensity over north Texas. Part I: Supercells; Mon. Weather Rev. 135 3281–3302 D (2007).

Torii, T., Sugita, T., Kamogawa, M. et al., Migrating source of energetic radiation generated by thunderstorm activity, Geophys. Res. Lett. 38, L24801, (2011).

Tsuchiya, H., Enoto, T., Yamada, S. et al., Long-duration gamma ray emissions from 2007 and 2008 winter thunderstorms, J. Geophys. Res. 116, D09113 (2011).

Williams E. R.,Weber M.E., Orville R.E., The Relationship Between Lightning Type and Convective State of Thunderclouds, JGR, 94, 13,213 – 13,220 (1989).

Williams E. R.,: The electrification of severe storms. *Severe Convective Storms*, *Meteor. Monogr.*, No. 50, Amer. Meteor. Soc., 527–561 (2001).

PHYSICAL REVIEW D **82,** 043009 (2010)

Ground-based observations of thunderstorm-correlated fluxes of high-energy electrons, gamma rays, and neutrons

A. Chilingarian,* A. Daryan, K. Arakelyan, A. Hovhannisyan, B. Mailyan, L. Melkumyan, G. Hovsepyan, S. Chilingaryan, A. Reymers, and L. Vanyan

Artem Alikhanyan National Laboratory, Alikhanyan Brothers 2, Yerevan 36, Armenia

(Received 28 April 2010; published 23 August 2010)

The Aragats Space Environmental Center facilities continuously measure fluxes of neutral and charged secondary cosmic ray incidents on the Earth's surface. Since 2003 in the 1-minute time series we have detected more than 100 enhancements in the electron, gamma ray, and neutron fluxes correlated with thunderstorm activities. During the periods of the count rate enhancements, lasting tens of minutes, millions of additional particles were detected. Based on the largest particle event of September 19, 2009, we show that our measurements support the existence of long-lasting particle multiplication and acceleration mechanisms in the thunderstorm atmosphere. For the first time we present the energy spectra of electrons and gamma rays from the particle avalanches produced in the thunderstorm atmosphere, reaching the Earth's surface.

DOI: 10.1103/PhysRevD.82.043009 PACS numbers: 92.60.Pw, 13.40.−f, 94.05.Dd, 96.50.S−

I. INTRODUCTION

Charles Thompson Rees Wilson in 1924 [1] realized that a "particle started with suitable velocity in the electrical field of the thundercloud may be expected to continue to acquire kinetic energy at the rate of many thousand volts per cm." In 1992 Alexander Gurevich, Gennady Milikh, and Robert Roussel-Dupre [2] introduced the theory of the generation of fast "runaway" electrons from the MeV electrons of the extensive air showers (EAS) initiated by the energetic proton or nuclei incident on the top of the atmosphere. However, the nature of seed particles is still under debate; an alternative source of the seed particles is connected with the lightning leaders [3,4]. Although there is no exact measurements yet of the possible strength of the electric field, in [5] it was suggested that streamer heads can produce fields up to several tens of millions volts per meter. The electrical fields in the thunderstorm atmosphere gave the cosmic ray shower and/or electrons from the lightning leaders a boost by increasing the number of energetic particles through a multiplication process initially called runaway breakdown (RB), and now referred to as relativistic runaway electron avalanche (RREA) [6–8]. The RREA mechanism can create large amounts of high-energy electrons and subsequently the gamma rays, as well as x rays and neutrons. Unfortunately, this model has not yet been able to demonstrate the creation of the hot plasma channel and lightning itself.

Astonishingly, the physical processes in the low atmosphere were observed by the orbiting gamma observatories at 400–600 km above the Earth's surface. Terrestrial gamma flashes (TGF), very short (tens of μ sec) bursts of high-energy gamma rays, have been routinely observed by satellite gamma ray detectors during the last 20 years (see Ref. [9]). Recently the TGF have been observed in correlation with strong thunderstorms in the equatorial regions [10]. The spectra of the flashes are roughly expressed by a power-law function with an exponential decaying term; some of them extending up to several tens of MeV. In Ref. [7] these events were interpreted as by-products of the massive number of runaway electrons being generated within thunderclouds.

Surface detections of the RREA process, although having a long history, are discrepant and rare. Early measurements [11,12] discovered the existence of electron flux simultaneously, or earlier, than lightning located 30 kms apart. Atop Mt. Lemmon (altitude 2800 m) at the lightning research facility of the University of Arizona, the simultaneous detection of the cosmic ray flux (by the 10-cm diameter and 10-cm length plastic scintillator) and electrical field (by an electrical field mill) demonstrate ~10% enhancement of the 1-minute count [13]. The average excess duration was ~10 minutes; the threshold energy of the particle detector ~100 keV. The Italian EAS-TOP surface array [14] measures significant excesses in the air shower counting rate lasting 10–20 minutes. The enhancements with maximum amplitude of 10%–15% were attributed mostly to highest energy EAS (large shower sizes, $>10^6$ electrons), and to zenith angles of incidence smaller than 20°; "thickness" (time distribution of the EAS particles arrival) of shower was slightly larger than in normal conditions [15].

A radiation monitoring post in a nuclear power plant in Japan reports on a comprehensive observation of a gamma ray burst emission lasting less than 1 min—correlated with snow and lightning activity. Enhancements were detected only during winter time, when thunderclouds are as low as several hundred meters [16]. The summer thunderstorm was observed by the same group at the top of Mt. Fuji (3776 m high). The flux of high-energy gamma rays had a

*chili@aragats.am

continuous energy spectrum up to 10 MeV, prolonged up to 20 min. The authors of [17] claim that the bremsstrahlung photons generated by the energetic electrons were produced continuously due to an intense electric field in the thundercloud rather than having originated in the process of lightning discharge.

A Japanese group on another Japanese power plant also detected short (less than 1 min) gamma bursts during winter thunderstorms [18]. The same authors reported a simultaneous detection of gamma rays and electrons at a mountain observatory Norikura located 2770 m above sea level [19]. Two emissions, lasting 90 sec, were associated with thunderclouds. At the same research station, Norikura in the Japanese Alps operates a large multilayered particle detector, primarily intended to register solar neutron events. In August 2000 on account of thunderstorms, particle flux enhancement was detected in 3 layers of a 64 m^2 area detecting system [20].

In experiments at the Baksan Neutrino Observatory of the Institute for Nuclear Research, the time series of cosmic rays are continuously measured along with precise measurements being taken of the electric field and monitoring of thunderstorms [8]. Intensity changes of the soft cosmic rays (below 30 MeV) and hard cosmic rays (>100 MeV) were studied [21]. It was shown that the critical field and particle energy for this process are $\sim$300 kV/m and $\sim$10 MeV, respectively [8].

The network of the NaI detectors along with EAS triggering system is located at Tien-Shan Cosmic Ray station of the Lebedev Physics Institute, at altitude 3340 m. The goal of the research is to detect runaway breakdown initiated by EAS with energy above 1000 TeV—so-called RB-EAS discharge. Based on short gamma flashes (less that 200 μ sec) detected by the network of gamma detectors, the authors of [22] claim that RB-EAS is a rather rare event ($\sim 1\%$ of all EAS registered during thunderstorms) requiring coincidence of several conditions, the most important of them being that the strong electrical field should be located not higher than 400–500 m above the detector.

The neutron production was claimed to correlate with the lightning process [23]; however, the mechanism by which neutrons can be generated by the lightning plasma are not well understood or even formulated [24]. The photonuclear reactions caused by gamma rays originated by bremstrahlung of the RREA electrons can be the origin of the neutron enhancements. On the other hand, absorption of neutrons in the dense lower atmosphere is so strong that the photonuclear neutron yield seems to be insufficient to account for the increase of neutron flux observed on the Earth's surface [25].

From the brief review above, it is apparent that many major problems connected with particle multiplication and acceleration in the thunderstorm atmosphere remains unsolved. Usually only one of the secondary cosmic ray species is measured; the additional particle flux is not too large and the number of detected "thunderstorm particle events" is very modest. Available experimental data cannot yet provide sufficient information to confirm the RREA theory. The energy spectra of RREA electrons and gamma rays are derived from a number of simulations; however, the experimental evidence is lacking till now.

Ground-based observations by a variety of the surface particle detectors systematically and repeatedly measuring the gamma rays, electrons, muons, and neutrons from atmospheric sources are necessary for answering these and other questions concerning high-energy phenomena in the atmosphere. Energy spectra and correlations between different particle fluxes, measured on the Earth's surface, address the important issues of where this radiation and particles come from and what kind of role they play in the lightning initiation.

The particle detectors of the Aragats Space Environment Center (ASEC) [26,27] observe charged and neutral fluxes of secondary cosmic rays by the variety of particle detectors located in Yerevan (1000 m a.s.l.) and on slopes of Mt. Aragats at altitudes 2000 and 3200 m. ASEC detectors measure particle fluxes with different energy thresholds and angles of incidence as well as EAS initiated by primary proton or stripped nuclei with energies greater than 50–100 TeV. Numerous thunderstorm-correlated events, detected by the ASEC facilities, constitute a rich experimental set to investigate the high-energy phenomena in the thunderstorm atmosphere. In this paper we will discuss the largest ever measured enhancement of cosmic ray fluxes on the Earth's surface, which occurred on September 19, 2009, at Mt. Aragats in Armenia.

II. PARTICLE DETECTORS OF THE ARAGATS SPACE ENVIRONMENTAL CENTER

The Aragats Space Environmental Center [26,27] of the Yerevan Physics Institute is located on the highland 3250 m above sea level, 5 km from the southern peak of Aragats (3750 m), near a large lake. The thunderstorm activity on Aragats is extremely strong in May–June. Sometimes, lightning continuously hits the ground in the vicinity of the station during an hour or longer. Thunderstorm clouds are usually below the southern peak (i.e., not higher than 500 m above) and sometimes 100–200 m above the station.

Along with solar modulation effects, ASEC detectors register several coherent enhancements associated with thunderstorm activity. Nearly 50 such events detected in 2007–2009, at solar cycle minimum, unambiguously pointed on the thunderstorm-correlated particle acceleration and multiplication. The experimental techniques used allowed for the first time to simultaneously measure fluxes of the electrons, muons, gamma rays, and neutrons correlated with thunderstorm activity[28].

Most of particle detectors are located in the MAKET building (see Fig. 1) and nearby. Along with 16 plastic

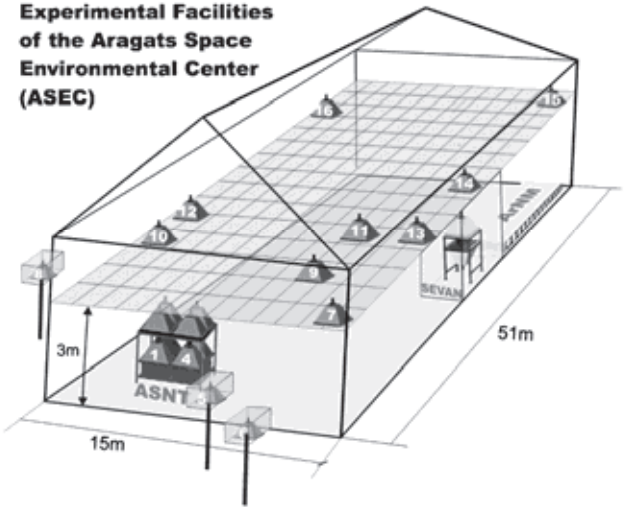

FIG. 1 (color online). The MAKET building at Aragats station, now hosting also ASNT, SEVAN, ArNM detectors, 3250 m above sea level.

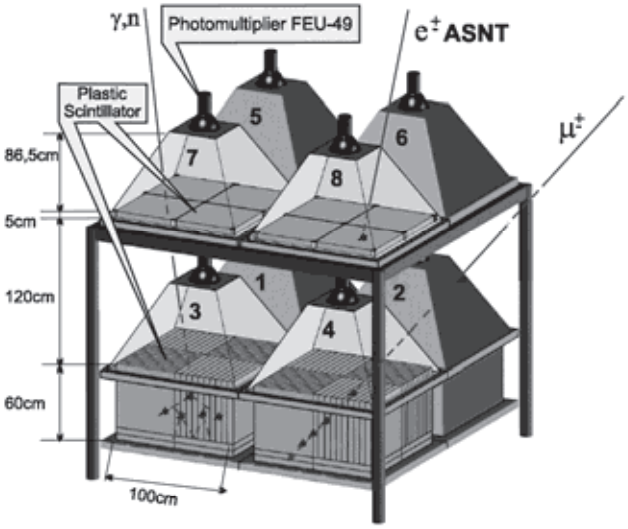

FIG. 2 (color online). Aragats Solar Neutron Telescope (ASNT).

scintillators belonging to the already finished MAKET-ANI surface array, in operation are Aragats Solar Neutron Telescope (ASNT); Aragats Neutron Monitor (ArNM) of 18NM64 type; and SEVAN (Space Environmental Viewing and Analysis Network) particle detectors. ArNM is detecting neutrons and ASNT and SEVAN are both neutral and charged species of the fallen secondary cosmic ray flux. Detailed descriptions of these particle detectors and appropriate references are presented in the following subsections.

A. Aragats Solar Neutron Telescope

Aragats Solar Neutron Telescope (ASNT, see Fig. 2) is part of the worldwide network coordinated by the Nagoya University (see details in [29]) aiming primarily to measure the fluxes of the neutrons born in the violent solar flares. In 2006, after setting up new data acquisition electronics [30], ASNT measures stopping particle energy in the range 7–120 MeV.

Histograms of the energy releases in the thick scintillators are measured and stored each minute, providing the exact pattern of the energy releases during solar transient events and during thunderstorms. The ASNT consists of 4 up and 4 bottom scintillators, each having the area of 1 m^2. The distance between layers is ~1.2 m. The data acquisition system can register all coincidences of detector signals from the upper and lower layers, thus, enabling measurements of the arrival of the particles from different directions. The signals ranging from 0.5 mV to 5 V, from each of 8 photomultipliers, are passed to the programmable threshold discriminators. The output signals are fed in parallel to the 8-channel logical OR gate triggering device and to a buffer. If there is a signal in the channel we will denote it by 1 and the channels that were not fired within the "opening" of the gate ($\sim 1\ \mu$ sec) by 0. The ASNT trigger condition is defined by detecting at least one signal in the 8 data channels. The trigger rate of the entire detector system does not exceed 10 kHz. The duration of the entire data readout and signal processing procedure is less than 10 μ sec . There are 23 different possibilities of so-called "basic states." Sixteen of them carry information about the direction of the incident particle. For example, the state configuration 0010 for the upper layer and 0010 for the lower layer corresponds to the charged particle traversal through the third upper and third lower scintillators (zenith angle between 0° and 30°). Combination 0010 and 1000 corresponds to the traversal through the third upper and the first lower scintillator (zenith angle between 20° and 40°). The other 7 possibilities give additional valuable information on the particle flux incident on the detector. For instance, the combination 01, i.e., no signal in the upper and the signal in the lower layer can be attributed to the traversal of a neutral particle. However, due to small sizes of the anticoincidence shielding (see Fig. 2), several charged particles can hit the detector from the side. Nonetheless, if the particle beam is near vertical (it is just the case of electron-gamma avalanche hitting ASNT), we can measure the energy release spectrum of the thunderstorm-correlated gamma rays. The combination 01 selects neutral particles, and viceversa the combination 10 selects low-energy charged particles (due to energy losses in the roof the threshold energy is ~15–17 MeV). The top scintillators have the thickness of 5 cm (energy release for the vertical electrons and muons is ~10 MeV) the combination 11 will select charged particles with energy greater that 25–27 MeV. The advanced data analysis system (ADAS) provides registration and storage of all logical combinations of the detector signals for further

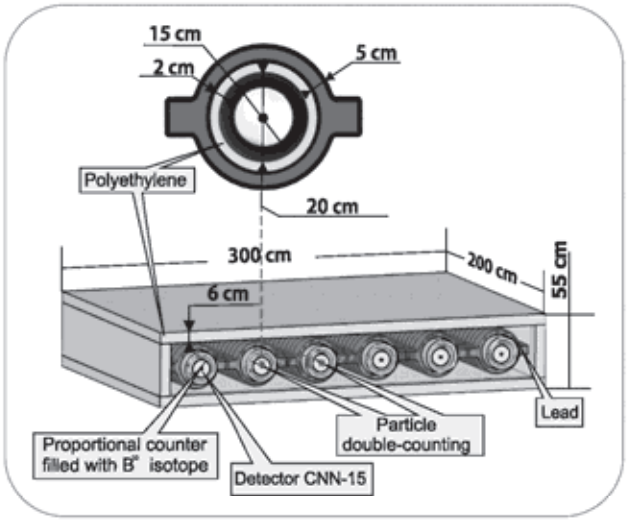

FIG. 3 (color online). Section of Aragats Neutron Monitor 18NM64 type; ArNM consists of 3 separate sections with 6 proportional chambers in each.

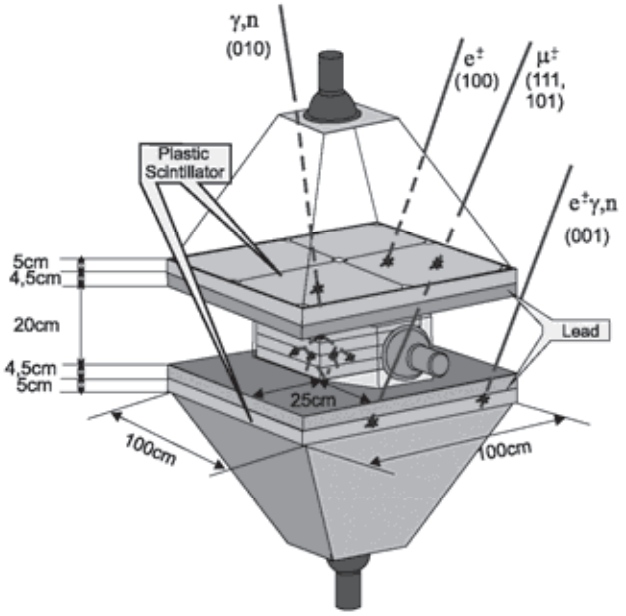

FIG. 4 (color online). SEVAN detector measuring charged and neutral secondary cosmic rays.

offline analysis and for issuing warnings and alerts on the dangerous space weather conditions [31].

B. Aragats Neutron Monitor (ArNM)

The standard neutron monitor (NM) of 18NM-64 type, see Fig. 3, consists of 18 boron-filled proportional chambers, located below 5 cm of lead (producer) and 10 cm of polyethylene (moderator).

Secondary protons and neutrons interacting with the lead producer give birth to numerous neutrons of smaller energies which release energy in polyethylene (thermalized) and enter the proportional counter filled with gaseous boron. A small fraction of these neutrons ($\sim 5\%$), are absorbed by ^{10}B isotope and generate alpha-particles detected by the proportional chamber. The neutron monitors are equipped with DAQ electronics, providing 3 different values of the detector dead time—0.4, 250, and 1250 μs. Only incident hadrons can be detected by the neutron monitor; the sensitivity of ArNM to electrons, muons, and gamma rays is vanishingly small.

C. SEVAN particle detectors

The new particle detector system, named SEVAN (Space Environmental Viewing and Analysis Network [32,33]), simultaneously measures fluxes of most species of secondary cosmic rays, thus representing an integrated device used for the exploration of the solar modulation effects.

The basic detecting unit of the SEVAN module (see Fig. 4) is assembled from standard slabs of $50 \times 50 \times 5$ cm^3 plastic scintillators. Between two identical assemblies of $100 \times 100 \times 5$ cm^3 scintillators (4 standard slabs) are located two $100 \times 100 \times 5$ cm^3 lead absorbers and thick $50 \times 50 \times 20$ cm^3 scintillator stacks (4 standard slabs). A scintillator light capture cone and photomultiplier tubes (PMTs) are located on the top, bottom, and intermediate layers of the detector. Incoming neutral particles undergo nuclear reactions in the thick 20 cm plastic scintillator and produce protons and other charged particles. In the upper 5-cm thick scintillator, charged particles are registered very effectively; however, for the nuclear or photonuclear interactions of neutral particles there is not enough substance. When a neutral particle traverses the top thin (5 cm) scintillator, usually no signal is produced. The absence of the signal in the upper scintillators, coinciding with the signal in the middle scintillator, points to neutral particle detection (gamma ray or neutron). The coincidence of signals from the top and bottom scintillators indicates the traversal of high-energy muons, traversing 10 cm of lead (minimal energy ~250 MeV).

D. Surface arrays: Aragats Multichannel Muon Monitor and MAKET ANI

Two detector assemblies measuring the extensive air showers operate on the Aragats research station. The main goal of the GAMMA [34] and MAKET-ANI [35] detectors is to measure the energy spectra of cosmic rays to understand their origin and particle acceleration mechanisms. Both detectors use the plastic scintillators overviewed by photomultipliers to determine the number of electrons in the shower and infer the energy and type of the primary particle. About 300 detecting channels formed from 5-cm thick plastic scintillators with area 1 m^2 each are located at the highland of Mt. Aragats at altitudes

3200–3250 m. EAS detectors are triggered arrays; however, each detector counts all incident particles measuring the time series of the changing fluxes of cosmic rays. High count rate ($\sim 30,000$ counts per m^2 per minute), combined with the large area of the detector assembly makes surface arrays ideal detectors for measuring additional electron flux correlated with thunderstorms. We select several detectors from both surface arrays and implement special trigger conditions for detecting additional fluxes of cosmic rays and large particle bursts in correlation with thunderstorm activity. Twenty-six of 1 m^2, 5-cm thick scintillators, located in iron boxes, comprise the surface array of the Aragats Multichannel Muon Monitor (AMMM). Another 16 same type scintillators comprise a surface array named MAKET, located inside and in the vicinity of the building where most of the other particle detectors are located, see Fig. 1. AMMM and MAKET detectors measure the charged species of secondary cosmic rays with very high accuracy: the relative error of the mean 1-minute count rates are 0.13% and 0.18% correspondingly. Each of MAKET standalone detectors provide measurements of the incident particles and the array on the whole also provides count of, so-called, EAS triggers (''firing'' of more than 8 detectors of array within the time window of 400 nsec). From the collected triggered events we can select other firing combinations of detector channels (for instance, events with all 16 channels firing). These 2 selections (>8 and all 16 firing channels) routinely collect EAS with sizes $\sim 10^4$ and $\sim 2^*10^4$ electrons correspondingly. However, when thunderstorm clouds are ''sitting'' on Mt. Aragats, the RREA process triggers the array and the stable count rate of EAS events goes up abruptly.

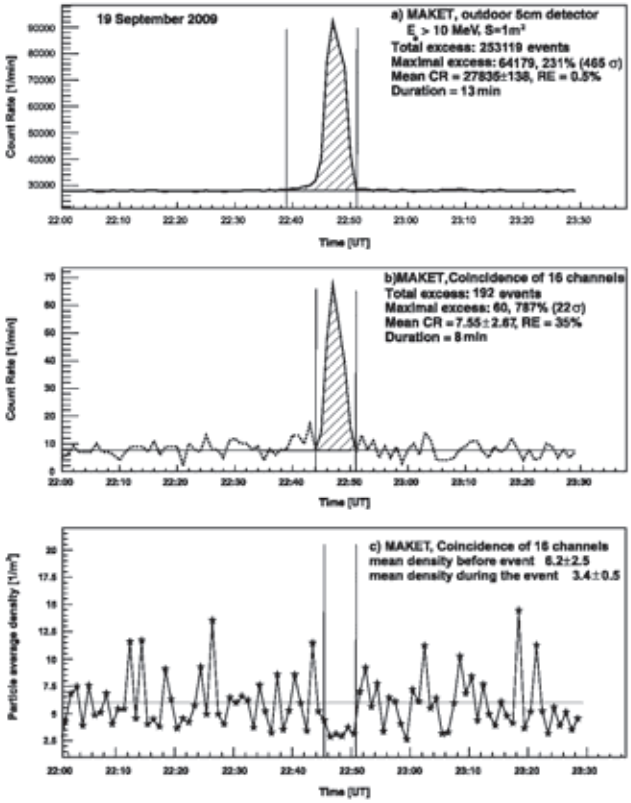

FIG. 5. One-minute time series detected by the MAKET array. (a) Count rate of the standalone outer detector. (b) Count rates of the ''EAS triggers''—all 16 scintillators give signal within 400 nsecs. (c) The mean density of the particles generating the MAKET trigger conditions.

III. DETECTION OF THE THUNDERSTORM-CORRELATED COSMIC RAY FLUXES

On September 19, 2009 all ASEC detectors measured large enhancements, seen as huge peaks in the 1-minute count rates (see Figs. 5, 6, and 8). According to the staff report and information from the Armenian meteorological service, the thunderstorm clouds height was 100–200 m and lightning accompanied with snow and rain were seen at $\sim$21–22 UT, a half an hour before the particle event.

In the legends of Figs. 5, 6, and 8, we depict a total enhancement during the event, the maximal enhancement occurred during 1 min, and statistical significance of the detected peaks in percents and numbers of standard deviations (σ). The mean count rate and variance of the count rate and the relative error were estimated by the 1-hour data before the start of enhancement when the mean and variance of the count rate corresponds to the detector typical operation.

In Fig. 5(a) one can see the enhancement of the count rate measured by the outdoor 5-cm thick scintillator of MAKET array (energy threshold 7–8 MeV, scintillator N 5 in Fig. 1. The observed enhancement above the background is really huge—10 times more than any reported ''thunderstorm particle'' flux by the other groups. The count rates of ''triggered'' events (signals in all 16 plastic scintillators within a time window of 400 nsec) although is only 0.1% of the 1-minute total count rate, enhanced $\sim$8 times compared with the background value. The background for the triggered events is EAS generated by the primary proton or stripped nucleolus entering terrestrial atmosphere. From the mean background count rate we can estimated the threshold energy of the primary proton to be 50–100 TeV. During the ''thunderstorm event'' the nature of the additional triggers is completely different from the EAS events. The mean value of the particle density is considerably lower as we can see in Fig. 5(c). A huge number of particles born in a very short time covering large surfaces on the ground possibly pointed on the new source of seed particles, different from the ambient population of the MeV secondary cosmic rays. Possibly seed particles come from the electrons accelerated by very large electrical fields in the plasma of intracloud lightning [4,36].

Also in Fig. 5 we can see that the duration of the particle enhancement measured by the standalone scintillator is much larger than the duration of the ''short flashes'' of particles—13 and 7 min correspondingly. The duration of the event was determined by visually examining the time series; the enhancement is demonstrating itself as a characteristic peak in the time series. Usually we do not need a more formal definition for very large events. However, the peak searching algorithm defines the start as the initial point in the time series starting from which 3 consequent enhancements are greater than 2.5σ. Nonetheless, the big variety of the peaks requires visual check as a final procedure.

IV. ELECTRONS AND GAMMAS DETECTED BY ASNT

In Fig. 6 we present the excess measured by the ASNT detector at the same time, on September 19, 2009. The statistical significances of the peaks are extremely high. We assume that additional flux was due to the RREA process and additional particles are mostly electrons and gamma rays. Plastic scintillators can register both electrons and gammas and first of all we performed GEANT4 [37] simulations of the detector response to estimate the probability of detection of particles of different types by selecting various ASNT operation options (namely, 01, 10, and 11 combinations).

For each combination we calculate the efficiencies of the registration of the particle of a definite type and contaminations of its counterparts. Gamma rays can be registered by a 5-cm scintillator, with efficiency less than 10% (imitating electron) and in a 60-cm scintillator with efficiency ~20%.[1] The electron can be registered in the top scintillator with efficiency above 95% or miss detection in the top scintillator and be detected in the lower one (imitating gamma ray) with efficiency less than 5%. Taking into account the energy of the minimal ionizing particle, giving a signal in the scincillator, and amount of the matter above the scintillator (roof, scintillator housing), we estimate the threshold energy to detect electron or gamma ray by the top layer of the ASNT to be equal ~15–17 MeV. Several indoor MAKET detectors located near walls of the building have energy thresholds of 11–13 MeV. The energy of electrons detected in both layers of ASNT (11 combination) is above 25 MeV).

The start of the enhancement of gamma rays (energy above 7 MeV) is 4 min earlier compared to the start of the enhancement of electrons with energy above 15 MeV; see Figs. 6(a) and 6(b).

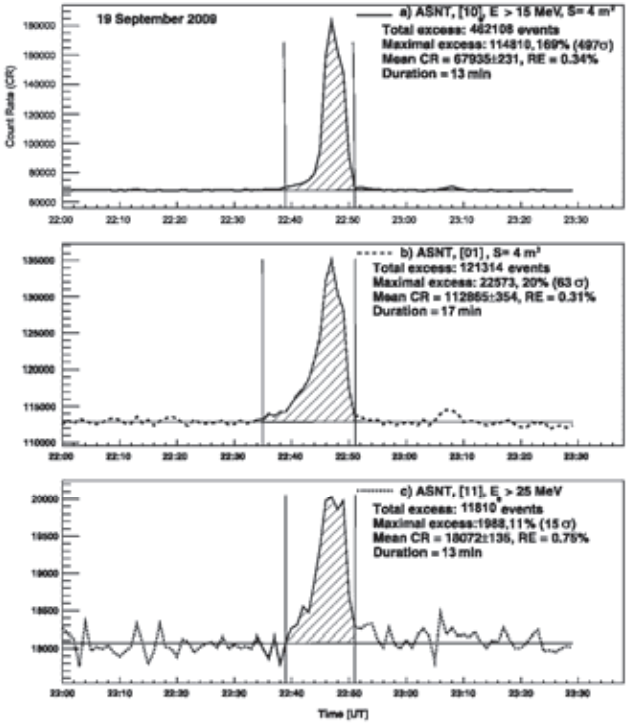

FIG. 6. One-minute time series of the particle fluxes measured by ASNT. (a) 10 combination, signal only in top layer, mostly electrons with energy greater than 15 MeV. (b) 01 combination—mostly gamma rays with contamination of neutrons and electrons. (c) 11 combination—electrons and/or gamma rays with energy above 25 MeV. Additional particles are demonstrated by the dashed areas.

V. RREA ELECTRON AND GAMMA-RAY ENERGY SPECTRA

By the 60-cm thick scintillator of the ASNT we measure not only count rates but also spectra of energy releases [the distribution of the PMT amplitude heights enumerated as ADC (amplitude-to-digital converter) codes]. However, we are interested not in the energy release spectrum, which is dependent on the detector response, but in the flux of gamma rays before entering the roof and detector. Thus, we have to solve the inverse problem of cosmic ray physics—reconstruct by the measured spectrum of energy releases the spectrum that is fallen on the detector or on the roof of the building where the detector is located. We solve the inverse problem and ''unfold'' the gamma ray energy spectrum by multiple solutions of the direct problem: assuming the analytic form of the RREA gamma ray spectra (power, exponential, or power with cutoff), we tune free parameters (normalizing coefficients, spectral indexes) by minimizing the ''quality'' function describing the closeness of simulated with GEANT4 energy releases histogram to an experimentally measured one. As a quality function we use the sum of the square differences between bin values of 2 histograms. The electrons and gamma rays

[1]Neutrons also are detected by the thick scintillator with considerable efficiency. However, the cross section of the neutron photoproduction is not large and additional neutrons can comprise only very few percents of the gamma rays.

were traced through the material of the roof above the detector and through the substance of the detector. Light absorption in the plastic scintillators was also taken into account in GEANT 4 simulation. Light attenuation coefficients were taken from [29]. We use the random search procedure for selecting the parameters of the energy spectra (see, for example, [38]).

The RREA electron spectrum was obtained using count rates measured by 5-cm thick scintillators of MAKET, ASNT, and SEVAN detectors. From Fig. 1 you can see that the MAKET 5th, 6th, and 8th scintillators are located outdoors and ASNT, SEVAN, and other 13 MAKET scintillators are located indoors. These detectors are of the same type; however, their energy thresholds are different due to different electronics thresholds and a various amount of substance above. Using enhancements (peaks) detected in these 18 5-cm thick scintillators, we select groups corresponding to 4 diverse energy thresholds. The energy thresholds were determined by comparing the mean count rates of scintillators with "theoretical" values, obtained from simulations of the EAS propagation in the atmosphere.

The electron integral spectrum is shown in Fig. 7 along with a gamma ray spectrum. The electron spectrum in the energy range 7–20 MeV is fitted by exponential function—$A \bullet e^{b \bullet E}$. The spectral index is -0.18 ± 0.06; corresponding fit quality—$\chi^2/\mathrm{ndf} = 0.34$. The horizontal error bars in the electron energy spectrum reflect uncertainties in determination of the energy thresholds, due to the complicated structure of the roof substance. The electron spectrum abruptly ended at ~30 MeV, as there is no evidence of additional electrons detected by 11 coincidence of ASNT. The peak seen in Fig. 6(c) was found to be caused by the gamma rays giving signals both in the top 5-cm and bottom 60-cm thick scintillators.

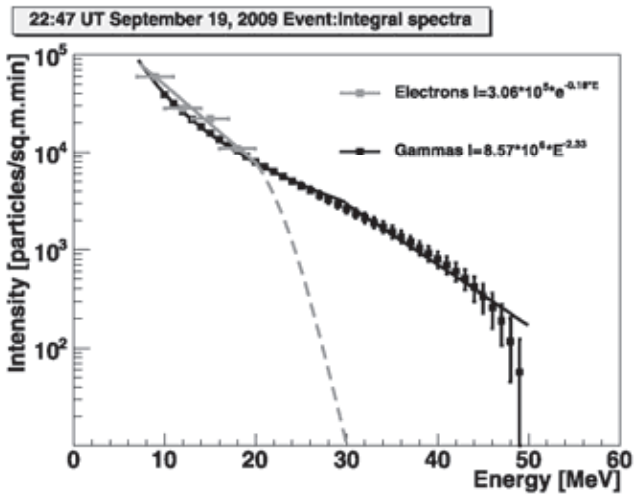

FIG. 7. Unfolded electron and gamma ray spectra fitted by exponential and power functions.

Using obtained electron spectrum, we estimate the number of electrons contaminating the energy release spectrum measured by the 60-cm thick scintillator and afterward correct the gamma ray energy spectrum. In turn, after reconstructing the gamma ray spectrum we correct the electron spectrum. The efficiency of gamma ray detection was checked by GEANT4 simulation; the probabilities of gamma rays to be detected in outer MAKET and ASNT 5-cm detectors are ~3.5% and ~10%, respectively. There is significant roof substance (metallic tilts, wood) above ASNT in which gamma rays create additional electron-positron pairs, increasing the probability of gamma rays to be detected in the 5-cm thick detector under the roof. The reconstructed energy spectrum of the incident gamma rays described by power function is continued till ~50 MeV. The gamma ray energy spectrum is fitted by power function—$A \bullet E^b$ in the range 7–30 MeV ($\chi^2/\mathrm{ndf} \sim 2.4$); in the energy range 30–45 MeV, the gamma ray spectrum is rather well described by the exponential function with slope equal to -0.14 and afterwards abruptly vanished near 50 MeV; see Fig. 7. Error bars of the gamma ray energy spectrum are statistical ones.

Details of the electron and gamma ray energy spectra at 3250 m are posted in Table I.

VI. NEUTRONS IN THE RREA: ARNM EVIDENCE

In Figs. 8(a) and 8(b) we compare the enhancements of the neutrons detected by the ArNM and all neutral particles in the SEVAN detector (signal only in the middle scintillator, combination 010). Placed in a few meters from SEVAN, ArNM's enhancement is consistent with neutral

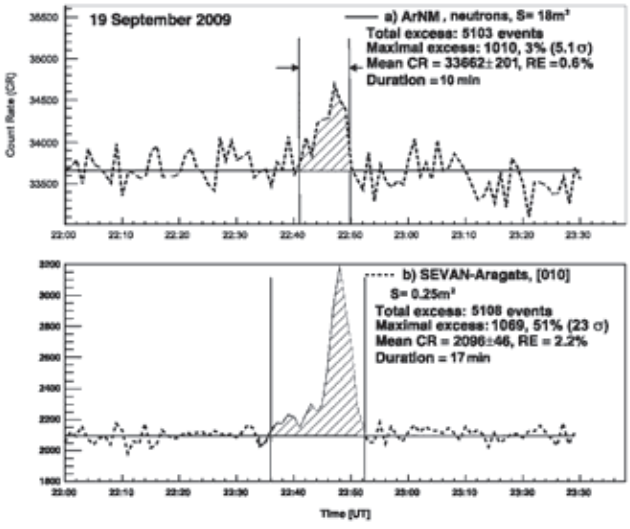

FIG. 8. One-minute time series of the particle flux detected by the SEVAN and ArNM detectors (a) 1-minute time series of ArNM. (b) 1-minute time series of SEVAN (010 combination). The additional particles are demonstrated by the dashed areas.

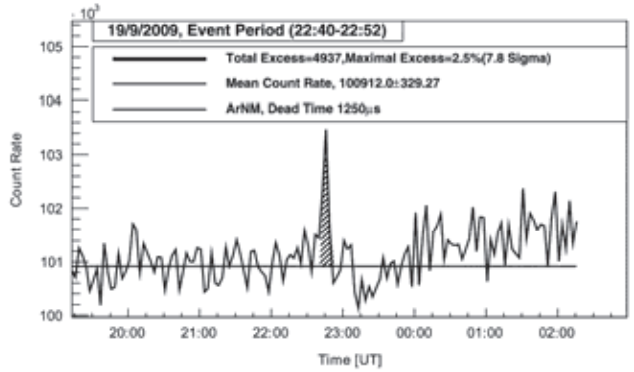

FIG. 9. 3-minute time series of ArNM on September 19, 2009.

fluxes registered by ASNT and SEVAN detectors. ASNT and SEVAN measure all neutral particles; there is no possibility of distinguishing between gamma rays and neutrons. The neutron monitor is a device with suppressed efficiency to measure leptons (see [39,40]).

Additional protons of the cosmic ray flux can also generate an enhancement in NM; however, the conditions of interplanetary magnetic fields were very stable on September 19 and there is absolutely no reason to expect extra proton flux. Therefore, although the enhancement of neutrons in ArNM is not so significant as detection of neutral particles by ASNT and SEVAN (5.1σ against 63σ and 23σ), nonetheless, the peak in ArNM time series proves the detection of neutrons. The source of additional neutrons is located in the atmosphere; the high-energy gamma ray flux generates neutrons in photonuclear reactions with air atoms (see details in [41]). A simultaneous measurement of electrons and gammas on September 19 provides unambiguous confirmation of the photonuclear mechanism for neutron production and is another demonstration that RREA was developing very close to the ASEC detectors on September 19, 2009.[2] The duration of a neutron event is 7 min shorter as compared with the duration of a gamma enhancement. The start time and duration of the gamma ray enhancement detected by the SEVAN detector coincide with the ones detected by the ASNT detector, located 30 m from SEVAN in the same building.

Taking into account the importance of proving neutron production, we form 3-minute time series from initial 1-minute ones, summing counts of the 3 succeeding minutes (a standard practice in time series statistical analysis; see Fig. 9). Obtained significance of the 3-minute neutron peak, equal $\sim 7.8\sigma$, is overwhelming. Calculating the chance probability of obtaining a peak in the 3-minute time series, we take into account the number of attempts we made to obtain the maximal peak significance. Three-minute time series can be obtained by 1-minute time series in 3 ways. Taking only one time series from 3 possible ones, we alter the statistical distribution used for calculation of chance probability (see details of statistical techniques used in [42,43]; see Web calculator in [44]). Final obtained chance probabilities of order $\sim 10^{-14}$ leave absolutely no doubts of the neutron detection on September 19, 2009.

VII. DISCUSSION

For the quantitative description of the RREA process in the thunderstorm atmosphere the most difficult problem is to determine the height of the cloud and structure and value of the electrical field in it. Nonetheless, despite the fact that we do not measure the height of the thundercloud and the structure of the electrical field in it, we can make rough estimates of some phenomenological parameters of the RREA process based on the measured particle energy spectra and neutrons. The energy spectra of the RREA electrons and gamma rays, as well as the measured flux of the neutrons, contain information on the strength and elongation of the electrical field in the thunderstorm cloud and on the height of the cloud above the detector.

To estimate the multiplication rate of the electrons in the thundercloud and overall number of electrons in it, we first have to estimate the height of the thundercloud on September 19, 2009, above the ASEC detectors. From the measured electron energy spectrum we can conclude that at least 20 MeV electrons reached ground level and were detected by the 5-cm scintillators inside the MAKET building. We can assume that maximal energy of the RREA electrons reached 40–50 MeV.[3] Therefore, assuming the average ionization losses of these electrons at $\sim$3500 m altitude equal to $\sim$200 KeV per meter, the most probable height of the cloud will be 100–150 m, well coinciding with the observations of the Armenian meteorological service. Taking for granted the height of 130 m, we estimate the RREA electrons spectrum just at the entrance from the thundercloud by selecting the trial electron spectrum at 3380 m and simulating with GEANT4 the electron-gamma avalanche till 3250 m. By trying different trial spectra (analogically to recovery of the gamma ray energy spectrum above the roof), evaluating the avalanche from 3380 till 3250 m and comparing each obtained spectrum with an experimental one (shown in Fig. 7 and Table I) we have found that the best approximation of the spectrum at 3380 m have again a exponential functional form; the spectral index is -0.15 ± 0.2. The number of electrons with energies greater than $\sim$30 MeV at 3380 m is 350, 000/sq m min only 90, 000/sq m min electrons with energy greater than 7 MeV (minimal ionizing particle energy of the 5-cm thick scintillators) survive traveling

[2]Neutrons attenuate very fast in dense atmosphere and survival probability of neutrons born high above the detector is very low.

[3]At least the AGILE gamma observatory detects one gamma ray with energy 40 MeV [10].

TABLE I. Parameters of the electron and gamma ray energy spectra fits measured on September 19, 2009, (maximal minute intensities) at altitude 3250 m above sea level.

Spectra fit function	A (coeff.)	b (slope)	Mean Energy (MeV)
Electron $A^*e^{-b^*E}$ (from 7 till 20 MeV)	$(3.1 \pm 0.3) \bullet 10^5$	-0.18 ± 0.06	5.6 ± 0.2
Gamma A^*E^{-b} (from 7 till 30 MeV)	$(8.57 \pm 0.53) \bullet 10^6$	-2.33 ± 0.02	4 ± 0.8 ($E_{min} = 1$ MeV)

till 3250 m. The mean electron energy is estimated to be $\sim 6.7 \pm 0.8$ MeV at the lower edge of the thundercloud at 3380 m. This value is in rather good agreement with that obtained from simulations of value 7.3 MeV [45]. From the measured RREA electron spectrum and spectrum of secondary cosmic ray electrons at 3380 m [46], we have calculated the multiplication rate (avalanche growth factor) in the thundercloud electric field. The obtained RREA energy spectrum on the 3380 m height (assumed end of the thundercloud and large electrical field in it) was extrapolated until 7 MeV; the number of electrons above 7 MeV was calculated and divided by the secondary cosmic ray electron number calculated according to [47]. Obtained multiplication factor equals ~ 330, corresponding to ~ 6 e-folding. Assuming a cross section area of electric field with radius 500 m (maximal distance between ASEC detectors measuring the thunderstorm-correlated particle enhancements), we will get a total number of electrons above 7 MeV $\sim 3.8^*10^{12}$.

The maximal energy gain of electrons per one avalanche length is approximately independent of the atmosphere density and electrical field value and equals ~ 7 MeV [45]. Thus, based on the calculations of the multiplication rate we obtain maximal energy of electrons ~ 40 MeV in good agreement with our assumptions and measurements.

To calculate the value of the e-folding length we need to know the elongation of the electrical field in the thundercloud. This length we estimate taking into consideration the neutron detection by the Aragats Neutron Monitor; see Figs. 8 and 9. The nuclear fusion origin of the thunderstorm-correlated neutrons was ruled out in [27]. Assuming the flux of the gamma rays with a spectrum stretching up till 50 MeV, well above the photonuclear reaction threshold for nitrogen (~ 10.5 MeV), the (γ, n) reaction becomes the best candidate for the neutron generation [25]. On September 19, 2009, ArNM detected ~ 70 additional neutrons per square meter at a maximal intensity minute. In the GEANT4 simulation, after the passage of 1500 m, bremsstrahlung photons had generated ~ 2250 neutrons. The number of gammas in simulation was taken to be 1×10^6, which corresponds to the 100 000 gammas after the passage of 1500 m (close to the experimental value). The obtained neutron energy spectrum can be fitted by the exponential function with slope -0.45; the maximal energy of neutrons was 14 MeV. The probability of the photonuclear reactions of gamma rays with atmosphere nucleus is rather low ($\sim 1\%$) in comparison with the probability of electromagnetic interactions. That is why the neutron flux is smaller in comparison with the gamma ray flux. Besides, the efficiency of the neutron monitor to register neutrons with energy below 15 MeV is much smaller than the efficiency of detecting neutral particles by ASNT and SEVAN. However, according to [48,49], even neutrons with energy less than 1 MeV still can be detected by the NM 64 neutron monitor. According to their estimates of the neutron detecting efficiency, we calculate the number of the neutrons expected to be registered by the ArNM to be ~ 20. The discrepancy between experiment and simulation can be due to other sources of neutron production [24] not taken into account in simulation or by greater than assumed efficiency of the NM 64 to detect low-energy neutrons, or by a too simplified model used for simulation. From the multiple trials of simulations started at the different heights in the atmosphere, we found that the maximal neutron yield was obtained when the starting point was ~ 1500 m above the detector. Therefore, from the estimate of the electrical field elongation of 1500 m, we can estimate the e-folding length as 250–300 m and the electrical field strength (if we assume its uniform distribution), according to equation (1) in [45] will be 180–200 kV/m.

A very long duration of the electron and gamma ray fluxes detected on the ground (~ 10 orders of magnitude greater than duration of the terrestrial gamma ray flashes) requires a permanent stable source of the seed particles, and secondary cosmic rays fulfill this condition. On the other hand, we do not decline that the intracloud lightning leader can provide another source of the seed particles. Detection of very short (within 400 nsec) flashes of the electrons detected by the MAKET air shower array is just a demonstration of this possibility. Existence of the alternative seed particle source did not put under question our calculations because a fraction of particles from this source does not exceed 0.1% of the total observed enhancement.

VIII. CONCLUSION

During the particle event on September 19, huge enhancements of the electrons, gamma rays, and neutrons, as well as short particle bursts, counting millions of the additional particles and distributed over a large area, were detected. The observations of ASEC monitors prove the existence of the long-lasting electron-photon avalanches developing in the atmosphere during thunderstorms.

Simultaneous measurements of the gamma rays and neutrons provide confirmation of the photonuclear mechanism for neutron production.[4]

For the first time we measured the electron and gamma ray energy spectra and made quantitative estimates of some phenomenological parameters of the RREA process based on detected particle fluxes. The exponential spectrum of the RREA electrons is in good agreement with simulations [45], and gamma ray power energy spectrum do not contradict recent observations of the TGF by orbiting gamma observatories [10]. However, we recognize that we measure only high-energy tails of the energy spectra of electrons and gamma rays; to measure bulk of particles of lower energies we need new particle detectors with much lower energy thresholds, under construction now.

[4]However, only ~20% of the detected neutrons can be explained by the photonuclear reaction according to our simulations

ACKNOWLEDGMENTS

This work was partly supported by the Armenian government grants and by ISTC Grant No. A1554. Authors are grateful to Arnold Wolfendale for his stimulating interest to the applied cosmic rays field.

[1] C. T. R. Wilson, Proc. Cambridge Philos. Soc. **22**, 534 (1925).
[2] A. V. Gurevich, G. M. Milikh, and R. A. Roussel-Dupre, Phys. Lett. A **165**, 463 (1992).
[3] Z. Saleh, J. Dwyer, J. Howard, M. Uman, M. Bakhtiari, D. Concha, M. Stapleton, D. Hill, C. Biagi, and H. Rassoul, J. Geophys. Res. **114**, D17210 (2009).
[4] B. E. Carlson, N. G. Lehtinen, and U. S. Inan, J. Geophys. Res. **114**, A00E08 (2009).
[5] G. D. Moss, V. P. Pasko, N. Liu, and G. Veronis, J. Geophys. Res. **111**, A02307 (2006).
[6] L. P. Babich, E. N. Donskoi, I. M. Kutsyk, and A. Yu. Kudryavtsev, Phys. Lett. A **245**, 460 (1998).
[7] J. R. Dwyer, Phys. Plasmas **14**, 042901 (2007).
[8] N. S. Khaerdinov, A. S. Lidvansky, and V. B. Petkov, Atmos. Res. **76**, 346 (2005).
[9] D. M. Smith *et al.*, Science **307**, 1085 (2005).
[10] M. Marisaldi *et al.*, J. Geophys. Res. **115**, A00E13 (2010).
[11] B. F. J. Schonland, Proc. R. Soc. A **130**, 37 (1930).
[12] B. F. J. Schonland and J. P. T. Viljoen, Proc. R. Soc. A **140**, 314 (1933).
[13] G. E. J. Shaw, Geophys. Res. Bull. **72**, 4623 (1967).
[14] M. Aglietta *et al.*, Nucl. Instrum. Methods Phys. Res., Sect. A **277**, 23 (1989).
[15] S. Vernetto (EAS-TOP Collaboration), *Proceedings of the 27th International Cosmic Ray Conference (ICRC)* (Copernicus Gesellschaft, Hamburg, Germany, 2001), Vol. 10, pp. 4165–4168.
[16] T. Torii, M. Takeishi, and T. Hosono, J. Geophys. Res. **107**, 4324 (2002).
[17] T. Torii, T. Sugita, S. Tanabe, Y. Kimura, M. Kamogawa, K. Yajima, and H. Yasuda, Geophys. Res. Lett. **36**, L13804 (2009).
[18] H. Tsuchiya *et al.*, Phys. Rev. Lett. **99**, 165002 (2007).
[19] H. Tsuchiya *et al.*, Phys. Rev. Lett. **102**, 255003 (2009).
[20] T. Takamil *et al.*, *Proceedings of the 27th International Cosmic Ray Conference (ICRC)* (Copernicus Gesellschaft, Hamburg, Germany, 2001), Vol. 10, pp. 4027–4030.
[21] A. S. Lidvansky and N. S. Khaerdinov, Izvestiya Rossiiskoi Akademii Nauk. Seriya Fizicheskaya **73**, 418 (2009) [Bulletin of the Russian Academy of Sciences: Physics **73**, 400 (2009)].
[22] A. V. Gurevich *et al.*, Phys. Lett. A **373**, 3550 (2009).
[23] G. N. Shah, H. Razdan, C. L. Bhat, and Q. M. Ali, Nature (London) **313**, 773 (1985).
[24] L. P. Babich and R. A. Roussel-Dupre, J. Geophys. Res. **112**, D13303 (2007).
[25] L. P. Babich, L. I.Bochkov, I. M.Kutsyk, and R. A.Roussel-Dupré, J. Geophys. Res. **115**, A00E28 (2010).
[26] A. A. Chilingarian *et al.*, J. Phys. G **29**, 939 (2003).
[27] A. A. Chilingarian *et al.*, Nucl. Instrum. Methods Phys. Res., Sect. A **543**, 483 (2005).
[28] A. A. Chilingarian *et al.*, *Proceedings of the International Symposium on Forecasting of the Radiation and Geomagnetic Storms by Networks of Particle Detectors (FORGES 2008)* [Nor Amberd, Armenia, (Alikanyan Physics Institute, printed by Tigran Mets, Yerevan) 2009], pp. 121–126.
[29] A. Chilingarian, L. Melkumyan, G. Hovsepyan, and A. Reymers, Nucl. Instrum. Methods Phys. Res., Sect. A **574**, 255 (2007).
[30] K. Arakelyan *et al.*, *Proceedings of the International Symposium on Forecasting of the Radiation and Geomagnetic Storms by Networks of Particle Detectors (FORGES 2008)* [Nor Amberd, Armenia, (Alikanyan Physics Institute, printed by Tigran Mets, Yerevan) 2009], pp. , pp. 105–116.
[31] S. Chilingaryan, A. Chilingarian, V. Danielyan, and W. Eppler, Adv. Space Res. **43**, 717 (2009).
[32] A. A. Chilingarian and A. Reymers, Ann. Geophys. **26**, 249 (2008).
[33] A. Chilingarian *et al.*, Earth Moon Planets **104**, 195 (2009).
[34] A. Garyaka *et al.*, J. Phys. G **28**, 2317 (2002).
[35] A. Chilingarian *et al.*, Astropart. Phys. **28**, 58 (2007).
[36] J. R. Dwyer, M. A. Uman, and H. K. Rassoul, J. Geophys. Res. **114**, D09208 (2009).
[37] S. Agostinelli *et al.*, Nucl. Instrum. Methods Phys. Res., Sect. A **506**, 250 (2003).
[38] A. A. Chilingarian, N. Gevorgyan, A. Vardanyan, D.

Jones, and A. Szabo, Math. Biosci. **176**, 59 (2002).
[39] J. M. Clem and L. I. Dorman, Space Sci. Rev. **93**, 335 (2000).
[40] S. Shibata *et al.*, Nucl. Instrum. Methods Phys. Res., Sect. A **463**, 316 (2001).
[41] L. P. Babich, JETP Lett. **84**, 285 (2006).
[42] A. Chilingarian, G. Hovsepyan, G. Gharagyozyan, and G. Karapetyan, Int. J. Mod. Phys. A **20**, 6753 (2005).
[43] A. Chilingarian, Adv. Space Res. **43**, 702 (2009).
[44] A. Chilinarian, http://se.crd.yerphi.am/chapman_calculator
[45] J. R. Dwyer, J. Geophys. Res. **113**, D10103 (2008).
[46] We accept here that RREA seed particles are electrons from the EAS initiated by primary proton and stripped nuclei. The seed electrons were simulated by the WEB generator of secondary cosmic rays (http://phits.jaea.go.jp/expacs/).
[47] T. Sato, EXPACS: Excel-based Program for calculating Atmospheric Cosmic-Ray Spectrum. User's Manual, http://phits.jaea.go.jp/expacs/, 2009.
[48] C. J. Hatton, *Progress in Elementary Particle and Cosmic-Ray Physics*, edited by J. G. Wilson and S. A. Wouthuysen (North Holland, Amsterdam, 1971), Vol. 10, Chap. 1.
[49] E. A. Maurchev *et al.*, "*Simulation of the Neutron Monitor Response Function, Report to the 31st All Russian Cosmic Ray Conference, GEO_29, Moscow, MSU*, 2010 (unpublished).

PHYSICAL REVIEW D **83,** 062001 (2011)

Particle bursts from thunderclouds: Natural particle accelerators above our heads

Ashot Chilingarian,* Gagik Hovsepyan, and Armen Hovhannisyan

Artem Alikhanyan National Laboratory, Alikhanyan Brothers 2, Yerevan – 36, Armenia

(Received 13 November 2010; published 1 March 2011)

Strong electrical fields inside thunderclouds give rise to fluxes of high-energy electrons and, consequently, gamma rays and neutrons. Gamma rays and electrons are currently detected by the facilities of low orbiting satellites and by networks of surface particle detectors. During intensive particle fluxes, coinciding with thunderstorms, series of particle bursts were detected by the particle detectors of Aragats Space Environmental Center at an altitude of 3250 m. We classify the thunderstorm ground enhancements in 2 categories, one lasting microseconds, and the other lasting tens of minutes. Both types of events can occur at the same time, coinciding with a large negative electric field between the cloud and the ground and negative intracloud lightning. Statistical analysis of the short thunderstorm ground enhancement bursts sample suggests the duration is less than 50 μs and spatial extension is larger than 1000 m^2. We discuss the origin of thunderstorm ground enhancements and its connection to the terrestrial gamma flashes detected by orbiting gamma-ray observatories.

DOI: 10.1103/PhysRevD.83.062001 PACS numbers: 92.60.Pw, 13.40.−f, 94.05.Dd

I. INTRODUCTION

High-energy particles and radiation of an atmospheric nature is registered in space and on the Earth's surface. Terrestrial gamma-ray flashes (TGFs)—brief bursts of gamma rays[1] produced in the atmosphere—have been firmly established during the last decades by the gamma-ray observatories aboard low-Earth orbit satellites [2–5]. It is generally accepted that the gamma rays in TGFs come from the bremsstrahlung radiation of energetic electrons. Inside thunderclouds, the electric fields can grow large enough to force fast electrons to gain energy from the field larger than the braking force and "run away." As the runaway electrons travel through air, they undergo hard elastic scattering with atomic electrons, producing additional electrons that can also run away. In this way the electrical fields in the thunderstorm atmospheres give the ambient population of the MeV electrons from the cosmic-ray showers a boost by increasing the number of energetic particles through a multiplication and acceleration process called relativistic runaway electron avalanche (RREA) [6,7]. The source of TGFs is located in the space just above or even within thunderclouds (12–20 km above Earth's surface; see [1]). The RREA mechanism can create large amounts of high-energy electrons and subsequently the gamma rays. The nature of seed particles is still under debate; an alternative source of the seed particles could be connected with the lightning step leaders [8–10]. As we will demonstrate in this paper, the very short time span of the discovered thunderstorm ground enhancement (TGE) events supports their lightning origin. However, it is possible that some other mechanisms are responsible for the high-energy phenomena in thunderclouds. Until now there were surprisingly few observations on the electric field dynamics in the thunderstorm atmospheres.

The amount of the surface detection of the electron and gamma-ray fluxes correlated with thunderstorms is not too large (see the review in [11]). Only at the Baksan Neutrino Observatory of the Institute for Nuclear Research [12] and at the Tien-Shan Cosmic Ray Station of the Lebedev Institute, both Russian Academy of Sciences, have surface particle enhancements correlated with thunderstorms been studied for many years in a systematic way. Unfortunately, the location of the surface array in the Baksan valley did not allow registration of large fluxes. The array is located in a deep narrow valley, and thunderclouds are rather high. The Tien-Shan group has concentrated mostly on the research of the very rare process—runaway breakdown initiated by an extensive air shower (EAS) with energy above 1000 TeV, so-called runaway breakdown-EAS discharge [6].

However, if electron and gamma-ray fluxes are unambiguously detected by orbiting gamma-ray observatories ~500 km from the source, we can expect the intensive particle and radiation fluxes on the highland altitudes from thunderclouds located a few hundred meters above. The particle detectors of the Aragats Space Environment Center (ASEC) [13,14] continuously measure the time series of the charged and neutral fluxes of the secondary cosmic rays. ASEC detectors measure 1 min and 10 sec time series starting from the minimal energy of 3 until 250 MeV, as well as time series of numbers of the EASs initiated in the atmosphere by primary protons or stripped nuclei with energy greater than ~50 TeV. Numerous thunderstorm correlated enhancements of electrons, gamma rays, and neutrons, detected by the ASEC facilities at the minimum of the solar activity years, constitute a rich

*chili@aragats.am

[1]Recently, Ref. [1] reported that a substantial fraction of TGF events are not gamma rays but high-energy electrons; see also [2].

experimental set to investigate the high-energy phenomena in the thunderstorm atmospheres. The Aragats High-Mountain Research Station of the Artem Alikhanyan National Laboratory (former Yerevan Physics Institute) is located 3250 m above sea level near the southern peak of Aragats (3750 m above sea level); the other 3 peaks of Aragats are located from 10 to 15 km away. The thunderstorm activity on Aragats is strongest in May–June and September–October. Thunderclouds are usually below the southern peak and sometimes 100–200 m only above the station. In 2009–2010 we measured several long TGEs of tens of minutes duration. During the two most intense of these, on 19 September, 2009 and 4 October, 2010, the Maket surface array [15] also detected a series of electron/gamma-ray bursts—short TGEs—extended showers of the coherent particles simultaneously detected in the scintillators of the surface array within a time window of 1 μs. In this paper, we discuss the short TGEs detection by the surface facilities and its relation to the TGFs detected by satellite facilities. We will demonstrate that TGEs have a duration not greater than 50 μs and will discuss their origin.

II. DETECTION OF THE THUNDERSTORM CORRELATED COSMIC-RAY BURSTS ON 4 OCTOBER, 2010

Most of the ASEC particle detectors and field meters are located in the Maket building (see Fig. 1) and nearby. Along with 16 plastic scintillators belonging to the Maket surface array, in operation are the Aragats Solar Neutron Telescope (ASNT), the Aragats neutron monitor of type 18NM64, and the Space Environmental Viewing and Analysis Network (SEVAN) particle detectors

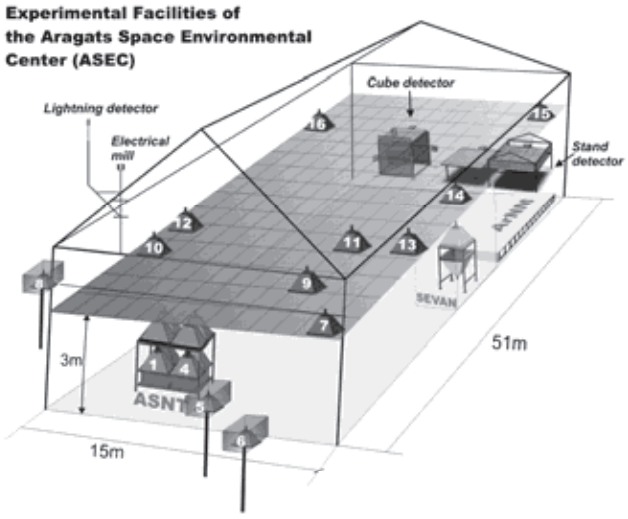

FIG. 1 (color online). Particle detectors and field meters of the Aragats Space Environmental Center operation during the 2010 measurement campaign.

(see the detailed description in [11]). In 2010, especially for the detection of low-energy electrons and gamma rays from thunderclouds, two new outdoor facilities were installed near the Maket building, namely, the Stand and Cube scintillation detectors. The Stand detector is a 3-layered pile of 1 cm thick and 1 m^2 area molded plastic scintillators with fiberglass wavelength shifters, fabricated by the High Energy Physics Institute, Serpukhov, Russian Federation. The same type of 3 cm thick scintillator is located also outdoors. The energy thresholds of the 1 cm thick scintillators are ~2, 6, and 10 MeV correspondingly from the top to the bottom: The energy threshold of the 3 cm thick scintillator is ~5 MeV. The energy thresholds of the rest of the ASEC scintillators range from 7 to 18 MeV (dependent on the amount of matter above); therefore in 2009 we reconstructed the energy spectra of RREA electrons and gamma rays starting from 7 MeV. The energy spectra of the 2010 campaign were reconstructed starting from 2 MeV. The aim of the Cube detector is to measure both charged and neutral fluxes separately, with enhanced purity of the neutral flux. For it the assembly of two 20 cm thick and 0.25 m^2 area plastic scintillators is fully surrounded by six 1 cm thick 1 m^2 area plastic scintillators, forming the veto for charged particles to enter the sensitive volume and hit the thick scintillators. The detector measures count rates of the neutral particles if there is at least one signal from the two inner scintillators without any signal from the surrounding veto scintillators. The histograms of the energy deposits in the two inner thick scintillators are stored every minute. The one-minute count rates of the surrounding 6 scintillators are measured and stored as well.

In 2010 we installed in the Maket building the magnetotelluric station LEMI-417, designed and commissioned by Lviv Center of the Space Research Institute of Ukrainian Academy of Science. One-second time series of the three-dimensional measurement of the geomagnetic field enter the ASEC database, which will highly improve the research of correlations of the geomagnetic parameters and changes of the fluxes of cosmic rays. The same device is measuring also components of the electric field. Additionally, on the roof of the building we installed an electrical field mill for measuring electrical fields between clouds and the ground and a lightning detector, measuring the broadband radio emissions by the intracloud, intercloud, and cloud-ground lightning (see Figs. 1 and 10).

In 2009–2010 we detected simultaneously large fluxes of electrons, gamma rays, and neutrons correlated with thunderstorm activity [11]. During the period of the count rate enhancements lasting tens of minutes, millions of additional particles were detected (see the appendix for discussion on the possible interferences with electronic or natural induced signals).

On October 4, 2010, all ASEC particle detectors measured a large enhancement of count rates seen as huge

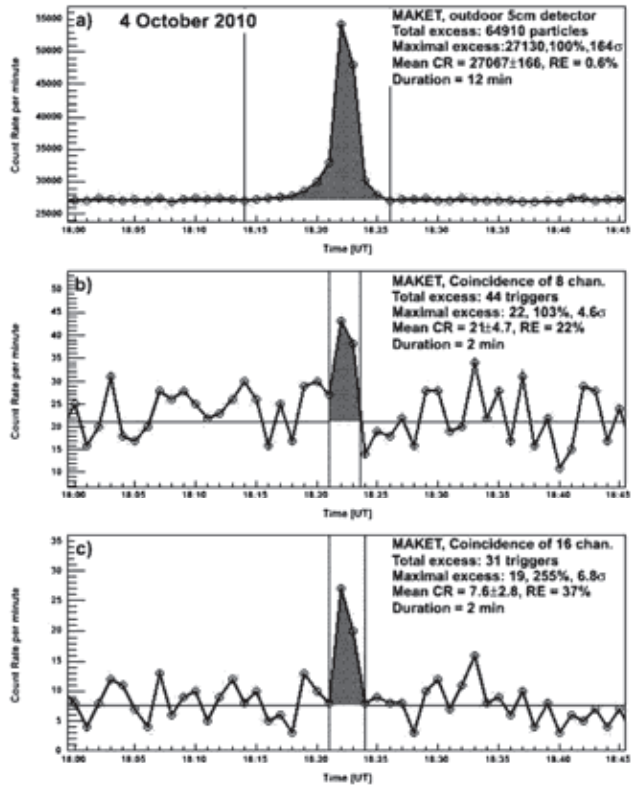

FIG. 2. One-minute time series detected by the Maket array. (a) Count rate of the standalone outer detector (energy threshold ~7 MeV); (b) count rates of the "EAS hardware trigger"—9 scintillators give a signal within 1 μs); (c) count rate of the EAS software triggers—off-line selection of events where all 16 scintillators give a signal within 1 μs.

peaks in the time series (see Fig. 2). In the legend of Fig. 2, we depict a total enhancement during the event, the maximal enhancement that occurred during 1 min, and the statistical significance of the detected peak in percents and numbers of standard deviations (σ). The mean count rate (CR), the variance, and the relative error (RE) of the time series were estimated by the 1-hour data before the start of enhancement when the mean and variance of the count rate correspond to the detector typical operation.[2] In Fig. 2(a), one can see the huge enhancement of the count rate measured by the outdoor scintillator of the Maket array (energy threshold 7 MeV) with maximal enhancement at 18:23 (100%, 164σ). In the time series of the number of the Maket hardware triggers (as minimum 9 "fired" scintillators), the maximal enhancement of the count rate can be seen during the same minute [Fig. 2(b)]—the peak of ~103% magnitude and ~4.6σ significance.[3] When we apply software trigger and select events with all 16 scintillators fired, this enhancement magnifies up to ~250% and ~7σ [Fig. 2(c)]. It is indirect evidence that the TGE events cover much larger space than "background"[4] EAS events (we will discuss the size of the EAS and TGE events in more detail in the following section).

III. CLASSIFICATION OF THE EAS AND TGE EVENTS

Based on the expected systematic difference of the EAS and TGE event densities, we perform a two-way classification of showers detected on 19 September and 4 October, 2010[5] We select the 10-minute sample of the pure background—EAS events measured during quiet weather. Having 2 samples, one containing the pure background and the other a signal contaminated by background, we can pose the problem of the signal "purification," i.e. selecting the decision boundary in the measured parameter space and performing cuts of the experimental sample containing signal and background. The boundary in the space of measured characteristics (decision boundary) should be optimized in such a way as to keep as many as possible of the signal events and suppress as many as possible of the background events. Obviously, we cannot keep 100% of the signal and reject all background events, because of the overlapping signal and background distributions; therefore, we have to select a compromise. The typical particle density distribution of the EAS hitting Earth's surface is a bell-like two-dimensional distribution with a large fraction of the shower particles near the core of EAS. The TGE event that originated from multiple avalanches of electrons with maximal energy not exceeding 50 MeV [11] is expected to be uniform without any significant particle density peaks.

Almost all of the additional Maket triggers [Figs. 2(b) and 2(c)] have mean density not exceeding 7–8 particles/m^2, and we can restrict ourselves by the one-dimensional classification scheme, using only the mean density of an event. However, as we can see in Fig. 3, to the right from the decision line in the region of low density there is a population of events with rather large maximal density. We treat these events as background small EAS events with their shower axes fallen in the array.

[2]Mean count rates and variances of the ASEC particle detectors were very stable in 2009–2010 due to continuous maintenance and the absence of the solar modulation effects during an unusual long period of a quiet Sun.

[3]The coherent short bursts of the thunderstorm correlated particle fluxes were first detected during the event of 19 September, 2009 (see details in [11]).

[4]The background for the triggered events is extensive air showers routinely generated by primary protons or stripped nuclei entering the atmosphere. Comparing the mean background count rate with the intensity of the primary cosmic rays, we estimate the threshold energy of the primary proton flux detected by the Maket array to be 50–100 TeV.

[5]We form a joint sample of events (total 613) containing background—EAS—and "signal"—TGE—events.

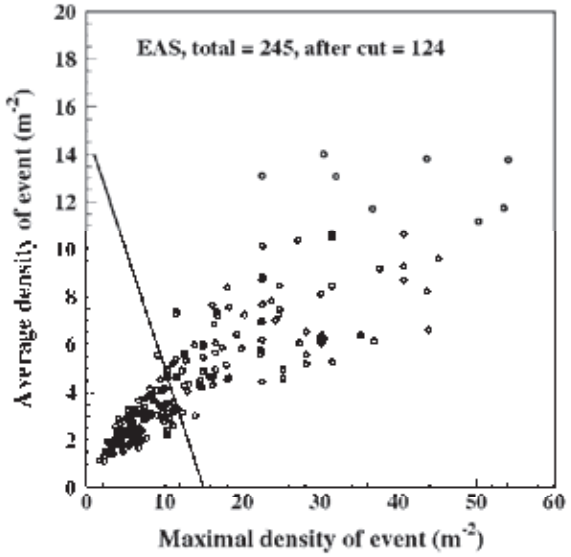

FIG. 3. Scatter plot of the registered at quiet weather Maket triggers; pure EAS events.

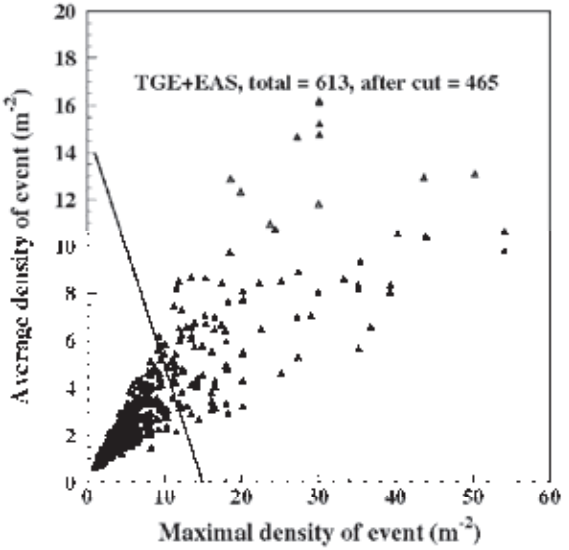

FIG. 4. Two-way classification of the showers detected on 19 September, 2009, and 4 October, 2010, during thunderstorms.

To additionally suppress such events we add the second discriminator—the maximal density within an event. Thus, the mean and maximal densities of Maket scintillators that detected the shower were used for classification. The selection procedure is visualized in Figs. 3 and 4. The showers with parameters in the region to the left from the linear decision boundary are classified as TGE events and the events to the right as EAS events.

Selected classification criteria suppress ~50% of the EAS events (121 from 245; see Fig. 3) but only losing ~25% of the joint EAS and TGE events (148 from 613; Fig. 4). Among the selected 465 signal events we expect about 121 background events; therefore, the expected purity of the selected TGE sample is rather high: ~75%. The 25% of contamination could not be significantly reduced due to large EAS with axes far from the Maket array. The long tails of EASs generate events with low mean and maximal densities and could not be distinguished from TGEs.

Further evidence of the difference of the two classes of events is apparent from Fig. 5. The density distribution of EAS events follows a power law as many other distributions generically connected with population of the galactic cosmic rays falling on the atmosphere. In contrast, the density distribution of the TGE events (obtained by subtraction of the pure EAS sample from the joint TGE + EAS sample) follows an exponential curve, as expected from an avalanche process. The average value of the mean density of EAS and TGE classes is ~6 and 2.5 particles/m^2, correspondingly. The density spectra of the TGE + EAS and pure EAS events are drastically different in the region of small densities (less than 7–8 particles/m^2) and identical for higher densities.

The comparison of the spatial extension of both classes is shown in Fig. 6. All 16 Maket array scintillators used for the detection of particle showers are located on the area of ~1000 m^2.

If in the off-line analysis we require more than 9 scintillators (hardware trigger condition) to be fired, the number of events diminishes with enlarging the number of scintillators participating in the software trigger. However, the speed of the decrease of events significantly differs for the EAS and TGE classes. In Fig. 6, we can see that the

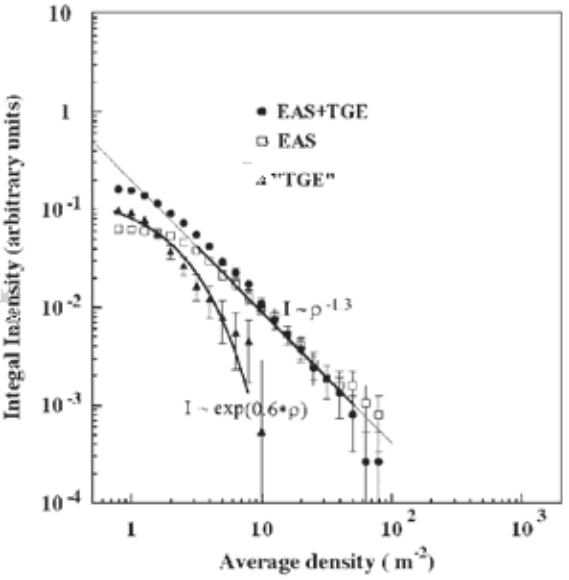

FIG. 5. Integral density distribution of the events from the joint TGE + EAS, statistically reconstructed TGE, and pure EAS classes.

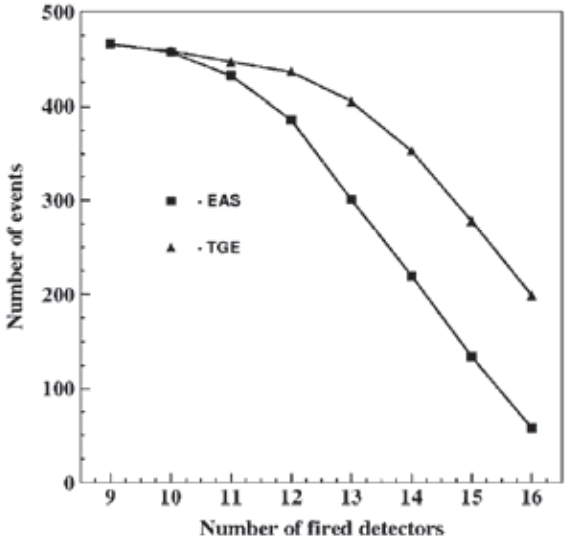

FIG. 6. Numbers of events detected with 9–16 scintillators of the Maket array for the two classes of events, both containing 465 events at hardware trigger conditions (9 scintillators fired).

number of EAS events is fast decreasing (from 465 at the trigger to 50 when all 16 scintillators are required). This can be explained by the small sizes of the EASs at rather low Maket array threshold energies ~50 TeV. The number of events of the TGE class is decreasing much slower. There are two possible reasons for the detected decrease in the number of events: the smaller than array dimension size of the event and the non-100% efficiency of the scintillators. We model the second possibility with 90% scintillator efficiency to register a charged particle.[6] Obtained trigger frequencies rather well coincide with the binomial law assuming a probability of success of 0.9. Therefore, we can state that there is no experimental evidence that the spatial elongation of the TGE events is less than 1000 m^2 (limit caused by the finite size of the Maket detector). Most of the EAS events are more compact.

IV. ESTIMATION OF THE MAXIMAL DURATION OF THE SHORT TGE EVENTS

The duration of the TGF events detected by gamma observatories on board low elevation satellites varies from several tens of microseconds to a few milliseconds, with a mean value of ~0.5 ms. At the present time we did not install megahertz flash amplitude-to-digital converters to measure the duration of the short TGE events directly; however, we establish the limits on the duration of the surface events by statistical analysis of the TGE event temporal distribution. The maximal duration of the surface particle bursts was estimated by exploiting the measured distribution of the TGE events in each of the seconds within a minute of the maximal flux (124 triggers at 22:47, 19 September, 2009). The data acquisition (DAQ) electronics and software operates as described below (see details in [16]):

(i) The Maket trigger system opens the window of ~1 μs after receiving the signal above the discriminator level from each of 16 channels.
(ii) If trigger conditions are fulfilled (8 selected +1 arbitrary scintillators are fired), 16 energy deposits are written in the temporary memory of the filled programmable gate arrays.
(iii) The duration of operations 1 and 2 is at most 50 μs, and it is the dead time of the Maket DAQ system.
(iv) The events (strings of 16 energy deposits) are collected during a second and then are transferred to permanent memory in an on-line ADAS personal computer.[7] Each event has a time stamp reporting when it was written in the temporary mass storage.
(v) ADAS joins the events collected in 1 s and transforms them to a 1-minute time series, storing them along with other information for sending to an MSQL database, where the ASEC time series are permanently stored.
(vi) If the duration of the event will exceed 50 μs after finishing of the dead time, another event will be generated and stored.

In Fig. 7, we present the distribution of the TGE triggers for the 3 selected minutes according to how many triggers were detected in a second. If, say, there is continuous detection of particles (discharge between a thundercloud and the ground) during a second, we can detect ~20 000 triggers (because of the 50 μs dead time of the DAQ electronics). If the TGE events have a duration exceeding the dead time of the detector, then several events will be detected within the same second; i.e. the detected events will be highly correlated and a very large number of events will fall in the particular second. However, even for the minute when the largest count rate occurred, at most 6 triggers per second were registered. It gives us a hint that the burst events are not correlated; however, we have to prove it formally by using the Neyman-Pearson technique of statistical hypothesis testing. As is usual in statistical hypothesis testing, we have to formulate the null hypothesis (H_0). It must be numerically exact—if it is valid, the distribution of the experiment outcomes (the distribution of the number of bursts in a second) should have a very definite shape close (within statistical errors) to the well known analytic distribution, thus allowing us to calculate the measure of the difference. If the calculated difference is

[6]Because of the aging of the scintillators (they have been in operation for ~20 years), the assumed efficiency is a realistic estimate.

[7]The Advanced Data Analysis System (ADAS) is a special software developed for on-line analysis and storing data from ASEC particle detectors; see details in [15].

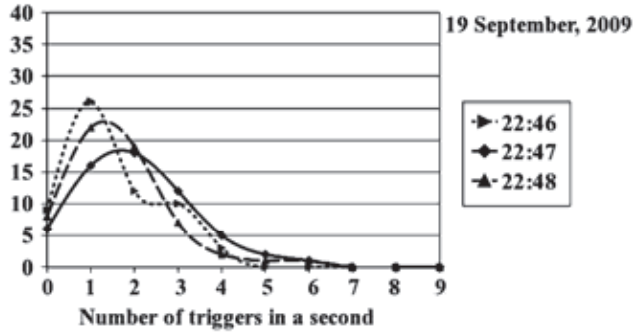

FIG. 7. Distribution of the Maket hardware triggers by the number of triggers per second at 3 minutes of 19 September, 2009.

greater than the preselected threshold value, we can state that the experimental results do not support H_0 and reject it (H_0 is rejected only for a first kind error—reject H_0 when it is true—is very unlikely). If the experimental distribution is close to the theoretical one, we accept H_0 stating that there is no evidence to reject it. Therefore, we formulate H_0 in the following way:

H_0 = there is no correlation between particle bursts measured by the Maket surface array.

The alternative hypothesis consists in the statement that particle bursts are correlated.

As we will see below, if H_0 is valid, we can numerically calculate the probabilities of having 1, 2, 3... bursts in a second using binomial, multinomial, and χ^2 analytical distributions. It is why we did not invert our procedure of the hypothesis testing and do not accept as H_0 the alternative hypothesis (bursts correlated). It will be very difficult (if even possible) to find the analytical distributions for arbitrary correlation of the bursts (TGEs).

The statistical hypothesis we have testing, the H_0 hypothesis (no correlation), consisted in several substatements. The distribution of the number of TGEs in a second can be described by the binomial distribution:

$P(X = r) = C^n{}_r p^r (1\text{-}p)^{n-r}$, where the combinatorial coefficient is $C^n{}_r = (n!/(n\text{-}r)!)/r!$.

The binomial model is valid when there are exactly two mutually exclusive outcomes of a trial. These outcomes are appropriately labeled success (TGE occurs in the selected second) and failure (TGE occurs during one of the other 59 seconds). The binomial distribution is used to obtain the probability of observing **r** successes in **n** trials, with the probability of success on a single trial denoted by **p** (in our case, $\mathbf{p} = 1/60$). The most important assumption of the binomial statistical model is the independent and identically distributed assumption: Trials (outcomes) of the experiment (TGEs) are independent, identically distributed variables, i.e. the assumption of no correlation between TGEs. To check this assumption we first will calculate binomial probabilities with a Web calculator [17] for the minute 22:47, 19 September, 2010; see column 3 in Table I.

For each minute we have a string of numbers. At the minute 22:47 of 19 September, 2009, we have, from 60 seconds, 6 seconds with no TGEs, 16 seconds with 1 TGF, 18 seconds with 2 TGFs, etc. To deal with the statistical experiment producing not only 2 outcomes as the binomial model but several outcomes, we have to adopt another statistical model, i.e. a multinomial model that has the following properties:

(i) The model consists of n repeated trials.
(ii) Each trial has a discrete number of possible outcomes (0 TGEs in a second, 1 TGE in a second, 2 TGEs in a second, ..., 124 TGE in a second).
(iii) On any given trial, the probability that a particular outcome will occur is constant.
(iv) The trials are independent; that is, the outcome of any of the trials does not affect the outcome of other trials.

To check the validity of the multinomial model, we have to compare the numbers of the experimentally obtained frequencies (column 3 of Table I) and expected frequencies calculated by binomial low (column 4 of Table I).

TABLE I. Comparison of the multinomial (H_0), simulated, and measured frequencies.

N of TGEs	Binomial probability $-\pi_i$	Experimental frequency at 22:47 (x_i)	Theoretical frequency $E_i = \pi_i * 60$	$(x_i - E_i)^2/E_i$	Simulated averaged frequency if TGE < 50 μs
0	0.124	6	7	1/7	7.5
1	0.261	16	16	0	15.8
2	0.273	18	17	1/17	16.2
3	0.188	12	11	1/11	11
4	0.096	5	6	1/6	5.6
5	0.039	2	2	0	2.3
6	0.013	1	1	0	1.4
>6	0.004	0	0	0	0.3
Sum	1.0	60	60	0.46	59.7

The validity of the null hypothesis was tested by using Pearson's chi-square test

$$\chi^2 = \sum_{i=1}^{k} \frac{(x_i - E_i)^2}{E_i},$$

where $E_i = N\pi_i$, $N = 60$, is the expected theoretical frequency. The normalized sum of deviations converges to a chi-square distribution with $k - 1$ degrees of freedom when the null hypothesis is true. From Table I we estimate the Pearson's χ^2 test value of 0.46 for 6 degrees of freedom. The corresponding chance probability of H_0 being false we can get from another Web calculator [18]. The chance probability of H_0 being false is 0.2% only; therefore, we do not have enough evidence to reject H_0, and we have to accept it; i.e. the particle bursts detected at 22:47, 19 September, 2010, are independent and identically distributed. From the physical analysis point of view it means that the TGE duration does not exceed 50 μs. We perform also a Monte Carlo study of the problem, generating trials of the short burst with durations less than 50 μs, greater than 50 μs, and less than 100 μs. If the duration of TGE events is greater than 50 μs and less than 100 μs, we can detect only even numbers of TGEs per second: 2, 4, 6, ... And, of course, the χ^2 test will rocket to very high values, thus signaling that events are correlated. Obtained frequencies (averaged by 100 independent trials) are posted in the last column of Table I. Frequencies are in very good agreement with analytical calculations proving the independence of the TGE events with the confidence level 99%. Frequencies of the greater than 50 μs and less than 100 μs trials do not agree with both experimental and analytically obtained frequencies.

V. THE ELECTRICAL FIELD STRUCTURE DURING TGE EVENT ON 4 OCTOBER

The static electric field between the thunderclouds and the ground was measured with the Boltek EFM-100 electrical mill installed on Aragats research station at altitude 3250 m just on the Maket building where particle detectors are located. The electrical field measurements were taken 2 times in a second. In Fig. 8, we see the disturbance of the electrical field at Aragats station during the thunderstorm on 4 October, 18:00–18:40 UT. After a period of ~10 minutes of a large positive electrical field (~30 kV/m), the electrical field changed polarity and during another ~10 minutes reached values of about −30 kV/m (right vertical axes). The large negative field was accompanied by a huge flux of particles measured by the ASEC detectors [the 250% enhancement of the Maket triggers, left vertical axes; see, for details, Fig. 2(c)]. The zoomed pattern of the 2 minutes of the maximal flux, namely, 18:22—18: 24, is shown in Fig. 9 along with gamma-ray time series measured by the 01 combination of the ASNT (10 second time series) and lightning occurrence times.

In Fig. 9, we can see the correlations of electrical field, particle flux, and lightning occurrence in much more detail compared with the 1 minute time series. The decreasing of the electrical field is strongly correlated with the rising gamma-ray flux. Flux is reaching the maximal values near the maximum of the absolute value of the negative electrical field.

By the rectangles the intracloud-lightning occurrence time is denoted, measured by the Boltec storm tracker located on the Maket building. All lightnings within a radii of 5 km around the Maket building are depicted in Fig. 9.

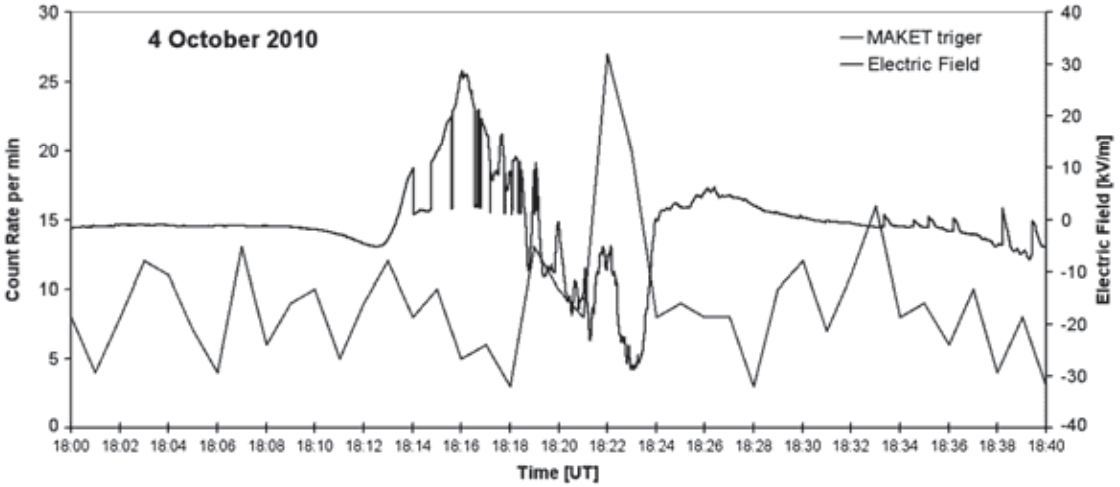

FIG. 8 (color online). The temporal structure of the electrical field disturbances and the time series of the Maket triggers detected on 4 October, 2010.

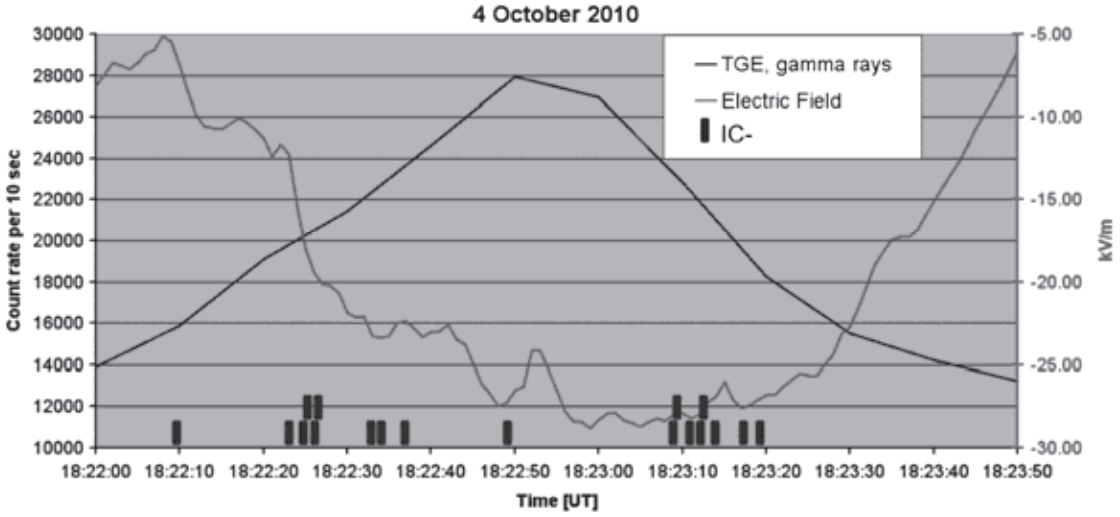

FIG. 9 (color online). Disturbed electric field and count rate of the gamma rays (energy >10 MeV) measured by the 01 combination of the Aragats Solar Neutron Telescope: 4 October, 2010, 18:22–18:24.

Remarkably, only 18 negative intracloud lightnings were detected during the maximal flux of the TGE, no intracloud positive, and no cloud-ground lightning was detected.

VI. DISCUSSION

We report the new observed phenomenon of the short TGEs (duration less than 50 μs) detected by the surface particle detectors at mountain altitudes. Short particle bursts occur during a large negative electrical field measured between cloud and the ground accompanied by numerous negative intracloud lightnings. In two episodes on September 19, 2009, and October 4, 2010, lasting totally 10 minutes, $(8 + 2) \sim 340$ short TGE events were detected. Observed short TGEs, in contrast to prolonged ones (described in detail in our previous paper, Ref. [11]) can be compared with TGFs routinely detected by orbiting gamma-ray observatories [3,5].

(i) The origin of the TGFs was estimated to be in (or just above) thunderclouds in the upper troposphere and lower stratosphere, at altitudes 15–21 km [19,20].

(ii) The mean duration of a TGF is $\sim$500 μs and mean fluence $\sim$1 particle/cm^2 [Ramaty High Energy Solar Spectroscopic Imager (RHESSI) observations].

(iii) Maximal energy—up to 50 MeV by Fermi [2] and AGILE observations [4] and even 100 MeV [21].

(iv) Cummer *et al.* [22] based on a subsample of RHESSI TGFs establish TGF correlation with lightning discharges: 50% of analyzed 26 TGFs are found to occur within $-3/+1$ ms of the positive intracloud (+ IC) lightning discharges inside a $\sim$300 km radii circle around the RHESSI subspacecraft position.

(v) Fermi gamma burst monitor data [23] confirm this finding, establishing an association of the 15 from a total of 50 TGFs with individual discharges. Surprisingly, both associations did not establish the time order of lightning-TGF occurrence.[8]

The observed rich phenomenology of the TGFs shortly presented above poses rather stringent constraints on the physical process responsible for TGF generation. According to analysis in [8,20] the huge upward ($\sim 10^{17}$) flux of the gamma rays is responsible for the observed TGFs. A sufficient amount of the seed electrons necessary for the production of 10^{17} gamma rays by the RREA developing (see Fig. 10) is provided by the streamers and stepped lightning leaders [8–10] in the intracloud positive lightning (+ IC [20]; see Fig. 10). The proposed mechanism also naturally supported the harmony of the time scales of the electron emission and TGF duration (see Table 2 in [8]).

Downward development of the RREA requires a positive electrical field in the cloud and, therefore, a negative field between clouds and the ground (see Fig. 10). The posed limit on the event maximal duration of 50 μs also puts severe restrictions on the physical mechanism responsible for the short TGEs. And again stepped leader propagation fits best to submit seed particles in the time scale adequate to the short TGEs. Consequently, the negative intracloud lightning (− IC) could provide seed particles for the TGEs detected by the Maket detector. As we can see in Fig. 9, the measured electrical field and observed negative intracloud lightnings support the model depicted in Fig. 10.

Thus, the generation mechanisms of the space TGFs and short TGEs are close to each other and symmetric: *RREA*

[8]The estimated mean delay of the RHESSI TGFs relative to lightning is −1.24 ms [22].

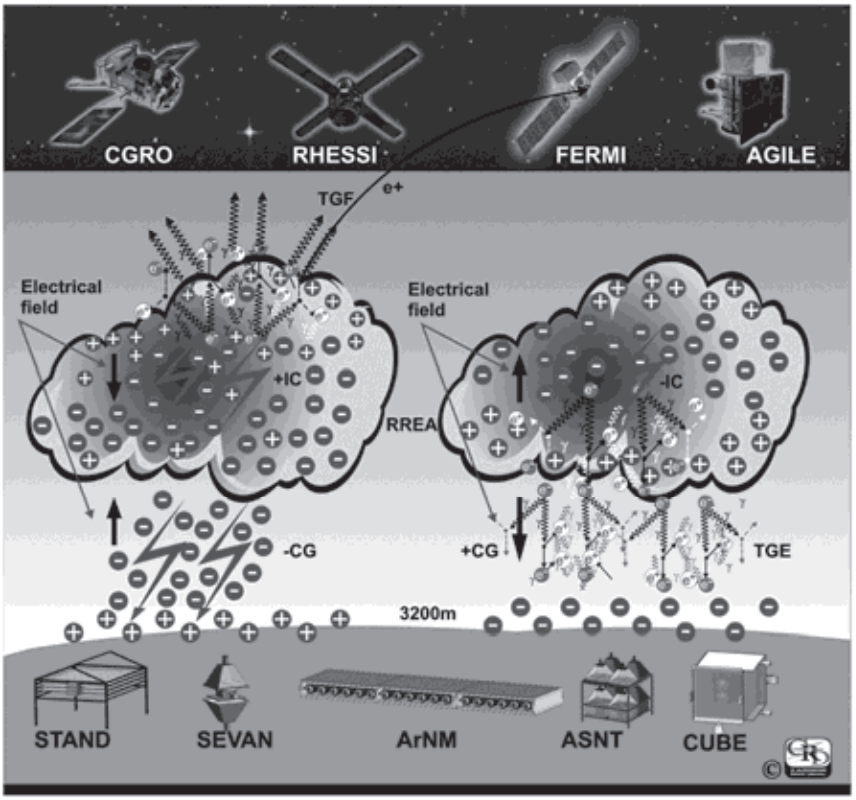

FIG. 10 (color online). Symmetry of the TGFs and TGEs.

uses as the seeds the electrons from the current pulses along the step leaders ($\pm$ IC) *and developing in consequent negative and positive electrical fields.*

Seed electrons for the long TGEs are provided by the ambient population of MeV electrons from the secondary cosmic rays. As we show in [11] the population of the secondary electrons from the particle showers initiated by the primary hadron entering the terrestrial atmosphere is sufficient to generate via the RREA process enough particles to explain the huge surface enhancement on 19 September, 2010.

However, there are significant differences in TGE and TGF events.

(i) Short TGEs are very rare events (detected at Aragats about once a year); the Maket array observes the sky just above the detector ($\sim 10^6$ m^2). Fermi and AGILE are observing huge areas reaching $\sim 10^{12}$ m^2; therefore, the number of detected TGFs is much larger, reaching hundreds per year.

(ii) Nonetheless, because of the closeness of the particle beam, the number of detected TGEs in 2 series of detection is rather large: ~325. TGE develops in a rather dense atmosphere; only the close location of the thundercloud to the ground and rather large elongation of the strong electrical field in the thundercloud can provide unique possibilities of detection of TGE electrons and gamma rays (see details in [11]).

(iii) The duration of the TGE is more than an order of magnitude shorter than the ones of TGF. Gamma rays arriving at satellite altitude are covering at least 3 orders of magnitude longer path length compared to TGEs and arrive spread over a pulse of ~500 μs. TGEs come from thunderclouds just above our heads and cover less than 500 m; therefore, they come in pulses with a duration less than 50 μs.

VII. CONCLUSION

We discover new energetic atmospheric phenomena, namely, short TGEs tightly connected with the ones detected by orbiting gamma-ray observatories, i.e. TGFs. The basis of high-energy emissions from the thunderstorm atmospheres is believed to be large electrostatic fields within thunderclouds, the mechanism—RREA); seed particles—ambient population of MeV electrons from EAS (for long TGEs) and electrons from current pulses of step leaders of intracloud lightning.

ACKNOWLEDGMENTS

This work was partly supported by the Armenian government grants and by ISTC Grant No. A1554.

The authors are grateful to participants of the conference TEPA-2010 and to members of the seminar of the cosmic-ray division of Alikhanyan national lab for useful discussion.

APPENDIX: DISCUSSION ON THE POSSIBILITY OF INTERFERENCES AND ELECTRONIC OR NATURAL INDUCED SIGNALS TO GENERATE PEAKS IN TIME SERIES OF THE ASEC PARTICLE DETECTORS

There are numerous sources of natural and electronics emissions that can mimic the peaks in the time series of particle detector count rates. To answer if the peaks apparent in the time series of the ASEC particle detectors during thunderstorms can be fake, we performed an in-depth analysis of the enhancements of the ASEC detectors and collected evidence demonstrating the existence of the indisputable additional particle fluxes responsible for the detected peaks.

400 m apart at Aragats are in operation same type detectors (AMMM—Aragats Multichannel Muon Monitor—and Maket) with fully independent cabling and DAQ electronics demonstrate similar time-coherent peaks (see Fig. 11).

The enhancements detected by the ASNT are concentrated only in the region of the small energy deposits; the large energy deposits remain unchanged (see Fig. 12).

The ASNT detector measures the incoming directions of the detected particles. The count rates of the near vertical and inclined particles are dramatically different. If we observe huge enhancement in the near vertical direction (expected arrival direction of the RREA particles), at the same time on the same detector using the same DAQ electronics and analysis software we measure a deficit in the inclined particle flux (maybe due to stopping positive muons; see Fig. 13).

The SEVAN particle detector measured 3 types of particle fluxes: low-energy charged particles, neutral particles, and high-energy particles (above 250 MeV, mostly muons). In Fig. 14, we can see a deficit of high-energy muons ($E_\mu > 250$ MeV) and a huge peak in the time series of neutral particles (there is also a peak in the time series of the low-energy charged particles). All 3 types of particle fluxes are detected by the SEVAN detector with one and the same cabling and DAQ electronics.

Nonetheless, we detect some induced signals in a few from hundreds of the ASEC detectors due to radio emission of the lightning. Lightning is a powerful broadband radio signals emitter. The pulse power of the radio signals can reach 100 GW. And if the detector is poorly grounded, or some of the cables have bad isolation, the radio signals induced peaks in these channels. We systematically monitor and repair failure equipment. However, lightning-induced signals in the poorly grounded counters have a very specific shape and follow the pattern of the lightning activity, now also monitored by the ASEC facilities. Therefore, it is not very difficult to outline fake peaks and repair the malfunctioning channels.

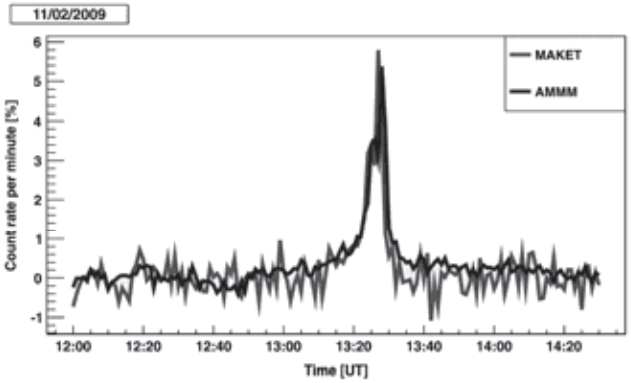

FIG. 11. Time series of the AMMM outdoor 5 cm scintillator and the Maket outdoor 5 cm scintillators located at a distance of 400 m from AMMM; TGE on 2 November, 2009.

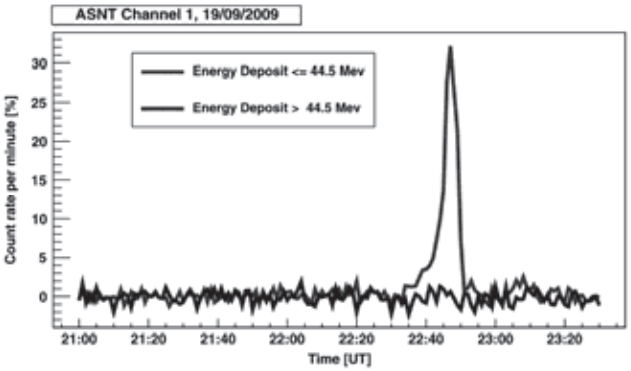

FIG. 12. Time series of the ASNT corresponding to different energy releases during TGE on 19 September, 2009.

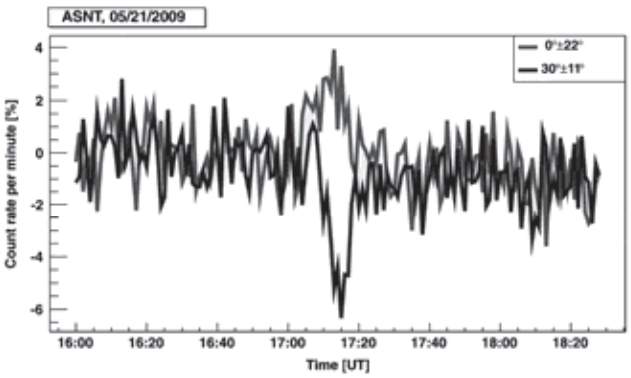

FIG. 13. Time series of ASNT corresponding to different directions of the incoming particle flux; TGE on 21 May, 2009.

[1] J. R. Dwyer, B. W. Grefenstette, and D. M. Smith, Geophys. Res. Lett. **32**, L22804 (2005).
[2] M. S. Brigs *et al.*, J. Geophys. Res. **115**, A07323 (2010).
[3] G. J. Fishman *et al.*, Science **264**, 1313 (1994).
[4] M. Marisaldi *et al.*, J. Geophys. Res. **115**, A00E13 (2010).
[5] D. M. Smith *et al.*, Science **307**, 1085 (2005).
[6] A. V. Gurevich, G. M. Milikh, and R. A. Roussel-Dupre, Phys. Lett. A **165**, 463 (1992); A. V. Gurevich *et al.*, Phys. Lett. A **373**, 3550 (2009).
[7] C. T. R. Wilson, Proc. Cambridge Philos. Soc. **22**, 534 (1925).
[8] B. E. Carlson, N. G. Lehtinen, and U. S. Inan, J. Geophys. Res. **114**, A00E08 (2009).
[9] G. D. Moss, V. P. Pasko, N. Liu, and G. Veronis, J. Geophys. Res. **111**, A02307 (2006).
[10] Z. Saleh, J. Dwyer, J. Howard, M. Uman, M. Bakhtiari, D. Concha, M. Stapleton, D. Hill, C. Biagi, and H. Rassoul, J. Geophys. Res. **114**, D17210 (2009).
[11] A. Chilingarian *et al.*, Phys. Rev. D **82**, 043009 (2010).
[12] N. S. Khaerdinov, A. S. Lidvasky, and V. B. Petkov, Atmos. Res. **76**, 346 (2005).
[13] A. Chilingarian *et al.*, J. Phys. G **29**, 939 (2003).
[14] A. Chilingarian *et al.*, Nucl. Instrum. Methods Phys. Res., Sect. A **543**, 483 (2005).
[15] A. Chilingarian *et al.*, Astropart. Phys. **28**, 58 (2007).
[16] K. Arakelyan *et al.*, in *Proceedings of the Third International Conference Solar Extreme Events, National & Kapodistrian University of Athens, Greece* (National & Kapodistrian University of Athens, Athens, 2009), pp. 363–367.
[17] http://stattrek.com/Tables/Binomial.aspx.
[18] http://www.physics.csbsju.edu/stats/chi-square_form.html.
[19] J. R. Dwyer, B. W. Grefenstette, and D. M. Smith, Geophys. Res. Lett. **35**, L02815 (2008).
[20] E. Williams *et al.*, J. Geophys. Res. **111**, D16209 (2006).
[21] M. Tavani *et al.*, Phys. Rev. Lett. **106**, 018501 (2011).
[22] S. A. Cummer, Y. Zhai, W. Hu, D. M. Smith, L. I. Lopez, and M. A. Stanley, Geophys. Res. Lett. **32**, L08811 (2005).
[23] V. Connaughton *et al.*, J. Geophys. Res. **115**, A12307 (2010).

Atmospheric Research 114–115 (2012) 1–16

Contents lists available at SciVerse ScienceDirect

Atmospheric Research

journal homepage: www.elsevier.com/locate/atmos

Recovering of the energy spectra of electrons and gamma rays coming from the thunderclouds

Ashot Chilingarian, Bagrat Mailyan *, Levon Vanyan

A. Alikhanyan National Laboratory, Yerevan Physics Institute, Alikhanyan Brothers 2, Yerevan, Armenia

ARTICLE INFO

Article history:
Received 9 October 2011
Received in revised form 25 April 2012
Accepted 11 May 2012
Available online 19 May 2012

Keywords:
Thunderclouds
Atmospheric electricity
Lightning

ABSTRACT

Strong electric fields inside thunderclouds give rise to enhanced fluxes of high-energy electrons and, consequently, gamma rays and neutrons. During thunderstorms at Mount Aragats, hundreds of Thunderstorm Ground Enhancements (TGEs) comprising millions of energetic electrons and gamma rays, as well as neutrons, were detected at Aragats Space Environmental Center (ASEC) on 3200 m altitude. Observed large TGE events allow for the first time to measure the energy spectra of electrons and gamma rays well above the cosmic ray background. The energy spectra of the electrons have an exponential shape and extend up to 30–40 MeV. Recovered energy spectra of the gamma rays are also exponential in energy range 5–10 MeV, then turns to power law and extends up to 100 MeV.

1. Introduction: Thunderstorm ground enhancements (TGEs)

The attempts to discover high-energy phenomena in the atmosphere, so called, Thunderstorm Ground Enhancement (TGE), in spite of a long history since prediction of C.R.T. Wilson in 1924 (Wilson, 1925), were discrepant and rare. Early measurements (Schonland, 1930; Schonland and Viljoen, 1933) reported the existence of electron flux simultaneously, or earlier, than lightning located 30 km apart. Atop Mount Lemmon (altitude 2800 m) at the lightning research facility of the University of Arizona, the simultaneous detection of cosmic ray flux (by the 10-cm diameter and 10-cm length plastic scintillator) and electric field (by an electric field mill) demonstrates ~10% enhancement of the 1-minute count (Shaw, 1967). The average excess duration was ~10 min; the threshold energy of the particle detector was ~100 keV. The Italian EAS-TOP surface array (Aglietta et al., 1989) measures significant excesses in the air shower count rate lasting 10–20 min. The enhancements with maximum amplitude of 10%–15% were attributed mostly to the highest energy Extensive Air Showers (EAS; large shower sizes, $>10^6$ electrons), and to zenith angles of incidence smaller than 20°; "thickness" (time interval of the EAS particles arrival) of shower was slightly larger than in normal conditions (Vernetto et al., 2001).

A radiation monitoring post in a nuclear power plant in Japan reports on a comprehensive observation of a gamma ray burst emission lasting less than 1 min—correlated with snow and lightning activity. Enhancements were detected only during wintertime, when thunderclouds are as low as several hundred meters (Torii et al., 2002). The same group observed a summer thunderstorm at the top of Mount Fuji (3776 m high). The flux of high-energy gamma rays had continuous energy spectrum up to 10 MeV, prolonged up to 20 min. The authors of Torii et al. (2009) claim that the bremsstrahlung photons generated by the energetic electrons were produced continuously due to an intense electric field in the thundercloud rather than having originated in the process of lightning discharge.

A Japanese group on another Japanese power plant also detected short (less than 1 min) gamma ray bursts during winter thunderstorms (Tsuchiya et al., 2007). The same authors reported a simultaneous detection of gamma rays and electrons at a mountain observatory Norikura located 2770 m above sea level (Tsuchiya et al., 2009). Two emissions, lasting 90 s, were associated with thunderclouds. At the same research station at Norikura in the Japanese Alps a large multilayered particle

* Corresponding author.
E-mail address: mbagrat@gmail.com (B. Mailyan).

0169-8095/$ – see front matter © 2012 Elsevier B.V. All rights reserved.
doi:10.1016/j.atmosres.2012.05.008

detector operates, primarily intended to register solar neutron events. In August 2000 on account of thunderstorms, particle flux enhancement was detected in 3 layers of a 64 m^2 area detecting system (Muraki et al., 2004).

In experiments at the Baksan Neutrino Observatory of the Institute for Nuclear Research, the time series of hard and soft components of secondary cosmic rays are continuously measured along with measurements of the electric field and monitoring of thunderstorms. Intensity changes of the soft cosmic rays (below 30 MeV) and hard component (>100 MeV) were studied (Lidvansky and Khaerdinov, 2009). It was shown that the critical field and particle energy for this process are ~300 kV/m and ~10 MeV respectively (Khaerdinov et al., 2005).

A network of the NaI detectors along with EAS triggering system is located at Tien-Shan Cosmic Ray station of the Lebedev Physics Institute, at altitude of 3340 m. The goal of the research is to detect runaway breakdown initiated by EAS with energy above 1000 TeV—so-called RB-EAS discharge. Based on short gamma flashes (less that 200 μs) detected by the network of gamma ray detectors, the authors of Gurevich et al. (2009) claim that RB-EAS discharge is a rather rare event — occurring in only ~1% of all EAS registered during thunderstorms, requiring coincidence of several conditions. The most important of them being that the strong electric field should be located not higher than 400–500 m above the detector.

Recently Japanese groups perform new measurements of gamma ray emission and detect the source of the radiation in thundercloud moving across locations of several nuclear power plants (Torii et al., 2011; Tsuchiya et al., 2011).

Facilities of the Aragats Space Environment Center (ASEC) (Chilingarian et al., 2003, 2005) observe charged and neutral fluxes of secondary cosmic rays by the variety of particle detectors located in Yerevan and on slopes of Mount Aragats at altitudes 1000, 2000 and 3200 m. ASEC detectors measure particle fluxes with different energy thresholds as well as EAS initiated by primary proton or stripped nuclei with energies greater than 50–100 TeV (Chilingarian et al., 2010). Abrupt enhancements of particle detector count rates correlated with thunderstorm activity, so called Thunderstorm Ground Enhancements (TGEs) detected during 2008–2011 bring vast amounts (243 TGE events) of small and very few large TGEs (only 6 TGE events with amplitude exceeding 20%) allowing the detailed analyses and taxonomy of the new high-energy phenomena in the atmosphere.[1] The flux enhancement is presented in percent relative to rather stable background of the ambient population of secondary cosmic rays. As we can see in the left corner of the histogram (Fig. 1), majority of TGE events have amplitude less than 10%. These small TGEs and analogical TGEs reported by other groups can be explained by the modification of the energy spectra of charged particles in the electric field of thunderclouds. Due to asymmetry of positive-to-negative flux of secondary cosmic rays in the terrestrial atmosphere, peaks and dips can arise in time series of count rates of surface particle detectors. These effects have been theoretically analyzed in Dorman and Dorman (2005) and detected on Mount Norikura (Muraki et al., 2004) and in Baksan, Russia (Alexeenko et al., 2002). Measurements at ASEC and simulations with GEANT4 package (Agnsotelli et al., 2003) confirm additional flux of gamma rays up to 1000% in the energy range of 2–20 MeV and up to 10% in the energy range up to 100 MeV. Simultaneously dips in the muon flux at energies above 200 MeV were obtained by GEANT4 simulations and detected by ASEC detectors.

Few very large enhancements seen in the right corner of Fig. 1 can be explained only by invoking the Runaway Breakdown (RB) process (Gurevich et al., 1992), also referred as Relativistic Runaway Electron avalanche (RREA, Dwyer, 2003, 2007; Carlson et al., 2008). Ambient population of secondary cosmic ray electrons in the electric fields with strength greater than the critical value[2] unleashes the electron-gamma ray avalanches and total number of particles on the exit from cloud can be multiplied by several orders of magnitude. Proceeding from the measurements of the charged and neutral fluxes as well as from the energy deposit of particles in thick scintillators, we recover the energy spectra of TGE electrons and gamma rays for the 2 largest TGE events of September 19, 2009 and October 4, 2010. Installation of Aragats field meters (Boltek firm electric mill EFM100, http://www.boltek.com/efm100.html) and lightning detectors (LD250 powered by the software from Astrogenic systems, http://www.boltek.com/ld250.html) allows correlating the measured particle fluxes with near-surface electric field disturbances and with occurrences of lightning of different types.

In Fig. 1, we present the histogram of the 243 TGE amplitudes (relative enhancements above cosmic ray background) measured by the MAKET detector in 2008–2011; the dates of 4 largest TGE events are displayed as boxed text. Lightning occurrences, as well as sketch of the RREA process in upper and lower dipoles also are depicted. The indispensible condition of TGE initiation is the creation of the lower dipole accelerating electrons downward. The temporarily emerging lower positive charge region (LPCR, Qie et al., 2009) is smaller than the mid-level negative and upper positive layers of the main upper thundercloud dipole (Williams, 1989). Therefore TGE phenomena are local and its duration coincides with the duration of the LCPR, which is usually ~10 min.

The critical electric field strength for the conventional discharge in thunderclouds is very large (~10 times more than RREA critical field) and was never measured in thunderclouds. Therefore, electron-gamma ray avalanches could initiate lightning by creating the initial conductive channel (Gurevich et al., 1999; Dwyer, 2005). Lightning in turn can provide the RREA process with additional seed electrons from the current pulses along developing lightning leader channels (Carlson et al., 2009; Lu et al., 2010, 2011; Cummer et al., 2011).

For the Terrestrial Gamma-ray Flashes (TGFs, Fishman et al., 1994) the physical model is symmetric. The electrons are accelerated upward by the negative field between main negative layer in the middle of the cloud and main positive layer near the top of the cloud. The additional seed electrons are provided by the positive intracloud lightning occurrences usually accompanying the detection of TGFs by the orbiting

[1] Time series of changing particle fluxes registered from ASEC monitors, as well as magnetometer and electrical mill measurements are available from http://adei.crd.yerphi.am/adei/.

[2] The critical electric field $E_t = 1.534$; 1.625, and 1.742 kV/cm at 4500, 4000 and 3400 m respectively. E_t dependence on altitude follows the air density dependence on altitude.

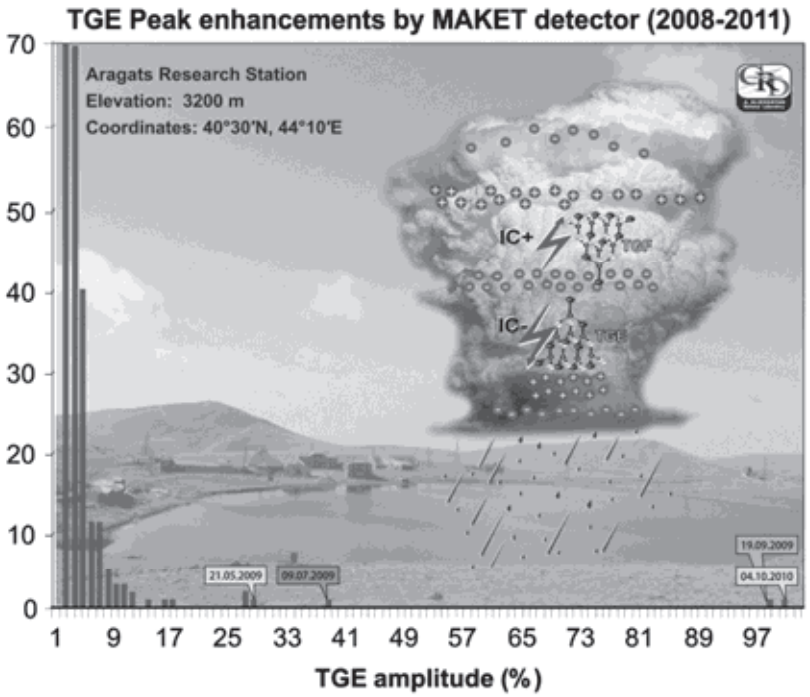

Fig. 1. The histogram of the amplitudes of TGE events detected by ASEC detectors in 2008–2010. The peak values of the cosmic ray flux increase above rather stable secondary cosmic ray background were measured by the outdoor plastic scintillators.

gamma ray observatories (Stanley et al., 2006; Cummer et al., 2005).

2. Dynamics of TGE events

Despite big varieties of measurements in the thundercloud electric field profiles the following basic structure of the electric field in thunderclouds is widely accepted: from the ground up to the cloud base there is usually a low magnitude field (both positive or negative); relatively small positively charged "pocket" (comprising only ~20% of negative charge higher) is responsible for the larger positive field prolonged up to negatively charged layer at 1–2 km above cloud base; and the negative field is extended about 1–4 km above the negative layer where the main positive charge is located (Stolzenburg et al., 1998). In presence of the positive electric field (pointed upward)[3] within the cloud, the electrons are accelerated downward and, dependent on the strength of the field, the flux of electrons and gamma rays reaching earth surface may exhibit significant amplification. As shown in Fig. 1, most of TGE events have rather small amplitudes; sometimes (less often than once per year) under yet fully unknown conditions the RREA process is unleashed and surface detectors measure huge TGEs surpassing rather stable cosmic ray background flux several times. The necessary condition for the RREA process is the creation of the considerably large positively charged layer in the bottom of the cloud. The manifestation of the existence of such layer is the absence of the cloud-to-ground lightning occurrences (leader attempts) due to the "blocking" of descending negative leader from reaching the ground. Simultaneously, significant enhancement of the intracloud negative lightning (Cui et al., 2009) occurrences took place due to the "converting" potential of the cloud-to-ground flash to an intracloud one (Nag and Rakov, 2009). On May 27, 2011, we detected a large TGE event by the 5 NaI crystals of size $30\times12.5\times12.5$ cm^3 newly installed at Aragats.

In Fig. 2, we can see the abrupt increase of the near-surface electric field at 13:07 UT caused by the negative cloud to ground (−CG) lightning flash that contained several strokes to the ground; thereafter the polarity of the electric field starts to reverse.[4] After 13:08 UT the TGE started (green curve) and −CG lightning occurrences stopped after 13:10 UT. At 13:12–13:15 UT we detect numerous intracloud negative discharges (−IC) in radii of 3 km, suggesting the screening of the ground by lower positive charge region (LPCR). The lightning stepped leader may provide the RREA process with additional seed electrons (by the "cold" runaway process, Moss et al., 2006) and at 13:12–13:15 UT the gamma ray intensity peaked at ~70% level above the background when the near surface electric field reaches its minimum.

The LPCR with main negative layer in the middle of the cloud forms lower dipole, responsible for the downward electron acceleration and also playing major role in initiation of cloud-to-ground (−CG) and intracloud (−IC) lightning

[3] We adopt the "atmospheric electricity" sign convention: the positive field (E kV/m) accelerates electrons downward in the direction of the Earth; the negative field (−E kV/m) vice-versa accelerates electrons upward in the direction of space.

[4] The rapid changes of the near-surface electric field usually are accompanied also with rapid change of the electric field within thundercloud (Standler and Winn, 1979).

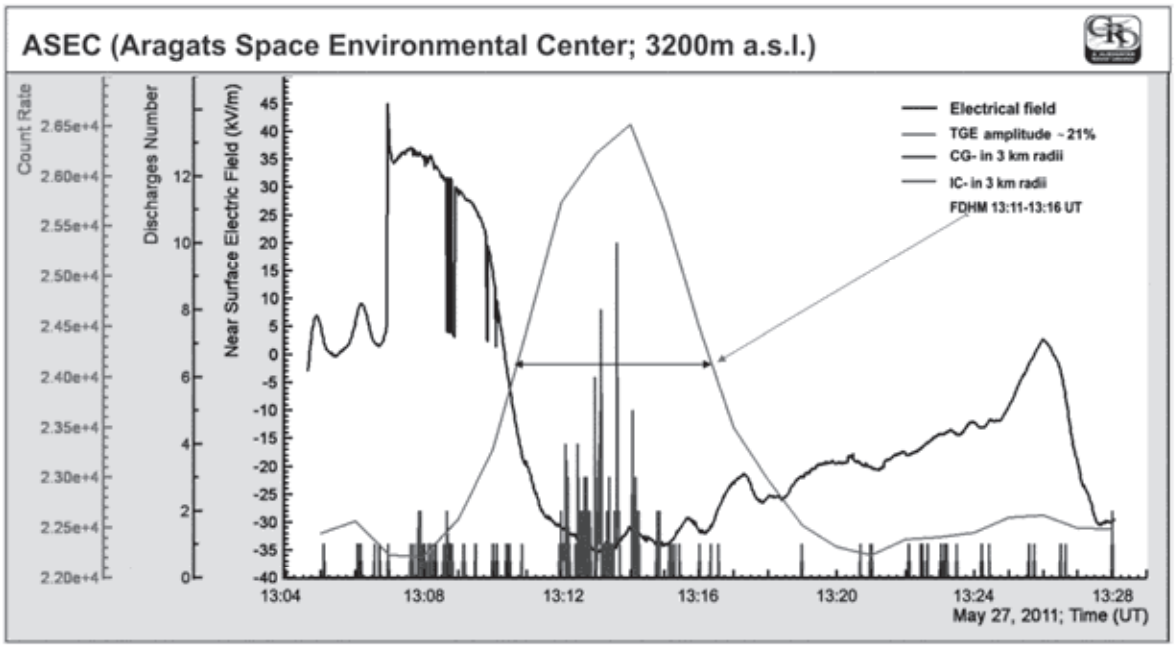

Fig. 2. The near-surface electric field (black curve) and frequency of lightning occurrences measured by the Bolter detector each second (2 left vertical axes). 143-CG − lightning occurrences were detected at 13:05–13:10 UT in the radii of 10 km (blue) and 139 IC − lightning occurrences − at 13:12–13:15 UT, radii of 3 km (red). Time series of the NaI crystals count rate (green curve, right vertical axes) demonstrate ~70% enhancement on May 27, 2011 at Aragats, 3200 m a.s.l. (For interpretation of the references to color in this figure legend, the reader is referred to the web version of this article.)

occurrences. Many researchers outline the dominant role that LCPR plays in initiating/triggering an intracloud and cloud-to-ground lightning discharges (Pawar and Kamra, 2004; Nag and Rakov, 2009; Qie et al., 2009). We suggest that development of the LCPR also has a major role in TGE initiation. The locality of the RREA can be explained by the small sizes of the lower positive charge region and the transient character of LCPR can explain the duration of the TGE. Based on the detection of the winter thunderstorms by Japanese authors of Tsuchiya et al. (2011), they estimate the radii of the circle of intense RREA radiation to be 600 m. Another Japanese group (Torii et al., 2011) detects moving at the speed of 7 m/s energetic radiation source at the height of 300 m along with the negatively charged region within the thundercloud at the height of around 1 km. The radiation was emitted from a downward hemispherical surface with radii of 700 m. These findings demonstrate the locality of the RREA process and imply that the number of additional gamma rays can vary significantly depending on the "impact parameter" of the thundercloud relative to the detection site (see also Babich et al., 2010).

Therefore, it is not always the lower dipole that initiates TGE; an evidence of the emerging LPCR without initiated TGE can be seen in Fig. 3. On June 8, 2011, the fair weather field was changed by moderate positive field at 11:29 UT; then electric field reversal happened at ~11:33 UT and field reach negative value was ~−30 kV/m. At 11:55 UT, electric field abruptly changes the polarity and simultaneously the (−CG) lightning occurrences stopped and the intracloud negative lightning (−IC) occurrence started. From Figs. 2 and 3, using the model sketched in Fig. 1, we can conclude that the creation of LCPR stopped −CG lightning occurrences and initiated −IC lightning occurrences. At the same time, near surface electric field changes the polarity and turns from positive to negative. It is also worth mentioning that during this thunderstorm we do not observe any significant TGE in charged and neutral fluxes. The reason of it can be the much higher intensity of the −IC lightning occurrences, comparing with May 27 TGE, which does not allow the development of the mature RREA process. Another reason can be the distant location of the positive bottom layer; only if the positive layer is above the detectors the RREA process can accelerate electrons downward in the direction of the observer.

Continuous measurements of the lightning activity, near-surface electrical field and particle fluxes give a possibility for the first time to investigate the interrelations of these geophysical parameters and estimate the intracloud (IC-) to cloud-to- ground (CG)-lightning flash ratio (Z, Pinto et al., 2007; De Souza et al., 2009) during thunderstorms at Aragats. The Z ratio gives information about the electrical activity in thunderstorms and can be a clue about how the centers of the charge are disposed in the clouds. Our finding that Z is peaked at the minimal near-surface electrical field and the maximum of RREA particle flux confirms that Z is directly correlated with LPCR development.

In Fig. 4, we demonstrate another type of the TGE event: relatively small near-surface electric field and absence of any kind of lightning occurrences accompanied by the moderate count rate enhancement. At 8:35 UT, October 16, 2010 we observe abrupt decrease of the electric field, followed after 2 min by a ~7% enhancement of the count rate of the outdoor plastic scintillators. No lightning occurrence within 10 km was observed during ~10 min of negative field duration and TGE detection.

As the strength of the near-ground electric field was 2 times less than at 27 May and there were no lightning occurrences we can assume that the LCPR was not well developed, and RREA process was not started.[5] The TGE initiation at 16 October can be connected with Modification Of the energy Spectra

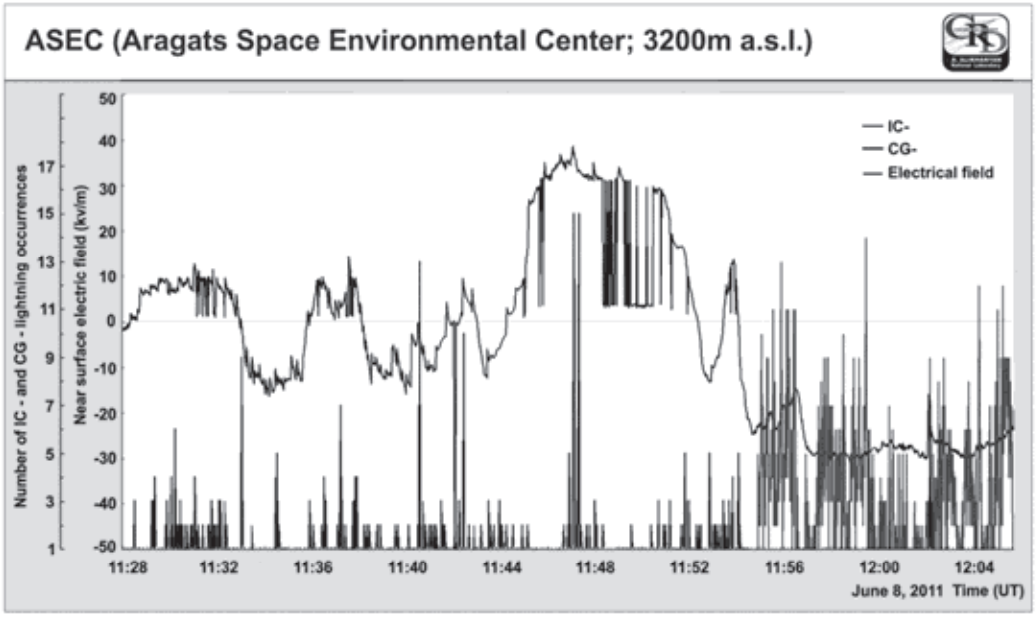

Fig. 3. The disturbances of near-ground electric field and frequency of cloud to ground (−CG) lightning occurrence at Aragats, 3200 m on June 8, 2011.

(MOS) of charged cosmic rays entering the region of the strong electric field within the thundercloud. Thus we introduce 2 types of the TGE origin: RRE avalanches responsible for very rare huge particle multiplication in the thunderclouds (up to 1000%) and MOS process — responsible for much often but small and modest (less than 10%) TGEs.

3. Acceleration and deceleration of the secondary charged cosmic rays in weak electric fields

From the consideration of the three thunderstorm events above, we can conclude that by no means electric fields in thunderclouds ultimately result in TGE, and far not all TGEs are due to RREA process. In the database of ASEC time series, we can find significant non-random variations of cosmic ray intensity in the absence of any lightning occurrences, indicating that the electric field strength in the cloud is below the RREA threshold. In Dorman and Dorman (2005), the theory of the modulation of the secondary cosmic ray by the various meteorological effects, including strong electric fields within thunderclouds is developed. Electrons and negative muons are accelerated downwards by a lower dipole before reaching particle detector. The positrons and positive muons as well as protons will be decelerated in the lower dipole. The positive charge of primary cosmic rays (mostly protons and stripped nuclei) introduces several asymmetries between particles and antiparticles born in atmospheric cascades. The intensity of the MeV electrons is larger than the intensity of positrons of the same energies in energy range of 1–50 MeV; the intensity of positive muons above 100 MeV is larger than the intensity of the negative muons, see Figs. 5 and 6 (obtained by EXPACS package, Sato et al., 2009).

We can see in Fig. 5 that the number of electrons with energies below 50 MeV at 5000 m altitude is significantly larger than the positrons. It means that positive electric field in the thundercloud will significantly alter the total intensity of low energy charged particles registered by scintillators at the Earth surface. The changes of intensity will manifest themselves as peaks and dips in the time series of count rates of particles registered by the scintillators located on the Earth surface. The energy spectrum of electrons will be shifted to the right (mean energy becoming larger) leading to the additional bremsstrahlung gamma rays; energy spectrum of positions shifted to the left is not sufficient to compensate these enhanced counts. The attenuation of the electrons in the atmosphere is much larger than the one of the gamma rays. Therefore, most TGE events are detected in the fluxes of gamma rays born by accelerated electrons.

Interestingly, positive fields have opposite influence on counts of muons at energies above 200 MeV. Among ASEC particle detectors there are scintillators with energy threshold greater than 200 MeV and the electron acceleration described above will not influence their count rate. Due to the abundance of the positive muons over the negative muons (1.2–1.3 times, at 100–500 MeV energies, Wentz et al., 2003, see Fig. 6) the braking of positive muons in the positive electric field cannot be compensated by the acceleration of the negative muons in the same field. The consequences of this asymmetry are indicated in Fig. 7. On October 4, 2010, we detected ~5% deficit in the flux of muons with energies greater than ~200 MeV, which concurred with a huge excess of low energy gamma rays and electrons.

[5] Of course, the combination of measurements on the microsecond scale of the lightning occurrences of different types and of the TGE in electron and gamma ray fluxes, as well as the electric field strength within the thundercloud is needed for the definite conclusion on the interrelations of these phenomena.

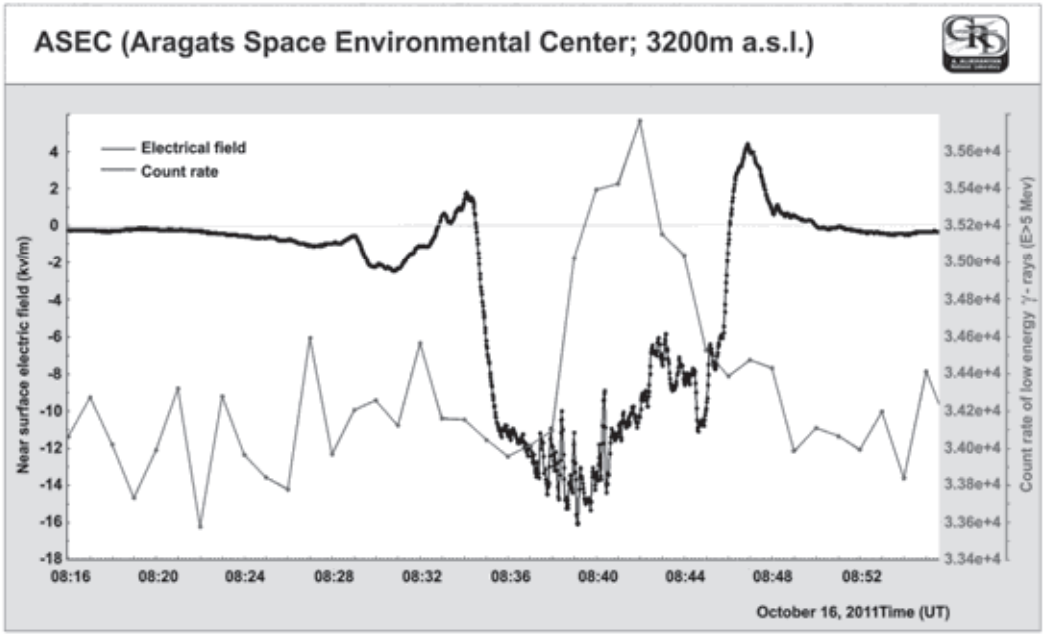

Fig. 4. The TGE event on 16 October 2010, the bold black line is the near-surface electric field strength; the gray line is the minute count rate of the 3 cm thick outdoor scintillator (energy threshold 4 MeV).

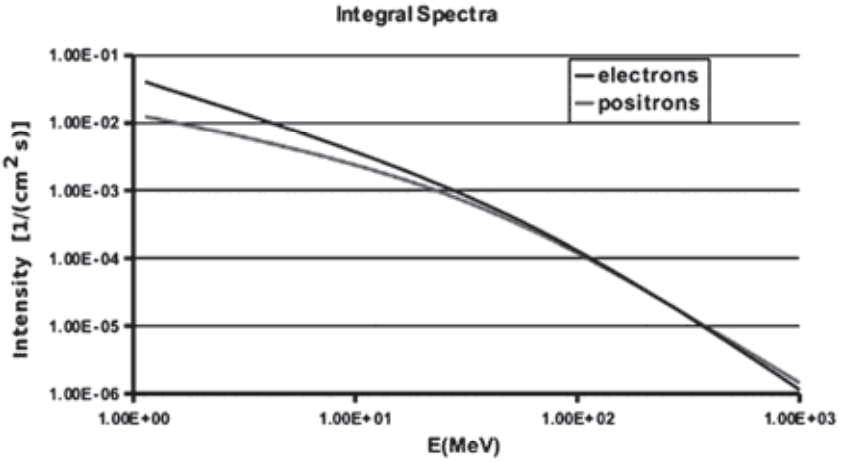

Fig. 5. The energy spectra of electrons and positrons at altitude of 5000 m a.s.l.

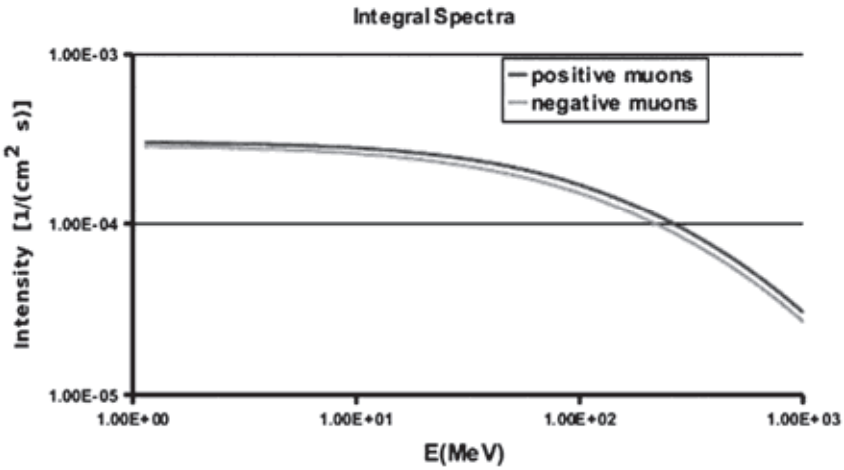

Fig. 6. Energy spectra of muonsat altitude 5000 m a.s.l.

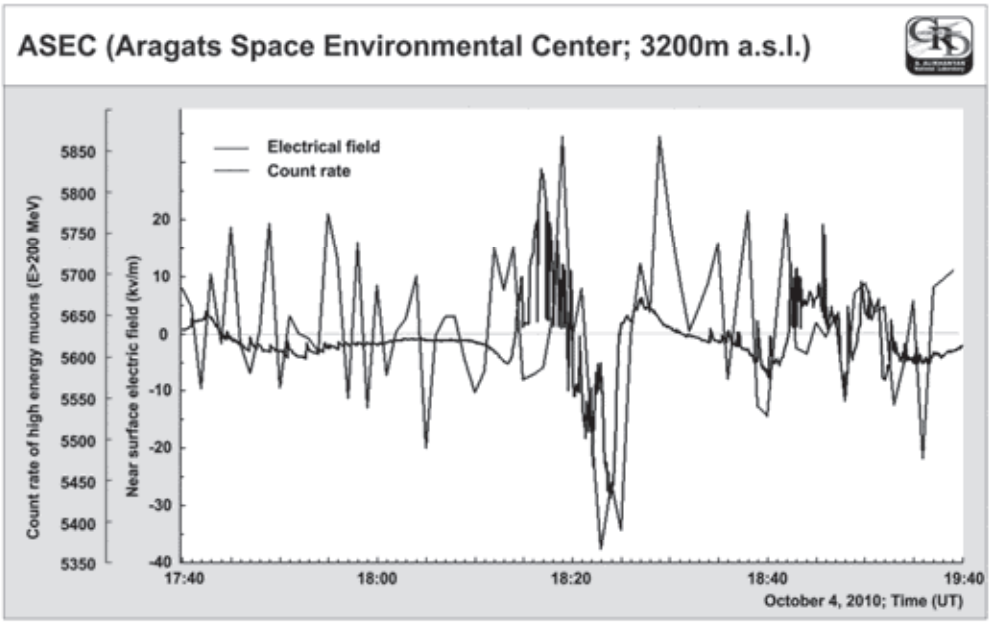

Fig. 7. The positive field in the thundercloud (electrons are accelerated downwards) stops positive muons; charge ratio of positive-to-negative muons is ~1.2–1.3, therefore we detect ~5% deficit of the flux of high-energy muons (energy > 200 MeV); simultaneously huge TGE in gamma ray and electron fluxes were measured.

4. GEANT4 simulations of particle propagation in strong electrical fields of thunderclouds

To get clues in the mechanisms of electron acceleration in the thunderclouds we implement simulations using a simple model of the electric fields in the thundercloud. GEANT4 simulations of the particle propagation in thunderclouds were performed with an electric field of 1.8 kV/cm spread uniformly from 5000 m till 3600 m a.s.l. Secondary Cosmic Ray (CR) electrons as seed particles in the energy range of 1–300 MeV and with fixed energy 1 MeV (simulating "pure" RREA process, ~1 MeV electrons commit minimal ionization losses in the atmosphere) were used. We chose the uniform electrical field strength above the critical energy of the RREA process at altitudes from 5000 m to 3400 m (1.7 kV/m) and fields below this threshold to illustrate the influence of the modification of secondary CR particle spectra (MOS process), as was described in the previous section.

In Fig. 8, we can apparently see 2 modes of particle generation. The RREA mode with maximal energy of electrons is 30–40 MeV and gamma rays — 20–30 MeV and MOS mode accelerating electrons up to 60–70 MeV; gamma ray spectrum prolonged up to 80–90 MeV. The electron and gamma ray energy spectra in the energy range of 1–10 MeV demonstrate large multiplication of electrons in the RREA process and huge amplitudes of the TGEs. MOS regime is fast fading after 50 MeV and needs large surfaces of particle detectors to be measured above the background of ambient population of secondary cosmic rays.

The high-energy tail of the gamma ray spectrum is due to enhanced bremstrahlung radiation of the higher energy electrons traversing the electric field of the cloud. Because of the highly enlarged radiation losses, high energy electrons cannot unleash the RREA, however, the additional flux of gamma rays radiated by these electrons can reach the mountain altitudes and be registered as small and modest enhancement over CR background — see the histogram in Fig. 1.

To prove our hypothesis on 2 component origin of TGE, we perform the same simulation with a fixed flux of 1 MeV seed electrons. The shape of electron and gamma ray spectra coincides with spectra obtained with 1–300 MeV electron seeds (exponential function — reflecting the particle multiplication in the avalanche process), however there are no high energy tails, see Fig. 9. Thus, pure RREA process with chosen electrical field parameters cannot produce TGE electrons with energies above 30–40 MeV and gamma rays with energies above 20–30 MeV.

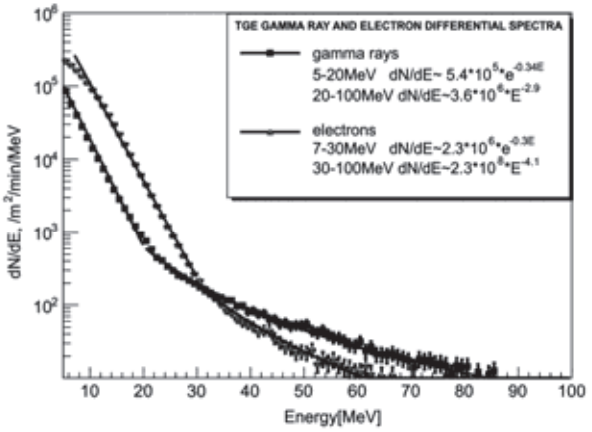

Fig. 8. TGE electron and gamma ray spectra obtained from GEANT4 simulation of RREA process in an electric field of 1.8 kV/cm with seed electrons of 1–300 MeV.

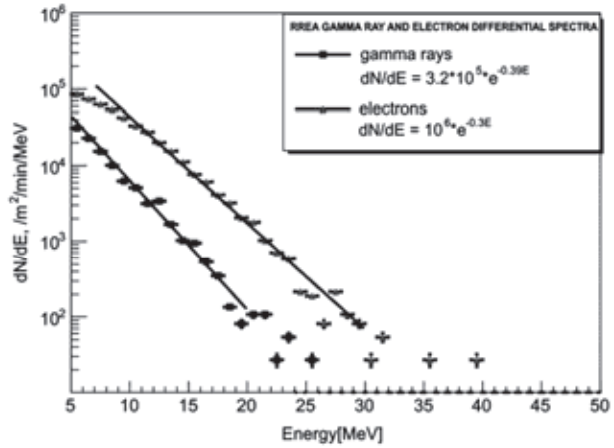

Fig. 9. The electron and gamma energy spectra obtained in electric field of 1.8 kV/m prolonged from 5000 till 3400 m with 1 MeV electron as seeds.

To prove that MOS process can provide high-energy gamma rays we perform simulations of the electron propagation in the moderate electric field below RREA initiation threshold (1.5 kV/m). In Fig. 10 we see that only the modification of the energy spectra of electrons can significantly enlarge the yield of the gamma rays reaching the earth surface. Electrons attenuate in the atmosphere after exiting from the cloud; however, as we can see from Fig. 10, the gamma rays survive.

5. The energy spectra of TGEs

5.1. TGE electron spectrum

The ultimate check of the RREA process detected on the ground is the measuring of the energy spectra of electrons and gamma rays well above the background of cosmic rays. Among hundreds of TGE events detected at ASEC only

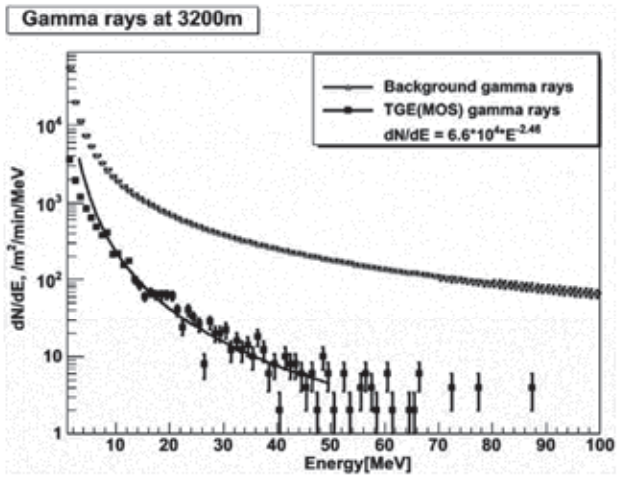

Fig. 10. Comparison of background gamma ray spectrum with the surplus gamma ray spectrum generated by electrons accelerated in the field of strength 1.5 kV/m below the critical field for the RREA initiation; the background cosmic ray gamma ray flux and TGE gamma ray flux are calculated at 3200 m altitude after exiting from the uniform electrical field at 3350 m altitude.

September 19, 2009 and October 4, 2010 TGEs allow the electron energy spectra recovering. After the estimation of the gamma ray flux, we subtract the obtained gamma-ray contamination, taking into account the efficiencies to register gamma rays by the particular detector and recover electron integral energy spectrum using several detectors with different energy thresholds. In Fig. 9, electron spectra of September 19, 2009 and October 4, 2010 TGEs are presented. The spectrum of September 19, 2009 TGE was obtained by additional counts of plastic scintillators with energy threshold of 9, 12, 15, 18 and 25 MeV (52, 826, 21,773, 15,967, 6750 and 506 electrons per minute per m^2, were registered respectively). The spectrum was approximated with exponential function (see fit parameters in the legend of Fig. 9); corresponding exponential mean energy equals to ~3.3 MeV. Scintillators with thresholds of 2, 7 and 12 MeV (36,089, 3896 and 459electrons per minute per m^2,was registered correspondingly) were used to recover the October 4, 2010 TGE electron integral spectrum; for this event the mean energy equals to ~2.3 MeV; both values are significantly smaller comparing with estimates based on simulations of the RREA (Lehtinen et al., 1999; Dwyer, 2004, ~7.2 MeV); however the 7.2 MeV value was obtained for the electrons just exiting the electrical field and for rather large electrical field strengths, 2 considered measurements at Aragats were made according to our estimates 50–150 m below the thundercloud (Fig. 11). For the details of separation of electrons and gamma rays and October 4, 2010 TGE electron spectrum recovery, see Appendix A.

5.2. The energy spectra of the TGE gamma rays

The energy spectra of September 19, 2009 and October 4, 2010 TGE gamma rays are recovered based on the energy deposit spectra measured by Cube and ASNT detectors (see details of detector operation in Chilingarian et al. (2010) and details of spectra recovery in the Appendix B). Both Cube and ASNT detectors are measuring the energy deposit histograms and store them each minute. These histograms reproduce the

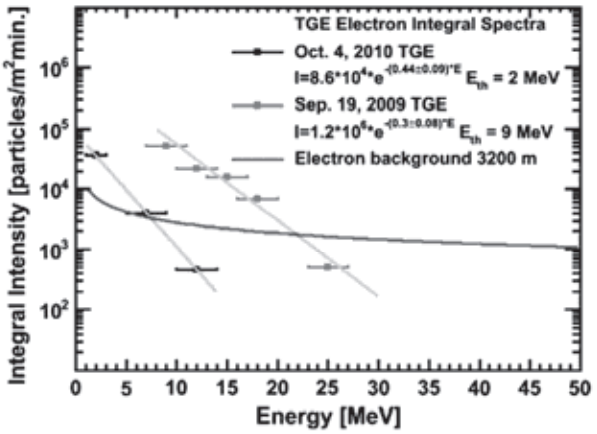

Fig. 11. Electron integral energy spectra of the September 19, 2009 and October 4, 2010 TGEs measured at 3200 m compared with the energy spectrum of the ambient population of the cosmic ray electrons at the same altitude (background).

energy spectrum of gamma rays, however they are folded by the detector response very differently for Cube and ASNT detector assemblies. Recovering the energy spectrum by the energy deposit histograms, i.e. solving the inverse problem of cosmic ray physics is rather a complicated task and we use multiple trial spectra for solving it (see for details Appendix B). The outdoor Cube detector was installed at Aragats in Spring 2010, near MAKET building, providing lower threshold of detected particles than indoor detector ASNT. Thus, only for October 4, 2010 TGE, we recover the gamma ray energy spectrum in the range of 5–10 MeV. The spectrum was approximated by both exponential and power law functions. Exponential function with mean energy of ~3.8 MeV provides slightly better approximation of the measured energy deposit with simulated one, than power law fit with index −1.8. χ^2/ndf were ~2 and ~3 for the exponential and power functions respectively.

Since the maximal energy deposit in Cube detector is less than 40 MeV (the scintillator thickness is only 20 cm, comprising ~0.5 radiation lengths), we can reliably recover the spectrum at energies higher than 40 MeV with the ASNT detector assembly only (4 independent detectors comprising scintillators of 60 cm thickness, ~1.5 radiation length).

We use the Cube energy deposit spectra for the calibration of ASNT detector response. By the energy deposit spectra measured by Cube detector we cannot estimate the maximal energy of the gamma rays. We use the energy deposit spectra measured by ASNT to decide on the maximal energy of the gamma ray spectra (see Appendix B). Above 10 MeV the energy spectra are better approximated with power law. The spectral indices of gamma ray differential energy spectra were estimated to be 3.3 ± 0.7 and 3.4 ± 0.25.

The recovered gamma ray energy spectra posted in Fig. 12 have no error bars due to the spectra recovering method; we chose a particular power index (the power was found to be the best model), which provides simulated energy deposit histogram (obtained by simulation of the detector response) closest to the experimentally measured one (see details in Attachment B). The uncertainties of the procedure, including the possible errors in estimating detector response are included in the errors of the estimated power law indices.

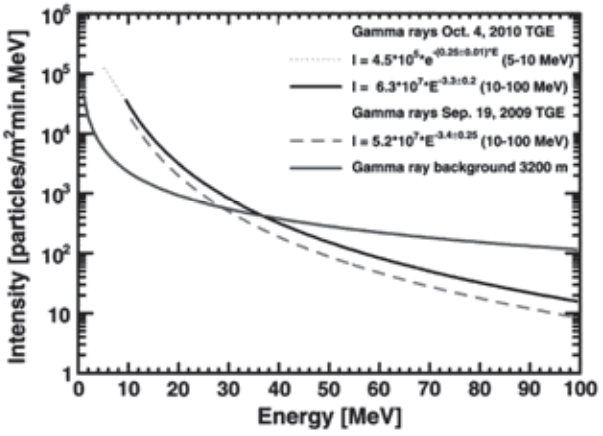

Fig. 12. The differential energy spectra of the gamma rays detected on September 19, 2009 and October 4, 2010.

6. Discussion and conclusion

The high elevation (~3200 m) of ASEC provides a good opportunity to detect thunderstorm-correlated particles, which attenuate rapidly in the atmosphere. We measure fluxes of the RREA electrons and gamma rays with intensities ~10 times above the cosmic ray background, thus, proving the existence of the runaway mechanism in thunderstorm atmospheres theoretically predicted by Gurevich et al. (1992). Both electron spectra measured on September 19, 2009 and October 4, 2010 are exponential. The gamma ray spectrum in the energy range 5–10 MeV (4 October 2010 TGE) also is better fitted with exponential function, in agreement with our simulations, see Fig. 9.

The estimated mean energies of the electron integral spectra are equal to ~2.3 and 3.3 MeV for October 4, 2010 and September 19, 2009 TGEs. The mean energy of the gamma ray differential energy spectrum in the energy range of 5–10 MeV is estimated to be 3.8 MeV.

It is less than derived from the simulations that the values of mean equal to 7.2 MeV (Dwyer, 2004). However, these values are in good agreement with values obtained from our simulations. Values of the mean energy of the 3 brightest electron/positron Terrestrial gamma flashes (TGFs) measured by the GBM, Fermi also are less than 7.2 varying from 2.3 to 4.6 MeV (Briggs et al., 2011).

Power law describes gamma-ray spectra at energies higher than 10 MeV. The energy spectra of the gamma rays extend till 100 MeV and demonstrate no exponential cutoff at high energies as obtained in many simulations of the RREA process (Dwyer and Smith, 2005). We suggest that the modification of the cosmic ray electron energy spectra in the electric field of the thundercloud leads to additional bremsstrahlung radiation reaching the Earth and sustaining the tail of TGE gamma ray spectra (the MOS process). As the cosmic ray spectra are power law, the high-energy tail of TGE gamma ray spectra is also a power law.

In the discussion section of Chilingarian et al. (2010), we estimate the height of thundercloud on September 19, 2009 TGE by assuming the maximal energy of RREA electrons ~50 MeV and calculating the distance in the air in which these electrons will lose 20–25 MeV (the maximal energy of measured electrons of September 19, 2009 TGE was estimated to be 25–30 MeV). After simulating the RREA process we come to the estimate of maximal energy of RREA electrons to be 30–40 MeV. Therefore we have to re-estimate the thundercloud elevation above detectors on September 19, 2009. Also we introduce a parameter, namely the ratio of electron to gamma ray flux, for estimation of the cloud (electric field) height, see Appendix C. With newly estimated thundercloud height, we re-estimate several phenomenological parameters of the RREA process as the following: the most probable height of thundercloud (and electrical field therein) is ~50 m. The number of electrons with energies above 1 MeV at the exit from the cloud is $1.97 * 10^7$ electrons/m^2/min; if we assume that the radiation region in the thundercloud has a radius of 1 km the total number of electrons crossing this region in a minute is $\sim 6 * 10^{13}$.

The same method applied to October 4, 2010 TGE gives the thundercloud height of 130 m. Taking into account that maximal energy of the detected electrons on October 4 was

12–14 MeV, we come to the estimate of the maximal energy of the RREA electrons to be 30–40 MeV, which is in good agreement with our simulations (Fig. 9). The most probable height of thundercloud (and electrical field therein) is ~130 m. The number of electrons with energies above 1 MeV on the exit from the cloud is $\sim 1.5*10^9$ electrons/m^2/min; if we assume that the radiation region in the thundercloud has a radius of 1 km the total number of electrons crossing this region in a minute is $\sim 5*10^{15}$.

The dynamics of the TGE increase (shown in Fig. 2) suggests that the largest TGE started by RREA having as seed particles the secondary cosmic ray MeV electrons; the particle avalanche developing in the direction to the Earth from the main negative charge layer in the middle of the thundercloud may create the initial conductive channel for the negative intracloud lightning discharge (Babich et al., 2011). The −IC lightning in turn may provide RB process with additional seed electrons from the current pulses along developing lightning leader channels thus enhancing the intensity of the electron and gamma ray fluxes.[6] Detection of the −IC lightning occurrences during the TGE events supports the suggested model. However, we recognize that the time scales of the lightning and TGE are drastically different and for definite conclusions on the possible seeds from the stepping leader we should compare on microsecond time scale the particle fluxes and lightning occurrences. Nonetheless the discovery of very short (less than 50 μsec) particle bursts within TGEs, coinciding with minute of the maximal flux (see for details, Chilingarian et al., 2011), illustrates the possible link between TGE and lightning.

The scenario of the TGF initiation is symmetric to the TGE: the electron-gamma avalanche is developing upward from the main negative charge layer to the main positive charge layer; coming out of the cloud, gamma rays are moving by straight lines to be detected by the orbiting gamma ray observatories. TGF gamma rays on their way to orbiting gamma observatories generate by Compton scattering and pair production high-energy electron-positron beams (TEBs, Dwyer, 2012), which follow the geomagnetic field line in the inner magnetosphere and may be observed thousands of kilometers away. The RREA developed in the upper dipole usually initiates positive intracloud lightning IC+ (Cummer et al., 2005; Shao et al., 2010; Lu et al., 2010) and the stepping leader of lightning may provide the RREA process with vast numbers of seed electrons.

7. Possible systematic errors

We do not measure the electric field within the thundercloud; near surface electric field is not a good proxy of the intracloud fields accelerating electrons downward. We also do not measure vertical extension of the field and only estimate the height of the cloud. Therefore, simulations of the RREA process in the atmosphere with chosen parameters, although are in an agreement with the available measurements of electric fields in the thunderclouds, cannot be used for direct comparisons with TGE measurements. However, these simulations give us understanding of the RREA scale and MOS processes and expected behavior of the energy spectra.

The radiation length of the ASEC electromagnetic calorimeters is 0.5 for Cube and 1.5 for ASNT, light attenuation in the thick scintillator significantly decreases the light incident on the PM cathode, and consequently the PM output pulse. Nonetheless, due to large gamma ray fluxes, energy deposit histograms collected during 1 min of peak intensity give a possibility to recover differential energy spectra of the gamma rays. To check the obtained gamma ray spectra and used attenuation coefficients several calorimeters were used for inter-calibration.

Due to particle bursts (Chilingarian et al., 2011) incident on colorimeter several large energy deposits may be because of multiple particle traversals. These effects are difficult to simulate and our method of the multiple spectra testing can give optimistically biased maximal energy of TGE gamma rays. Therefore, we do not include in the energy spectra recovering procedure 2 largest bins of the energy deposit histogram.

The electron/gamma separation is made by using veto scintillators with non-zero efficiency to detect charged flux. Nonetheless multilayered detectors with dedicated coincidence logic help to check the estimated fraction of TGE electrons and gamma rays and make appropriate corrections.

Several detecting devices are placed at high altitude, under snow and strong winds and it is very difficult to keep stable detecting channel parameters (high voltage, electronics thresholds and other) influencing the operation of detectors. However, high altitude station staff maintained detector operation 24 h daily for 12 months yearly and on-line visualization programs ADAS (Chilingaryan et al., 2008) and ADEI (Chilingaryan et al., 2010) provide possibilities of the remote monitoring and control of the key parameters of detectors.

8. Conclusions

We introduce 2 component model of the TGE origin: the RRE avalanches in energy domain up to 30–40 MeV and Modification Of energy Spectra (MOS) process operating on all energy scales and providing extension of gamma ray energy spectra up to 100 MeV. The RREA process can multiply particle flux up to 10 times above ambient background of secondary cosmic rays; the MOS process can provide several percent excess above cosmic rays, however for the much higher energies.

The TGE process is well correlated with near-surface electrical field and with lightning occurrences. All TGEs occur at the large negative near-surface electrical field and particle flux is accompanied with intracloud lightning occurrences (IC−) and suppression of cloud-to-ground lightning occurrences (CG−)). Measured structure of lightning occurrences supports creation of developed lower positive charge region (LPCR) as a fundamental condition of TGE origination.

Acknowledgements

This work was partly supported by the Armenian government grants, NFSAT-CRDF-ECSP-09-69 grant and by ISTC A1554 grant. Authors thank Karen Arakelyan, Karen Avagyan,

[6] Calculations of the flux of runaway electrons produced by the lightning streamers suggests that stepped leaders produce a considerable number of energetic electrons, which is in an agreement with the number of energetic photons observed from satellites in terrestrial gamma ray flashes (Celestin and Pasko, 2011).

David Pokhsraryan, Arthur Reymers and David Sargsyan for assembling and launching Cube and STAND detectors. Authors are grateful to the members of the seminar of the cosmic ray division of Alikhanyan national lab for useful discussions and to S. Chilingaryan for developing ADEI multivariate visualization tool (Chilingaryan et al., 2010) for the treatment of the ASEC data flow. Gagik Hovsepyan helped in understanding asymmetries of the secondary cosmic ray flux and Laura Melkumyan made the histogram of the TGE events. Authors thank them for collaboration.

Appendix A. Disentangling of charged and neutral fluxes by ASEC detectors

The largest TGEs measured by the ASEC detectors originated from RREA process in thunderclouds located above Aragats research station. The electrons and gamma rays from the RREA are continuing their path in direction of the Earth after avalanche growth stopped reaching LPCR. Depending on the distance from LPCR to particle detectors the relative fraction of electrons to gamma rays is changing. Measured huge enhancement of count rates is due to electrons and gamma rays, because both neutral and charged particles can generate signals in plastic scintillators, although with different efficiencies. Therefore, to estimate energy spectra of electrons and gamma rays we need to disentangle the mixture of electrons and gamma rays. Special experimental facilities were designed and installed at Aragats for separating electron and gamma ray fluxes. Two 20 cm thick plastic scintillators located inside the Cube detector are completely surrounded by 1 cm thick molded plastic scintillators, which are shown in Fig. 13. Thick scintillators detect charged flux with very high efficiency (99%) and also neutral flux with efficiency of 20–30%. Thin scintillators also detect charged flux with very high efficiency (98–99%), though the efficiency of detecting neutral flux is highly suppressed and equals to 1–2%. Using advanced coincidence technique it is possible to purify the neutral flux detected by inside scintillators, rejecting the charged flux by signals from surrounding thin scintillators. The calibration of Cube detector proves that veto system (preventing counting signal in the thick scintillator if there is a signal in at least one of surrounding six thin scintillators) can reject 98% of the charged flux. Number of TGE particles detected by upper thick scintillator (detector surface 0.25 m^2, see Fig. 13) at 18:23, October 4, 2010 was $N(20\ cm) = 43{,}439$ with veto and $N^v(20\ cm) = 44{,}956$ without veto, the difference is $N - N^v = 1517$. By these counts we can recover the flux (number of particles per m^2 per minute) of electrons N_e and gamma rays N_g above the detector.

$$\begin{aligned} N(20\,cm) &= N_e p(20\,cm/e) + N_g p(20\,cm/g) \\ N^v(20\,cm) &= N_e p^v(20\,cm/e) + N_g p^v(20\,cm/g), \end{aligned} \quad (1)$$

where p(20 cm/e) and p(20 cm/g) are the conditional probabilities to register electron or gamma ray by 20 cm scintillator. Accordingly p^v(20 cm/e) and p^v(20 cm/g) are the conditional probabilities to register electron or gamma ray by Cube 20 cm scintillator with veto switched on. By calibration, confirmed with detector response simulations, we estimate these conditional probabilities as follows:

$$\begin{aligned} &p(20\,cm/e) = .99 \\ &p(20\,cm/g) = 0.2 \\ &p(1\,cm/e) = 0.98 \\ &p(1\,cm/g) = 0.02 \\ &p^v(20\,cm/e) = (1 - p(1\,cm/e))p(20\,cm/e) = (1-0.98)0.99 = 0.0198 \\ &p^v(20\,cm/g) = (1 - p(1\,cm/g))p(20\,cm/g) = (1-0.02)0.2 = 0.196. \end{aligned} \quad (2)$$

Solving the system of Eq. (1) with coefficients (2) we readily get: $N_e = 1560$ and $N_g = 215{,}000$. Thus, on October 4, most of TGE particles were gamma rays, the fraction of electrons was less than 1%. From additional 1560 particles detected by 20 cm thick Cube scintillators only 31 can be electrons, i.e. less than 2%. Therefore, by examining the histograms of the energy deposits released in the thick scintillators of Cube we can recover the energy spectrum of the gamma rays of the TGE that happened on October 4, 2010 (see the techniques of the energy spectra recovering in the Appendix B). Of course, our calculations did not include the energy dependence of the efficiencies to detect gamma ray or electron by plastic scintillators; we assume that conditional probabilities are constant, according to Eq. (2). However, estimation of the energy dependence of these efficiencies by detector response function calculation with GEANT 4 code does not significantly alter our results. The ultimate check of the particle classification and energy spectra recovering will be an independent estimate of the particle enhancements registered with other ASEC detectors using those obtained by Cube energy spectra. The energy spectrum of gamma rays (Eq. (3)) obtained by the Cube detector was used to calculate the detector response of the STAND detector.

$$\begin{aligned} &dE/dN = 5.4e+07{*}\exp(-0.25{*}E) \\ &\quad \text{for the energy range of 5–10 MeV;} \\ &dE/dN = 1.93e+08{*}E^{-3.3} \text{ for the energy range of } 10-50\,MeV; \end{aligned} \quad (3)$$

Another outdoor detector STAND, see Fig. 14, consists of three 1 cm thick scintillators of the same type as Cube veto scintillators. STAND detector DAQ electronics stored statistics of all possible coincidences of the 3 scintillator "firings".

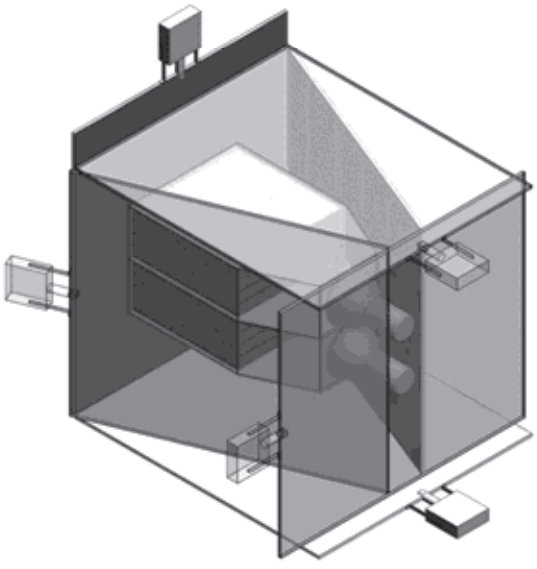

Fig. 13. Cube outdoor detector; thick scintillators located inside are measuring neutral flux with purity 98%.

Denoting the scintillator, which detected a particle by "1" and the scintillator, which has not registered a particle by "0" we get 7 meaningful combinations (combination 000 has no sense). For instance, combination "100" corresponds to the case when low energy particle stops in the upper layer and does not reach the layers below; "111" combination corresponds to high-energy particle generating signal in all 3 scintillators.

In Table 1 we compare the measurement at 18:23 4 October 2010 coincidence statistics with simulated detector response on reconstructed by Cube gamma ray energy spectrum (3).

Rather good coincidence of the sum of the simulated electrons and gamma rays with measured particle confirms that used gamma ray energy spectrum (3) is valid. Furthermore, by the electron fraction of the total counts we can recover integral spectrum of the TGE electrons.

Appendix B. The method of TGE gamma ray and electron spectra recovery

The data acquisition (DAQ) electronics of the ASNT and Cube detectors stores each minute energy deposit histograms, digitized by Amplitude to digital converter (ADC) output analog signals of the photomultipliers (PM) overviewed the 60 cm and 20 cm thick scintillators located in the lightproof housings. On the basis of these histograms, using Monte Carlo techniques we recover differential energy spectra of the gamma rays. We solve the inverse problem and "unfold" the gamma-ray spectra by multiple solutions of the direct problem and comparisons of simulated and measured energy deposit histograms. Assuming the analytic form of the RREA gamma-ray spectra (power, exponential, or power with exponential cutoff) we tune free parameters (number of gamma-rays fallen on the roof and spectral indices) by minimizing the "quality" function describing the closeness of simulated with GEANT4 energy deposit histogram with the experimentally measured one. Gamma rays were traced through the material of the roof above the detector and trough the detector itself. The following steps were performed for the unfolding of the ASNT gamma ray spectrum above the roof of the MAKET building at an altitude of 3200 m:

Table 1
Measured and simulated STAND statistics; 18:23, 4 October 2010.

	100	110	111
Experiment	95,025	7366	1836
Simulated gamma rays	62,832	3929	1377
Simulated electrons	32,193	3437	459

- An energy spectrum with initial parameters randomly chosen from predetermined interval is generated;
- This spectrum is used to simulate the traversal of gamma rays through roof and ASNT detector components to finally obtain the energy deposit in thick scintillator;
- The obtained histogram of simulated energy deposits is compared with experimental one; the discrepancy (quality function) and initial spectrum parameters are stored;
- The simulations are continued till obtaining the histograms of energy releases corresponding to the whole interval of chosen spectrum parameters.

Having the dependence of the quality function on the test gamma ray spectra parameters, we fit these data by a second order polynomial function and find the minimum corresponding to the test gamma-ray spectrum, which generates an energy deposit spectrum closest to the experimentally measured one. For estimating the bias and accuracy of the above formulated procedure we simulate 150,000 gamma rays with energies distributed by power law with chosen spectral index equal to 3, i.e., $f(E) \sim E^{-3}$. Each gamma ray was followed by GEANT4 code, traversing the roof and detectors, and energy deposit in the scintillators was enumerated and stored. The obtained energy deposit histogram was taken as an "experimental" one and was further used for the energy spectrum recovery procedure. The gamma-ray spectra with power indices from −2 to −4 with step −0.01 were generated and corresponding energy deposit histograms were

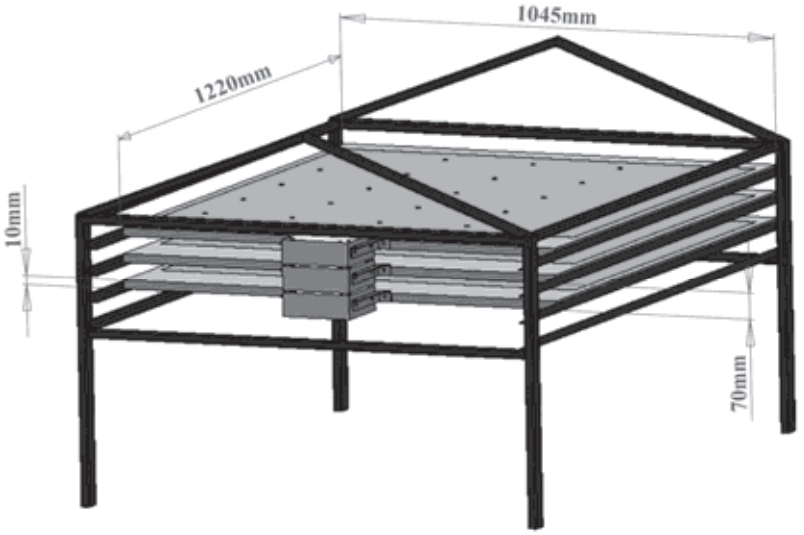

Fig. 14. STAND detector consisting of three layers of 1 cm thick scintillators.

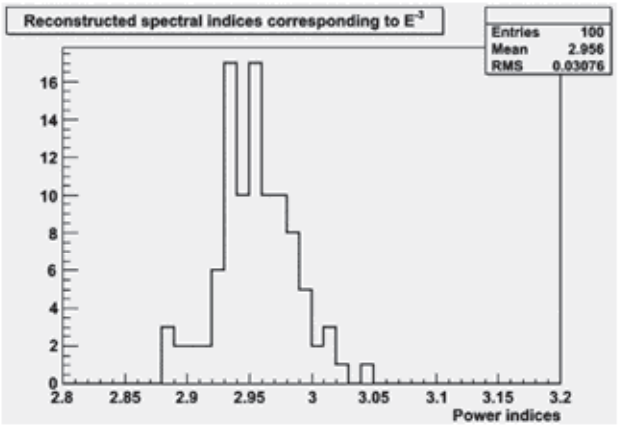

Fig. 15. Test of the spectral index recovery using a simulated spectrum as $f(E) \sim E^{-3}$.

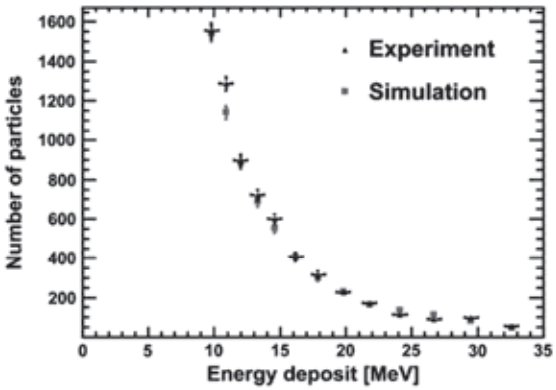

Fig. 17. Measured and simulated energy deposit histograms of Cube upper scintillator.

generated. Quality functions between "measured" and simulated spectra were calculated; the value of power index corresponding to the minimum of the quality function was obtained. We have repeated this procedure with hundred independent random samples, which serve as experimental ones and for each of hundred we repeated the spectra recovery procedure. As we can see from the legend of Fig. 15 the negative bias of the method is 0.044 and RMS is ~0.031. The corresponding relative error of the power index estimate is ~2%, which is 3 times less than the statistical error.

The test spectra for the recovering of the gamma ray spectrum of October 4, 2010 TGE were simulated according to power law with spectral indices varying in the range of −2 to −4 with step 0.01. Simultaneously, both spectra measured by top and bottom 20 cm thick Cube scintillators were simulated. Two hundred trials were performed and quality functions were calculated each time to describe the closeness of the energy deposit obtained in simulation with the experimental one. In Fig. 16, the dependence of the quality function on spectral index is shown for upper and lower Cube scintillators. For the quality function the χ^2/ndf was chosen. The power spectra were found to give closer results to the experiment. The values of the quality functions corresponding to the different indices of the power function are approximated by the second order polynomial and as the final estimate the power index corresponding to the minimum of the curve was chosen (see Fig. 16). The χ^2/ndf for the best-fit parameters is less than 1.

The obtained gamma-ray spectra by both Cube 20 cm detectors are in very good agreement with each other. The estimated gamma-ray spectrum by Cube upper scintillator for October 4, 2010 TGE is $\sim E^{-3.3\pm0.2}$in the energy range >10 MeV; the gamma ray flux is ~150,000 particles/m^2/min at 18:23 UT on 4 October, 2010, at altitude of 3200 m above sea level. The recovered spectrum by Cube lower scintillator is $\sim E^{-3.3\pm0.2}$. The October 4, 2010 TGE gamma-ray spectrum at energies 5–10 MeV is flatter and can be better described by the exponential function with index ~−0.25, the intensity is equal to ~400,000 particles/m^2/min. The "theoretical" (obtained by simulation, assuming power law spectrum of gamma rays above the outdoor Cube detector) and the measured energy deposit histograms of upper Cube scintillator are shown in Fig. 17.

However, the high-energy gamma rays will deposit small fraction of its energy in 20-cm thick scintillator and it will lead to possible biases in the high-energy spectra recovering.

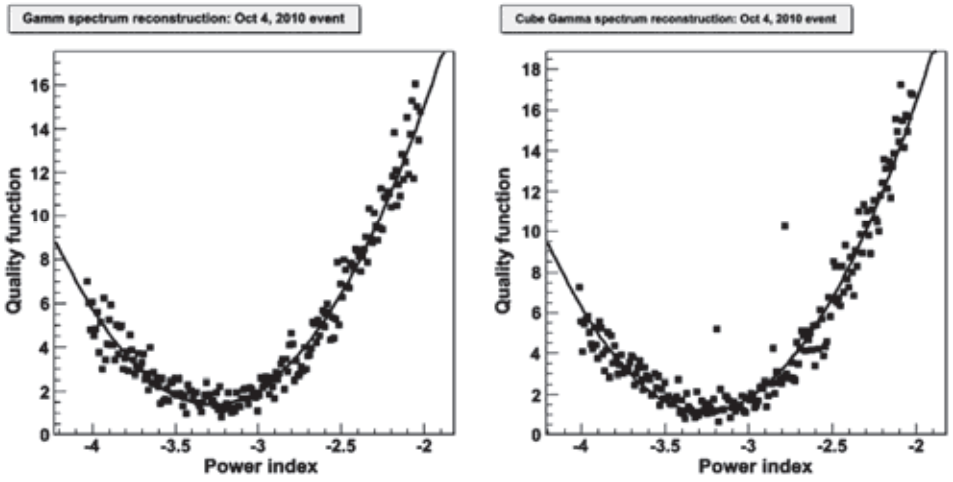

Fig. 16. The 200 trial spectra fitted by the second order polynomial (2 cube detectors data on 4 October, 2010).

As we are interested in proving the existence of high-energy tail, for gamma ray spectra recovering above 10 MeV we use 60 cm thick ASNT scintillators, more sensitive for high energies. The energy deposit histogram measured by one of the four ASNT scintillators with the best performance at low threshold (calibrated with spectra measured by Cube detector) was used for energy spectra recovering in high-energy domain. The gamma ray differential energy spectra above detector were estimated by multiple tests of propagation of the trial spectra through detector using GEANT4 code. Simulations in the energy range above 10 MeV were performed with power-law spectra in 2 versions: with maximal gamma-ray energy equal to 50 MeV and 100 MeV. In Fig. 18, the simulated energy deposit spectra obtained with assuming 50 MeV and 100 MeV along with the measured one are presented. The higher value of gamma ray maximal energy made the simulated spectrum closer to the experimental one. The error bars include the uncertainty in determination of the light attenuation coefficients in thick scintillator of ASNT detector. The quality function (χ^2/ndf) describing the closeness of simulated and measured histograms has a smaller value in case of 100 MeV maximal energy of incident gamma rays — ~3 instead of ~250 for 50 MeV.

Large values of χ^2/ndf reflect both possible errors in the used light attenuation coefficients and 2 modes of TGE origin. The fast decrease of experimental energy deposit spectrum at 17 MeV maybe is the illustration of the mode change of the TGE particle initiation.

The recovered gamma ray energy spectrum was checked by SEVAN detector, which can also distinguish neutral and charged fluxes. SEVAN DAQ electronics stores all possible combinations of signals (denoted by 1), and absence of signal (denoted by 0) in 3 layers. Combination "100" selects the low energy charged particles; coincidence "010" selects neutral particles, and combination "111" selects high-energy muons (see details in Chilingarian and Reymers, 2008). Simulating the passage of the recovered gamma-ray flux through the roof above and detector and taking into account the detector response to gamma rays and electrons, we have estimated the expected number of gamma rays detected by the "010" combination to be 1459 respectively. This value is in good agreement with experimentally measured value of 1452 ± 42.

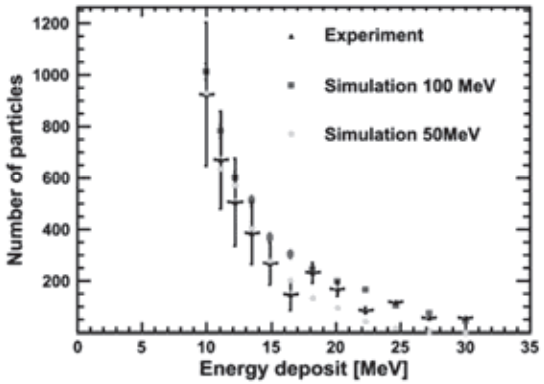

Fig. 18. Simulated and measured energy deposit spectra in the 60 cm thick scintillator of ASNT detector. Test power law spectra above detector were simulated in 2 versions: with maximal energy of 50 and 100 MeV.

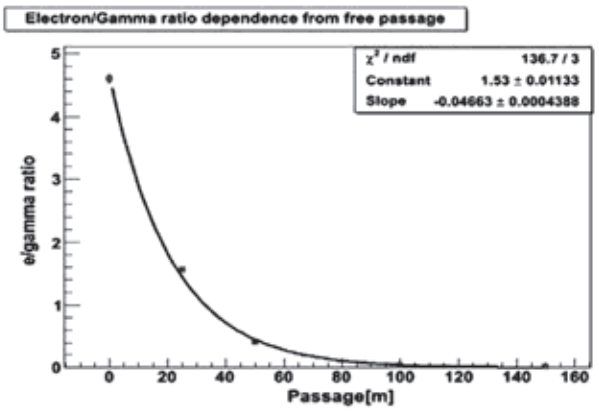

Fig. 19. Dependence of the electron/gamma ray ratio on the free passage distance after quitting the electrical field region.

Appendix C. Thundercloud height estimation; electron number estimation

From the estimated integral energy spectra of electrons and gamma rays of October 4, 2010, we can estimate the approximate altitude of the thundercloud (the altitude from where the electron flux is not accelerated anymore, but only attenuated). This distance can be estimated by the dependence of the electron/gamma ray ratio on these particles' passage in the atmosphere obtained by the simulations of the RREA process followed by the passage of particles in the air. Using the GEANT 4 code we simulate the electron-gamma ray avalanche in an electric field of 1.8 kV/cm prolonged 1.6 km and then — obtain the electron/gamma ray ratio for various passage distances. In Fig. 19, the electron/gamma ray ratio dependence on the passage distance is presented for particles with energies greater than 7 MeV.

From Fig. 20, where we presented integral energy spectra of electrons and gamma rays with energies higher than 1 MeV, along with cosmic ray background electrons and gamma rays at 3200 m, we readily get the electron/gamma ray ratio of 0.0135 for 7 MeV particles. From Fig. 18, we find that the passage distance value corresponding to the observed electron/gamma ray ratio equals ~130 m. The maximal energy of the detected electrons on October 4 was 12–14 MeV, therefore we

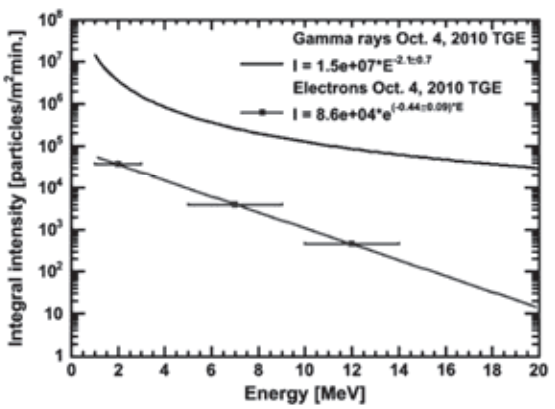

Fig. 20. Electron and gamma ray integral energy spectra of 4 October 2010 TGE as measured on 3200 m.

can estimate the maximal energy of the RREA electrons to be 30–40 MeV.

References

Aglietta, M., et al., EAS-TOP Collaboration, 1989. The EAS-TOP array at E0 = 1014–1016 eV: stability and resolutions. Nucl. Instrum. Methods Phys. Res., Sect. A 277, 23–28.

Agnsotelli, S., Allison, J., Amako, K., et al., 2003. GEANT4—a simulation toolkit. Nucl. Instrum. Methods Phys. Res., Sect. A 506, 250–303.

Alexeenko, V.V., Khaerdinov, N.S., Lidvansky, A.S., Petkov, V.B., 2002. Transient variations of secondary cosmic rays due to atmospheric electric field and evidence for pre-lightning particle acceleration. Phys. Lett. A 301, 299–306, http://dx.doi.org/10.1016/S0375-9601(02)00981-7.

Babich, L.P., Bochkov, L.I., Kutsyk, I.M., Roussel-Dupre, R.A., 2010. Localization of the source of terrestrial neutron bursts detected in thunderstorm atmosphere. J. Geophys. Res. 115, A00E28.

Babich, L.P., Bochkov, E.I., Kutzyk, I.M., 2011. Lightning initiation mechanism based on the development of relativistic runaway electron avalanches triggered by background cosmic radiation: numerical simulation. Russ. J. JETF 139, 1028–1036.

Briggs, M.S., Fishman, G.J., Connaughton, V., et al., 2011. Electron-positron beams from terrestrial lightning observed with Fermi GBM. Geophys. Res. Lett. 38, L02808.

Carlson, B.E., Lehtinen, N.G., Inan, U.S., 2008. Constraints on terrestrial gamma ray flash production from satellite observation. J. Geophys. Res. Lett. 34, L08809.

Carlson, B.E., Lehtinen, N.G., Inan, U.S., 2009. Terrestrial gamma ray flash production by lightning current pulses. J. Geophys. Res. 114, A00E08, http://dx.doi.org/10.1029/2009JA014531.

Celectin, S., Pasko, V.P., 2011. Energy and fluxes of thermal runaway electrons produced by exponential growth of streamers during the stepping of lightning leaders and in transient luminous events. J. Geophys. Res. 116 (A03315), 14, http://dx.doi.org/10.1029/2010JA016260.

Chilingarian, A., Reymers, A., 2008. Investigations of the response of hybrid particle detectors for the Space Environmental Viewing and Analysis Network (SEVAN). Ann. Geophys. 26, 249–257.

Chilingarian, A., Avagyan, K., Babayan, V., et al., 2003. Aragats Space-Environmental Center: status and SEP forecasting possibilities. J. Phys. G: Nucl. Part. Phys. 29, 939–952.

Chilingarian, A., Arakelyan, K., Avakyan, K., et al., 2005. Correlated measurements of secondary cosmic ray fluxes by the Aragats Space-Environmental Center monitors. Nucl. Instrum. Methods Phys. Res., Sect. A 543 (2–3), 483–496.

Chilingarian, A., Daryan, A., Arakelyan, K., et al., 2010. Ground-based observations of thunderstorm-correlated fluxes of high-energy electrons, gamma rays, and neutrons. Phys. Rev. D 82, 043009.

Chilingarian, A., Hovsepyan, G., Hovhannisyan, A., 2011. Particle bursts from thunderclouds: natural particle accelerators above our heads. Phys. Rev. D 83, 062001.

Chilingaryan, S., Chilingarian, A., Danielyan, V., Eppler, W., 2008. The Aragats data acquisition system for highly distributed particle detecting networks. J. Phys. Conf. Ser. 119, 082001.

Chilingaryan, S., Beglarian, A., Kopmann, A., Voekling, S., 2010. Advanced data extraction infrastructure: web based system for management of time series data. J. Phys. Conf. Ser. 219, 042034.

Cui, H., Qie, X., Zhang, Q., Zhang, T., Zhang, G., Yang, J., 2009. Intracloud discharge and the correlated basic charge structure of a thunderstorm in Zhongchuan, a Chinese Inland Plateau region. Atmos. Res. 91, 425–429.

Cummer, S.A., Zhai, Y., Hu, W., Smith, D.M., Lopez, L.I., Stanley, M.A., 2005. Measurements and implications of the relationship between lightning and terrestrial gamma ray flashes. Geophys. Res. Lett. 32, L08811, http://dx.doi.org/10.1029/2005GL022778.

Cummer, S.A., Lu, G., Briggs, M.S., Connaughton, V., Xiong, S., Fishman, G.J., Dwyer, J.R., 2011. The lightning–TGF relationship on microsecond timescales. Geophys. Res. Lett. 38, L14810, http://dx.doi.org/10.1029/2011GL048099.

De Souza, P.E., Pinto Jr., O., Pinto, I.R.C.A., Ferreira, N.J., Dos Santos, A.F., 2009. The intracloud/cloud-to-ground lightning ratio in Southeastern Brazil. Atmos. Res. 91, 491–499, http://dx.doi.org/10.1016/j.atmosres.2008.06.011.

Dorman, L.I., Dorman, I.V., 2005. Possible influence of cosmic rays on climate through thunderstorm clouds. Adv. Space Res. 35, 476–483.

Dwyer, J.R., 2003. A fundamental limit on electric fields in air. Geophys. Res. Lett. 30, 2055.

Dwyer, J.R., 2004. Implications of X-ray emission from lightning. Geophys. Res. Lett. 31, L12102, http://dx.doi.org/10.1029/2004GL019795.

Dwyer, J.R., 2005. The initiation of lightning by runaway air breakdown. Geophys. Res. Lett. 32, L20808.

Dwyer, J.R., 2007. Relativistic breakdown in planetary atmospheres. Phys. Plasmas 14, 042901.

Dwyer, J.R., 2012. The relativistic feedback discharge model of terrestrial gamma ray flashes. J. Geophys. Res. 117, A02308, http://dx.doi.org/10.1029/2011JA017160.

Dwyer, J.R., Smith, D.M., 2005. A comparison between Monte Carlo simulations of runaway breakdown and terrestrial gamma-ray flash observations. Geophys. Res. Lett. 32, L08811.

Fishman, G., Bhat, P.N., Malozzi, R., et al., 1994. Discovery of intense gamma-ray flashes of atmospheric origin. Science 264, 1313–1316.

Gurevich, A.V., Milikh, G.M., Roussel-Dupre, R., 1992. Runaway electron mechanism of air breakdown and preconditioning during a thunderstorm. Phys. Lett. A 165, 463–468.

Gurevich, A., Zybin, K., Roussel-Dupre, R., 1999. Lightning initiation by simultaneous effect of runaway breakdown and cosmic ray showers. Phys. Lett. A 254, 79–87.

Gurevich, A.V., Mitko, G., Antonova, V., et al., 2009. An intracloud discharge caused by extensive atmospheric shower. Phys. Lett. A 373 (39), 3550–3553.

Khaerdinov, N.S., Lidvansky, A.S., Petkov, V.B., 2005. Cosmic rays and the electric field of thunderclouds: evidence for acceleration of particles (runaway electrons). Atmos. Res. 76, 346–354.

Lehtinen, N.G., Bell, T.F., Inan, U.S., 1999. Monte Carlo simulation of runaway MeV electron breakdown with application to red sprites and terrestrial gamma ray flashes. J. Geophys. Res. 104 (A11), 24,699–24,712.

Lidvansky, A.S., Khaerdinov, N.S., 2009. Strong variations of cosmic ray muons during thunderstorms. Izv. Ross. Akad. Nauk, Ser. Fiz. 73, 415–417 [Bulletin of the Russian Academy of Sciences: Physics 73, 400 (2009)].

Lu, G., Blakeslee, R.J., Li, J., Smith, D.M., Shao, X.-M., McCaul, E.W., Buechler, D.E., Christian, H.J., Hall, J.M., Cummer, S.A., 2010. Lightning mapping observation of a terrestrial gamma-ray flash. Geophys. Res. Lett. 37, L11806, http://dx.doi.org/10.1029/2010GL043494.

Lu, G., Cummer, S.A., Li, J., Han, F., Smith, D.M., Grefenstette, B.W., 2011. Characteristics of broadband lightning emissions associated with terrestrial gamma ray flashes. J. Geophys. Res. 116, A03316, http://dx.doi.org/10.1029/2010JA016141.

Moss, G.D., Pasko, V.P., Liu, N., Veronis, G., 2006. Monte Carlo model for analysis of thermal runaway electrons in streamer tips in transient luminous events and streamer zones of lightning leaders. J. Geophys. Res. 111, A02307, http://dx.doi.org/10.1029/2005JA011350.

Muraki, Y., Axford, W.I., Matsubara, Y., et al., 2004. Effects of atmospheric electric fields on cosmic rays. Phys. Rev. D 69, 123010.

Nag, A., Rakov, V.A., 2009. Some inferences on the role of lower positive charge region in facilitating different types of lightning. Geophys. Res. Lett. 36, L05815, http://dx.doi.org/10.1029/2008GL036783.

Pawar, S.D., Kamra, A.K., 2004. Evolution of lightning and the possible initiation/triggering of lightning discharges by the lower positive charge center in an isolated thundercloud in the tropics. J. Geophys. Res. 109, D02205.

Pinto Jr., O., Pinto, I.R.C.A., Naccarato, K.P., 2007. Maximum cloud-to-ground lightning flash densities observed by lightning location systems in the tropical region: a review. Atmos. Res. 84, 189–200.

Qie, X., Zhang, T., Chen, C., Zhang, G., Zhang, T., Kong, X., 2009. Electrical characteristics of thunderstorms in different plateau regions of China. Atmos. Res. 91, 244–249.

Sato, T., Endo, A., Zanki, M., Petoussi-Henss, N., Niita, K., 2009. Fluence-to-dose conversion coefficients for neutrons and protons calculated using the PHITS code and ICRP/ICRU adult reference computational phantoms. Phys. Med. Biol. 54, 1997.

Schonland, B.F.J., 1930. Thunder-storms and the penetrating radiation. Proc. R. Soc. Lond. A 130, 37.

Schonland, B.F.J., Viljoen, J.P.T., 1933. On a penetrating radiation from thunderclouds. Proc. R. Soc. Lond. A 140, 314.

Shao, X.M., Hamlin, T., Smith, D., 2010. A closer examination of terrestrial gamma-ray flash-related lightning processes. J. Geophys. Res. 115, A00E30, http://dx.doi.org/10.1029/2009JA014835.

Shaw, G.E.J., 1967. Cosmic count increase associated with thunderstorms. Geophys. Res. Bull. 72, 4623.

Standler, R.B., Winn, W.P., 1979. Effects of coronae on electric field beneath thunderstorms. Quart. J. Roy. Meteor. Soc. 105, 285–302.

Stanley, M., Shao, X.M., Smith, D., et al., 2006. A link between terrestrial gamma-ray flashes and intracloud lightning discharges. Geophys. Res. Lett. 33, L06803, http://dx.doi.org/10.1029/2005GL025537.

Stolzenburg, M., Marshall, T.C., Rust, W.D., 1998. Electrical structure in thunderstorm convective regions 2. Isolated storms. J. Geophys. Res. 103, 14079.

Torii, T., Takeishi, M., Hosono, T., 2002. Observation of gamma-ray dose increase associated with winter thunderstorm and lightning activity. J. Geophys. Res. 107, 4324, http://dx.doi.org/10.1029/2001JD000938.

Torii, T., Sugita, T., Tanabe, S., Kimura, Y., Kamogawa, M., Yajima, K., Yasuda, H., 2009. Gradual increase of energetic radiation associated with

thunderstorm activity at the top of Mt. Fuji. Geophys. Res. Lett. 36, L13804, http://dx.doi.org/10.1029/2008GL037105.
Torii, T., Sugita, T., Kamogawa, M., et al., 2011. Migrating source of energetic radiation generated by thunderstorm activity. Geophys. Res. Lett. 38, L24801, http://dx.doi.org/10.1029/2011GL049731.
Tsuchiya, H., Enoto, T., Yamada, S., et al., 2007. Detection of high-energy gamma rays from winter thunderclouds. Phys. Rev. Lett. 99, 165002.
Tsuchiya, H., Enoto, T., Torii, T., et al., 2009. Observation of an energetic radiation burst from mountain-top thunderclouds. Phys. Rev. Lett. 102, 255003.
Tsuchiya, H., Enoto, T., Yamada, S., et al., 2011. Long-duration gamma ray emissions from 2007 and 2008 winter thunderstorms. J. Geophys. Res. 116, D09113, http://dx.doi.org/10.1029/2010JD015161.
Vernetto, S., for EAS-TOP Collaboration, 2001. The EAS counting rate during thunderstorms. Proceedings of the 27th International Cosmic Ray Conference (ICRC) (Copernicus Gesellschaft, Hamburg, Germany, 2001), 10, pp. 4165–4168.
Wentz, J., Brancus, I.M., Bercuci, A., Heck, D., Oehlschlager, J., Rebel, H., Vulpescu, B., 2003. Simulation of atmospheric muon and neutrino fluxes with CORSIKA. Phys. Rev. D 67, 073020.
Williams, E.R., 1989. The tripole structure of thunderstorms. J. Geophys. Res. 94, 13151–13167.
Wilson, C.T.R., 1925. The acceleration of b-particles in strong electric fields such as those of thunderclouds. Proc. Camb. Philos. Soc. 22, 534–538, http://dx.doi.org/10.1017/S0305004100003236.

PHYSICAL REVIEW D **85,** 085017 (2012)

Neutron bursts associated with thunderstorms

A. Chilingarian,* N. Bostanjyan, and L. Vanyan

A. Alikhanyan National Laboratory (Yerevan Physics Institute), Armenia

(Received 14 June 2011; revised manuscript received 23 January 2012; published 16 April 2012)

The basis of our analysis is the observation of the simultaneous enhancements of the gamma ray and neutron fluxes detected in 2009–2010 during thunderstorm ground enhancements at the mountain altitude of 3200 m. We investigate the correlated time series of the gamma rays and neutrons measured by the surface particle detectors of Aragats Space Environmental Center. The photonuclear reactions of the gamma rays born in the runaway breakdown (RB, now referred to as relativistic runaway electron avalanche, RREA) process with air were considered as the main process responsible for the copious neutron production. We consider also the mesoatom nuclei decay as a possible source of the additional neutrons registered by the neutron monitor due to enhanced population of the negative muons accelerated in the thunderclouds.

DOI: 10.1103/PhysRevD.85.085017 PACS numbers: 92.60.Pw, 13.40.−f, 94.05.Dd

I. INTRODUCTION

The idea of neutron production during thunderstorms comes from the experimentation with fibers exploded after applying high voltage pulses. Neutron production in high voltage discharges forcing the explosion of fibers containing hydrogen or deuterium is reported in several papers (see [1], and references therein). An average neutron yield approached $\sim 10^{10}$ and neutron energy spectra peaked at 2.48 MeV. Based on these investigations, it was postulated that natural lightning discharges could produce neutrons as a mixture of deuterium contained in the atmospheric water vapor. However, the attempt to measure these neutrons in correlation with lightning strokes gives fluxes consistent with the cosmic ray background [2].

The first evidence of neutron generation in lightning discharges comes from Gulmarg, India, altitude 2743 m [3]. Neutrons were detected by the low-energy lead-free neutron monitor (GNM) comprising 21 proportional counters filled with BF_3 gas enriched by the B^{10} isotope ($\sim 3\%$ registration efficiency for 2.5 MeV neutrons). The counters were arranged in the form of a pile and were placed over 28 cm thick paraffin wax slabs 8 m above the ground. The counters were also covered by 7.5 cm thick paraffin wax. During the 3-year operation of the detector several lightning correlated neutron events were detected, the biggest one comprising 60 neutrons. The authors suggest a nuclear fusion [deuterium-deuterium, $(^2H, n)^3He$] mechanism for producing 2.45 MeV neutrons occurring in the lightning channel. The neutron counting timing accuracy ($> 300\ \mu$ sec) was large compared to the duration of a lightning stroke, though, and there was no possibility to establish a one-to-one relation between lightning and detected neutrons.

Another Indian group running a neutron detection system at Mumbai (sea level) by statistical analysis also claims correlation of neutron bursts with lightning [4]. The experimental device consisted of 16BF3 detectors of 0.05 m diameter, embedded in polyethylene neutron slowing-down material. The neutron burst was identified by the multiplicity greater than 2 (more than 2 neutrons detected by the system of 16 tubes within ~1 millisecond). During the low-altitude lightning occurrences the frequency of counts was significantly higher and multiplicities of 6 and 7 were observed (which were not observed during other weather conditions, including rain). The counts obtained during lightning were 4.8σ higher than the background. Therefore, the authors stated that neutron bursts were associated with lightning.

Recently the data acquisition electronics of the GNM has been significantly modified to record the time profiles of the neutron bursts with microsecond accuracy [5]. Despite a rather small amount of detected neutrons (the biggest event comprises 63 neutrons) and large millisecond delays of neutrons relative to lightning, the authors confirm the previous GNM claim of the production of neutrons in atmospheric discharges.

In the city of Sao Jose dos Campos, Brazil, at sea level a standard lead- and moderator-free He^3 tube (area 70 cm^2; type 25291; Ludlum, USA) detected a burst of neutrons which coincided with a lightning strike within a short distance of the detector (< 0.5 km). The minute count of 690 (the mean minute count rate was ~0.8) corresponds to the flux ~20 neutrons/cm^2, which in turn corresponds to about 10^{12}–10^{13} neutrons produced by the lightning discharge [6].

A less exotic neutron source is associated with the excitation by gamma rays of natural oscillations of protons relative to neutrons, the so-called giant dipole resonance. When the gamma ray energy exceeds the energy of a giant resonance (the binding energy of the nucleon in the nucleus), neutrons that absorb the gamma rays escape from the nucleus [7].

*chili@aragats.am

Whether neutrons observed in correlation with lightning are produced by nuclear fusion or by photonuclear reaction remains uncertain. According to [8], though, the maximum bulk plasma temperature attained in lightning discharge is far too low to initiate fusion reactions. Photonuclear reactions in the air initiated by the gamma rays generated in the relativistic breakdown (RB, [9]), now referred as runaway electron avalanches (RREAs, [10]) seem to be a more probable process. Nonetheless, authors of Ref. [5] claim that there are some hot spots in the lightning channel where the pinch effect could create plasma configurations in which ions may have competing peak energies to induce fusion reactions.

Therefore, the problem of the neutron origin still is challenging. We need simultaneous detection of the gamma rays, neutrons, and lightning occurrence to disentangle this complicated problem. During last year's campaign at Aragats Space Environmental Center (ASEC, 2003, 2005) numerous thunderstorm ground enhancements (TGEs) were detected; some of them also include significant enhancements of the count rate of the Aragats Neutron Monitor (ANM). In this paper we present analysis of the simultaneous gamma ray and neutron enhancements and discuss possible explanations of the peaks in the ANM time series coinciding in time with gamma ray intensity increases.

A. Neutron enhancements detected by Aragats Neutron Monitor during thunderstorm ground enhancements

Registration of high-energy neutrons at ASEC was performed with the standard neutron supermonitor (NM-64, [11]), located at the slopes of Mt. Aragats near a lake at altitude of 3200 m. The neutron monitor registers basically the atmospheric neutrons in a wide range of energies, although with various efficiency, going down at low energies [12]. Eighteen cylindrical proportional counters of type CHM-15 (length 200 cm, diameter 15 cm) are filled with BF_3 gas enriched by a B^{10} isotope. The proportional chambers are surrounded by 5 cm of lead (producer) and 2 cm of polyethylene (moderator). The neutron supermonitor consists of 3 sections, 6 chambers in each. The cross section of lead producer above each section has a surface of $\sim$6 m^2, and a total surface of 3 sections—18 m^2. The atmospheric hadrons produce secondary neutrons in nuclear interactions in lead; then the neutrons get thermalized in a moderator, enter the sensitive volume of the counter, and in interactions with boron gas bear L_i^7 and the α particle. The α particle accelerates in the high electrical field inside the chamber and gives a pulse registered by the data acquisition electronics. The NM response to incident hadrons can contain several pulses depending on the number of secondary low-energy neutrons entering the volume of the counter and reacting with boron gas. Usually high-energy hadrons generate a larger number of secondary neutrons and have greater chances to generate more than one pulse. If we want to count all pulses initiated by the incident hadron (i.e., estimate so-called multiplicities) we have to keep the dead time of the NM very low (the ANM has a minimal dead time of 0.4 μs); if we want to count incident hadrons only (a one-to-one relation between count rate and hadron flux) we have to keep the dead time as much as all secondary neutron collecting time to avoid double counting (for ANM—1250 μs).)

For the detection of the thermal atmospheric neutrons on top of the ANM we install two proportional chambers without moderator and producer, only "bare" proportional counters. The 1 min time series of two chambers as well as 18 chambers of ANM are being entered in the MSQL database at CRD headquarters in Yerevan (available online from http://adei.crd.yerphi.am/adei/), and the database of the Euro-Asian consortium of neutron monitors (NMDB@.eu.org).

Other particle detectors of the ASEC [13,14] are continuously registering charged and neutral species of the secondary cosmic rays. The main building blocks of the particle detectors are plastic scintillators (both polished and molded pressed) located in the lightproof housings; the scintillation light is collected directly or via fiberglass light-shifting wires and overviewed by the photomultipliers. From the standard scintillation pieces of 5 cm thickness were assembled scintillator slabs from 20 to 60 cm thickness. The thin scintillators have very high efficiency to detect charged particles (mostly electrons and muons); the thick ones to detect neutral particles (gamma rays and neutrons). Thick detectors register also the energy deposit of traversing particles, thus giving the possibility to recover the energy spectra of the gamma ray flux. The coincidence technique allows significantly suppressing charged particle contamination to counts of thick scintillators and significantly purifying detected gamma ray flux. We use a 01 combination of the Aragats Solar Neutron Telescope (ASNT, 01 combination means no signal in the upper 5 cm thick scintillator and a signal in the 60 cm thick bottom scintillator) and 010 combination of the SEVAN[1] three-layered detector (signal only in the middle 20 cm thick scintillator). Details on detector operation can be found in [16].

In contrast to thick plastic scintillators, sensitive to both neutrons and gamma rays, the neutron monitor is sensitive only to incident hadrons (registration efficiency of electrons and gamma rays is negligible). The relative standard error of the particle detector 1 min time series is rather small (see Table I), ranging from 0.56% to 2%; therefore few percent peaks are significant and if the neutron peaks are correlated with electron and gamma ray peaks the chance probability of random coincidences is vanishingly

[1]SEVAN is the worldwide network of hybrid particle detectors measuring neutral and charged components of the secondary cosmic rays, primarily aimed at space weather research and forecasting (see [15]).

TABLE I. Characteristics of ASEC particle detectors and parameters of the 4 October 2010 TGE.

Detector	Mean count rate per minute	Standard deviation (σ) and relative standard deviation	Percent of enhancement at 18:23, 4 October 2010	Number of standard deviations in peak at 18:23, 4 October 2010
SEVAN 010	2040	45 (2%)	73%	66σ
ASNT 01	31750	178 (0.56%)	32%	57σ
ANM	37700	285 (0.76%)	5.8%	7.6σ

small. We are also monitoring possible interferences and radio induced fake peaks and cleanup data from the suspicious channels.

The neutron event selection criteria consist of detection of the significant peaks in the neutron monitor 1 min time series coinciding in time with large peaks in gamma ray and electron fluxes measured by other ASEC particle detectors. An example of such an event is posted in Fig. 1.

At 18:23, 4 October 2010, all ASEC particle detectors registered large enhancements; see Fig. 1 and Table I.

Aragats neutron monitors were well maintained and corrected to atmospheric pressure changes and electronics aging [17]. In 2009–2010 when there were no interferences with peaks due to solar modulation effects (ground level enhancements and geomagnetic storms), we detected 12 peak enhancements of the neutron count rate observed by the ANM in coincidence with the enhanced gamma ray flux measured by other ASEC detectors; see Table II.

The first column of Table II provides the date of the TGE event.

In the second column we display the number of additional neutrons in the peak normalized to 1 m^2.

In the third column we display the relative enhancement of neutrons in percent of the mean background, estimated by 1 h data before the start of the TGE,[2] and in the number of standard deviations.

In the fourth column we provide the neutron intensity at 3200 m obtained by the NM counts using the shape of the energy spectrum of the photonuclear neutrons and energy dependence of NM efficiency. The simulations were made by GEANT4 code; the primary gamma ray source was located at a height of 5000 m. The obtained neutron energy spectrum (see Fig. 2) coincided well with the spectrum presented in [18], Fig. 1. The energy dependence of the neutron monitor efficiency was taken according to Refs. [19–21].

In the fifth column we put the number of additional gamma rays in the peak detected by the ASNT. Also, we put in the fifth column the values of the reconstructed integral energy spectrum of gamma rays above 10 MeV. Only the two largest TGE events allow reliable gamma ray spectra recovering; for the rest of the events the histograms of energy deposits in the 60 cm thick plastic scintillates of the ASNT detector (see details in [16]) are too scarce to allow reliable retrieving of the gamma ray energy spectra.

In the sixth column we put the relative enhancement of gamma rays in percent of the mean background and in number of standard deviations.

In the seventh column we put the recovered intensities of gamma rays for the 2 largest TGE events.

In the column 8 we put the ratio of neutron-to-gamma rays (for the largest two events also, the ratio of neutron-to-gamma ray intensities), which reveals some important features of neutron and gamma ray propagation in the atmosphere. As we see in column 8 for the 2 largest events the ratio of detected neutrons to detected gamma rays is substantially smaller compared with 10 other events. Thus, TGE events by gamma ray content fall in two groups: events detected on 19 September 2009 and 4 October 2010 and 10 other events.

In Fig. 3 we put the scatter plot of detected additional neutrons (x axis, from column 2 of Table II) vs number of additional gamma rays (y axis, from column 5 of Table II). In the scatter plot the existence of 2 distinct groups introduced above is apparent.

The existence of 2 distinct groups in the TGE events with different gamma ray content suggests that the parent gamma rays generated by the bremsstrahlung of the electrons accelerated in the RREA process have rather narrow lateral distribution. Only TGEs initiated by the RREA

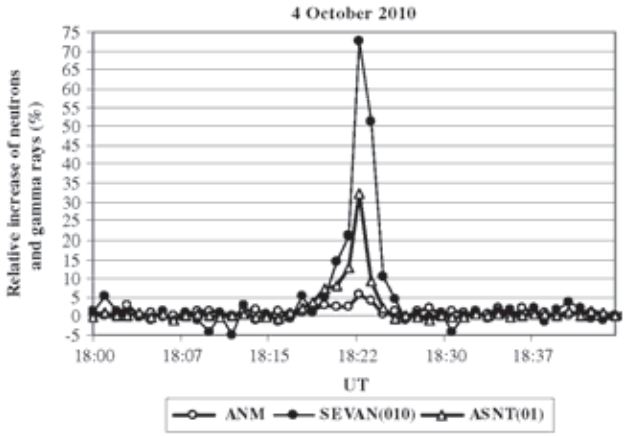

FIG. 1. The count rates of the ANM, SEVAN, and ASNT (01) combination on 4 October 2010.

[2]See for instance the mean count rate, standard deviation, and relative standard deviation of the background on 4 October 2010 in Table I.

TABLE II. The list of the parameters of the 12 TGE events with neutron content (2009–2010).

Day/month/year	Number of additional neutrons detected by ANM at minute of maximal excess (min^{-1}, m^{-2})	Relative increase of neutrons detected by ANM (%)/$N(\sigma)$	Recovered neutron intensity at 3200 m (min^{-1}, m^{-2})	Number of additional gamma rays detected by ASNT (combination 01) at minute of maximal excess min^{-1}, m^{-2}	Relative increase of gamma rays in (%)/$N(\sigma)$	Recovered gamma ray intensity at 3200 by (min^{-1}, m^{-2})	Ratio of neutron to gamma ray flux/ ratio of intensities for largest TGE events
21/05/09[a]	83	3.8/5	3420	1920	7/12		0.043
21/05/09[a]	94	4.3/5.7	3847	1921	7/12		0.049
03/06/09[a]	88	3.9/5.2	3613	1215	4/7		0.072
03/06/09[a]	89	3.9/5.2	3666	1076	3.6/6		0.083
08/07/09[a]	63	2.7/3.5	2591	1116	3.3/5.3		0.056
08/07/09[a]	64	2.7/3.6	2624	1290	4.1/6.5		0.050
09/07/09	74	3.2/4.2	3050	1690	5.3/9.5		0.044
20/08/09	51	2.3/3.2	2110	940	3/4.8		0.054
02/09/09	50	2.5/3.3	2032	900	3/5.2		0.055
19/09/09	63	2.8/3.7	2574	7452	23/41	104 000	0.008/0.025
02/11/09	50	2.3/3.1	2041	1101	3.3/6		0.045
04/10/10	124	5.8/7.7	5091	10280	32/58	153 000	0.012/0.033

[a]Events occurred during 1 d but different times.

process above the particle detectors can sustain large gamma ray fluxes. The majority of the TGE events originate due to either modification of the energy spectra of cosmic ray electrons or the RREA process being launched outside the detector location site; in both cases the number of detected gamma rays will be significantly less.

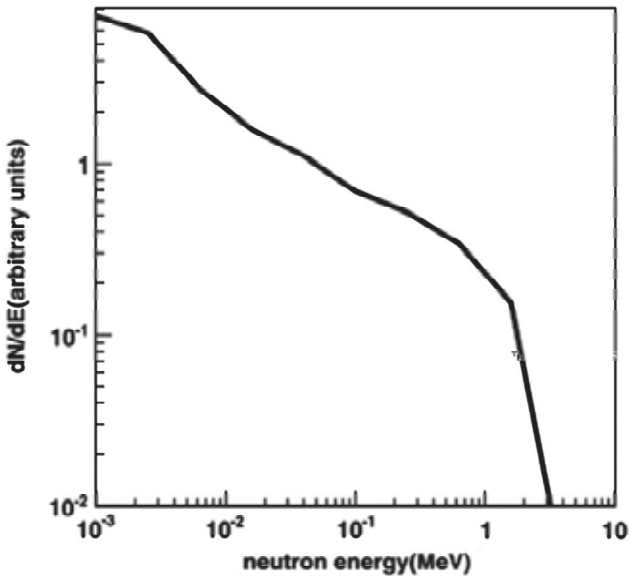

FIG. 2. Energy spectrum of neutrons born in photonuclear reaction; gamma ray source is located at 5000 m, and neutron detectors at 3200 m.

B. Contribution of the negative muons to ANM counts

The shift of the energy spectrum of the electrons/positrons and negative/positive muons entering a large electrical field region in thunderclouds can lead to dips and peaks in the time series of the count rates of surface particle detectors (see the theory of meteorological effects in [22] and numerical calculations in [23]). The charge ratio of positive-to-negative muons above 200 MeV equals ~1.3 [24,25]. Therefore, if an electrical field in the thundercloud is positive and accelerates electrons and negative muons downward, the same field will also decelerate positive muons. And, due to significant enhancement of the

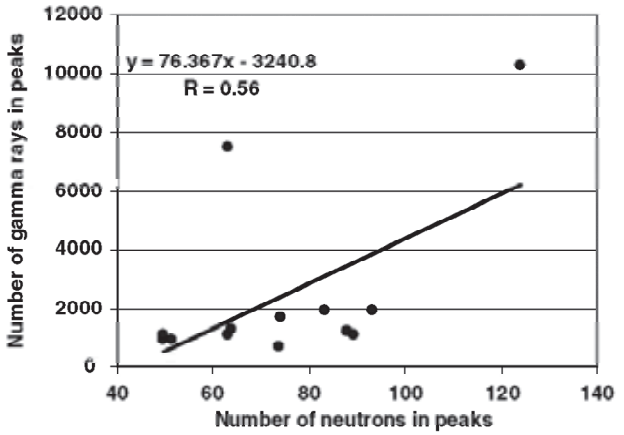

FIG. 3 (color online). Scatter plot of 12 TGE events detected in 2009–2010. R is correlation coefficient.

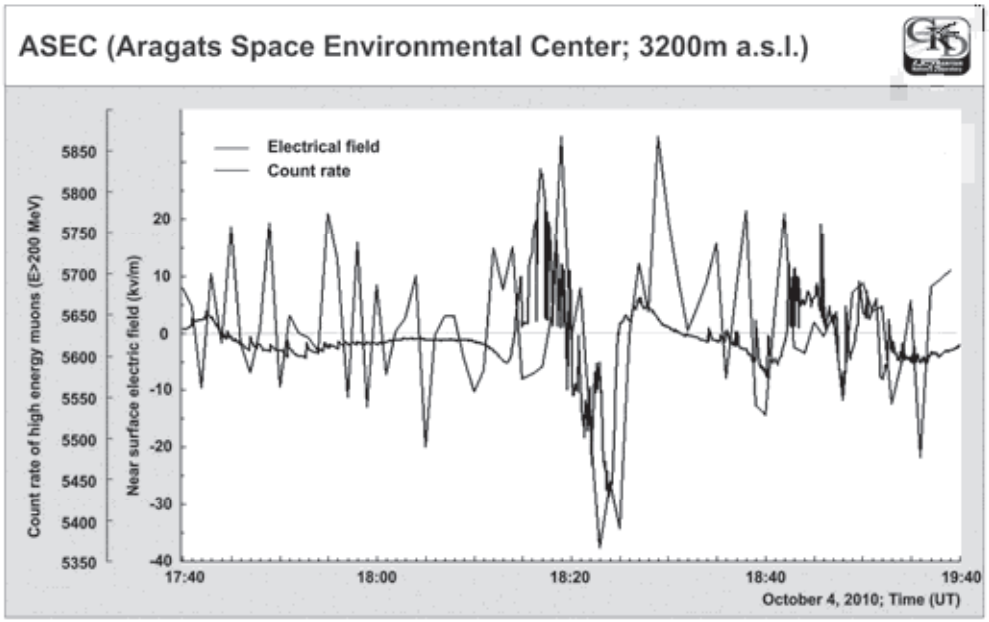

FIG. 4. Deficit of the >200 MeV muons during large negative near surface electrical field.

positive muons compared with the negative ones, we expect a dip in the time series of the high-energy muons at the same time when we detect enhancements of electrons and gamma rays. A SEVAN detector cannot distinguish between negative and positive muons—both charged particles are contributed to the time series registered by the detector—therefore, the detector count rate (the sum of negative and positive muons) after crossing the electrical field diminished because in the cosmic ray flux positive muons are 1.3 times more abundant than negative muons.

On 4 October we detected a deficit of the high-energy muons registered by SEVAN detectors' 111 combination (signals in each of the 3 layers of the assembly of 3 stacked scintillators interlayered by 10 cm of lead); see Fig. 4. As we can see in Fig. 4 the dip in the time series of high-energy muons coincides with a large negative field measured by an electrical mill located on the roof of the building where particle detectors are located.[3] At the same time, with the same detector (see Fig. 1) we detect a huge enhancement of the gamma ray flux (a combination 010 of SEVAN).

The detected dip in the high-energy muon count rate indicates that the positive field in the thundercloud stopped the positive muons. Because the number of positive muons in the secondary cosmic rays' flux is ~1.3 times more compared with negative muons, we detect overall depletion of the muon flux (see Fig. 4). From the measured dip of ~6% in muon flux we calculate an expected deficit of the positive muons and enhancement of the negative muons. GEANT4 calculations indicate that the enhancement of the negative muons can reach ~15% (consequently the reduction of positive muons is 20%). Consequently, the additional negative muons' incident on the ANM can be captured in the 5 cm thick lead producers of the ANM and form so-called mesic atoms where an electron orbiting the atom nucleus is substituted by the muon. Deexcitation of the nucleus occurs with emission of several MeV energy neutrons [22]. The details of nuclear muon capture and consequent decay with emission of several neutrons can be found in the review [26]. Therefore, several fractions of the neutron count rate enhancement can be attributed to these negative muons.

In Fig. 5 we depict the energy dependence of the efficiency of a negative muon to generate NM counts [27]. The efficiency of neutron detection is significant only in the energy range of 50–230 MeV. However, as demonstrated by our simulations the enhancement of the number of negative muons in this energy range after crossing the

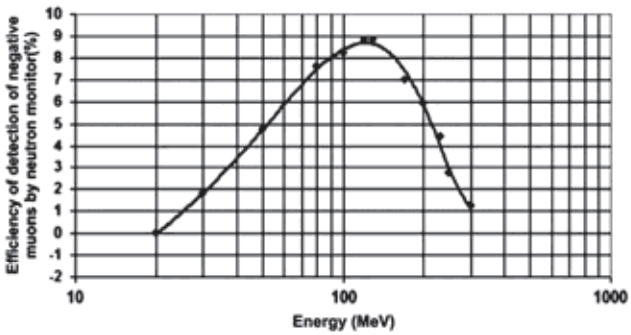

FIG. 5. Energy dependence of the NM detection efficiency of the negative muons.

[3]Almost all TGEs are detected during an abrupt decrease of the near surface electrical field down to ~ -30 kV/m.

electrical field is not very large. Therefore, from this calculation we cannot expect any significant (greater than 10–20) excess of NM count rate due to enhancement of the negative muons.

Another estimate of the additional count rate due to an enhanced number of negative muons [Eq. (30) from [22]] gives ~20 additional counts of the ANM. A simpler way to calculate additional NM counts is based on the estimate that 5%–7% of the overall NM counts is due to negative muons [28]. Let us assume that 6% of the NM count rate is generated by the negative muons; taking from Table I the ANM count rate (all 18 proportional tubes, ~1 m^2 surface each) we will obtain $37\,700 \times 0.06 = 2262$ additional counts from ambient population of secondary negative muons. On 4 October we estimated maximally ~15% of additional negative muons; therefore we can expect an additional $2262 \times 0.15 = 340$ NM counts; normalizing the additional flux to 1 m^2 we get ~20 additional counts among 124 detected on 4 October 2010.

C. Evidence of the "bare" proportional chamber

The bare (without lead producer and polyethylene moderator) proportional counter CNM-15, of the same type as is used in the ANM, was located directly above the ANM for detection of the low-energy neutrons. The bare counter registered enhancement on 4 October 2010 was well correlated with the ANM peak (see Fig. 6).

The number of neutrons detected during the 4 October 2010 TGE normalized to 1 m^2 was less than that of the ANM (54 and 124 correspondingly). Our simulations demonstrate that the MeV neutron flux incident on the neutron monitor thermalized in the polyethylene moderator and a significant fraction of the thermal neutrons is emitted upwards from the polyethylene moderator covering the ANM

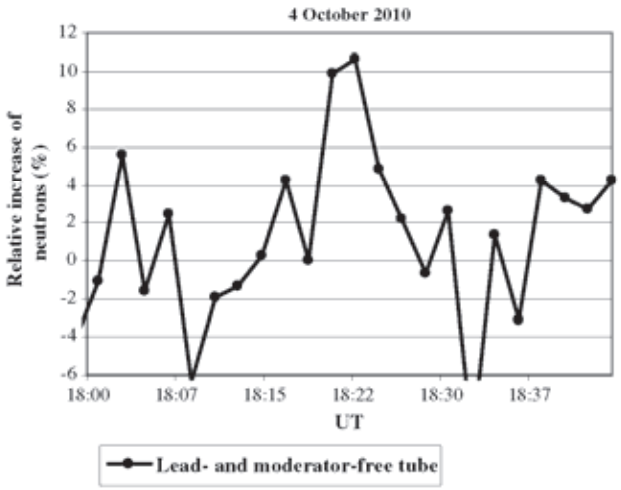

FIG. 6 (color online). Time series of the neutrons detected by bare proportional counter, located just on the ANM, 4 October 2010.

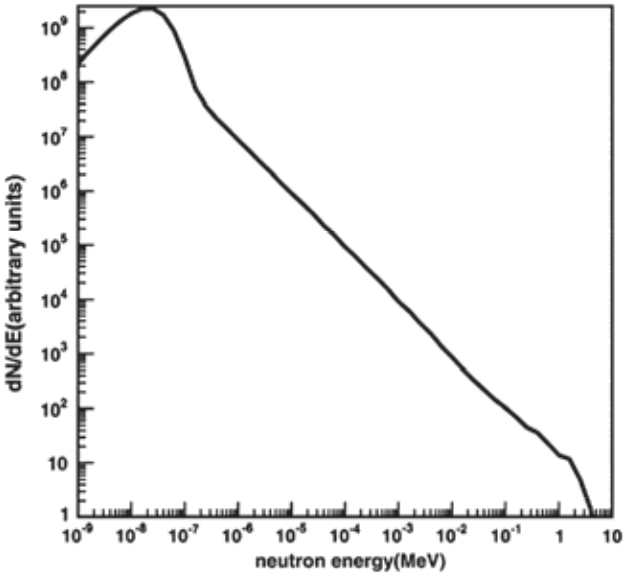

FIG. 7. Energy spectrum of the neutrons emitting upward from the polyethylene top layer of the ANM (logarithmic energy scale).

(the energy spectrum of the thermalized neutrons is depicted in Fig. 7).

The bare counter registered these neutrons having energies in the range (0.025–0.1 eV) with high efficiency [29]. Proceeding from the photonuclear neutron energy spectrum (Fig. 2) and the upward thermal neutron spectrum (Fig. 7), we simulate the expected number of hits in the bare counter on 4 October 2010 and come to an estimate of the neutron flux comparable with one we obtain by the NM counts.

II. DISCUSSION

Simultaneous detection of the electrons, gamma rays, and neutrons by experimental facilities of the Aragats Space Environmental Center provides a convincing confirmation of the photonuclear mechanism for neutron production during thunderstorms. The "lightning" origin of the neutrons can be ruled out because not all TGEs were accompanied by lightning occurrences[4] and because the time scale of the neutron peaks in TGEs (minutes) drastically differs from the lightning time scale (milliseconds). The origin of the TGE is an extended region within a thundercloud between a negative charged layer and a positive charged layer in the bottom of the cloud (see Fig. 10 in [30]). Despite big varieties of electrical field profiles measured in the thundercloud the following basic structure of the electrical field in thunderclouds is widely accepted: from the ground up to the cloud base there is usually a low

[4]During the largest by neutron content 4 October 2010 TGE, with the neutron enhancement lasting ~5 minutes, we detected only one intracloud lightning occurrence.

magnitude field (both positive and negative); a relatively small positively charged "pocket" is lowermost just in the cloud base (comprising only ~20% of the negative charge higher up); a larger positive field prolongs up to a negative charge layer at 1–2 km above the cloud base; and the main positive charge is located about 1–4 km above the negative layer [31]. The lower positive charge region with the main negative layer in the middle of the cloud form, the so-called lower dipole, is responsible for the downward electron acceleration and also plays a major role in initiation of cloud-to-ground and intracloud lightning occurrences. Many researchers outline the dominant role the lower positive charge region plays in initiating/triggering intracloud and cloud-to-ground lightning discharges [32–34]. We suggest that development of the lower positive charge region also has a major role in TGE initiation.

The locality of the RREA can be explained by the small sizes of the lower positive charge region. Based on the detection of the winter thunderstorms in Japan, the authors of [35] estimate the radii of the circle of intense RREA radiation to be 600 m. Another Japanese group [36] detected movement at the speed of 7 m/ sec of an energetic radiation source at the height of 300 m along with the negatively charged region within a thundercloud at the height of around 1 km. The radiation was emitted from a downward hemispherical surface with radii of 700 m. These findings demonstrate the locality of the RREA process and imply that the number of additional gamma rays can vary significantly depending on the "impact parameter" of the thundercloud relative to detection site (see also [37]). Therefore, a large discrepancy of the gamma ray content can be explained by the existence of 2 types of TGE events: one with a thundercloud above the detector location, and the second outside the detector location.

Gamma rays within the RREAs are radiated in a rather narrow cone; therefore they are illuminated in a limited area below the thundercloud. Only if RREAs occurred occasionally just above the site where particle detectors are located can we expect large fluxes of the RREA electrons and gamma rays like we detected during the 19 September 2009 and 4 October 2010 TGEs. The location of the majority of TGE events is outside the detector location site and detectors measure scattered gamma ray flux; the flux enhancement usually is rather small; the amplitude of 99% of TGEs is less than 10% of the cosmic ray background. Neutrons born in the photonuclear reactions have a much wider lateral distribution and can hit a neutron monitor even if the RREA is far from the detector site. And we can expect that the ratio of neutron-to-gamma ray content of the TGE will rise proportionally to the distance of the detector from the projection of the "center" of the lower dipole on the Earth's surface.

To prove this statement we simulate RREA development and register gamma rays and neutrons in the circles of growing radii around the symmetry axes of the electron-gamma ray avalanche. We again put the gamma ray source at 5000 m above the detector site located at 3200 m. The number of neutrons and gamma rays was counted in concentric rings of radii enlarging on each step by 20 m. As we can see from Fig. 8 the gamma content at distances less than 100 m is prevailing and the ratio is below 2%; however, at distances above 100 m the neutron-to-gamma ray ratio starts to rise very quickly reaching 12% at 160 m. As we can see in the last column of Table II the neutron-to-gamma ray ratio reconstructed for the 2 largest events is 2.5% and 3.3%; for the rest of the events, although we cannot recover intensities of the particle flux, proceeding from the measured count rate ratio we can expect a much larger value of neutron-to-gamma ray intensities. Of course, we recognize that the TGE is due to multiple RREA processes started from numerous points in an extended region in the thundercloud; however, as we discuss above, this region is local and the edge effect will lead to dependence of the neutron-to-gamma ray ratio similar to the one we display in Fig. 8.

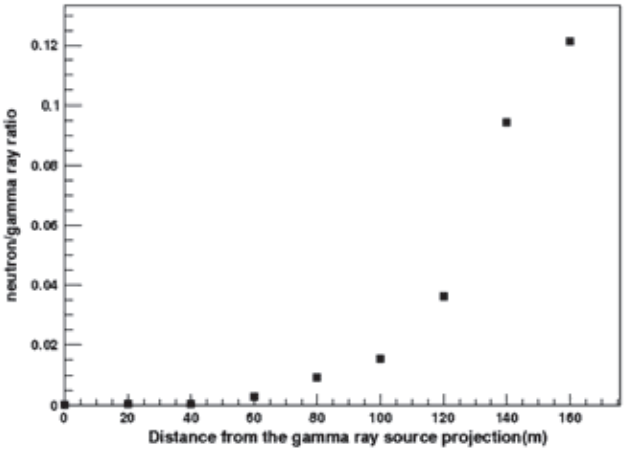

FIG. 8. Dependence of the detected-in-TGE neutron/gamma ray ratio on the distance from RREA center.

III. CONCLUSIONS

We unambiguously prove the existence of the neutron flux linked to theTGEs and well correlated with the gamma ray flux. The mechanism of the neutron generation in the thunderclouds is the photonuclear reaction of the gamma rays born in the electron–gamma ray avalanches unleashed in the strong electrical fields of the thunderclouds (the RREA process).

Detection of the dips in the time series of the high-energy muons simultaneously with detection of very large peaks in low-energy gamma rays proves the existence of a large positive electrical field in the thunderclouds that accelerates electrons downward and demonstrates the developed positively charged layer in the bottom of the thundercloud.

ACKNOWLEDGMENTS

This work was partly supported by Armenian government grants and by Grant No. A1554 ISTC. The authors are grateful to participants of the conference TEPA-2010 and to members of the seminar of the cosmic ray division of the Yerevan Physics Institute for useful discussion and to S. Chilingaryan for developing the ADEI multivariate visualization tool [38] for the treatment of the ASEC data flow. One of the authors (A. C.) is grateful to Brant Carlson for useful discussions on the start of work explaining the neutron content of TGE.

[1] D. Klir *et al.*, Phys. Plasmas **15**, 032 701 (2008).
[2] R. L. Fleischer, J. Geophys. Res. **80**, 5005 (1975).
[3] G. N. Shah, H. Razdan, C. L. Bhat, and Q. M. Ali, Nature (London) **313**, 773 (1985).
[4] A. Shyam and T. C. Kaushik, J. Geophys. Res. **104**, 6867 (1999).
[5] G. N. Shah, P. M. Ishtiaq, S. Mufti, and M. A. Darzi, in Burst Profile of the Lightning Generated Neutrons Detected by Gulmarg Neutron Monitor, 30th International Cosmic Ray Conference, Merida, Mexico, 2007.
[6] I. M. Martin and M. A. Alves, J. Geophys. Res. **115**, A00E11 (2010).
[7] J. Chadwick and M. Goldhaber, Nature (London) **134**, 237 (1934).
[8] L. P. Babich and R. A. Roussel-Dupré, J. Geophys. Res. **112**, D13303 (2007).
[9] A. V. Gurevich, G. M. Milikh, and Roussel-Dupre, Phys. Lett. A **165**, 463 (1992).
[10] J. R. Dwyer, B. W. Grefenstette, and D. M. Smith, Geophys. Res. Lett. **35**, L02815 (2008).
[11] H. Carmichael, "Cosmic Rays" (IQSY Instruction Manual, #7), London, 1964.
[12] C. J. Hatton, in *Progress in Elementary Particles and Cosmic Ray Physics*, edited by J. G. Wilson and S. A. Wouthuysen (North Holland, Amsterdam, 1971), Vol. 10, p. 1.
[13] A. Chilingarian *et al.*, J. Phys. G **29**, 939 (2003).
[14] A. Chilingarian *et al.*, Nucl. Instrum. Methods Phys. Res., Sect. A **543**, 483 (2005).
[15] A. Chilingarian and A. Reymers, Ann. Geophys. **26**, 249 (2008).
[16] A. Chilingarian, A. Daryan, K. Arakelyan, A. Hovhannisyan, B. Mailyan, L. Melkumyan, G. Hovsepyan, S. Chilingaryan, A. Reymers, and L. Vanyan, Phys. Rev. D **82**, 043009 (2010).
[17] A. Hovhannisyan and A. Chilingarian, Adv. Space Res. **47**, 1544 (2011).
[18] B. E. Carlson, N. G. Lehtinen, and U. S. Inan, J. Geophys. Res. **115**, a00e19 (2010).
[19] J. M. Clem and L. I. Dorman, Space Sci. Rev. **93**, 335 (2000).
[20] E. A. Maurchev, B. B. Gvozdeckij, Yu. V. Balabin, and E. V. Vashenuk, Simulation of the Response Function of Neutron Monitors, official CD of Russian Cosmic Ray Conference, Moscow State Univ., 2010.
[21] K. Watanabe *et al.*, Astrophys. J. **592**, 590 (2003).
[22] L. I. Dorman and I. V. Dorman, Adv. Space Res. **35**, 476 (2005).
[23] Y. Muraki *et al.*, Phys. Rev. D **69**, 123010 (2004).
[24] J. Wentz, I. M. Brancus, A. Bercuci, D. Heck, J. Oehlschläger, H. Rebel, and B. Vulpescu, Phys. Rev. D **67**, 073020 (2003).
[25] M. Bahmanabadi, F. Sheidaei, M. Khakian Ghomi, and J. Samimi, Phys. Rev. D **74**, 082006 (2006).
[26] N. C. Mukhopadhyay, Phys. Rep. **30**, 1 (1977).
[27] J. M. Clem, in *26th International Cosmic Ray Conference* (Salt Lake City, 1999), Vol. 7, p. 317.
[28] E. B. Hughes and P. L. Marsden, J. Geophys. Res. **71**, 1435 (1966).
[29] T. W. Crane and M. P. Baker, *Passive Nondestructive Assay of Nuclear Materials*, edited by D. Reilly *et al.* (Los Alamos National Laboratory, Los Alamos, NM, USA, 1991), Chap. 13, Technical Report No. NUREG/CR-5550, LA-UR-90-732.
[30] A. Chilingarian, G. Hovsepyan, and A. Hovhannisyan, Phys. Rev. D **83**, 062001 (2011).
[31] M. Stolzenburg, T. C. Marshall, and W. D. Rust, J. Geophys. Res. **103**, 14 079 (1998).
[32] A. Nag and V. A. Rakov, Geophys. Res. Lett. **36**, L05815 (2009).
[33] S. D. Pawar and A. K. Kamra, J. Geophys. Res. **109**, D02205 (2004).
[34] X. Qie, T. Zhang, C. Chen, G. Zhang, T. Zhang, and X. Kong, Atmos. Res. **91**, 244 (2009).
[35] H. Tsuchiya *et al.*, J. Geophys. Res. **116**, D09113 (2011).
[36] T. Torii, T. Sugita, M. Kamogawa, Y. Watanabe, and K. Kusunoki, Geophys. Res. Lett. **38**, L24801 (2011).
[37] L. Babich, E. Bochkov, I. Kutsyk, and R. Roussel-Dupre, J. Geophys. Res. **115**, A00E28 (2010).
[38] S. Chilingaryan, A. Beglarian, A. Kopmann, and S. Vöcking, J. Phys. Conf. Ser. **219**, 042 034 (2010).

List of Participants

Arakelyan	Karen	Armenia	Alikhanyan National Labaratory	karen@yerphi.am
Chilingarian	Ashot	Armenia	Alikhanyan National Labaratory	chili@aragats.am
Gemmeke	Hartmut	Germany	Karlsruhe Institute of Technology	hartmut.gemmeke@ipe.fzk.de
Hovhannisyan	Armen	Armenia	Alikhanyan National Labaratory	harmen@yerphi.am
Kanoyan	Hakob	Armenia	Alikhanyan National Labaratory	hakob91@gmail.com
Karapetyan	Tigran	Armenia	Alikhanyan National Labaratory	ktigran79@yerphi.am
Knapp	Johannes	UK	Physics & Astronomy University of Leeds	j.knapp@leeds.ac.uk
Mailyan	Bagrat	Armenia	Alikhanyan National Labaratory	bagrat_mailyan@yerphi.am
Mkrtchyan	Hripsime	Armenia	Alikhanyan National Labaratory	hripsime@mail.yerphi.am
Mirzoyan	Razmik	Germany	Max Planck Institute for Physics	razmik.mirzoyan@mpp.mpg.de
Reymers	Arthur	Armenia	Alikhanyan National Labaratory	artur@yerphi.am
Rostomyan	Hasmik	Armenia	Alikhanyan National Labaratory	hasmik_rostomyan@yerphi.am
Sargsyan	David	Armenia	Alikhanyan National Labaratory	david@ yerphi.am
Sargsyan	Stepan	Armenia	Alikhanyan National Labaratory	sargsyan@yerphi.am
Tsakanyan	Hovhanes	Armenia	Alikhanyan National Labaratory	hovhannes.ht@gmail.com
Vanyan	Levon	Armenia	Alikhanyan National Labaratory	levon@mail.yerphi.am

TEPA-2010

Cosmic Ray Summer School-2012

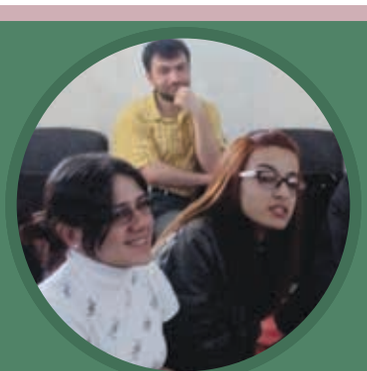

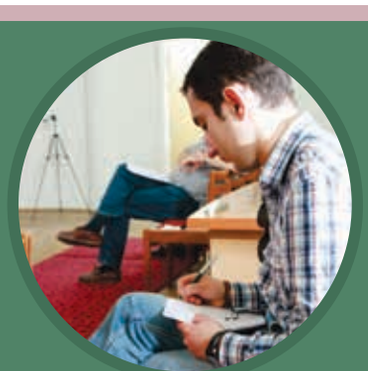

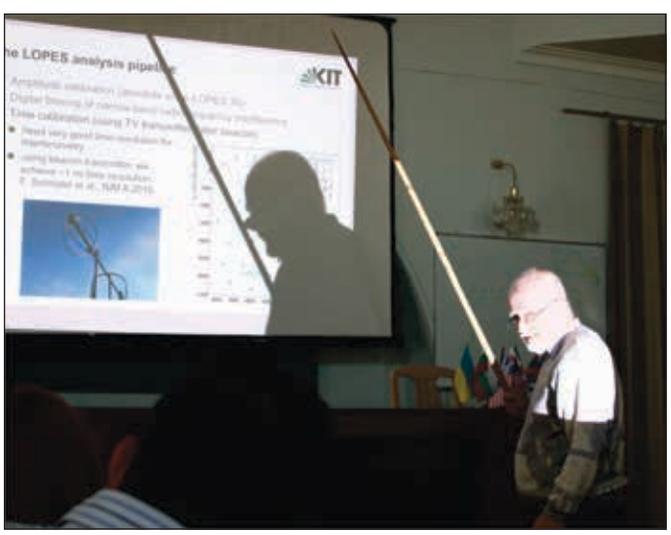
KIT

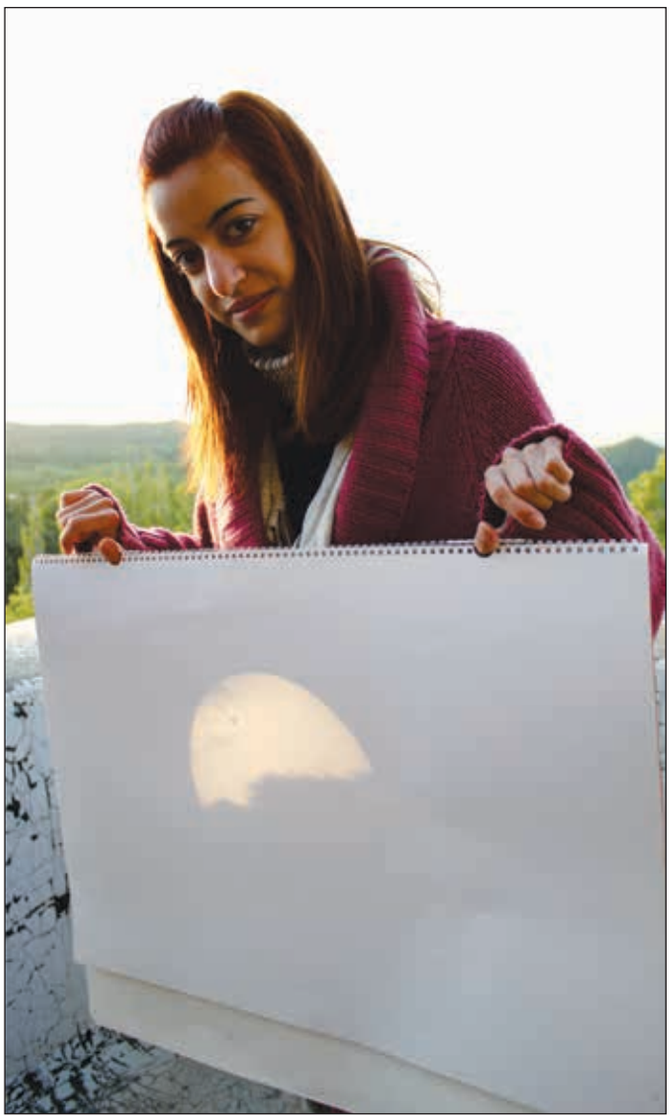

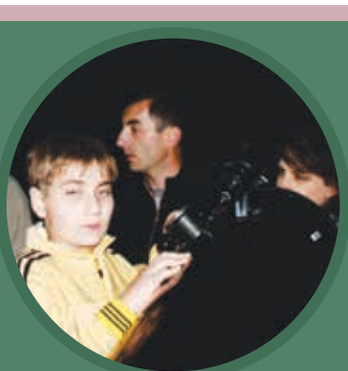

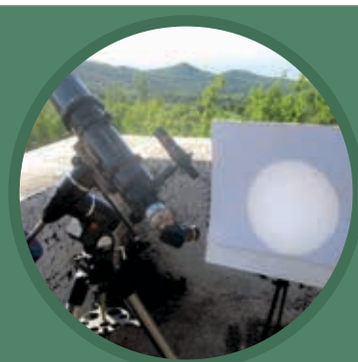

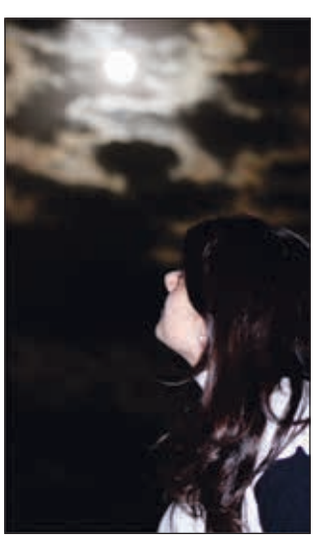

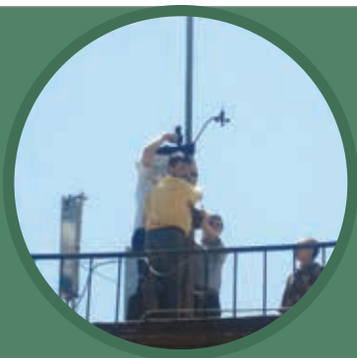

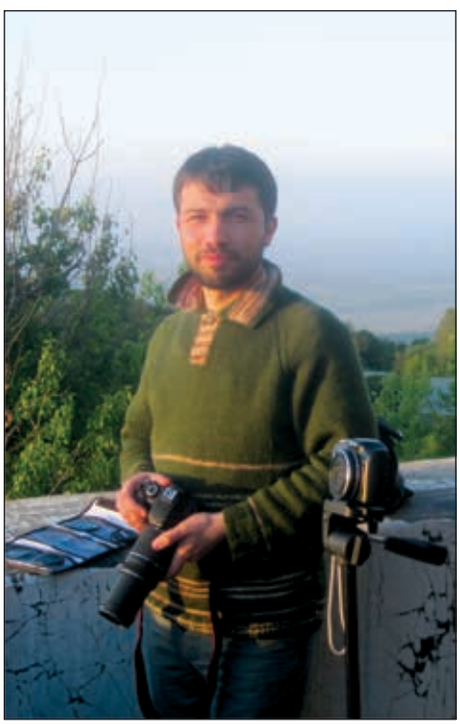

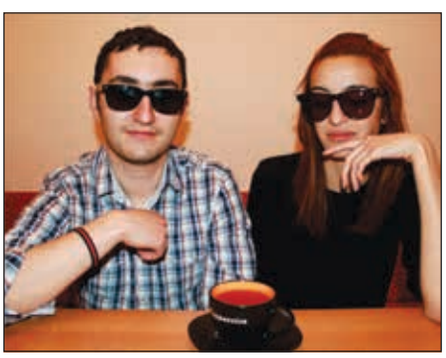

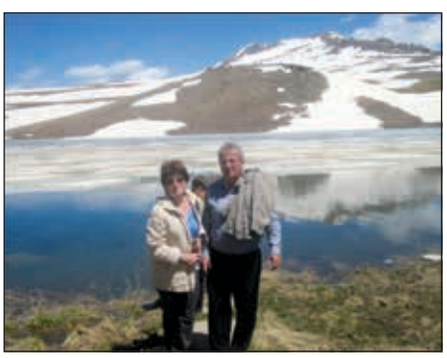

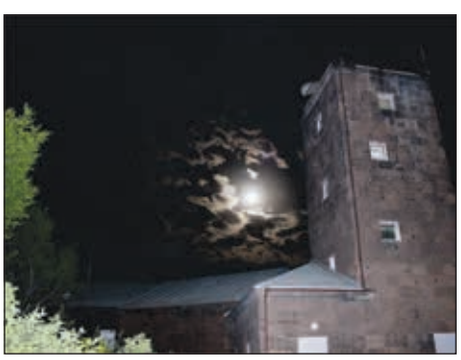

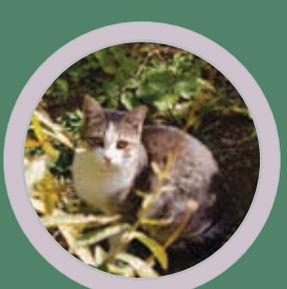

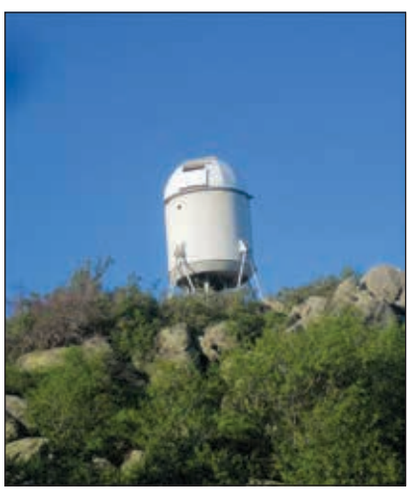

CRD Bikathone 2012